Josip Juraj Strossmayer University of Osijek
University of Dubrovnik
Ruđer Bošković Institute, Zagreb

Interdisciplinary doctoral studies Molecular Biosciences

Ana Petelinec

THE ROLE OF KINESIN-8 AND CELL SHAPE IN MITOTIC PROGRESSION IN HEALTHY AND TUMOR CELLS

Doctoral thesis

Osijek, 2025.

This doctoral thesis was done in the Laboratory of Cell Biophysics, Department of Molecular Biology, at the Ruđer Bošković Institute, Zagreb, under the supervision of Dr. Iva M. Tolić, Head of Laboratory. This work was funded by the "Young Researchers' Career Development Project – Training New Doctoral Students" (DOK-2021-02-4097) of the Croatian Science Foundation.

TEMELJNA DOKUMENTACIJSKA KARTICA

Sveučilište Josipa Jurja Strossmayera u Osijeku **Doktorski rad**
Sveučilište u Dubrovniku
Institut Ruđer Bošković
Doktorski studij Molekularne bioznanosti

Znanstveno područje: Interdisciplinarno područje znanosti
Znanstvena polja: Biologija i Temeljne medicinske znanosti

ULOGA KINEZINA-8 I OBLIKA STANICE U TIJEKU MITOZE U ZDRAVIM I TUMORSKIM STANICAMA

Ana Petelinec

Doktorski rad je izrađen u: Laboratorij za biofiziku stanice, Zavod za molekularnu biologiju, Institut Ruđer Bošković, Zagreb

Mentor: dr. sc. Iva M. Tolić, znanstvena savjetnica u trajnom izboru

Kratki sažetak doktorskog rada:
Mitoza je dio staničnog ciklusa gdje se genetički materijal podijeli u dvije stanice pomoću diobenog vretena. Protein KIF18A regulira duljinu vretena i smanjuje oscilacije kinetohora, a neke stanice su osjetljive na njegov gubitak. Post-tetraploidne stanice osjetljivije su na gubitak KIF18A nakon inhibicije sa sovilnesibom. Mitoza je uspoređena između jednoslojnih kultura i sferoida, koji bolje prikazuju složenost tkiva. U ograničenom prostoru stanice i vretena su manji, a povećava se frakcija nepravilnih oblika i prometafaznih stanica.

Broj stranica: 161 stranice
Broj slika: 59 slika
Broj tablica: 0 tablica
Broj literaturnih navoda: 174 literaturnih navoda
Jezik izvornika: engleski jezik
Ključne riječi: post-tetraploidne stanice, KIF18A, sovilnesib, sferoidi, 2D kulture

Datum javne obrane:

Povjerenstvo za javnu obranu:
1. nasl. doc. dr. sc. Ana Čipak Gašparović, znanstvena savjetnica (predsjednica)
2. nasl. izv. prof. dr. sc. Andreja Ambriović Ristov, naslovna izvanredna profesorica, znanstvena savjetnica u trajnom izboru (članica)
3. izv. prof. dr. sc. Ivana Škrlec, izvanredna profesorica (članica)
4. dr. sc. Maja Sabol, viša znanstvena suradnica (zamjenska članica)

Doktorski rad je pohranjen u: Nacionalnoj i sveučilišnoj knjižnici Zagreb, Ul. Hrvatske bratske zajednice 4, Zagreb; Gradskoj i sveučilišnoj knjižnici Osijek, Europska avenija 24, Osijek; Sveučilištu Josipa Jurja Strossmayera u Osijeku, Trg sv. Trojstva 3, Osijek

BASIC DOCUMENTATION CARD

Josip Juraj Strossmayer University of Osijek **PhD thesis**
University of Dubrovnik
Ruđer Bošković Institute
Doctoral Study of Molecular biosciences

Scientific Area: Interdisciplinary area of science
Scientific Fields: Biology and Basic medical sciences

THE ROLE OF KINESIN-8 AND CELL SHAPE IN MITOTIC PROGRESSION IN HEALTHY AND TUMOR CELLS

Ana Petelinec

Thesis performed at: Laboratory of Cell Biophysics, Department of Molecular Biology, Ruđer Bošković Institute, Zagreb

Supervisor: Iva M. Tolić, PhD, Senior Scientist with Tenure

Short abstract:
Mitosis is a part of cell cycle that divides genetic material in two cells with mitotic spindle. KIF18A protein regulates spindle length and reduces kinetochores oscillations, and some cells are sensitive to its loss. Post-tetraploid cells are sensitive to KIF18A loss after sovilnesib inhibition. Mitosis was compared between monolayers and spheroids, that better mimic tissue complexity. Confined environment caused decrease in cell and spindle dimensions, followed with increase in irregular shapes and fraction of prometaphase cells.

Number of pages: 161 pages
Number of figures: 59 figures
Number of tables: 0 tables
Number of references: 174 references
Original in: English language
Key words: post-tetraploid cells, KIF18A, sovilnesib, spheroids, 2D cultures

Date of the thesis defense:

Reviewers:
1. Ana Čipak Gašparović, PhD, Senior Scientist (president of the committee)
2. Andreja Ambriović Ristov, PhD, Senior Scientist with Tenure, Associate Professor (committee member)
3. Ivana Škrlec, PhD, Associate Professor (committee member)
4. Maja Sabol, PhD, Senior Research Associate (substitute member)

Thesis deposited in: National and University Library in Zagreb, Ul. Hrvatske bratske zajednice 4, Zagreb; City and University Library of Osijek, Europska avenija 24, Osijek; Josip Juraj Strossmayer University of Osijek, Trg sv. Trojstva 3, Osijek

Acknowledgements

TABLE OF CONTENTS

ABBREVIATIONS

2D – two-dimensional
3D – three-dimensional
γ-TuRCs – γ-tubulin ring complexes
APC/C – anaphase promoting complex
ATCC – American Type Culture Collection
BP – blocking/permeabilization
CCAN – constitutive centromere-associated network
CENP-A – centromere protein A
CIN – chromosomal instability
DMSO – dimethyl sulfoxide
ECM – extracellular matrix
GFP – green fluorescent protein
HGSOC – high grade serous ovarian cancer
HPT – HCT166 post-tetraploid
KD – knockdown
KMN – Knl1, Mis12, Ndc80 subcomplexes
Mad2 – mitotic arrest deficiency protein
MAPs – microtubule-associated proteins
MCTS – multicellular tumor spheroid
MTOC – microtubule-organizing center
N.D. – not determined
NEBD – nuclear envelope breakdown
NuMA – Nuclear Mitotic Apparatus protein
PCM – pericentriolar material
PDMS – polydimethylsiloxane
PRC1 – Protein Regulator of Cytokinesis 1
PT – post-tetraploid
RPT – RPE1 post-tetraploid
SAC – spindle assembly checkpoint
siRNA – small interfering RNA
STED – stimulated emission depletion
WGD – whole genome doubling

1. INTRODUCTION

1.1. The cell cycle

The cell cycle in eukaryotes has a main function of dividing genetic material into two daughter cells. It is composed of two major phases, interphase, and M phase, that can further be divided. Interphase consists of G1 (gap 1) phase, S (synthesis) phase and G2 (gap 2) phase (Figure 1). Phases of cell cycle are temporally controlled and have checkpoints where proceeding to the next phase is approved (Alberts et al., 2002).

In G1 phase cells grow and synthesize proteins required for DNA replication, and it is the longest phase of the cell cycle. Also, it is decided if the conditions are favorable to continue to the next phase. In S phase DNA is duplicated, and it is followed by G2 phase, where cells are preparing for division. After interphase cells go into M phase, the shortest phase of the cell cycle. M phase has two main stages: mitosis, where genetic material is divided, and cytokinesis, where the cytoplasm and organelles are distributed to each new cell (Alberts et al., 2002) (Figure 1).

The cell cycle is regulated by various intracellular and extracellular signals. If conditions are unfavorable or a phase cannot be completed, the regulatory system will halt the cycle. Transitions between cell cycle phases are controlled by the cell cycle control system, which activates and monitors processes like DNA replication, mitosis, and cytokinesis based on the cells' conditions and environment (Alberts et al., 2002).

Cells that are actively growing and dividing are also called proliferative cells. Various extracellular and intracellular signals will regulate cell proliferation. If conditions are not favorable for cell division, cells will enter resting phase, G0 (gap 0), in which they can spend various amount of time, ranging from days to years, before re-entering the cell cycle (Figure 1). Reversible cell cycle arrest is called quiescence, and irreversible is called senescence (Alberts et al., 2002).

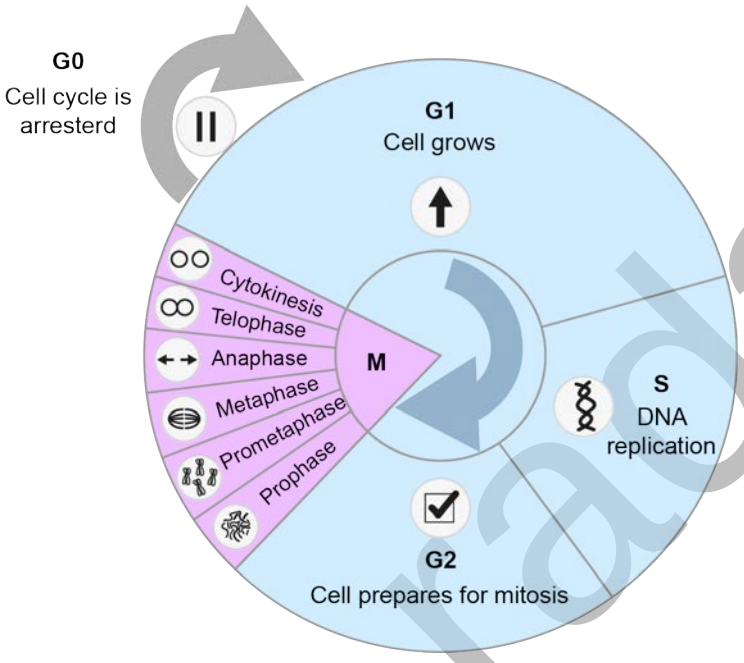

Figure 1. The cell cycle. The cell cycle is divided into interphase, consisting of G1, S and G2 phase, and M phase, consisting of mitosis and cytokinesis. In interphase cells grow, replicate its genetic material, and prepare for division. In M phase cells undergo nuclear division, where chromosomes are equally divided, and each daughter cell gets two copies of each chromosome. In cytokinesis, cytoplasm divides, resulting in the formation of two daughter cells. Adapted from (Alberts et al., 2002).

1.2. Mitosis

Mitosis is a multi-stage process that is vital for growth and tissue repair in multicellular organisms. It is important for precise distribution of genetic material to daughter cells, ensuring genomic stability. Mitosis is subdivided into prophase, prometaphase, metaphase, anaphase, and telophase (Figure 2). During prophase, before nuclear envelope breakdown (NEBD), chromatin, consisting of DNA molecules and histone proteins, condenses to form chromosomes, each composed of two sister chromatids joined at the centromere (McIntosh et al., 2012). The mitotic spindle, composed of microtubules and various proteins, starts to form between two centrosomes outside the nucleus. Prometaphase starts with NEBD and formation of mitotic spindle. Chromosomes are attaching to the microtubules via kinetochores, complex protein structures on the centromeric region of chromosomes, (Musacchio & Desai, 2017). Chromosomes start to congress to the future equatorial plane, where chromosomes are properly aligned in metaphase. Once all chromosomes are aligned in the metaphase plate, with sister chromatids attached to the microtubules from the opposite spindle pole, anaphase can start (Maiato et al., 2017).

Anaphase can be divided into anaphase A and anaphase B. In anaphase A sister chromatids start to segregate to the opposite poles by shortening of microtubules. It is followed with anaphase B, where centrosomes separate and spindle elongates, which further segregates the chromosomes (Vukušić et al., 2019). In telophase, the two chromosome masses are fully separated, chromosomes start to decondense, the nuclear envelope starts to form around each set of chromosomes, and mitotic spindle disassembles. Cytokinesis begins concurrently with anaphase, with the formation of contractile actomyosin ring in the equatorial plane that constrict the cell membrane and cytoplasm resulting in the formation of two daughter cells (Alberts et al., 2002).

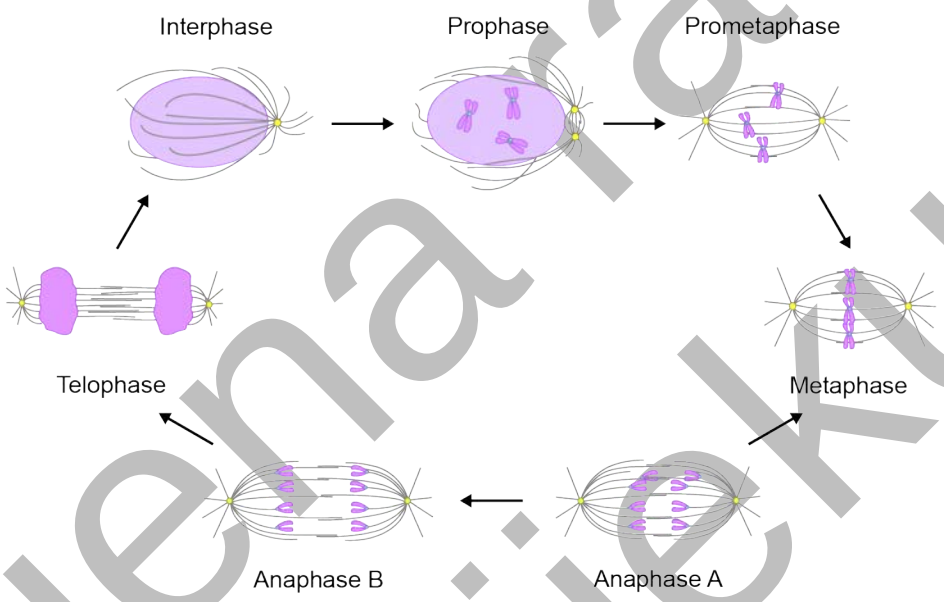

Figure 2. The phases of mitosis. Mitosis can be divided into five subphases: prophase, prometaphase, metaphase, anaphase, and telophase. In prophase, chromosomes condense, and in prometaphase mitotic spindle starts to form. Chromosomes attach to the microtubules and start to congress towards the spindle equator. When chromosomes are properly aligned in metaphase, anaphase starts, and chromosomes separate to the opposite sides. In anaphase A chromosomes move towards the spindle poles, and in anaphase B spindle elongates, further separating two chromosome mases. In telophase, chromosomes are fully separated and start to decondense. Two daughter cells are being formed. Adapted from (Walczak et al., 2010).

1.3. Mitotic spindle architecture

Mitotic spindle is a complex and dynamic structure that enables precise division of chromosomes into two daughter cells. It has the same function in all species, but its structure and components can change. In most somatic animal cells mitotic spindle is composed of microtubules and proteins that perform various functions. Spindles normally have two spindle poles and are called bipolar spindles (Alberts et al., 2002). In some cases, spindles can form more than two spindle poles and are called multipolar. These spindles can be tripolar, tetrapolar, pentapolar etc (Manchester, 1995).

Microtubules are protein tubes made from α- and β-tubulin subunits, that make heterodimers. Each microtubule is built from thirteen protofilaments, making a hollow cylindrical structure, that has a polarity, with α-tubulin on minus end and β-tubulin on plus end. Polymerization happens on the plus end, and depolymerization on the minus end. In the mitotic spindle, microtubules are organized in a way that their minus ends are anchored at the spindle poles, while their plus ends grow outward from the poles (Alberts et al., 2002). Tubulin subunits constantly move along the microtubules. Microtubule poleward flux is a constant poleward movement of tubulin subunits in the microtubules, coordinated with addition of tubulin subunits at the plus end, where microtubules polymerize, and removal of tubulin subunits at the minus end, where microtubules depolymerize. In that way the shape and size of spindle in metaphase remains constant (Mitchison, 1989).

Microtubules can be divided into several categories in respect to their function and localization, and individual microtubules can form microtubule bundles (Alberts et al., 2002). If microtubule ends at the kinetochore, it is called kinetochore microtubule, and they form parallel bundles called kinetochore fibers or k-fibers. Non-kinetochore microtubules can be individual, or they can form parallel and antiparallel bundles. Non-kinetochore microtubules can be divided on astral, polar and interpolar or overlap microtubules. Astral microtubules grow from the spindle pole towards cell cortex, and they have a role in positioning of the spindle to the cell cortex (Dumont & Mitchison, 2009). Polar microtubules are the ones that grow toward the spindle equator and have a free end. Overlap microtubules grow from each side of the spindle and form an antiparallel overlap in the center of the spindle (Alberts et al., 2002; Tolić, 2018) (Figure 3A).

Overlap microtubules can also form bridging fibers. These are overlap microtubule bundles that form during metaphase and early anaphase that are laterally attached to a pair of sister k-fibers, looking like a bridge between them, which is the reason why they are called bridging fibers (Kajtez et al., 2016; Vukušić et al., 2017) (Figure 3B). Their role is to balance the tension between sister kinetochores and maintain the curved shape of the spindle (Kajtez et al., 2016; Polak et al., 2017; Tolić, 2018; Tolić & and Pavin, 2016).

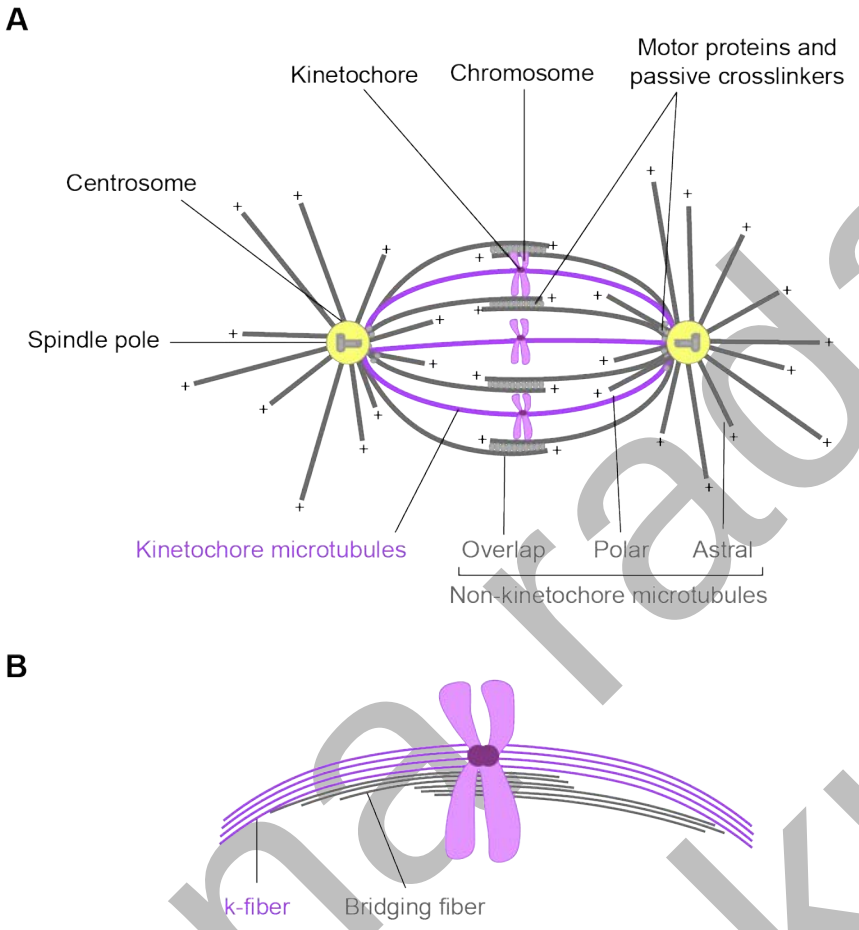

Figure 3. Mitotic spindle architecture. A) Microtubules in mitotic spindle can be divided into kinetochore (magenta) and non-kinetochore microtubules (grey). Kinetochore microtubules attach to chromosomes via protein complexes, kinetochores, and connect them to the spindle pole. Non-kinetochore microtubules can be divided into overlap, polar and astral microtubules. Overlap microtubules grow from the opposite sides of the spindle and form an antiparallel overlap. Polar microtubules grow toward the spindle equator and have the free end. Astral microtubules grow from the spindle pole towards the cell cortex. Spindle pole has a protein organelle, centrosome, that is a microtubule nucleation center. In addition to microtubules, mitotic spindle has various motor and passive crosslinking proteins, which help to maintain proper structure and functions of the spindle. **B)** Overlap microtubules are laterally attached to a pair of sister k-fibers and form an overlap that resembles a bridge, which is why they are called bridging fibers. Adapted from (Alberts et al., 2002; Tolić, 2018).

1.4. Centrosomes

Each spindle pole is focused around protein organelle centrosome, that consists of a pair of centrioles, surrounded with a matrix of pericentriolar material (PCM) (Figure 3A). In G1 phase of the cell cycle, each cell has one centrosome. Centrosome duplicates in the S phase, the same as DNA. Cell will enter mitosis with a pair of centrosomes, that will separate during mitosis, and each daughter cell will inherit one centrosome (Alberts et al., 2002).

PCM contains many signaling molecules, cell cycle regulators and proteins that nucleate and organize microtubules, so it is one of the most important microtubule-organizing centers (MTOCs). The amount of PCM significantly increases when cells prepare to enter mitosis, which is called centrosome maturation. During centrosome maturation γ-tubulin ring complexes (γ-TuRCs) are recruited to the PCM (Conduit et al., 2015). γ -TuRCs serve as a template to nucleate new microtubules, and they contain γ-tubulin protein and two accessory proteins that bind directly to it (Alberts et al., 2002).

1.5. Importance of proper kinetochore attachments to microtubules

To ensure correct and faithful segregation of all chromosomes during mitosis, it is important that all chromosomes are properly attached to spindle microtubules. Chromosomes are attached to the microtubules through a specific recognition site, with the help of kinetochores. This recognition site is localized within a specific region of the chromosome, called the centromere. This region contains a variant of histone H3, centromere protein A (CENPA), which plays a crucial role in defining the centromere and enabling kinetochore binding (McKinley et al., 2015).

Kinetochore proteins are organized into inner and outer kinetochore, where inner kinetochore interacts with chromosomes, and outer kinetochore binds to microtubules. The inner kinetochore contains a 16-subunit constitutive centromere-associated network (CCAN), which binds directly to CENPA, and other inner kinetochore components assemble to CCAN-CENPA complex (McKinley et al., 2015; Prosser & Pelletier, 2017). The outer kinetochore contains the KMN network, composed of Knl1, Mis12 and Ndc80 subcomplexes, and it is a microtubule binding site (Cheeseman et al., 2006) (Figure 4A).

For a proper chromosome attachment, the kinetochore on each sister chromatid must be connected to a k-fiber originating from the opposite spindle pole. This type of attachment is called amphitelic. Sister kinetochores that are properly attached to both spindle poles are called bioriented. If only one sister kinetochore is attached to a k-fiber, the attachment is monotelic. Syntelic attachment occurs when both sister kinetochores are attached to k-fibers from the same spindle pole. Finally, in merotelic attachments, one kinetochore is attached to

a k-fiber from one spindle pole, while other is attached to k-fibers from both spindle poles (Prosser & Pelletier, 2017) (Figure 4B).

Kinetochores have an error correction mechanism that is mediated by Aurora B kinase, which senses the tension at centromeres with incorrect attachments (Godek et al., 2015; Trivedi & Stukenberg, 2016). In addition, the spindle assembly checkpoint (SAC) also regulates kinetochore attachments (Lara-Gonzalez et al., 2021). SAC remains active until all kinetochores are correctly attached to the microtubules. However, it can fail to detect merotelic attachments, which can lead to chromosome segregation errors. Once the correct attachments are established, the SAC is silenced, allowing activation of the anaphase-promoting complex (APC/C), which triggers the onset of anaphase (Cimini et al., 2001; Prosser & Pelletier, 2017).

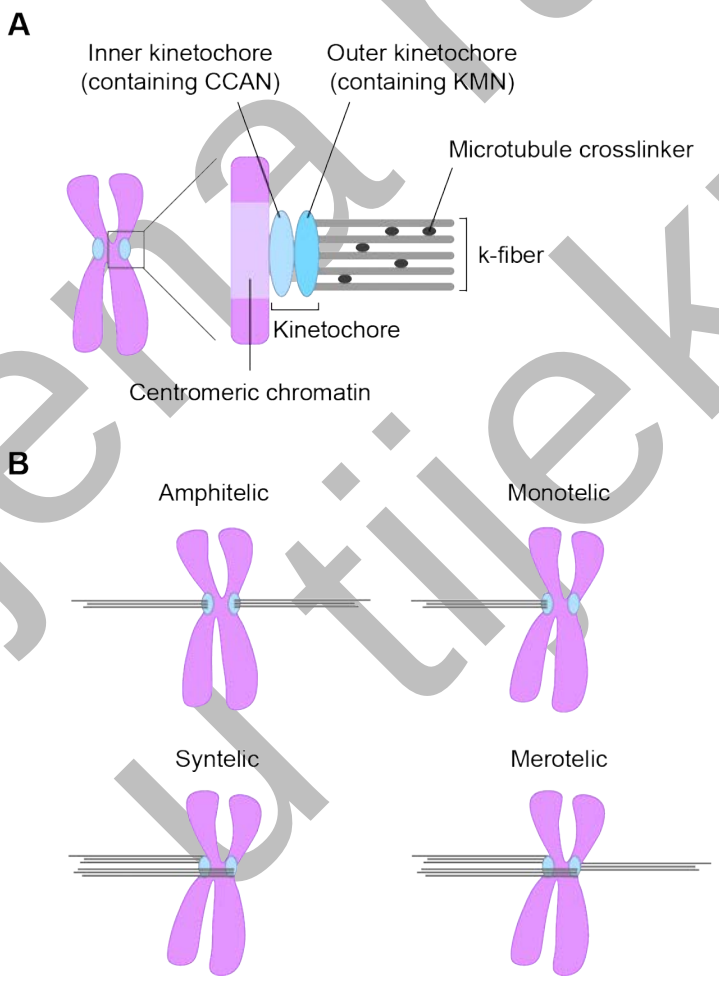

Figure 4. Caption on the following page.

Figure 4. Different types of kinetochore-microtubule attachments. A) Chromosomes connect to microtubules via kinetochores, a protein complex located on the centromeric region of each sister chromatid. The kinetochore complex consists of inner and outer kinetochore. **B)** Kinetochores can form different types of attachments with microtubules: amphitelic – the correct attachment, sister kinetochores are attached to the opposite poles, monotelic – only one kinetochore is attached, syntelic – sister kinetochores are attached to the same pole and merotelic – one kinetochore is attached to both poles. Adapted from (Prosser & Pelletier, 2017).

In some cases, chromosomes fail to align properly at the metaphase plate or form erroneous attachments, which can lead to mitotic errors. During prometaphase, cells may have unaligned chromosomes that remain behind the spindle poles or misaligned chromosomes located between the spindle poles and the metaphase plate. If they do not align correctly before the anaphase onset, further mis-segregation errors in anaphase can occur (Tucker et al., 2023; Vukušić & Tolić, 2022). Anaphase errors include lagging chromosomes, which are found between two segregating chromosome masses, and chromosome bridges, which occur when sister chromatids fail to separate properly and form a chromosome bridge between chromosome masses (Cimini et al., 2001; Ford & Correll, 2011). Lagging chromosomes often fail to integrate into the newly formed nucleus and instead form micronuclei (Potapova & Gorbsky, 2017), and chromosome bridges may persist into cytokinesis (Hong et al., 2021).

1.6. Microtubule-associated proteins

Microtubule-associated proteins (MAPs) are crucial for assembly and proper functioning of mitotic spindle. These large number of proteins are precisely coordinated, and they have diverse activities throughout the cell cycle. They can be divided into four groups depending on their function: crosslinking proteins that stabilize and organize microtubules; plus-end tracking proteins that regulate microtubule growth or connect them to the other structures; proteins that control microtubule destabilization; and motor proteins that move with respect to the microtubules (Alfaro-Aco & Petry, 2015; Lodish, 2008) (Figure 5).

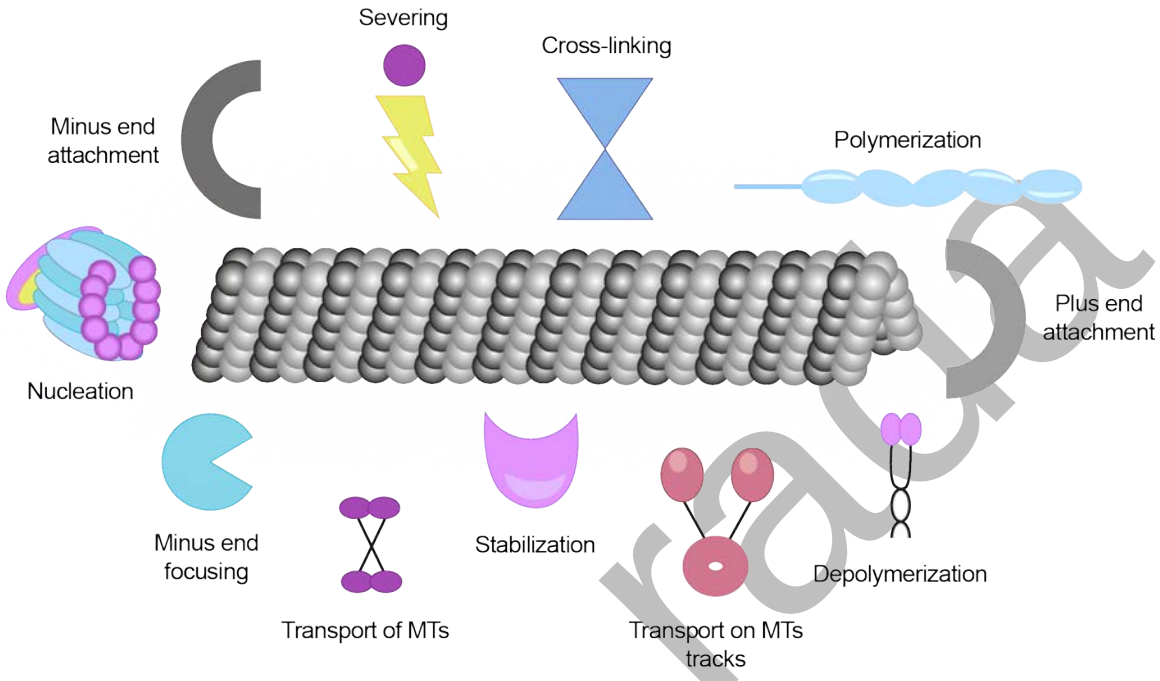

Figure 5. Microtubule-associated proteins. MAPs have different functions such as: microtubules polymerization and depolymerization, nucleation of microtubules, minus-end focusing, stabilization, severing, cross-linking, transport of microtubules, and transport of cargo. MAPs can attach to the minus-end and to the plus-end of the microtubules. Adapted from (Alfaro-Aco & Petry, 2015).

Motor proteins are a group of MAPs that transport cargo and play key roles in the assembly of mitotic spindle, influencing the stability of microtubules, and they can mediate the cross-linking and sliding apart of neighboring microtubules. In general, motor proteins can bind ATP and hydrolyze it to ADP, which means they are ATPases. During ATP hydrolysis energy releases and causes conformational change in the motor domain, enabling them to switch from bound and unbound state, in other word to “walk” along microtubules, using “hand-over-hand” motion. Motor proteins have preferable directionality of the movement with respect to the microtubules plus and minus-ends (Alberts et al., 2002) (Figure 6).

Motor proteins can be divided into kinesins and dyneins. Kinesins are a large ATP-dependent protein superfamily that have a motor domain in common (Alberts et al., 2002; Kapitein & Peterman, 2009). In humans, 41 different kinesin-like proteins have been described so far (Dagenbach & Endow, 2004). Kinesin family members have various roles during mitosis: kinesin-4, kinesin-8 and kinesin-14 can regulate growth and shrinkage of microtubules; kinesin-5, kinesin-6 and kinesin-13 can generate microtubule arrays that are polarity specific, and kinesin-7 can mediate interactions between chromosomes and microtubules (Kapitein & Peterman, 2009).

Most of the kinesins walks towards the plus-end of microtubules, but some of them can walk towards the minus-end, or they can walk in both directions (Alberts et al., 2002; Kapitein & Peterman, 2009). One of the main focuses of this thesis will be a member of kinesin-8 family, KIF18A protein, which will be described in more details.

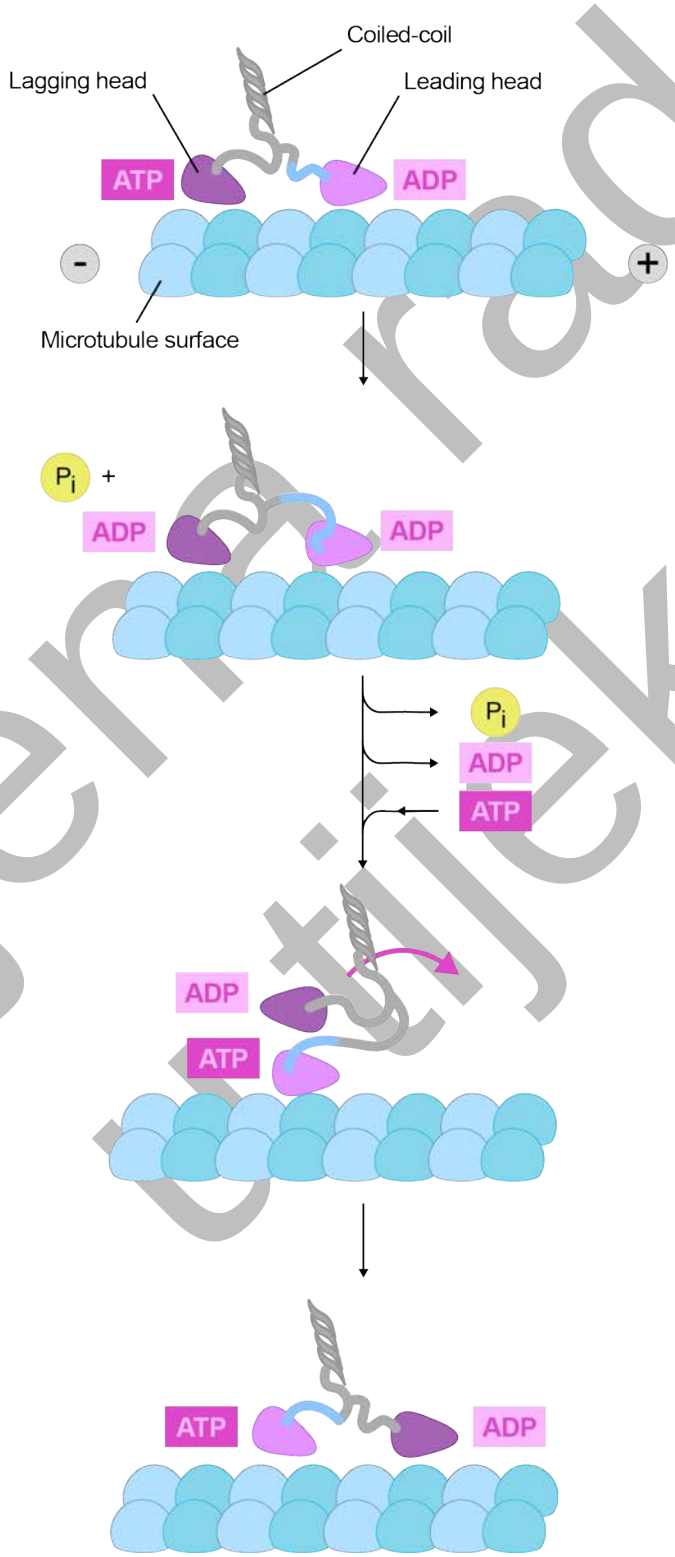

Figure 6. Caption on the following page.

Figure 6. Kinesins walking mechanism. Kinesin motor protein can bind ATP and hydrolyze it to ADP. Hydrolysis happens in the lagging domain, and energy release causes confrontational changes in the motor domain, so lagging head switches to a leading head and vice versa. The switch from bound to unbound state enables them to "walk" on the microtubules, using "hand-over-hand" motion. Adapted from (Alberts et al., 2002).

1.7. KIF18A regulates spindle length and chromosome alignment

Motor protein KIF18A is a member of the kinesin-8 protein family that has important roles in maintaining spindle architecture and chromosome alignment. It localizes on plus-end tips of k-fibers, distal to the outer kinetochore (Mayr et al., 2007; L. N. Weaver et al., 2011) (Figure 7). KIF18A depletion experiments show a delay in mitosis mediated by SAC activation, spindle elongation, and chromosome alignment defects (Janssen et al., 2018; Mayr et al., 2007; Stumpff et al., 2008; L. N. Weaver et al., 2011; Zhu et al., 2005).

Both *in vitro* and *in vivo* studies showed that kinesin-8 proteins, including KIF18A, are plus-end directed motor proteins that can depolymerize stable microtubules in a length-dependent manner, indicating that they directly regulate microtubule dynamics and length (Gupta et al., 2006; Mayr et al., 2007; Stumpff et al., 2008; Varga et al., 2006). KIF18A uses a combination of length-dependent accumulation and concentration-dependent regulation of k-fiber plus-end dynamics to control chromosome alignment (Stumpff et al., 2008). More KIF18A proteins will accumulate on longer microtubules, and they dissociate as the microtubule shortens (Mayr et al., 2007; Stumpff et al., 2008).

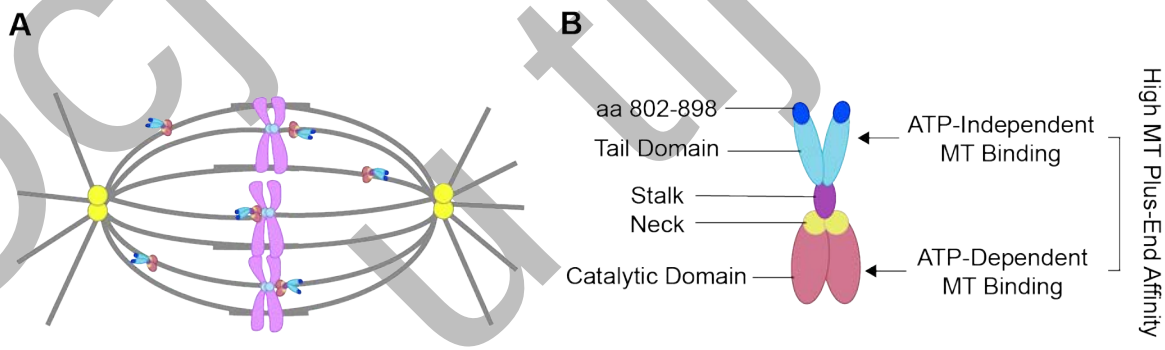

Figure 7. KIF18A protein. A) KIF18A is a motor protein with a plus-end directed movements. It localizes on the plus-end tips of the microtubules (MT). **B)** KIF18A consists of two microtubule-binding domains, catalytic domain is ATP-dependent, while tail domain is ATP-independent. They both consist of two heads, and they are separated by the stalk and the neck. Adapted from (L. N. Weaver et al., 2011).

During congression, both aligned and unaligned chromosomes move at a constant velocity. These movements are oscillatory because chromosomes abruptly change the direction of movement. In other words, they constantly move back and forth around the spindle equator (Rieder & Salmon, 1994; Skibbens et al., 1993). KIF18A limits the persistent movements of bioriented kinetochores in a motor-dependent manner and reduces the amplitude of oscillations (Stumpff et al., 2008). Kinetochores located at the periphery of the spindle exhibit reduced oscillations compared to those closer to the long spindle axis. When KIF18A is depleted, all kinetochores have increased movements, regardless of their position in the spindle (Stumpff et al., 2008).

Previous study showed that KIF18A is also localized on the bridging fibers. After the acute removal of the Protein Regulator of Cytokinesis 1 (PRC1) from antiparallel overlap, which leads to longer overlaps, KIF18A was also lost. The reduction of KIF18A on the bridging fibers following PRC1 removal was a consequence of reduced number of microtubules in the bridging fibers. KIF18A localization on k-fibers remained unaffected by PRC1 removal. It was additionally shown that overlap regions become longer after KIF18A depletion. According to this evidence, KIF18A regulates the overlap length of bridging microtubules (Jagrić et al., 2021).

1.8. KIF18A prevents mis-segregation errors

A model has been proposed to explain the link between KIF18A loss and chromosome segregation errors. After KIF18A depletion cells have problems with chromosome alignment due to increased chromosome oscillations. This prolongs mitotic duration, which is driven by SAC activation, and can ultimately result in unsuccessful mitosis. In this scenario, SAC is activated even though kinetochore-microtubule attachments are already formed, because the tension between sister kinetochores is insufficient. Lack of tension may be caused by chromosome hyperoscillations (Janssen et al., 2018) (Figure 8A).

Another model has been proposed to explain the link between KIF18A and mis-segregation errors, which is based on poleward flux-driven centering of kinetochores in metaphase plate, which helps to prevent lagging chromosomes and micronuclei formation (Risteski et al., 2022, 2024). KIF18A contributes to centering, because it is measuring microtubule length by binding on the microtubule lattice and walking toward the plus-end tips where it regulates the microtubule dynamics in a length-dependent manner (Varga et al., 2006).Centering mechanism is based on length-dependent pulling forces exerted by k-fibers onto the kinetochores. These forces pull kinetochores poleward, and they are generated at the plus-end tips (Risteski et al., 2022).

Misaligned sister kinetochores have a longer and shorter k-fiber, and the longer one has faster poleward flux, it pulls the kinetochores in the direction of his fiber, toward the spindle center, so that kinetochores align properly. Pulling forces increase with the increase in overlap length between bridging and k-fibers. Forces from the bridging fiber are transmitted to the k-fiber in a manner dependent on the coupling between them. Kinetochores are better centered in the spindle center when the overlaps between bridging and k-fibers are shorter, and the k-fiber flux is slower than the bridging fiber flux (Risteski et al., 2022) (Figure 8B).

To test whether poleward flux could prevent mis-segregation errors by centering kinetochores into metaphase plate, three approaches were used. KIF18A depletion led to faster k-fibers flux, longer antiparallel overlaps, and kinetochores were misaligned (Risteski et al., 2022, 2024). The mis-segregation errors were rescued by low-dose taxol treatment or co-depletion of HAUS8 or Nuclear Mitotic Apparatus protein (NuMA) in KIF18A depleted cells. Taxol stabilizes microtubules dynamics, HAUS8 depletion rescues chromosome misalignment, and NuMA depletion regulates the poleward flux of k-fibers. The treatments rescued errors in KIF18A depleted cells by shortening the antiparallel overlaps, slowing down the flux and the growth rate of kinetochore microtubules, thereby improving alignment, rather than by slowing microtubule growth in general (Risteski et al., 2024).

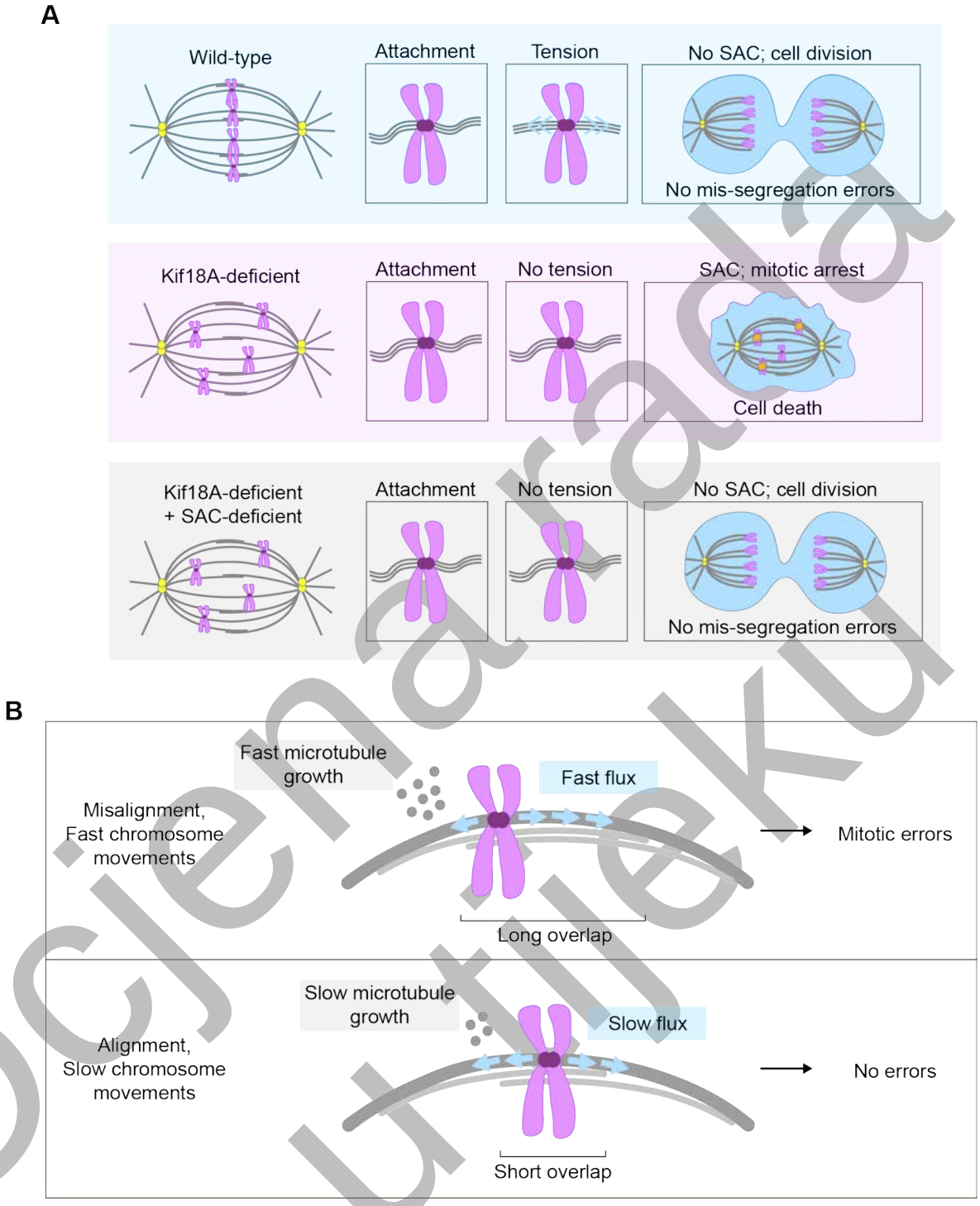

Figure 8. Caption on the following page.

Figure 8. Loss of KIF18A activates the SAC response. A) KIF18A reduces chromosomes oscillations when they are properly aligned in metaphase, stabilizes kinetochore-microtubule attachments, and has a role in tension generation. Chromosomes are segregated without errors (upper panel). KIF18A-deficient cells have increased oscillatory movements, resulting in tension defects and SAC activation, which ultimately leads to mitotic arrest and cell death (middle panel). SAC deficiency rescues the lethal effect caused by KIF18A loss (lower panel). Adapted from (Janssen et al., 2018). **B)** Misaligned kinetochores have a longer and shorter k-fiber. Longer k-fiber has a faster flux, while shorter k-fiber has a slower flux, and microtubule growth is increased. Overlap between bridging fiber is longer. Misalignment will result in mis-segregation errors in anaphase (upper panel). When sister kinetochores are properly aligned sister k-fibers are the same length. They have slow flux, and slow microtubule growth. Cell will divide without errors in anaphase (lower panel). Adapted from (Risteski et al., 2022, 2024).

1.9. Hallmarks of cancer

In multicellular organisms, homeostasis depends on the communication and collaboration of all cells, that are divided in tissues and organs, depending on the complexity of organism. Extracellular signals will give the information to each cell if it is supposed to grow, divide, differentiate, rest, or undergo apoptosis or cell death. When homeostasis is disturbed, a single cell may gain a selective advantage and starts to grow and divide more rapidly than the neighboring cells, which can lead to the formation of cancer cells. In other words, cancer cells are the ones that can grow and reproduce without control, and they invade and colonize other tissues. These cells can form a tumor or neoplasm, which is considered malignant when it can invade surrounding tissues. Tumor cells can separate from the primary tumor, invade other tissues, and form secondary tumors called metastases (Alberts et al., 2002).

Over the years the field of cancer research significantly expanded, and many characteristics of cancers have been described, and new ones are being found with the advancement of science. The principles that describe genotypic and phenotypic variabilities of cancers are called hallmarks of cancer (Figure 9). The hallmarks of cancer comprise of genome instability and mutations, cell death resistance and replicative immortality, deregulation of cellular metabolism, altered proliferative signaling, evading growth suppressors, avoiding immune destruction, tumor-promoting inflammation, invasion and metastasis and vascularization. Recently, additional enabling characteristics of tumors have been added to this list, such as phenotypic plasticity, non-mutational epigenetic reprogramming, a polymorphic microbiome and the role of senescent cells (Hanahan, 2022; Milane, 2022).

This work focuses on tetraploidy, as a part of genome instability. Other focus of this thesis is a specific three-dimensional (3D) architecture and microenvironment of mitotic cells in the tumors.

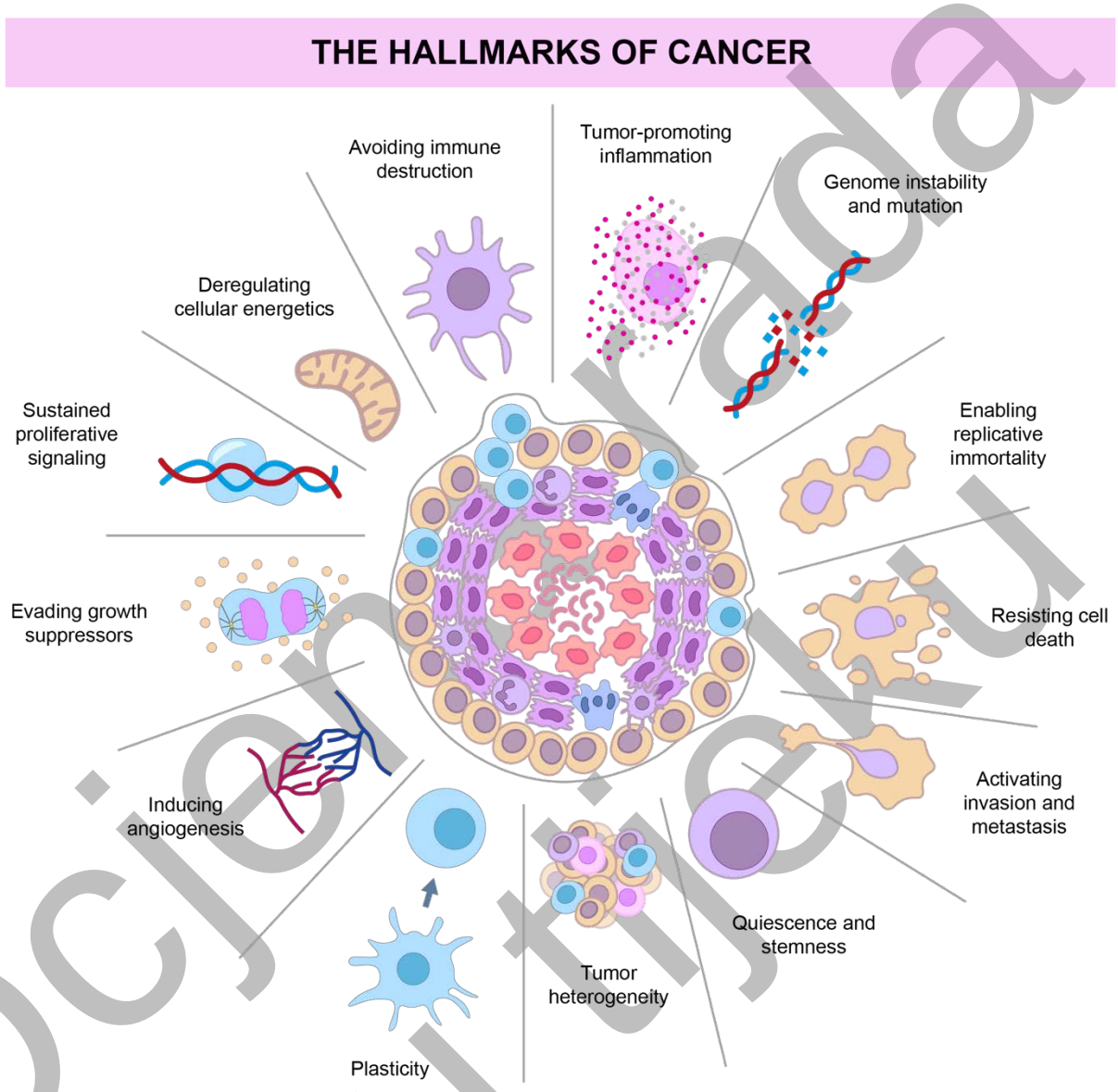

Figure 9. The hallmarks of cancer. The hallmarks of cancer represent the common set of traits or features that are acquired during tumorigenesis. Adapted from (Milane, 2022).

1.10. The connection between aneuploidy, polyploidy, and chromosomal instability

Genome instability refers to genetic alterations in cell that are often passed on to daughter cells during division. In small amounts it can promote diversity and evolution of organisms, but it is also frequently associated with pathological conditions, and it is classified as a hallmark of cancer. It can occur because of replication errors and DNA damage, or because of chromosome rearrangements, and these events are classified as micro- and minisatellite instability (Aguilera & Gómez-González, 2008).

Another form of genome instability is chromosomal instability (CIN), that occurs because of changes in chromosome number (Aguilera & Gómez-González, 2008). In other words, CIN is defined as a constantly elevated rate of chromosome gains and losses. It is often found in solid tumors, contributes to tumor heterogeneity, and is associated with poor patient prognosis (Burrell et al., 2013; Thompson et al., 2010).

Based on chromosome number, which depends on the success of chromosome segregation during mitosis, cells can be classified into three categories: euploid, aneuploid and polyploid. Cells that inherit two copies of each chromosome are euploid, representing a normal, successful division (Alberts et al., 2002). Cells with variations in chromosome numbers, due to segregation errors in mitosis are aneuploid (Orr et al., 2015). It is important to emphasize that aneuploidy refers to the karyotype of cells, while CIN is a persistent mis-segregation of chromosomes (Thompson et al., 2010). Cells that have more than two sets of chromosomes are polyploid. The most common form of polyploidy in human cells is tetraploidy, where cells have four sets of chromosomes, although higher ploidy levels can also occur (Davoli & de Lange, 2011).

In some cases, polyploidy is important for normal development and differentiation. Placental cells, trophoblasts, can reach ploidy as high as 64N (Ullah et al., 2008). Megakaryocytes become polyploid during endomitosis (Ravid et al., 2002), and hepatocytes in adult humans can become tetraploid or octoploid due to cytokinesis failure (Watanabe et al., 1978). Polyploidy is often observed in tumor cells, whose karyotypes may range from hypodiploid to hypertetraploid, indicating the presence of both aneuploidy and polyploidy in tumors (Davoli & de Lange, 2011).

Because of polyploidy, cells can have an increased volume (Otto, 2007). A study in yeast showed that mRNA and protein abundance scale allometrically with ploidy, due to reduced rRNA and ribosomal proteins abundance. Tetraploids had only a threefold increase in protein abundance compared to isogenic haploids. Downregulation of ribosomal proteins was also observed in near-tetraploid cell lines derived from colon cancer cell line HCT116 and RPE1. The authors hypothesize that reduced translation is a cellular response to increased ploidy (Yahya et al., 2022).

Polyploidy in yeast has also been shown to alter spindle geometry. The length of anaphase spindle and the size of kinetochores remained unchanged, while the spindle pole body was larger. This imbalance can cause syntelic attachments, that can result in chromosome mis-segregation (Storchová et al., 2006). Recent work described how spindle adapts to varying genome sizes among the species to conserve its function. In polyploid cells, a greater number of chromosomes creates a stronger interchromosomal pushing forces, which results in longer metaphase plates and wider spindles (Gudlin et al., 2025).

1.11. Development and characteristics of tetraploid cells

There are a few different ways how polyploid cells can be generated. The first one is cell fusion, which can occur spontaneously in cell culture, during the development of skeletal muscles (Taylor, 2002), or it can be induced by viruses. Next, cells can undergo endoreplication, where DNA is replicated, but mitosis is skipped. This cycle where cell goes through S phase but doesn't proceed to mitosis can be repeated several times. The third mechanism is an abortive cell cycle which refers to multiple defects during the cell cycle, such as problems with DNA replication, the mitotic spindle, and separation of sister chromatids. In these cases, cells can go into mitotic arrest or apoptosis. When defects happen during cytokinesis, forming daughter cells often fail to divide resulting in cytokinesis failure (Storchova & Pellman, 2004).

Tetraploid cells can have different cell fates. They can arrest at the G1 tetraploidy checkpoint, which can be followed by senescence or apoptosis. The G1 tetraploidy checkpoint is mediated by p53 and pRb, that can inhibit the G1 to S transition by binding E2F, the main activator of genes regulating this transition (Kirsch-Volders et al., 2025).

1.12. Post-tetraploid cell lines in polyploidy research

A model for studying tetraploidy *in vitro* was developed. One of the main challenges during model development was that p53 activation often impairs further cell proliferation. Cells would either fail to divide or stop dividing after the first tetraploid division, which is frequently accompanied by numerous mis-segregation errors. Kuznetsova and colleagues successfully developed a model to study long-term effects of tetraploidy on a p53 proficient cell lines (Kuznetsova et al., 2015) (Figure 10). They used chromosomally stable, near diploid, non-polyposis cancer cell line HCT116 and the diploid retinal pigment epithelium cell line RPE1. Tetraploid cells were generated by inducing cytokinesis failure through inhibition of the actomyosin ring using the actin depolymerizing drug cytochalasin D. The treatment induced tetraploidization of approximately 60% of cells. After the treatment, cells were seeded as single cells and expanded for six weeks. Clones that had a DNA content near tetraploid were selected. Established clones were HCT116 post-tetraploid (HPT) and RPE1 post-tetraploid (RPT) (Kuznetsova et al., 2015).

In this thesis the focus will be on two post-tetraploid (PT) RPE1 clones – RPT1 and RPT3, that were used to conduct a part of this research. Characterization of RPT1 and RPT3 revealed some interesting findings. PT clones had a slight increase in mitotic duration and a bit slower proliferation than the parental cell line, and they have a variability in chromosome number. The parental RPE1 cell line has 45 to 46 chromosomes with a modal number of 46. While it would be expected that PT clones have double the chromosome number, their chromosome counts varied between cells. The RPT1 clone has a range of 53-112 chromosomes and the RPT3 clone has a range of 38-95, with a modal number of 80 (Kuznetsova et al., 2015). This variability indicates that, after tetraploidization, cells undergo chromosome gains and losses in subsequent mitoses, which can lead to CIN (Storchova & Pellman, 2004).

Furthermore, RPT3 exhibited CIN, while RPT1 didn't show significant changes compared to the parental line. Differences in karyotypic heterogeneity between PT clones and CIN were induced by tetraploidization since such variability was not observed in the parental lines even after multiple generations. RPT3 showed a higher percentage of mitotic errors, but neither one of the clones didn't have an increase in centrosome number, suggesting that mitotic errors didn't come from multipolar divisions (Kuznetsova et al., 2015).

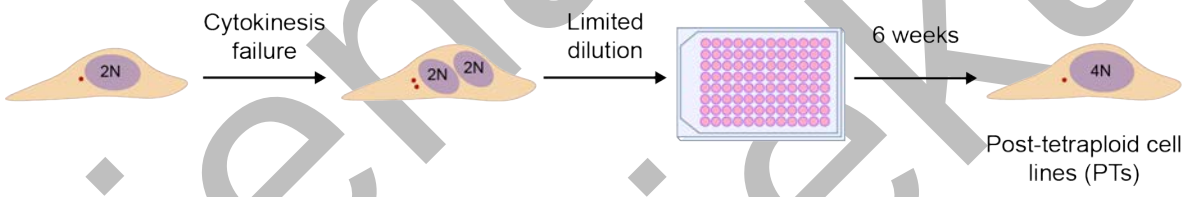

Figure 10. Generation of post-tetraploid cell lines. Tetraploidy is generated in diploid cells by inducing cytokinesis failure. Cells are seeded as single clones, and after six weeks stable, post-tetraploid clones are isolated. Adapted from (Kuznetsova et al., 2015).

1.13. Tetraploid non-tumor precursor cells

Research on cancer hallmarks such as CIN and tetraploidy has been extensive, yet numerous uncertainties persist regarding the mechanisms of mitotic events and their role in tumorigenesis. Multiple models have been proposed to explain the onset of tumorigenesis. These models focused on gene mutations, genetic instability, environmental factors, epigenetic and tissue organization. Also, there were models that combined these factors (Kirsch-Volders et al., 2024).

Initially, it was believed that the accumulation of mutations in oncogenes and tumor suppressor genes drives tumorigenesis, and increased aneuploidy was considered a consequence of tumor development. However, there were multiple evidence that would support the opposite mechanism, in which tetraploid non-tumor precursor cells can trigger tumorigenesis (Davoli & de Lange, 2011; Kirsch-Volders et al., 2024, 2025; Storchova & Kuffer, 2008; Storchova & Pellman, 2004), a hypothesis explored further in this work (Figure 11).

Studies on breast and colorectal cancer showed that tumor karyotypes are highly heterogeneous. Although tumors accumulate many mutations, only a subset appears to contribute directly to tumorigenesis (Sjöblom et al., 2006). Analysis of somatic copy-number alterations showed that around 37% of cancer undergone whole genome duplication (WGD) at some point in tumorigenesis (Quinton et al., 2021; Zack et al., 2013). Tetraploid cells are often found in early stages of tumor development, and it would be difficult to generate such a high number of chromosomes through consecutive aneuploidies (Storchova & Kuffer, 2008). In addition, tumor karyotypes can vary between hypodiploid to hypertetraploid. This diversity can be achieved through tetraploidization followed with aneuploidies and potentially elevated CIN rates (Ganem et al., 2009; Kuznetsova et al., 2015; Storchova & Pellman, 2004).

Fujiwara and colleagues gave direct evidence that supports the hypothesis that tetraploid cells can evolve into tumorigenic aneuploid cells (Fujiwara et al., 2005). Through cytokinesis failure they created tetraploid $p53^{-/-}$ mouse mammary epithelial cells that initiate tumor formation when transplanted into nude mice, whereas the isogenic diploid cells did not initiate tumor formation. Cells in newly formed tumors were near-tetraploid and had increased rates of mis-segregation errors (Fujiwara et al., 2005).

An increase in aneuploidy is also observed in a study by comparing high numbers of clinical tumor samples that had undergone WGD (WGD+) and tumors that did not go through WGD (WGD-). WGD+ tumors showed higher CIN rates and, correspondingly, more frequent aneuploidy, contributing to increased heterogeneity. These tumors also had more chromosomal losses, suggesting that genome doubling may act as a “buffer” against the harmful effects of DNA loss. Furthermore, WGD+ tumors had a greater number of whole-chromosome aneuploidies than the WGD- tumors (Prasad & Ben-David, 2023).

The hypothesis that tumorigenesis begins from a tetraploid intermediate is also supported by the fact that tumor cells frequently have multiple centrosomes (Storchova & Kuffer, 2008), which is observed in breast (Lingle et al., 1998), pancreatic (N. Sato et al., 1999), prostate (Pihan et al., 2001), lung and colon cancer (Pihan et al., 1998). It is important to emphasize that supernumerary centrosome can also arise from abnormal centriole biogenesis due to centriole overduplication and de novo assembly (Mittal et al., 2021), meaning they are not always the result of tetraploidization.

Baudoin and colleagues studied populations of newly formed tetraploid colorectal cancer cell line DLD1 and RPE1 cell lines, generated through cytokinesis failure (Baudoin et al., 2020). They observed that the first few divisions following tetraploidization were often multipolar, but highly aneuploid cells resulting from these divisions quickly disappeared from the population (Baudoin et al., 2020). Consequently, the rate of multipolar divisions declined over time. Also, cells with supernumerary centrosomes quickly disappeared from the population. This decline was attributed to asymmetric centrosome clustering, although some cells exhibited symmetric clustering and proceeded with bipolar division (Baudoin et al., 2020). Some WGD+ tumor cells also carry a mutation in PPP2R1A gene, which promotes centrosome clustering (Quinton et al., 2021). Multiple centrosomes that don't cluster during mitosis will cause the formation of multipolar spindles. In multipolar spindles many merotelic attachments are being formed which increases the probability of lagging chromosomes and the probability of unsuccessful mitosis (Ganem et al., 2009).

The evidence presented here Indicates that polyploidy is frequently followed with aneuploidy and elevated CIN rates. Spontaneously occurring tetraploid cells that may initiate tumorigenesis are defined as transient intermediates between diploidy and aneuploidy (Davoli & de Lange, 2011; Kirsch-Volders et al., 2024, 2025; Storchova & Kuffer, 2008; Storchova & Pellman, 2004).

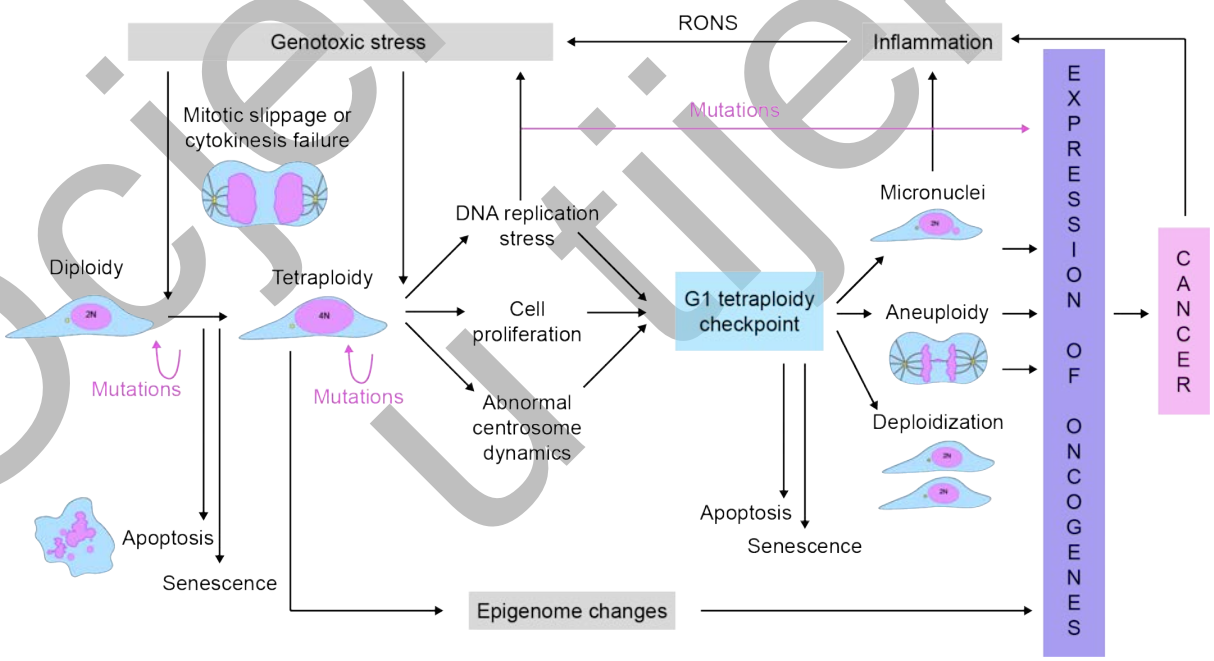

Figure 11. Caption on the following page.

Figure 11. Tetraploid non-tumor precursor cell model. Stress-induced polyploidization usually leads to p53 stabilization and cell cycle arrest, followed by senescence or apoptosis. If tetraploid cells escape the G1-tetraploidy checkpoint it can lead to uncontrolled proliferation that results in micronuclei formation, aneuploidy and diploidization. Micronuclei induce inflammation which can lead to additional tetraploidization. The combined effect of genetic and epigenetic changes leads to oncogene expression and to the onset of tumorigenesis. Polyploid cells represent an intermediate state between diploids and cancer cells. Adapted from (Kirsch-Volders et al., 2024).

1.14. Highly aneuploid cells show increased sensitivity to KIF18A depletion

Despite ongoing advancements in the development of anti-cancer drugs, the mission to successfully battle cancer is ongoing. Some of these drugs specifically target mitotic cells, as tumor cells are highly proliferative, but they have not proven to be the most successful, as they also affect healthy cells. New strategies for treating tumors are being developed with a focus on selectively targeting aneuploid tumor cells (Ben-David & Amon, 2020).

Several studies have analyzed the differences between diploid and polyploid cancer and non-cancer cell lines. The cell lines were also compared based on their CIN levels. Cohen-Sharir and colleagues compared around 1000 human cancer cell lines and categorized them based on their aneuploidy levels (Cohen-Sharir et al., 2021). They identified genes that are essential for highly aneuploid cancer cells. Those were SAC components MAD2 and BUB1B (Cohen-Sharir et al., 2021). This was also confirmed in another research, where it was shown that depletion of these genes increased mis-segregation errors (Quinton et al., 2021). Short-term effect of SAC inhibition was bigger on diploid cells, with low aneuploidy rates, but highly aneuploid cells had a greater long-term effect. These cells more rapidly escaped mitotic arrest after SAC was inhibited, but their divisions were often multipolar, followed with mis-segregation errors and micronuclei formation. This led to the accumulation of even more aneuploid and highly sensitive cells, and ultimately to increased cell death (Cohen-Sharir et al., 2021).

Cells with increased CIN and WGD+ cells also showed heightened sensitivity to KIF18A perturbations, which correlated with aneuploidy levels (Cohen-Sharir et al., 2021; Quinton et al., 2021). Both HPT and RPT cells had altered spindle geometry and decreased kinetochore-microtubule stability following siRNA-mediated KIF18A knockdown, compared to their parental cell lines. HPT cells also demonstrated a higher incidence of multipolar divisions. Interestingly, overexpression of KIF18A was able to restore their response to SAC inhibition (Cohen-Sharir et al., 2021). In WGD+ cells, mis-segregation and mitotic delay can also be triggered by altered spindle architecture. KIF18A depletion further increased spindle length and chromosome oscillation amplitude in tetraploids compared to diploids. Hyperoscillating

chromosomes often lose the attachments with microtubules, which activates SAC and causes prolonged mitosis. Chromosomes that do not have the proper attachments can also mis-segregate in anaphase (Quinton et al., 2021).

Marquis and colleagues further tested the effect that KIF1A KD has on cells with increased CIN (Marquis et al., 2021). CIN cells are characterized by elevated microtubule polymerization rates and increased turnover at kinetochore-microtubule attachments (Bakhoum et al., 2009). KIF18A reduces microtubule polymerization in CIN cells, which explains why it is essential for CIN cell viability. The loss of KIF18A leads to prolonged mitotic arrest and multipolar spindle formation (Cohen-Sharir et al., 2021; Marquis et al., 2021; Quinton et al., 2021).

To determine the origin of multipolarity, they examined centrosomes and spindle poles. In MDA-MB-231 cells, KIF18A knockdown did not cause centrosome amplification, as most cells retained four centrioles. However, around 60% of multipolar KIF18A KD cells exhibited γ-tubulin-containing MTOCs without centrioles, which was also confirmed in HT29 cells. Also, cells entered mitosis as bipolar, and during mitosis spindles became multipolar. These data suggest that KIF18A KD leads to multipolar spindles formation by inducing PCM fragmentation in CIN cells. They proposed a model in which the combined effect of increased microtubule growth in CIN cells and the absence of KIF18A-mediated suppression creates imbalanced forces within the spindle, leading to weakened centrosome integrity and eventual fragmentation (Marquis et al., 2021) (Figure 12).

Consistent with Cohen-Sharir's findings, KIF18A knockdown also induced mis-segregation and micronuclei formation in a subset of CIN cells (Cohen-Sharir et al., 2021; Marquis et al., 2021). Paclitaxel gave the similar phenotype as KIF18A KD, but its mechanism of action is opposite to KIF18A KD, as it increases microtubule dynamics. This suggests that any changes in microtubule dynamics in CIN cells can compromise spindle integrity. Also, it was shown that CIN cells show only dependency to KIF18A, but not to other kinesins, which makes it a suitable target to reduce cancer cells connected with CIN or aneuploidy (Marquis et al., 2021).

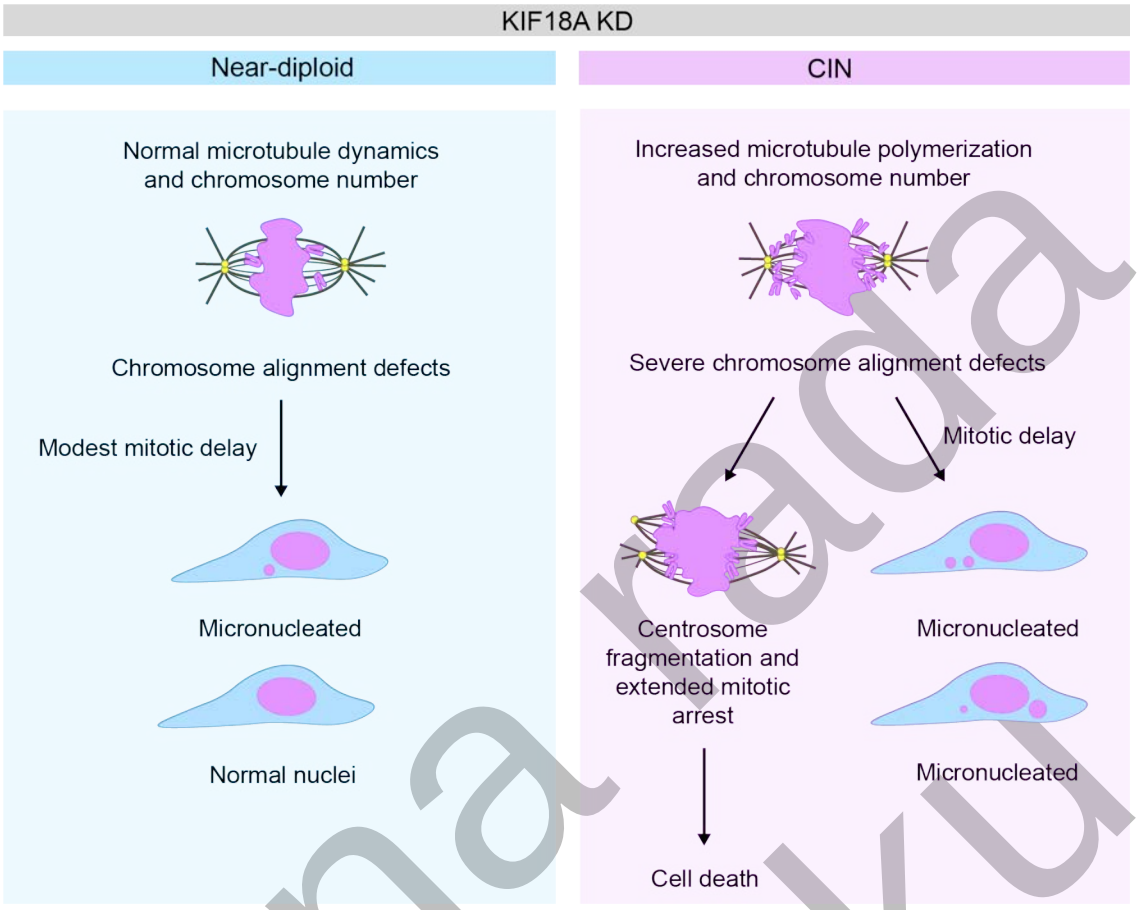

Figure 12. CIN cells show increased sensitivity to KIF18A loss. In near-diploid cells with low CIN levels, KIF18A loss causes minor chromosome alignment defects and prolongation of mitosis. The percentage of micronuclei formation is low (left panel). Cells with high CIN exhibit severe chromosome alignment defects due to increased microtubule polymerization and heightened chromosome number. A fraction of cells has centrosomes fragmentation and mitotic arrest that result in cell death, while other group has a mitotic delay and an increased frequency of micronuclei formation (right panel). Adapted from (Marquis et al., 2021).

1.15. KIF18A inhibitor as a potential anti-tumor drug

Previous findings demonstrate that KIF18A is essential for the survival of highly aneuploid cells (Cohen-Sharir et al., 2021; Marquis et al., 2021; Quinton et al., 2021), making it an excellent target for anti-tumor drugs that affect only mitotic tumor cells. This has encouraged the development of small-molecule KIF18A inhibitors. Several KIF18A inhibitors have been described; AM-0277, AM-1882, AM-5308, AM-9022 (Gliech et al., 2024; Payton et al., 2024), and Sovilnesib AM-650 (*Volastra - Short Circuiting Cancer's Chaos*, 2025), inhibitor that was used in this study.

These inhibitors act on the motor domain of KIF18A and prevent its “walking” along microtubules. The inhibitors have a lower risk of neurotoxicity compared to agents like paclitaxel, as they do not directly affect microtubule dynamics. Since the inhibited protein can no longer move along microtubules but still binds to them, it accumulates at the spindle poles due to microtubule poleward flux, as demonstrated in live-cell imaging of HeLa cells (Payton et al., 2024).

Payton and colleagues showed that protein inhibition has the same effect on the cells as depletion (Payton et al., 2024). CIN cell lines showed preferential sensitivity to inhibition of KIF18A, leading to SAC activation and prolonged mitosis, PCM fragmentation followed with multipolar spindle formation and apoptosis (Payton et al., 2024).

In a recent study, it was shown that some cell lines are more sensitive to KIF18A inhibition than others. Cell lines that were insensitive include HCT116, DLD1, RPE1, MCF10A, and MCF7, while sensitive cell lines include OVCAR-3, OVCAR-8, HeLa, HCC1806, and MDA-MB-157. The study demonstrated that in addition to SAC activation, APC/C also plays a role in sensitivity to KIF18A inhibition. KIF18A inhibition causes a modest increase in SAC signaling in all cell lines due to elevated chromosome misalignment. SAC signaling increases with ploidy level, and its intensity determines whether cells will proceed to anaphase. Sensitive cells may have weakened APC/C activity, which further prolongs mitotic delay (Gliech et al., 2024) (Figure 13).

In summary, persistent SAC signaling, which increases with ploidy levels, combined with weakened APC/C, which prevents the anaphase onset, drives sensitivity to KIF18A inhibition (Gliech et al., 2024). To support this model, it was shown that reducing SAC signaling decreases sensitivity to KIF18A inhibition (Gliech et al., 2024), and that MAD2 knockout increases cell viability after KIF18A depletion (Janssen et al., 2018). Similarly, increased basal APC/C activity reduces sensitivity to the inhibition (Gliech et al., 2024).

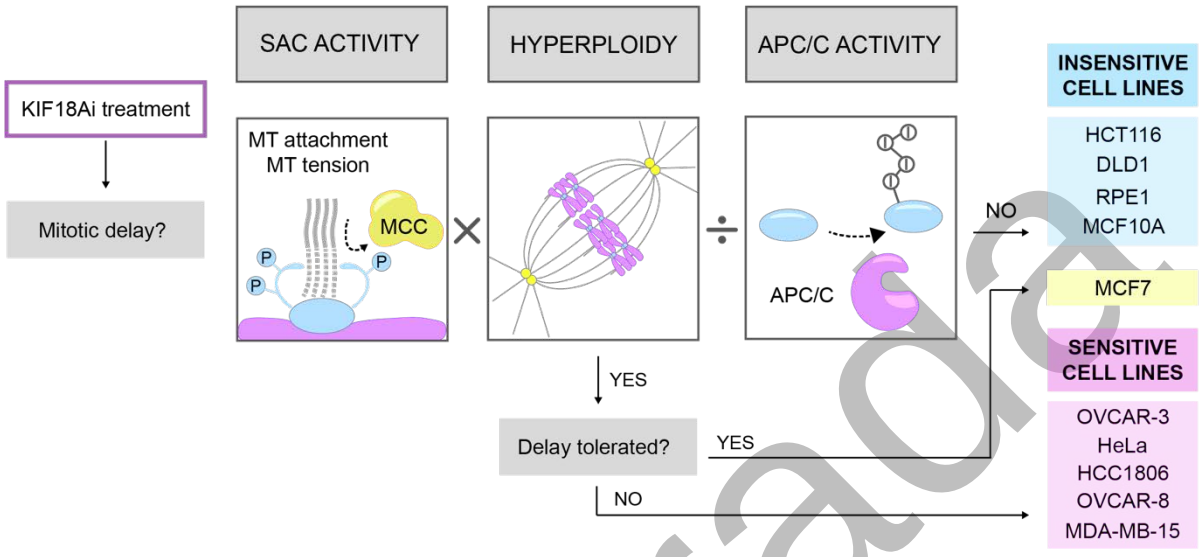

Figure 13. Factors that determine the sensitivity to KIF18A inhibition. Mitotic arrest after KIF18A inhibition depends on following factors: elevated SAC activity, ploidy levels and basal activity of the APC/C. The amount of elevated SAC activity increases with ploidy levels, while basal activity of the APC/C will reduce the sensitivity to inhibition. Insensitive cell lines go through a minor prolongation of mitosis, while sensitive cells do not tolerate mitotic delay. Adapted from (Gliech et al., 2024).

1.16. The emerging need for three-dimensional cell culture models

Numerous traits of both healthy and tumor cells have been unveiled through research in cell cultures, where cells typically adhere to a surface and grow in two dimensions (2D) as a monolayer. However, this research system neglects the structure and microenvironment complexity found within healthy tissues and tumors. To provide a more faithful representation of *in vivo* events, methods for cultivating cells in three-dimensional (3D) cultures have been developed (Langhans, 2018).

The development of anti-tumor drugs has highlighted the need for improved testing systems, as studies showing promising results in monolayers often failed in clinical trials. This has driven the emergence of various types of 3D cell cultures that revolutionized the fields of tumor biology, tissue engineering and developmental biology (Breslin & O'Driscoll, 2013; Desoize & Jardillier, 2000; Langhans, 2018). 3D cultures have also become a valuable tool for mitosis studies. Traditional monolayers often fail to capture the full complexity of mitosis as it occurs in the 3D environment of living tissues, because interactions of mitotic cell with its microenvironment and spatial constraint are not considered (Ćosić & Petelinec, 2024; Desoize & Jardillier, 2000).

1.17. Monolayers

Cells grown as monolayers are widely used model in cell biology, especially adherent cells, which easily attach to the surface of a culture flask or a petri dish. (Breslin & O'Driscoll, 2013). The surface is coated with ECM proteins, such as collagen or fibronectin, or with synthetic polymers, such as poly-L-lysine, which enable easy attachment (Hynes & Naba, 2012; Klimek & Ginalska, 2020; Langhans, 2018). This makes them the simplest and most convenient research model. They typically require low maintenance and allow fast production of big number of cells and experiment replicates. Monolayers are also more financially accessible in comparison with some types of 3D cultures and animal models.

Despite their practicality, cells grown in monolayers lack proper cell-cell interactions, tissue architecture and forces distribution, as well as molecule gradients (Figure 14A). Also, the production of extracellular matrix can differ between monolayers and tissues. Isolation from the tissue and transfer to a 2D environment alters both cell morphology and the mode of cell division (Kapałczyńska et al., 2018; Langhans, 2018; Pampaloni et al., 2007; A. G. Souza et al., 2018). In monolayers, cell polarity is artificial and imposed by the substrate. Cells adhere to the substrate through focal adhesions, while their upper side is exposed to the medium (Cukierman et al., 2001).

Monolayered cell cultures can be generated using either primary cells isolated directly from a donor, or established cell lines from bioresource centers such as the American Type Culture Collection (ATCC). Primary cells closely mimic the genetic features of the donor tissue but can be difficult to isolate and have a limited lifespan. In contrast, established cell lines are more uniform, which reduces the variability among replicates and experiments, and they can be cultured for extended period (Kapałczyńska et al., 2018).

1.18. 3D cell cultures

The first 3D cultures were developed by Boiron in 1968, marking the beginning of their role in cell culture research (Boiron et al., 1968). 3D cell cultures are *in vitro* systems that grow in three dimensions, aiming to mimic tissue morphology and functionality by simulating the tissue microenvironment (Ovsianikov et al., 2012; Taubenberger et al., 2019).

There are various types of 3D cell cultures. Based on the usage of scaffold or gels, 3D cultures can be scaffold-based, scaffold free in which case cells are cultured in the cell culture medium or cultured with hydrogels such as collagen and Matrigel that imitate ECM (Kyriakopoulou et al., 2023). Scaffold-based culturing methods produce more complex cultures, whereas scaffold-free methods allow cells to spontaneously form aggregates that vary in size and density, depending on cell number (Chen & Wang, 2020). Scaffold-free culturing methods include the hanging drop method, low adhesion plates, rotating bioreactors, and

magnetic cell levitation method (Chen & Wang, 2020; Kyriakopoulou et al., 2023; Lin & Chang, 2008; G. R. Souza et al., 2010). Next, cells within 3D cultures can be heterogeneous regarding to cell type, polarity, proliferation status and availability of nutrients (Kyriakopoulou et al., 2023) (Figure 14B). An interesting type of 3D cultures are organoids, miniaturized and simplified versions of organs, designed to mimic key structural and functional aspects. These structures originate from different type of stem cells that will self-organize *in vitro* into the different cell types comprising an organ (Clevers, 2016; Eiraku & Sasai, 2012; M. A. Lancaster & Knoblich, 2014). Organoids of various organs including brain, liver, kidneys, lungs, small intestine, colon, etc. have been developed (Cherry & Daley, 2012; Chin et al., 2014; Clevers, 2016; T. Sato et al., 2009). For example, intestinal organoids can be generated from Lgr5+ stem cells, showing key features of the native intestine, such as villus-like structures, functional crypts, and a central lumen (T. Sato et al., 2009) (Figure 14C). Organoids have an important role in personalized medicine since the establishment of patient-derived tumor organoids that can serve as a personalized models for investigating individual treatment responses and developing therapeutic strategies (Clevers, 2016; M. A. Lancaster & Knoblich, 2014; T. Sato et al., 2011).

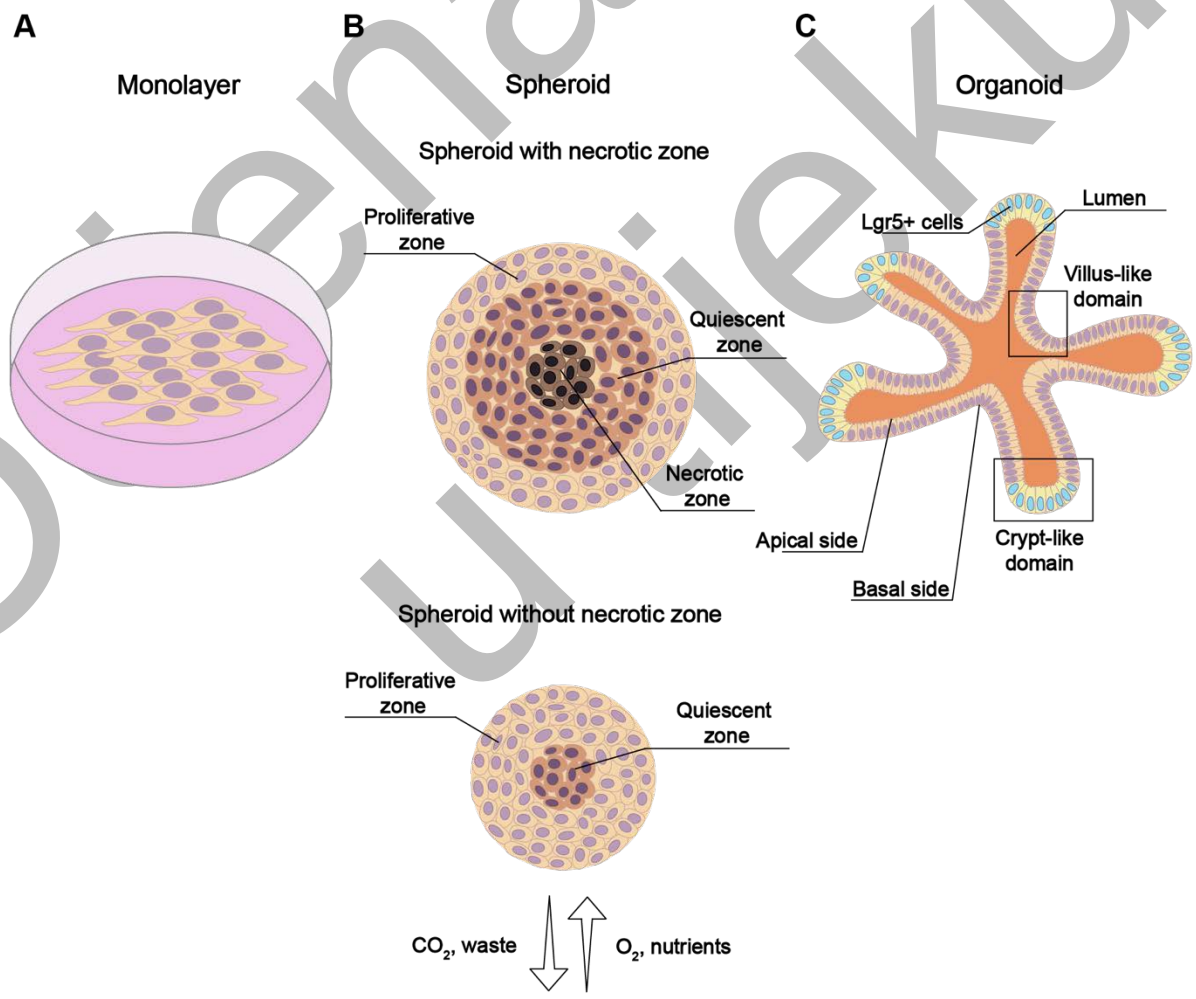

Figure 14. Caption on the following page.

Figure 14. Different types of cell cultures. A) Two-dimensional cell culture where cells grow as a monolayer and adhere to the surface. Cells are homogeneous with the same availability of nutrients and oxygen. **B)** Multicellular spheroid where cells grow in three dimensions. Spheroids have a proliferative, quiescent, and necrotic zone. Smaller spheroids may lack a necrotic zone. Cells in spheroids are heterogeneous based on their proliferation status and nutrients gradient. **C)** Three-dimensional architecture of a small intestine organoid. Organoids have a tissue structure, including a villus-like domain with differentiated cells, a crypt-like domain with dividing stem cells, and a central lumen. Cell polarity is defined by an apical side, facing the lumen, basal side, facing the basement membrane, and lateral sides that are in contact with neighboring cells. Taken from (Ćosić & Petelinec, 2024).

1.19. Multicellular Spheroids

Multicellular spheroids are a widely used type of 3D cultures, especially as a model for solid tumors (Hirschhaeuser et al., 2010; Molla et al., 2017; Nunes et al., 2019). Spheroids can be generated using scaffold free techniques such as hanging drop, low adhesion plates and magnetic cell levitation (Chen & Wang, 2020; Haisler et al., 2013; Kyriakopoulou et al., 2023; Lin & Chang, 2008; G. R. Souza et al., 2010).

Spheroids are often formed from a single cell line but display heterogeneous cellular arrangements. As in tumors, spheroids can be divided into several layers that consist of proliferative cells on the periphery, quiescent cells in the middle, and necrotic cells at the core (Desoize & Jardillier, 2000; Hirschhaeuser et al., 2010; Laurent et al., 2013; Lin & Chang, 2008; Sutherland, 1988). The thickness of these layers depends on the spheroid's size (G. R. Souza et al., 2010), various treatments, and mechanical stress (Dolega et al., 2017). Smaller spheroids may lack a necrotic core, with proliferative cells evenly distributed throughout the spheroid (Laurent et al., 2013).

Cells in spheroids can have unequal availability of nutrients and metabolic gases. They have a gradient of availability with outer layers having better access to oxygen, glucose, amino acids, and other medium components, while in the inner layers the availability is lower. Lactate and other metabolites can accumulate in inner layers leading to lower pH (Pampaloni et al., 2007; Sutherland, 1988; Trédan et al., 2007). These conditions can cause hypoxic regions and necrosis in the spheroid core. As such, spheroids are excellent models for studying micrometastases and non-vascularized tumor regions (Sutherland, 1988).

It is important to note that in these types of 3D cultures, only tumor cells or non-tumor cells with inactive p53 protein can divide. Non-tumor cells experience growth arrest due to contact inhibition, which is triggered by cell-cell interactions, and it also happens in monolayers when cells become too confluent. The p53 tumor suppressor protein promotes contact inhibition in response to cell culture density (Meerson et al., 2004).

1.20. Magnetic cell levitation method

One of the methods to generate multicellular spheroids is a scaffold-free, magnetic cell levitation method, that relies on magnetic forces and cell levitation in the medium. Cells are first grown as monolayers and incubated with a nanoparticle solution that has magnetic properties, consisting of iron oxide, gold nanoparticles and hydrogel. Magnetic nanoparticles diffuse into the cell cytoplasm or remain attached to membrane proteins. When a magnet is placed above the cells in suspension, they begin to float in the media solution meniscus, gradually forming aggregates and eventually multicellular spheroids (G. R. Souza et al., 2010) (Figure 15).

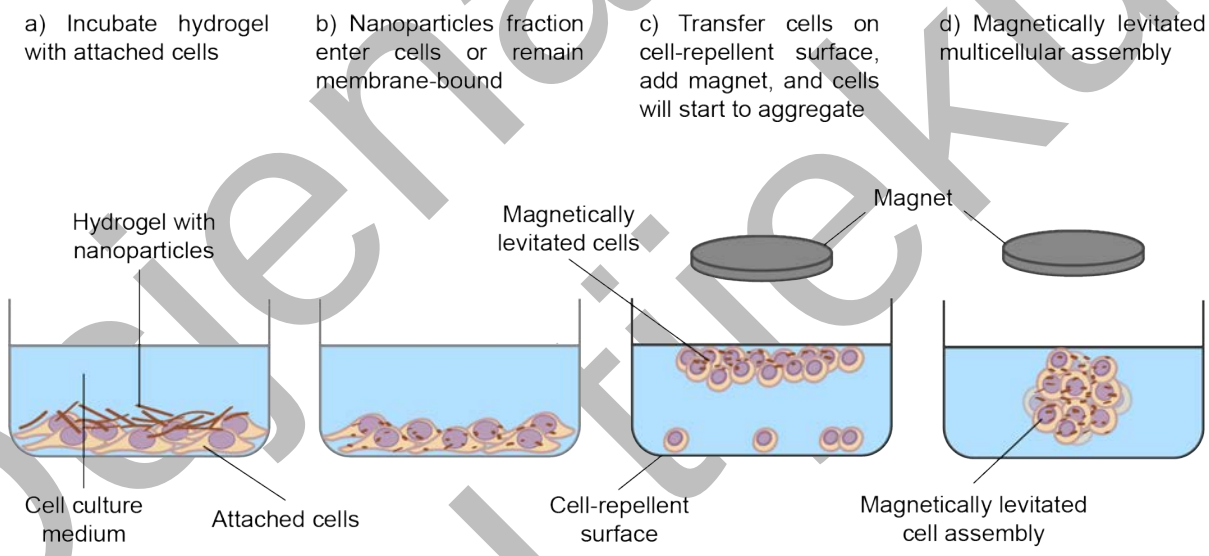

Figure 15. Magnetic cell levitation method. Cells cultured as monolayers are incubated with magnetic nanoparticles, which enter the cells or remain attached to the cell membrane. Cells in suspension are exposed to the magnet. Under the influence of magnetic forces cells start to aggregate and eventually form spheroids. Adapted from (G. R. Souza et al., 2010).

The efficacy of this method was studied by comparing the localization of N-cadherin in human glioblastoma cells cultured as monolayers, spheroids and human tumor xenografts implanted in mice. N-cadherin was localized in the cytoplasm and nucleus in monolayers, while in spheroids and xenografts it was localized in the cytoplasm, on the cell membrane and at adherens junctions (G. R. Souza et al., 2010). It plays a role in the formation of adherens junctions where its interactions with ECM components fibronectin, integrins and tensin are important for junction formation (Lefort et al., 2011), which indicates that components of the ECM are present in spheroids. Another study confirmed that N-cadherin is localized on the cell membrane in spheroids of A549 cells. Additionally, E-cadherin, mucin and cytokeratin-19 were present in spheroids, which implies that cells retained their function and phenotype characteristic for the cell line (Haisler et al., 2013).

An advantage of this method is that cells can form ECM components in the desired composition and quantities. 3D cultures generated with hydrogels have ECM of a predetermined composition, which can degrade over time, and the exact composition and compound concentrations of commercially available hydrogels, such as Matrigel, are often not disclosed (Kyriakopoulou et al., 2023; G. R. Souza et al., 2010). Another advantage is that spheroid size and shape can be regulated by the size and shape of the magnet, whereas in other methods for producing multicellular spheroids, only size can be regulated by the number of cells. It was shown that magnetic nanoparticles are not toxic, do not affect proliferation and cause the inflammatory response (G. R. Souza et al., 2010; Tse et al., 2012). Similar spheroids can be produced using hanging drop method and low adhesion plates, which are more affordable compared to magnetic cell levitation. In this work, the magnetic cell levitation method will be used to generate spheroids of different cell lines.

1.21. Key differences between 2D and 3D cell culture models

Multiple differences between monolayers and 3D cell cultures have been described. The most significant differences are in culture architecture and cell morphology, production of ECM components, cell proliferation and gene expression. All these differences can directly or indirectly impact division of cells in these systems.

As already mentioned, cells in spheroids are heterogeneous, they have both dividing and non-dividing cells, distributed in different parts of the spheroid. In contrast, monolayers are homogeneous, composed mostly of proliferative cells. Opposite to spheroids, cells in monolayers have unlimited access to nutrients and oxygen from the medium, and there is no accumulation of metabolic gasses and waste in certain areas. In spheroids, due to their tumor-like architecture, the distribution of nutrients and metabolic gases can be uneven (Chen & Wang, 2020; Pampaloni et al., 2007).

It Is important to highlight some key differences between organoids and 2D cultures. Unlike spheroids, organoids have a rigid tissue architecture with well-defined cell polarity, like in a healthy tissue. Organoids are composed of various cell types, including stem cells, which are difficult to maintain in monolayers. Moreover, a mixture of growth factors and supplements is required to sustain organoids in cell culture, which can affect the research outcomes and impact cell division (Clevers, 2013, 2016; T. Sato et al., 2009).

Spheroids show lower proliferation rates compared to monolayers. Proliferation rates in spheroids more closely resemble those in tumors than monolayers (Chignola et al., 2000). Lower cell proliferation has been shown in multiple cell lines when cultured in 3D compared to monolayers, such as prostate (Adcock et al., 2015; A. G. Souza et al., 2018), colorectal (Luca et al., 2013), osteosarcoma and breast cancer cell lines (Fallica et al., 2012). Proliferation in spheroids is influenced by the composition and quantity of ECM produced by the cells. For example, glioma cell lines differ in production of hyaluronic acid. Cell lines that produced more hyaluronic acid had higher proliferation rates, although this was not correlated with the overall extent of the ECM (Glimelius et al., 1988).

2D and 3D cell cultures exhibit different levels of gene expression. These differences are variable, and varying expression levels were observed in three different prostate cancer cell lines. For example, in PC-3 and LNCaP spheroids, ANXA1 and CD44 were upregulated, while in DU145 spheroids, they were downregulated (A. G. Souza et al., 2018). This is interesting because ANXA1 plays a role in apoptosis and proliferation (Shao et al., 2019), and CD44 is involved in cell-cell interactions and adhesion (Senbanjo & Chellaiah, 2017). Proteomic analysis of 2D and 3D neuroblastoma cultures showed overexpression of proteins related to metabolism, stress response, cytoskeleton components such as tubulin and actin, which are crucial for cell-cell interactions (Kumar et al., 2008). The described genes and proteins that are differently regulated in monolayers and 3D cultures are all involved in cell division, implying that findings from mitosis research conducted on 2D cultures should not be directly extrapolated to events in tissues without further research.

1.22. The role of extracellular matrix in 3D cultures

The ECM consists of different matrix proteins (e.g., collagens), glycoproteins (e.g., fibronectin), proteoglycans (e.g., heparan sulfate), cytokines and chemokines. It is a scaffold that provides a physical support to tissues and regulates cell proliferation. The ECM affects cell adhesion and migration, and it enables cell communication (Aumailley & Gayraud, 1998; Hohenester & Engel, 2002; Langhans, 2018; Streuli, 1999). One of the key differences between 2D and 3D cultures is the difference between ECM components and their localization (Frantz et al., 2010; Glimelius et al., 1988; Kleinman et al., 2003; Langhans, 2018).

Integrins are receptors for ECM components that have an important role in forming cell adhesions. These adhesions can differ between 2D and 3D cultures where they are called 3D-matrix adhesions (Yamada et al., 2003). Integrins can also influence tumor progression. The HMT-3522 healthy cells grow in acini and assemble the basement membrane, while tumor cells lose the tissue structure and grow in irregular colonies. Perturbations of integrins caused reversions from normal to tumor phenotype and vice versa (Weaver et al., 1997). It was also shown that depletion of β1 integrin in the PC3 prostate cancer cell lines impaired their 3D growth in Matrigel (Howe & Addison, 2012; Schooley et al., 2012).

Cells in monolayers showed increased drug sensitivity compared to spheroids that produce ECM components (Bulysheva et al., 2013; Desoize & Jardillier, 2000; Dhiman et al., 2005; Fayad et al., 2011; Langhans, 2018; Molla et al., 2017; A. G. Souza et al., 2018). Increased drug resistance is also related to a smaller fraction of proliferative cells, as drugs often affect dividing cells. Drug distribution in spheroids can be different because diffusion into the inner parts of spheroids is obstructed by tightly packed cells and ECM. In some cases, outer layers may be resistant to drugs, while inner layers, with fewer ECM components, may be more sensitive (Muranen et al., 2012; A. G. Souza et al., 2018).

1.23. Cell division in multicellular spheroids

Monolayers have served as a valuable model for mitosis research, especially in microscopy-based studies, due to their 2D growth, which is suitable for imaging. However, they often fail to capture the complexity of the 3D tissue environment (Ćosić & Petelinec, 2024; Desoize & Jardillier, 2000). A few studies have provided new insights into the challenges mitotic cells face in multicellular spheroids.

Molla and colleagues (2017) observed that mitoses in spheroids of three tumor cell lines, murine p53WT TSA/pc, HEK293, and HeLa, was often unsuccessful (Molla et al., 2017). The number of binucleated cells, resulting from a cytokinesis failure, increased by 20%. There were no problems with SAC signaling, so cells could proceed to anaphase. However, problems occurred in metaphase, where the metaphase plate rotated in all cells, leading to incomplete chromosome segregation. Additionally, more lagging chromosomes were observed in anaphase compared to monolayers. As a control, spheroids were allowed to spread on the surface overnight, after which cells divided normally. The authors hypothesize that contact with neighboring cells or cytoskeletal disruption might destabilize division axis, causing cytokinesis failure (Molla et al., 2017).

Few studies have addressed the impact of confinement and mechanical stress on mitotic cells in tumor spheroids, which is relevant because tumor microenvironment can apply compressive stress on a tumor, limiting its growth (Taubenberger et al., 2019). In HCT116 spheroids, mitotic cells were sensitive to mechanical stress generated by polydimethylsiloxane (PDMS) microdevice, which restricted spheroid growth (Figure 16). Spheroids adopted a rod-like shape, and showed altered distribution of proliferative cells, which were distributed throughout the whole spheroid (Desmaison, Frongia, et al., 2013; Desmaison, Lorenzo, et al., 2013). In contrast, proliferative cells in freely growing spheroids were mainly localized in the outer layer, as expected (Laurent et al., 2013; Molla et al., 2017). In the confined spheroids, mitotic cells accumulated in the inner regions due to mitotic arrest (Desmaison, Frongia, et al., 2013).

Also, bipolar spindle formation was impaired. Only 63% of mitotic cells formed bipolar spindles in confined spheroids compared to 89% in freely growing ones. Additionally, 22% of the spindles were monopolar (Desmaison, Frongia, et al., 2013), which can be caused by problems with centrosome separation or duplication (Tillement et al., 2009). As cell rounding was not impaired, mechanical stress is most likely the cause of mitotic arrest in confined spheroids (Desmaison, Frongia, et al., 2013). On the other hand, in the CT26 cell line, an increase in mechanical force led to a reduction in the number of proliferative cells, which were increasingly restricted to a thinner outer layer (Dolega et al., 2017). These contradictory findings may be explained by differences in cell lines, stress-induction methods, and exposure durations. Possibly, CT26 cells entered a quiescent state under mechanical stress, as the conditions were not optimal for cell division.

Additional evidence for the impact of confinement on mitosis in spheroids was provided. In freely growing HCT116 spheroids cells had elongated nuclei, oriented parallel to the surface of spheroid, and the division axis was also parallel. When confined with agarose gel, nuclei were less elongated and less parallel to the spheroids surface. Orientation of division axis also became less parallel to the surface. Interestingly, these changes were observed only in outer layers of spheroids, which would imply that in inner parts of the spheroid are already confined by the adjacent cells, making them less sensitive to additional external forces (Desmaison et al., 2018). Confinement also prolonged prometaphase (Desmaison et al., 2018), which could explain previous findings that mechanical stress in spheroids causes mitotic arrest (Desmaison, Frongia, et al., 2013). These results emphasize the extent to which different cell lines may behave differently in 3D systems. Consequently, various cell types may exhibit diverse behaviors in tissues, which must be considered when planning experiments and interpreting results.

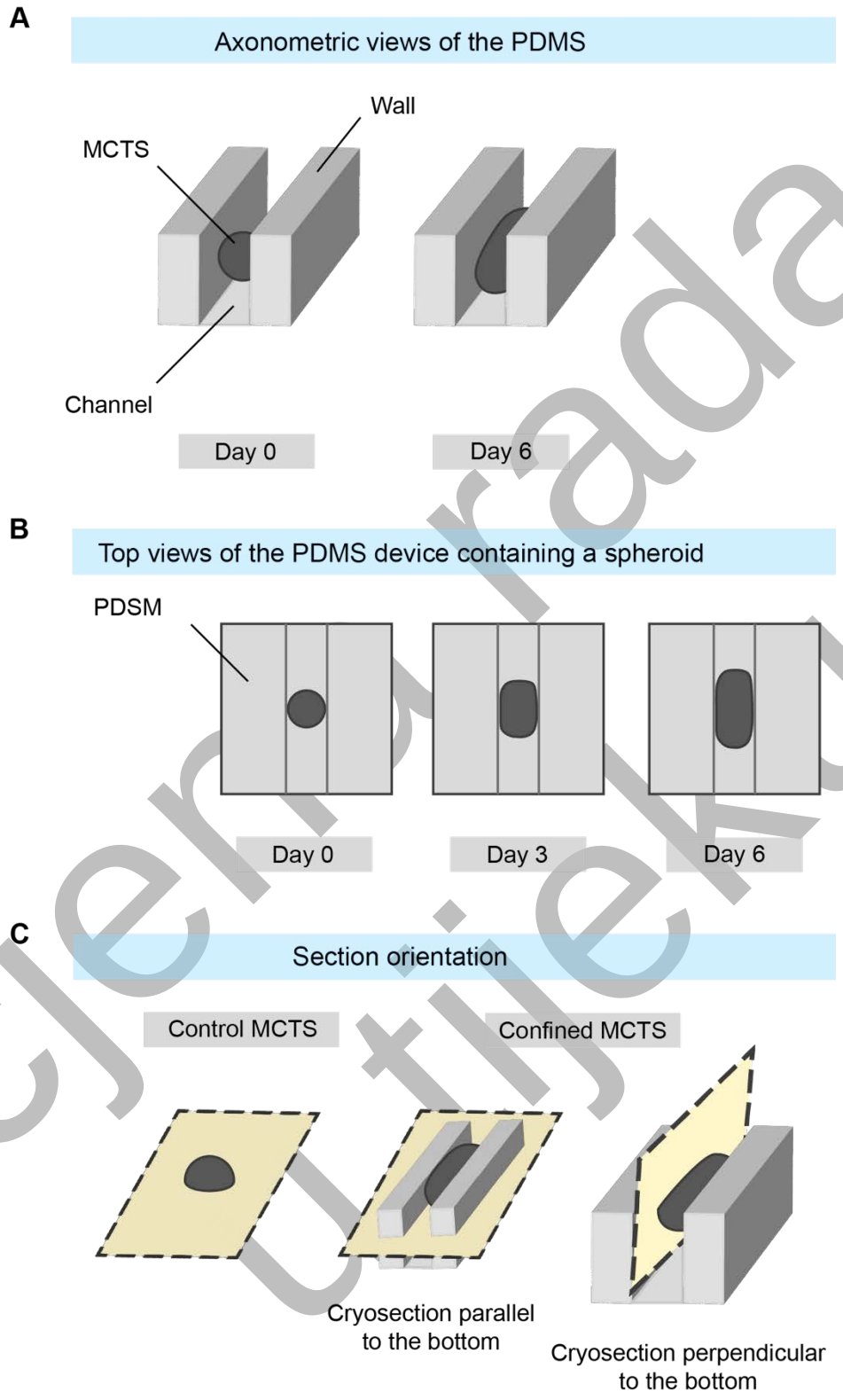

Figure 16. Caption on the following page.

Figure 16. PDSM microdevice. A) Axonometric view of the PDSM microdevice. Multicellular tumor spheroids (MCTS) change their shape after six days in confined condition. **B)** Transmitted-light images of a PDMS microdevice and of a spheroid at zero, three and six days of growing within the microdevice. **C)** Differences between spheroid that grows in non-confined conditions and mechanically confined conditions (oriented for cryosectioning). Taken from (Desmaison, Frongia, et al., 2013).

1.24. Spindle positioning in spheroids

Even though tissue architecture, polarity, and cell-cell interactions play critical roles in spindle positioning and the orientation of cell division, most studies on mitotic spindles have been conducted on monolayers, that lack the tissue complexity and have an artificial cell polarity (Cukierman et al., 2001). With the advancement of 3D culture systems and in vivo studies, interest has shifted toward investigating extrinsic factors, in addition to intrinsic factors, that influence the orientation of cell division (Nestor-Bergmann et al., 2014). Intrinsic factors are polarized cortical signals that interact with plus-end MAPs to align the spindle along a specific axis (Lu & Johnston, 2013). Extrinsic factors include mechanical forces exerted by the substrate in monolayers, neighboring cells, and ECM components (Nestor-Bergmann et al., 2014).

When unidirectional stretch was applied to HeLa cells and keratinocytes, the spindles rotated in the direction of the stretch. Rotation occurred because external forces polarize subcortical actin, which affected spindle orientation (Fink et al., 2011; Seldin et al., 2013). This example served as direct evidence how external cues can influence spindle orientation. In monolayers, the spindle generally aligns with the long axis of the interphase cell, which is known as the Hertwig's rule (Hertwig & Hertwig, 1884). It was demonstrated with HeLa cells, cultured on various micropatterns, that they will adjust their shape to the pattern accordingly. During the subsequent mitosis, the spindle aligns with the long axis of the newly formed shape (Théry et al., 2005).

Proper cell rounding is essential to ensure bipolar spindle formation and correct spindle orientation during mitosis. In confined environment, the actin cortex promotes cell rounding by generating forces that support the pressure increase within cells at the onset of mitosis, which is not essential in isolated cells (O. M. Lancaster et al., 2013). In HeLa cells cultured as monolayers, mechanical confinement impaired cell rounding and led to aberrant mitosis (O. M. Lancaster et al., 2013; Tse et al., 2012). In contrast, cell rounding was unaffected by mechanical confinement in HCT116 spheroids (Desmaison et al., 2018). This difference may be due to cell line-specific responses to mechanical stress. Another explanation could be that in spheroids, forces are distributed among neighboring cells, reducing the impact on individual cells.

This is another example that emphasize the importance of conducting research in 3D systems, as the results can be significantly different from the ones obtained in monolayers.

1.25. Mitosis in organoids is highly organized

Organoids have become valuable tools for studying mitosis, as they provide a more accurate representation of the conditions that closely resemble those in living organisms. Small intestine organoids form structures resembling native tissue. The epithelial layer is composed of densely packed columnar cells. The cells are polarized, with the apical side facing the lumen, the basal side facing the basement membrane, and lateral sides are in contact with neighboring cells (T. Sato et al., 2009).

During interphase, the nucleus is located on the basal side, and at the onset of mitosis it migrates apically in a process called interkinetic nuclear migration. The cell stays anchored to the basement membrane via actin cables, ensuring it returns to its correct position after mitosis (Carroll et al., 2017). Neighboring cells expand to fill the basal gap during mitosis. The metaphase plate aligns perpendicularly to the apical side, and cells divide symmetrically. After mitosis, the adjacent cells move apart, and daughter cells adopt their characteristic columnar shape (Carroll et al., 2017; McKinley et al., 2018; Saleh et al., 2023).

In summary, organoids are a great model for studying mitosis due to their capacity to mimic complex tissue architecture. In this model for healthy tissue, mitosis is well organized in space and each dividing cell is well coordinated with neighboring cells to preserve the tissue functions and integrity. Opposite to that, in multicellular tumor spheroids cells divide in the random positions. The only spatial regulation present is due to gradients of nutrients and oxygen in larger spheroids. Moreover, a significant portion of mitotic events in spheroids are unsuccessful, suggesting that neighboring cells do not assist in division but instead contribute to a confined environment.

2. AIMS OF THE RESEARCH

The aim of this research is to investigate the differences in sensitivity to KIF18A depletion and inhibition in diploid and post-tetraploid cells. Non-tumor diploid RPE1 cells, and their post-tetraploid derivatives, that underwent WGD and formed stable cell lines will be used. A sub-population of cells which requires KIF18A for proliferation will be described. First hypothesis is that sensitivity to KIF18A loss increases with aneuploidy levels, so highly aneuploid cells should show increased sensitivity to KIF18A perturbations. Post-tetraploid cells should have more problems with chromosome alignment, due to a higher chromosome number, which will cause increased sensitivity.

The second aim of the research is to describe cell division in 3D cultures, to get insights into the influence of 3D culture architecture, confinement, and adjacent cells on mitosis of tumor and non-tumor cell lines. Monolayers and spheroids will be compared to study the differences in spindle and cell morphology, as well as the error rates in two models. The hypothesis is that a change of cell shape and confinement will negatively impact different mitotic patterns in spheroids.

3. MATERIALS AND METHODS

3.1. Cell culture

To explore differences in sensitivity to KIF18A depletion and inhibition between diploid and post-tetraploid cell lines following cell lines were used: human diploid hTERT immortalized retinal pigment epithelial RPE1 cells stably expressing H2B-GFP, green fluorescent protein (throughout the text these cells will be referred to as RPE1 parental), and their post-tetraploid clones RPT1 and RPT3 (Kuznetsova et al., 2015), a gift from Zuzana Storchová (RPTU Kaiserslautern-Landau, Kaiserslautern, Germany), and human diploid hTERT RPE1 cells stably expressing both CENP-A-GFP and Centrin1-GFP (throughout the text these cells will be referred to as RPE1 CC) (Magidson et al., 2011), a gift from Alexey Khodjakov (Wadsworth Center, New York State Department of Health, Albany, NY, USA).

To explore differences between 2D and 3D cell cultures the following cell lines were used: human hTERT RPE1 cell line with a p53 knockdown (KD) stably expressing H2B-Dendra2 (throughout the text these cells will be referred to as RPE1 p53KD) (Soto et al., 2018) a gift from Rene Medema (Netherlands Cancer Institute, Amsterdam, Netherlands), unlabeled human breast cancer MDA-MB-231 cell line (ATCC Cat. N. HTB-26), a gift from Dragomira Majhen (Ruđer Bošković Institute, Zagreb, Croatia), unlabeled human osteosarcoma U2OS cell line, a gift from Marin Barišić (Danish Cancer Society Research Center, Copenhagen, Denmark) and unlabeled human high-grade serous ovarian cancer OVSAHO cell line (JCRB1046 Cell Bank, Tebubio, Le Perray-en-Yvelines, France).

All cell lines, except OVSAHO cells, were maintained in Dulbecco's Modified Eagle Medium (DMEM) medium, containing 1 g/L D-glucose, L-glutamine, phenol red and sodium pyruvate (Gibco, MT, USA). OVSAHO cell line was maintained in RPMI-1640 medium, containing L-glutamine, sodium bicarbonate and phenol red (Sigma-Aldrich, MO, USA). DMEM and RPMI-1640 medium were supplemented with 10% heat-inactivated fetal bovine serum (FBS, Sigma-Aldrich, MO, USA) and penicillin (100 IU/mL)/streptomycin (100 mg/mL) solution (Lonza, Basel, Switzerland). Cells were grown in a Galaxy 170S humidified incubator (Eppendorf, Hamburg, Germany) at 37°C with a 5% CO_2 atmosphere, and routinely passaged at the confluence of 70-80%. Cells were regularly tested for mycoplasma contamination with 1 µg/mL DAPI staining (D9542, Sigma-Aldrich, MO, USA).

For the experiments in which the difference in KIF18A loss sensitivity was tested cells were cultured for a maximum of five passages, to ensure that they don't gain additional mutations and variability among the clones. For the experiments were differences between monolayers and spheroids were determined, cells were cultured for a maximum of ten passages.

3.2. Spheroid generation using magnetic cell levitation

Spheroids were made using magnetic cell levitation method developed by Souza and colleagues (G. R. Souza et al., 2010).

To cultivate spheroids 6 Well Bio-Assembler™ Kit (Greiner Bio-One GmbH, Kremsmünster, Austria) was used. The kit contains 6-well plates with cell-repellent surface, lid with magnets for each well, a plastic barrier that prevents direct contact between the cell suspension and the magnets, and a nanoparticles solution NanoShuttle™-PL. Nanoparticles solution contains iron(III) oxide, Fe_2O_3, water soluble gold nanoparticles stabilized with citrate ion, with a diameter of less than 100 nm, and poly-L-lysine solution.

For generation of spheroids RPE1 p53 KD, MDA-MB-231, U2OS and OVSAHO cells were used. To achieve the optimal confluency of approximately 70% for treatment with nanoparticles solution, 250000 cells were seeded as monolayers in a 6-well plate one day prior to the addition of 1 µL/cm^2 of nanoparticles solution. The nanoparticles were incubated with the cells for approximately 18 hours. If the incubation lasts 24 hours or longer, the nanoparticles tend to exit the cells and detach from the cell membrane. On the third day, the cells were detached from the surface, and the cell suspension was transferred into a cell-repellent 6-well plate with a magnetic lid. Spheroids were incubated for five to seven days before immunostaining.

To investigate cell division in 3D cell cultures, 2D cell culture, where RPE1 p53 KD, MDA-MB-231, U2OS and OVSAHO cells were grown as monolayers, were also established as controls. 150000 cells were seeded on uncoated 18 mm coverslips. When cells were 50-70% confluent, 1 µL/cm^2 of nanoparticle solution was added and incubated for approximately 18 hours. Magnetic lid was placed over the wells and cells were incubated for an additional four hours before immunostaining. Extended incubation with the magnetic lid led to cell detachment from the substrate.

3.3. KIF18A depletion and inhibition

Small interfering RNA (siRNA) was used for depletion of endogenous KIF18A. RPE1 CC, RPE1 parental, RPT1 and RPT3 cells were seeded on 35 mm uncoated dishes with 0.17 mm glass thickness (Ibidi GmbH, Gräfeling, Germany) in 1 mL of cell culture medium. 40-50% confluent cells were transfected with targeting KIF18A siRNA (100 nM, s37882, Ambion, Thermo Fisher Scientific, MA, USA) or control siRNA ON-TARGETplus Control Pool Non-Targeting pool (100 nM, D-001810-10-20, Dharmacon, Lafayette, CO, USA) constructs, diluted in Opti-MEM medium (Life Technologies, Waltham, MA, US) and transfection was performed using Lipofectamine RNAiMAX Reagent (Life Technologies, Waltham, MA, US) according to the manufacturer's instructions. Four hours after transfection, the transfection mixture was replaced with cell culture medium. Cells were incubated 24 hours before live-cell imaging. For other experiments cells were incubated from 24 hours to seven days before immunostaining, depending on the experiment.

To inhibit KIF18A protein, small-molecule KIF18A inhibitor Sovilnesib (AMG-650, MedChemExpress, NJ, USA) was used in a range of concentrations on RPE1 CC, RPE1 parental, RPT1 and RPT3 cells. Inhibitor was dissolved in dimethyl sulfoxide (DMSO, Sigma-Aldrich, MO, USA) and control cells were treated with equivalent concentrations of DMSO. For live-cell imaging cells were treated with 250 nM Sovilnesib (and 0.05% DMSO) and incubated 30 minutes prior to imaging. For other experiments a range of concentrations between 10 nM to 500 nM was used (and 0.1% DMSO). Cells were incubated from 24 hours to seven days prior to immunostaining. To test if Sovilnesib has some non-specific effects, KIF18A was both depleted and inhibited in RPE1 parental and RPT3 cells. Transfection was conducted as already described, but after the removal of transfection mixture, cell culture medium with 250 nM Sovilnesib was added, and incubated for 24, 48 and 72 hours. Control cells were treated with control siRNA and 0.05% DMSO.

To determine how different treatments affect the growth of diploid and post-tetraploid cell lines, RPE1 CC, RPE1 parental, RPT1 and RPT3 cells were seeded at low confluency, 5-10%, on 35 mm uncoated dishes with 0.17 mm glass thickness (Ibidi GmbH, Gräfeling, Germany), and treated with 100 nM KIF18A siRNA, 100 nM control siRNA, 250 nM Sovilnesib or 0.05% DMSO, as already described. Cells were monitored using an inverted phase-contrast microscope (Optika Microscopy, Ponteranica, Italy) and imaged every 24 hours for up to thirteen days. During this period, the cell culture medium was not changed, and no additional treatments were applied. The percentage of confluency was determined daily from three randomly selected fields of view per sample.

3.4. Immunofluorescence

3.4.1. KIF18A visualization

To prepare samples for confocal imaging of control KIF18A depleted or inhibited cells, RPE1 CC, RPE1 parental, RPT1 and RPT3 cells were fixed with of ice-cold methanol for 1 min at -20 °C. Following fixation, cells were washed with PBS three times for 5 min at a room temperature. Cells were permeabilized in 0.5% Triton-X-100 for 15 min at a room temperature. To block unspecific bindings of antibodies, cells were blocked with 1% normal goat serum (NGS, Thermo Fisher Scientific, Waltham, MA, USA) for one hour, at a room temperature. Triton-X-100 and NGS were diluted in PBS.

Cells were incubated with 250 µL of primary antibodies diluted in 1% NGS overnight at 4 °C. The primary antibodies used were rabbit anti-KIF18A (diluted 1:300, A301-080A, Bethyl Laboratories) rat anti-tubulin (diluted 1:500, MA1-80017, Invitrogen) rabbit anti-centrin-3 (diluted 1:300, ab228690, Abcam). After the incubation with primary antibodies, cells were washed with PBS three times for 5 min at a room temperature, and then incubated with 250 µL of secondary antibodies diluted in 2% NGS for one hour at a room temperature, in the dark. Secondary antibodies used were donkey anti-rabbit Alexa Fluor 647 (diluted 1:500, ab150075, Abcam) to visualize KIF18A and centrin-3 and donkey anti-rat Alexa Fluor 568 (diluted 1:1000, ab175475, Abcam) to visualize tubulin. After incubation cells were washed three times with PBS, for 5 min at a room temperature.

Although RPE1 parental, RPT1, and RPT3 cells stably express H2B-GFP, all samples were additionally stained with 1 µg/mL DAPI for 15 min at a room temperature, to ensure consistent measurement of metaphase plate parameters, Furthermore RPE1 CC stably express CENP-A-GFP and Centrin1-GFP, were also stained with DAPI to visualize chromosomes and ensure equal measurements among the cell lines, so CENP-A-GFP and Centrin1-GFP were not imaged.

3.4.2. Immunofluorescence for STED microscopy

Superresolution stimulated emission depletion (STED) microscopy was used to investigate spindle architecture after KIF18A depletion in RPE1 parental, RPT1 and RPT3 cells. To remove the components of cytoplasm, a cytoplasm extraction buffer containing: 0.5% Triton-X-100, 0.1 M PIPES, 1 mM EDTA and 1 mM $MgCl_2$ was added for 15 sec. Cells were fixed with 3% paraformaldehyde and 0.1% glutaraldehyde solution for 10 min.

Quenching solution, 100 mM glycine in PBS, was added for 7 min and reduction solution, 0.1% sodium borohydride in PBS, was added for 10 min. Quenching and reduction solution were added to reduce the background fluorescence. Following, cells were incubated in

blocking/permeabilization (BP) buffer, containing 2% NGS and 0.5% Triton-X-100 in PBS, for 2 hours at a room temperature.

To visualize microtubules, primary antibody rat anti-tubulin (MA1-80017, Invitrogen) was diluted in 1:500 ratio in BP buffer and incubated overnight at 4 °C. Cells were washed with PBS three times for 5 min at a room temperature, and then incubated with secondary antibody donkey anti-rat Alexa Fluor 568 (ab175475, Abcam) diluted in 1:1000 ratio in BP buffer, for 1 hour at a room temperature, in the dark. Stably expressed H2B-GFP or 1 µg/mL DAPI were used to visualize chromosomes.

3.4.3. Immunofluorescence of spheroids

Spheroids of RPE1 p53 KD, MDA-MB-231, U2OS and OVSAHO cells were formed in 6-well plates, and prior to fixation were gently transferred by pipetting to 35 mm uncoated dishes with 0.17 mm glass thickness (Ibidi GmbH, Gräfelfing, Germany). In all steps of the protocol, 200 µL of solutions were added to keep the spheroid centered in a droplet of liquid, preventing it from sticking to the edges of the dish and breaking apart. Furthermore, the immunostaining protocol was optimized to minimize solution changes, as spheroids can easily be damaged during pipetting.

Samples were fixed with 4% paraformaldehyde, for 20 min at a room temperature. Spheroids were washed with PBS for 10 min. Next, BP buffer was added and incubated for 1 hour at a room temperature. Primary antibody rat anti-tubulin (MA1-80017, Invitrogen) was diluted in 1:300 ratio in BP buffer and incubated overnight at 4 °C. On the following day, spheroids were washed with PBS for 10 min and secondary antibody, diluted in 1:500 ratio in BP buffer, was incubated 1 hour at a room temperature, in the dark. For MDA-MB-231 and U2OS spheroids secondary antibody donkey anti-rat Alexa Fluor 488 (ab150153, Abcam) was used, and for RPE1 p53 KD and OVSAHO spheroids donkey anti-rat Alexa Fluor 647 (ab150155, Abcam) was used. Spheroids were washed with PBS.

MDA-MB-231 and U2OS spheroids were stained with 1 µg/mL DAPI and 4 µM SiR-actin dye (Spirochrome, Stein am Rhein, Switzerland), for 20 min at a room temperature, to visualize chromosomes and cell membrane. RPE1 p53 KD and OVSAHO spheroids were stained with 1 µg/mL DAPI and 5 µg/mL Wheat Germ Agglutinin, Alexa Fluor™ 594 Conjugate (Invitrogen, Waltham, MA, SAD) cell membrane dye. After PBS wash, spheroids were mounted with antifade aqueous embedding media (Abberior, Göttingen, Germany) and covered with a coverslip.

Control samples, in which cells were cultured as monolayers, were prepared using the same protocol. The only difference was that cells were grown on coverslips, so in the final step, the mounting medium was applied directly onto the coverslip, which was then placed onto a microscope slide.

3.5. Microscopy

Live-cell imaging of RPE1 CC, RPE1 parental, RPT1 and RPT3 was performed on the Lattice Lightsheet 7 system (Carl Zeiss, Germany), equipped with an illumination objective lens 13.3×/0.4 (at a 30° angle to cover the glass) with a static phase element and a detection objective lens 44.83×/1.0 (at a 60° angle to cover the glass) with an Alvarez manipulator. Automatic water immersion was applied from the dispenser at intervals of 25 minutes.

The CENP-A-GFP and Centrin1-GFP, as well as H2B-GFP were visualized with the 488-nm diode laser (power output 10 Mw) with laser power set to 2% and 15 ms exposure time. The detection module consists of a Hamamatsu ORCA-Fusion sCMOS camera. The LBF 405/488/561/642 emission filter was used. Cells were kept in a Zeiss stage incubation chamber system (Carl Zeiss) at 37°C and 5% CO2 atmosphere. The imaging area in the x dimension was set to 1.5 mm. The image was acquired every two minutes for 24 hours in ZEN 3.7 software.

Confocal imaging was performed on an Airyscan Zeiss LSM800 confocal laser scanning microscope with the 63x/1.4 Oil DICII objective (Carl Zeiss, Germany) and LSM 800 camera. Laser lines of 405 nm, 488 nm, 561 nm, and 640 nm were used to excite DAPI, Alexa Fluor 488, 568, 594 and 647 respectively. For experiments with KIF18A depletion/inhibition 31 z-slice were imaged for picture. The number of z-slices was adjusted individually for each cell during spheroid imaging, to capture the whole cell. The z-step size was set to 0.5 μm in all experiments. Images were acquired in ZEN Blue 3.5 software.

Superresolution imaging of RPE1 parental, RPT1 and RPT3 was performed on Expert Line easy3D STED microscope system (Abberior Instruments, Göttingen, Germany) using 100x/1.4NA UPLSAPO100x oil objective (Olympus, Tokyo, Japan) and avalanche photodiode (APD) detector. Depletion of red lines was performed with a STED 775 nm laser line during superresolution imaging. Line accumulation was set to 1, dwell time to 10 μs and pinhole size to 1.0 AU (Airy units). The xy pixel size was set to 20 nm the distance between z-planes was 300 nM. To determine the phase of mitosis chromosomes were visualized and with H2B-GFP or DAPI and imaged in confocal mode. Images were acquired using Imspector software.

3.6. Image processing and data analysis

All images were analyzed in Fiji/ImageJ (National Institutes of Health, Bethesda, MD, USA). Quantification and statistical analysis were performed in GraphPad Prism (GraphPad Software, Boston, MA, USA). No statistical methods were used to predetermine the sample size. Data are given as mean ± SEM (standard error of mean), unless stated otherwise.

The data were tested for normal distribution using Shapiro-Wilk normality test. When data were normally distributed, an unpaired two-tailed t-test was used to assess differences between two groups, while one-way ANOVA followed by Tukey's multiple comparison test was used for comparisons among multiple groups. If the data wasn't normally distributed, two groups were tested with Mann-Whitney test, while multiple groups were tested with Kruskal-Wallis test followed with Dunn's multiple comparison test. Proportions among the groups were statistically compared with Chi-Square test, or Fisher's exact test when the proportions of two outcomes were compared. A p-value < 0.05 was considered statistically significant. Statistically significant differences are indicated as follows: ns for not significant when $p \geq 0.05$, * for $0.01 < p < 0.05$, ** for $0.001 < p < 0.01$, and *** for $p < 0.001$. Data analysis was performed in GraphPad Prism (GraphPad Software, Boston, MA, USA). Figures and schemes were assembled in Adobe Illustrator CS5 and CC (Adobe Systems, Mountain View, CA, USA).

3.7. Measurements of cell and spindle parameters

All the images from live-cell imaging were analyzed from maximum intensity projections (MIPs) that were automatically generated by Zen 3.7 software.

To study the effect of KIF18A depletion and inhibition SUM intensity projections of z-stacks of individual cells were used. Only the spindles that were horizontal relative to the dish surface were analyzed. To determine KIF18A depletion and inhibition, KIF18A intensity was measured on the spindle and on the spindle pole. Spindle area was encompassed with the Polygon selection tool, and mean spindle intensity was measured. Mean intensity on the pole was measured using a 2x2 Oval selection tool, which was also used to measure the background intensity in the cytoplasm (Figure 17A). Mean background intensity was subtracted from the mean spindle intensity and the mean spindle pole intensity. Values were also divided with the mean background intensity to get normalized values.

Spindle length was measured as a distance between spindle poles, defined by the microtubule foci. Spindle width was measured in the spindle midzone and defined as the distance between the outermost microtubule bundles. Metaphase plate length was measured as the distance between the outermost chromosome ends perpendicular to the spindle axis, and metaphase plate width parallel to the spindle axis (Figure 17B). Spindles were defined as multipolar if they had more than two microtubule foci.

In analysis of mitotic cells in spheroids and monolayers cell dimensions were measured only when the whole cell was in the field of view. Spindle length and width were measured if the spindle was horizontal relative to the dish surface.

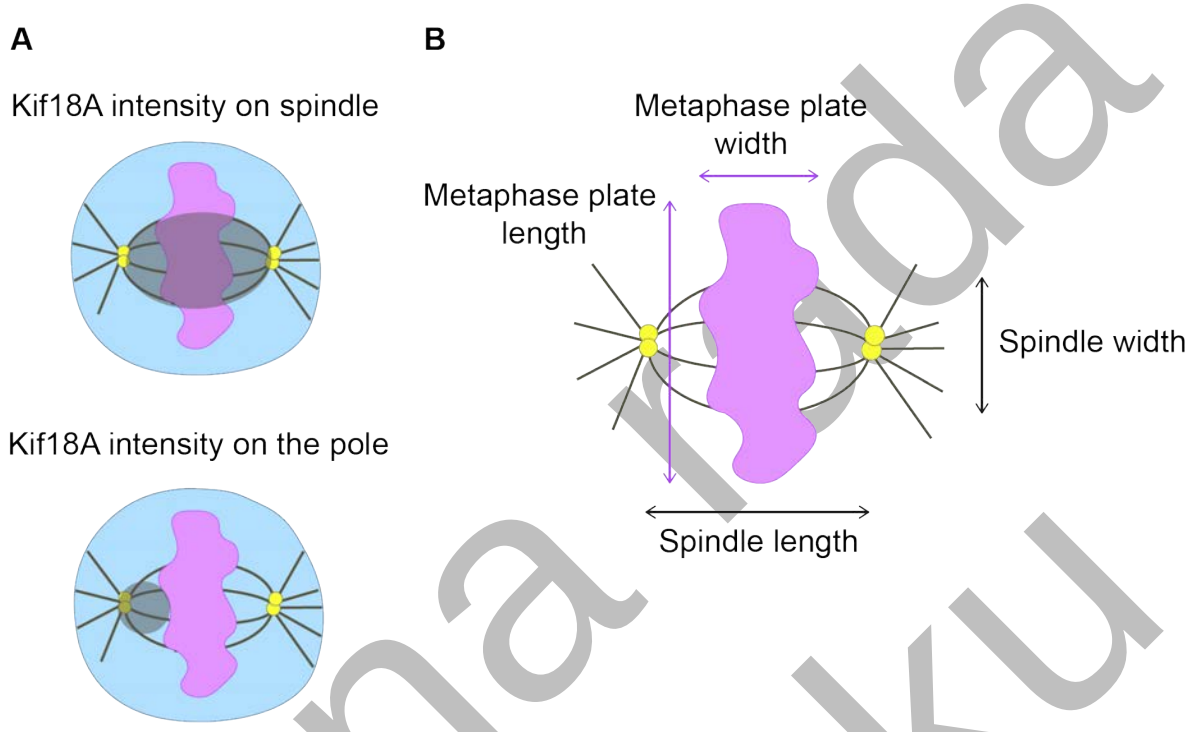

Figure 17. Measurement of cell and spindle parameters. A) Schematic view of the area (grey) that will be measured to determine KIF18A signal intensity on the spindle (upper), and on the spindle pole (lower). **B)** Schematic view of spindle parameters that will be measured; spindle length and spindle width (grey), and metaphase plate length and metaphase plate width (magenta).

4. RESULTS

In this thesis, two important features of tumors are investigated. The first part compares differences between diploid and PT cells, which, according to some theories, are precursors of tumor cells (Davoli & de Lange, 2011; Kirsch-Volders et al., 2024, 2025; Shackney et al., 1989; Storchova & Kuffer, 2008). The response of diploid and PT RPE1 cells to the loss of the KIF18A protein is examined by silencing the protein with siRNA and chemically inhibiting it using sovilnesib.

Tumor cells divide within a specific microenvironment. To date, tumor cell division has been mostly studied in monolayer cultures, which do not fully replicate the complex environment surrounding mitotic cells (Ćosić & Petelinec, 2024; Desoize & Jardillier, 2000). The second part of this thesis investigates how 3D architecture affects cell division by comparing mitosis in cell lines grown as monolayers and as spheroids.

4.1. KIF18A loss does not affect cell culture confluency over time

It was shown that KIF18A depletion and inhibition lead to a decrease in proliferation over time. Although the decrease in proliferation is more significant in sensitive CIN+ cell lines, it was also detectable in insensitive ones (Cohen-Sharir et al., 2021; Gliech et al., 2024). To test the proliferation rate over time four cell lines were used: RPE1 CC, RPE1 parental, RPT1 and RPT3. Cells were treated with 100 nM KIF18A siRNA or 250 nM sovilnesib, while control groups were treated with 100 nM non-targeting siRNA or 0.05% DMSO, respectively. Proliferation rate was measured by monitoring cell confluency over time.

Cell confluency was determined as the percentage of the surface area covered by cells in the field of view. Measurements were taken from three random fields of view at various time points ranging from 24 hours up to 13 days after treatment and are presented as mean values (Figure 18). Cells were seeded at low confluency, between approximately 5% and 15%, prior to treatment. Among the cell lines, RPT3 treated with both KIF18A siRNA and non-targeting siRNA showed the highest increase in proliferation, indicating the greatest growth rate (Figure 18E). In contrast, RPE1 parental cells exhibited the lowest confluency over time (Figure 18C).

Overall, there were no significant differences in confluency between treated and control groups or among the different cell lines. Most cell lines reached over 90% confluency by day 8. These results suggest that KIF18A silencing, and inhibition do not affect RPE1 cell culture confluency over time.

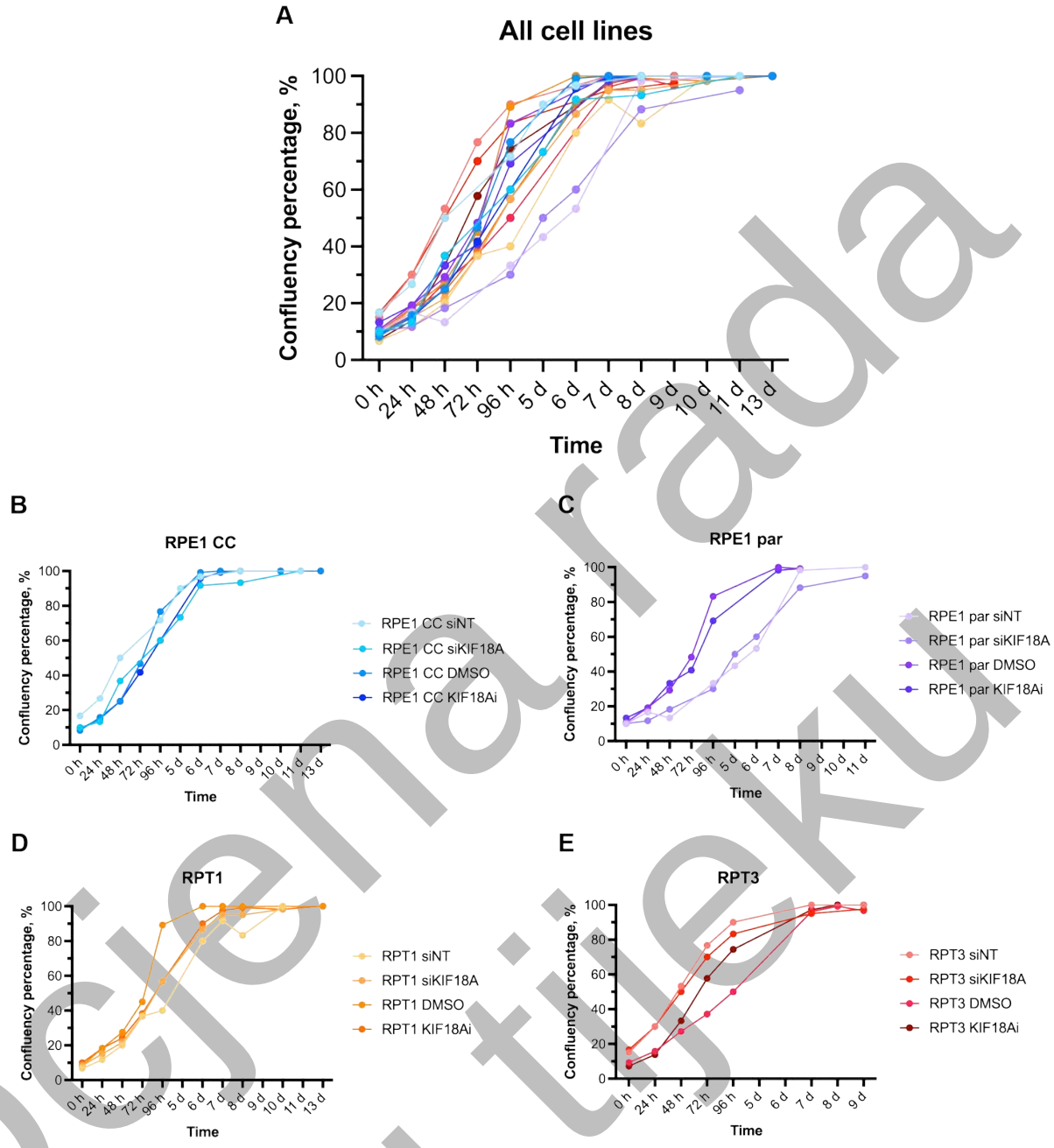

Figure 18. KIF18A silencing and inhibition do not affect cell culture confluency over time. RPE1 CC, RPE1 parental, RPT1 and RPT3 cell lines were treated with 100 nM KIF18A siRNA or 250 nM sovilnesib. Control groups were treated with 100 nM non-targeting siRNA or 0.05% DMSO, respectively. **A)** Cell culture confluency over time in all cell lines. Legends are provided in panels **B-E**, showing confluency changes in RPE1 CC, RPE1 parental, RPT1 and RPT3, respectively. Data is shown as a mean value. Results were obtained from one experiment for KIF18A depletion, and from two independent experiments for KIF18A inhibition, for all cell lines.

4.2. siRNA-mediated KIF18A depletion impairs mitosis for up to 96 hours

To test the efficiency of KIF18A depletion over time, RPE1 parental and RPT3 cells were treated with 100 nM KIF18A siRNA and incubated for 24, 48, 72 and 96 hours. Depletion was evaluated by immunostaining, KIF18A and tubulin were labeled, while DNA was visualized with DAPI.

In control cells, treated with non-targeting siRNA, KIF18A is localized on the spindle, mostly on the plus-end tips of microtubules. After KIF18A depletion there is no localization on the spindle, only the background cytoplasm signal is visible (Figure 19A). To confirm the distribution of KIF18A signal, line intensity profile was measured from one spindle pole to the other. Control cells showed two peaks corresponding to plus-end tips, while these peaks were absent after depletion (Figure 19B). KIF18A intensity on the spindle was significantly reduced in both cell lines compared to controls (Figure 20A). Additionally, RPT3 cells displayed a greater reduction than RPE1 parental cells at 72 and 96 hours, but not at earlier time points.

Spindle length did not differ significantly between RPE1 parental and RPT3 cells (Figure 20B). However, RPT3 cells showed wider spindles and longer metaphase phases, likely due to higher ploidy levels, as it was recently shown (Gudlin et al., 2025) (Figures 20C-D). Both cell lines exhibited a significant increase in metaphase plate width, indicating chromosome misalignment and confirming effective KIF18A depletion lasting for at least four days (Figure 20E).

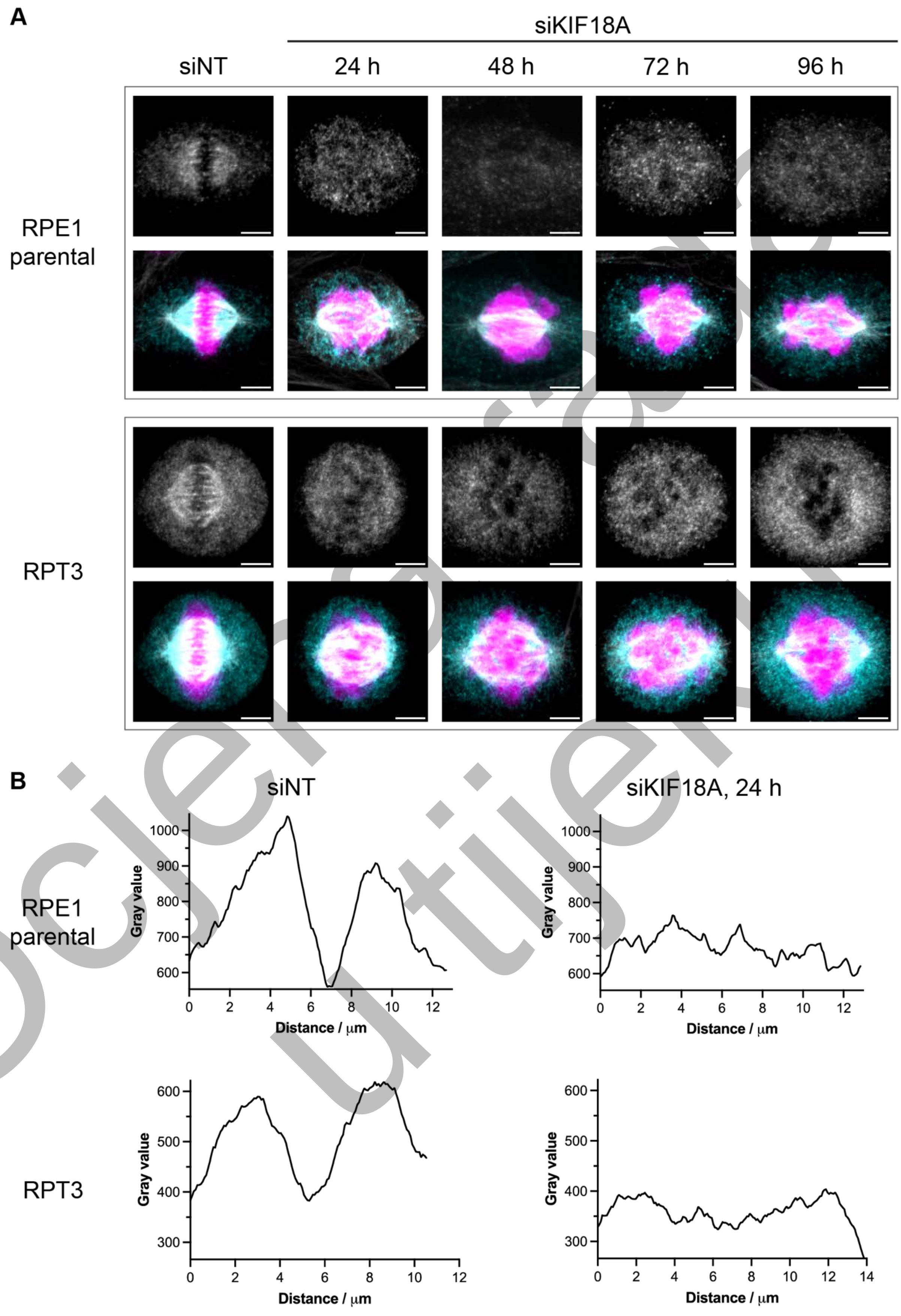

Figure 19. Caption on the following page.

Figure 19. KIF18A depletion effect lasts for four days. A) Confocal images of immunostained RPE1 parental and RPT3 cells, treated with 100 nM KIF18A siRNA for 24, 48, 72 and 96 hours. Control cells were treated with 100 nM non-targeting siRNA and incubated for 24 hours. Cells were immunostained for KIF18A and tubulin, while DNA was labelled with DAPI. Upper panels show KIF18A (grey), and lower panels show merged images for KIF18A (cyan), tubulin (grey) and DNA (magenta) for RPE1 parental and RPT3. Images are shown as a SUM intensity projections. Scale bars, 5 μm. **B)** Line profile intensity of KIF18A signal on the spindle, measured from one spindle pole to the other. RPE1 parental and RPT3 cells, incubated 24 hours, that have been measured are shown in **A**.

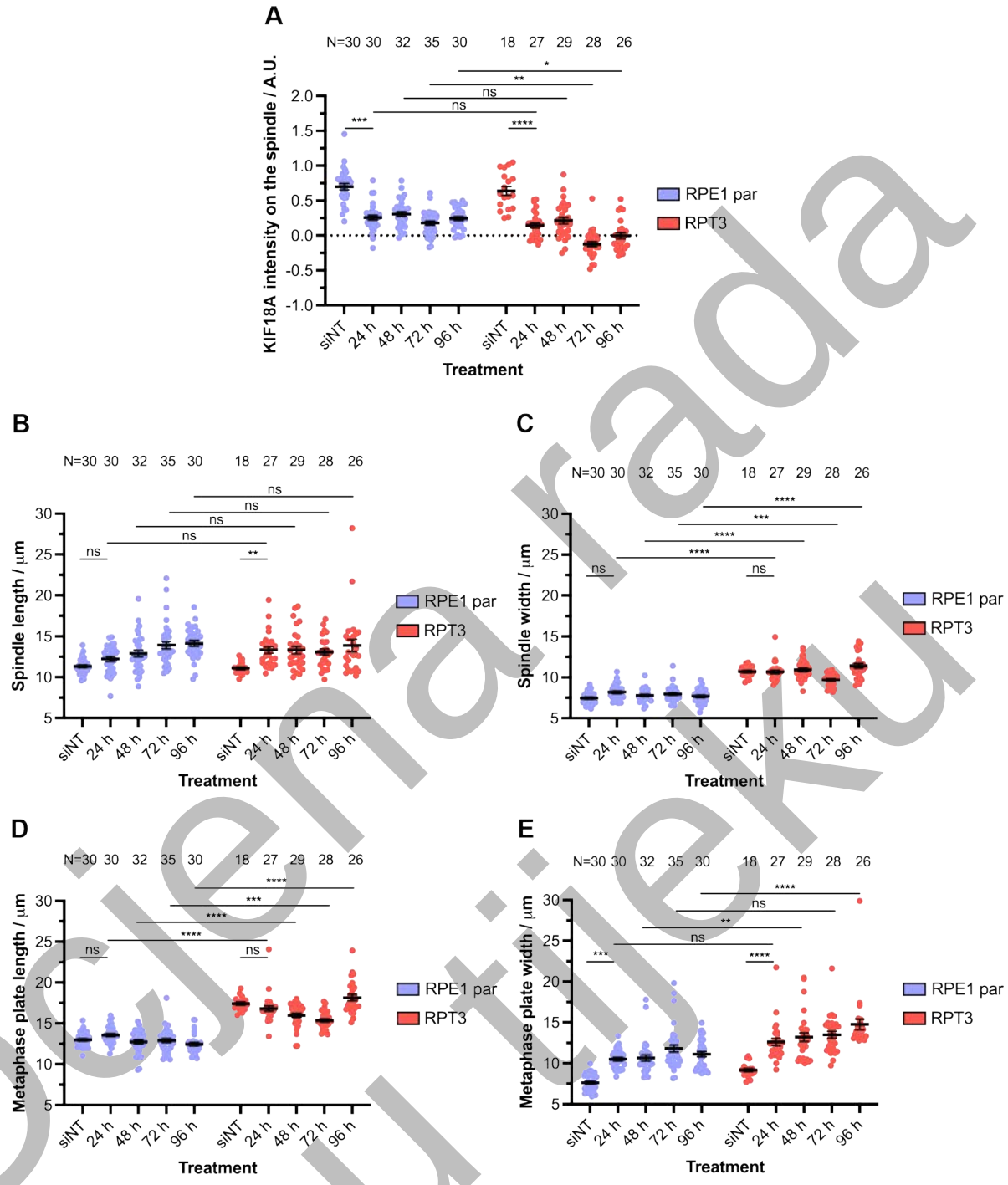

Figure 20. Caption on the following page.

Figure 20. KIF18A depletion affects spindle parameters in RPE1 parental and RPT3 cell lines. A) KIF18A intensity on the spindle after KIF18A depletion. The percentage of silencing efficiency in RPE1 parental is following: 24 h – 63.3%, 48 h – 56.2%, 72 h – 74.4% and 96 h – 64.8%. Silencing efficiency in RPT3 is following: 24 h – 77.2%, 48 h – 66.3%, 72 h – 80.7% and 96 h – 99.9%. **B)** Spindle length after KIF18A depletion. **C)** Spindle width after KIF18A depletion. **D)** Metaphase plate length after KIF18A. **E)** Metaphase plate width after KIF18A depletion. Error bars represent mean value and SEM. Results were obtained from one experiment. Statistical analysis: Kruskal-Wallis test with post-hoc Dunn's test was performed on a total number of cells for each incubation time.

4.2.1. A subpopulation of oversensitive cells occurs after KIF18A perturbations

A fraction of cells with a characteristic phenotype was observed. A subpopulation was characterized by elongated, irregular spindles, which were sometimes narrower, and chromosomes scattered on the whole spindle, even beside the spindle poles, implying that this fraction of cells had a severe chromosome alignment defects. This subpopulation of cells was referred to as oversensitive cells and was found in both diploid and PT cell lines. Also, it will be mentioned in the following results. These cells could also be multipolar (Figure 21A-B). A small fraction of multipolar cells without severe chromosome alignment defects was also observed (Figure 21B). These cells are referred to as normal multipolar cells and are distinguished from the oversensitive subpopulation.

Oversensitive cells were not detected in control groups. After KIF18A depletion, approximately 5% to 10% of the population consisted of oversensitive cells, peaking at 48 hours in both RPE1 parental and RPT3 cells (Figure 21C). By 96 hours, this fraction declined, possibly due to reduced siRNA efficiency or cell detachment during fixation, as these sensitive cells may have impaired adhesion. No significant differences in phenotype ratios were observed between RPE1 parental and RPT3.

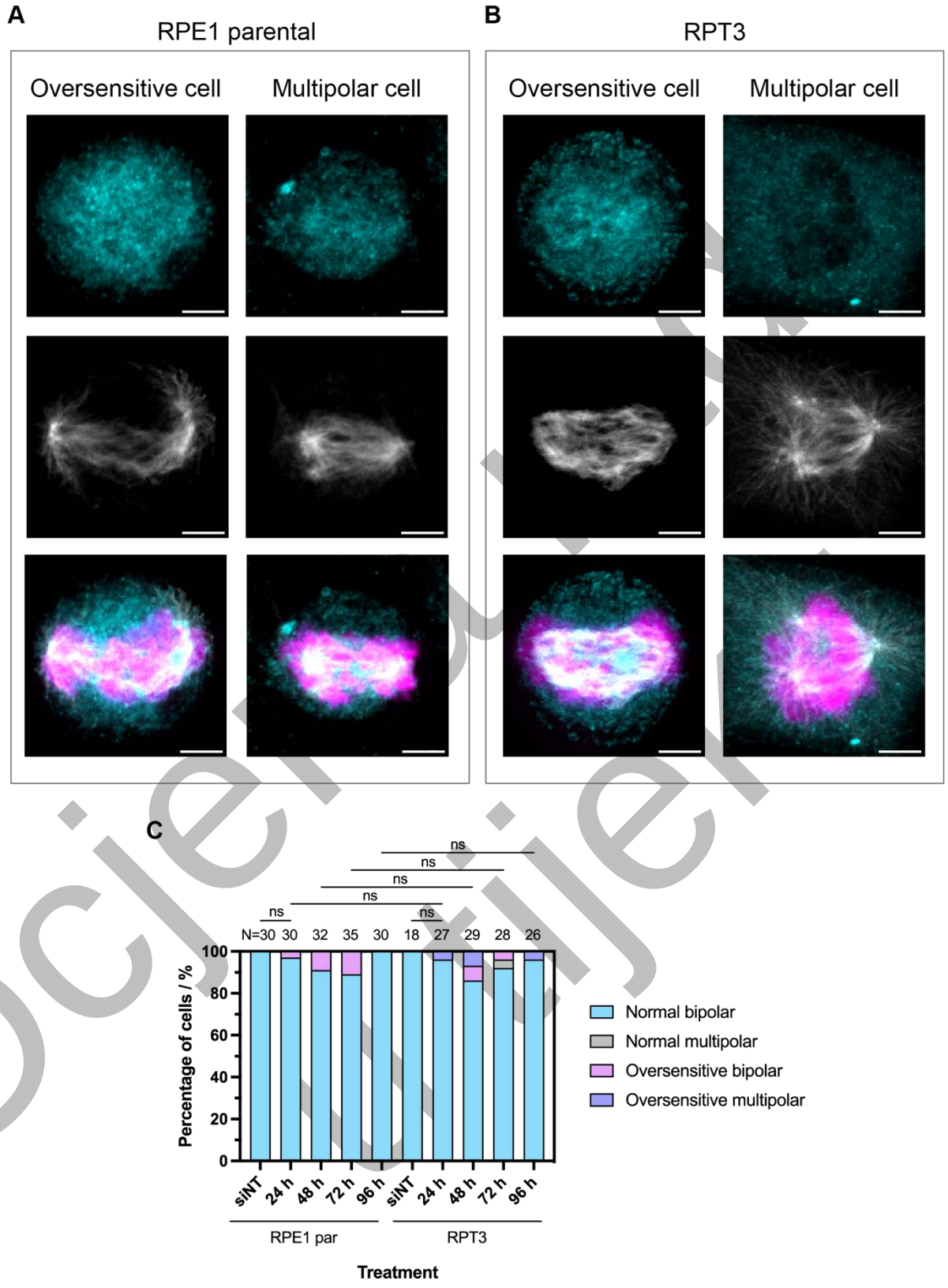

Figure 21. Caption on the following page.

Figure 21. A subpopulation of oversensitive cells occurs after KIF18A depletion. Confocal images of immunostained **A)** RPE1 parental cells and **B)** RPT3 oversensitive and multipolar cells. Cells were immunostained for KIF18A (upper panel, cyan), tubulin (middle panel, grey), while DNA was labelled with DAPI (lower panel, merged image, magenta). Images are shown as a SUM intensity projections. RPE1 parental multipolar cell is also an oversensitive cell, it has a minor, extra pole on the left side of the spindle. Scale bars, 5 µm. **C)** Distribution of phenotypes after KIF18A depletion. Results were obtained from one experiment. Statistical analysis: Fisher's exact test when compared groups had two outcomes, and Chi-square test if there were more than two outcomes (RPE1 par vs RPT3 – 48 h and RPE1 par vs RPT3 – 72 h). Ratio of outcomes was determined from a total number of cells for each incubation time.

4.3. Sovilnesib successfully inhibited KIF18A protein in both diploid and PT cell lines

Previous study showed that KIF18A inhibitor AM-1882 has a mild effect on diploid and tetraploid RPE1 cell lines, as these cells are considered insensitive, compared to sensitive cancer cell lines (Gliech et al., 2024). To evaluate how small molecule inhibitor sovilnesib affects diploid and PT cells, following cell lines were used: RPE1 CC, RPE1 parental, RPT1 and RPT3 cell line. Sovilnesib was tested at 100 nM, 250 nM, and 500 nM concentration to determine the optimal one. Cells were incubated with the inhibitor for 24 hours prior to fixation and immunostaining. Control cells were treated with 0.1% DMSO, corresponding to the amount used with the highest sovilnesib concentration. Cells were immunostained for KIF18A and tubulin, while DNA was visualized with DAPI (Figure 22).

In control cells, KIF18A is localized at microtubule plus-end tips, as previously observed. After sovilnesib treatment, KIF18A localization shifted toward the spindle poles (Figure 22). Line intensity profiles confirmed this shift in RPE1 parental and RPT3 cells (Figure 23A), with quantification showing increased KIF18A signal at the spindle poles in most groups, except RPE1 CC and RPT1 treated with 250 nM, where no significant increase was detected (Figure 23B). Other spindle parameters confirmed KIF18A inhibition (Figure 24), suggesting these exceptions may be due to microscopy limitations.

Spindle length increased in all cell lines following KIF18A inhibition, and PT cells had longer spindles than diploid cells (Figure 24A). Spindle width was generally greater in PT cells, which is associated with increased ploidy (Gudlin et al., 2025) (Figure 24B). Interestingly, spindle width decreased in PT cells after KIF18A inhibition, likely due to the oversensitive subpopulation with altered spindle geometry.

A similar effect was observed in metaphase plate length (Figure 24C). Metaphase plate width increased compared to controls across all lines, indicating impaired chromosome alignment, especially in PT cells (Figure 24D).

Following sovilnesib treatment, the fraction of oversensitive cells was significantly higher in PT cells than diploids. PT lines also had more oversensitive multipolar cells, and after 500 nM treatment they even had more oversensitive multipolar than bipolar cells. In conclusion, sovilnesib effectively inhibits KIF18A in both diploid and PT cell lines, with PT cells exhibiting greater sensitivity. 250 nM concentration was determined to be optimal for further experiments.

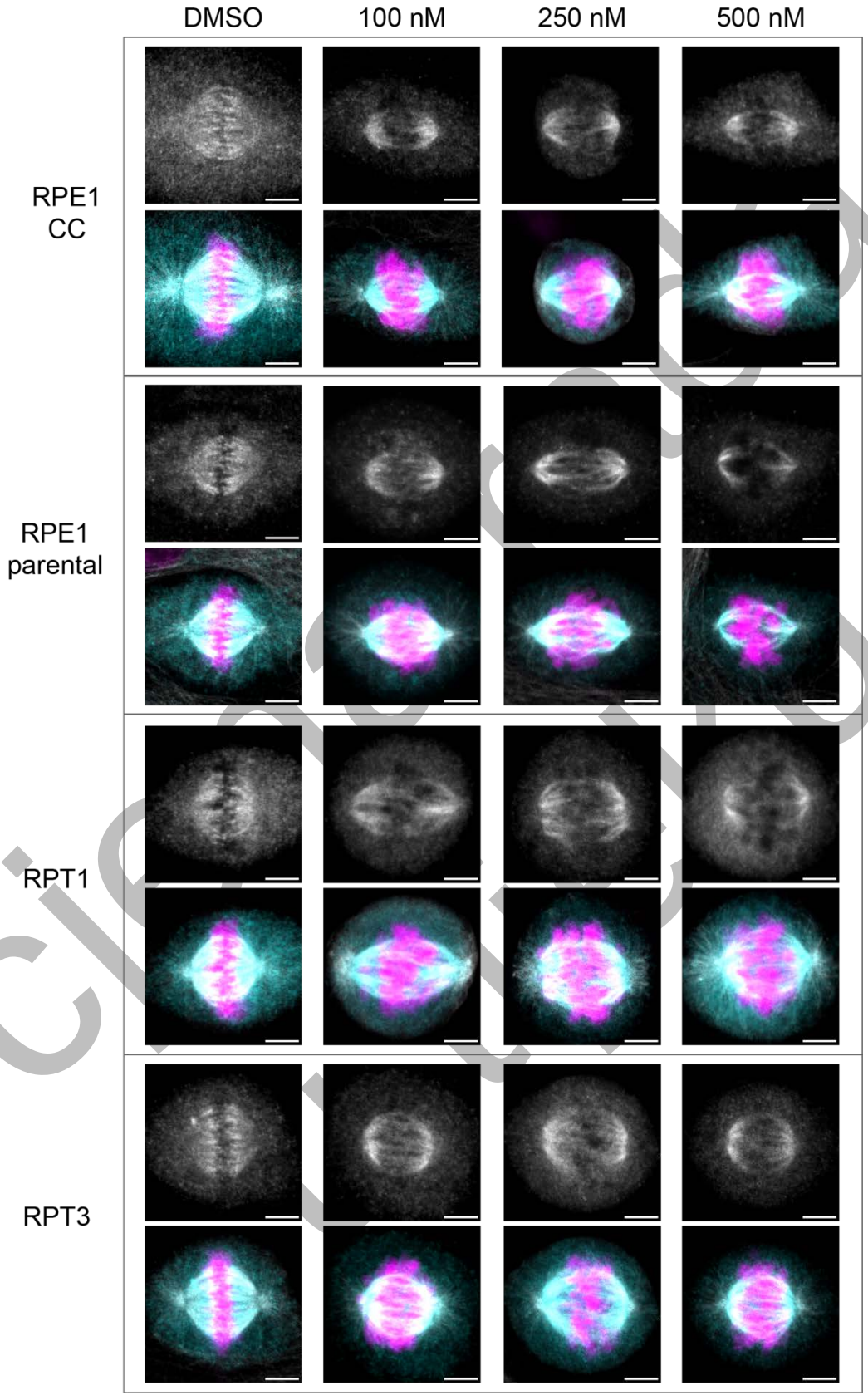

Figure 22. Caption on the following page.

Figure 22. Confocal images of diploid and PT cells after KIF18A inhibition. Immunostained RPE1 CC, RPE1 parental, RPT1 and RPT3 cells treated with 100 nM, 250 nM and 500 nM sovilnesib. Control cells were treated with 0.1% DMSO. Cells were fixed 24 hours after the treatment and immunostained for KIF18A and tubulin, while DNA was labelled with DAPI. Upper panels show KIF18A (grey), and lower panels show merged images of KIF18A (cyan), tubulin (grey) and DNA (magenta) for RPE1 CC, RPE1 parental, RPT1 and RPT3. Images are shown as a SUM intensity projections. Scale bars, 5 μm.

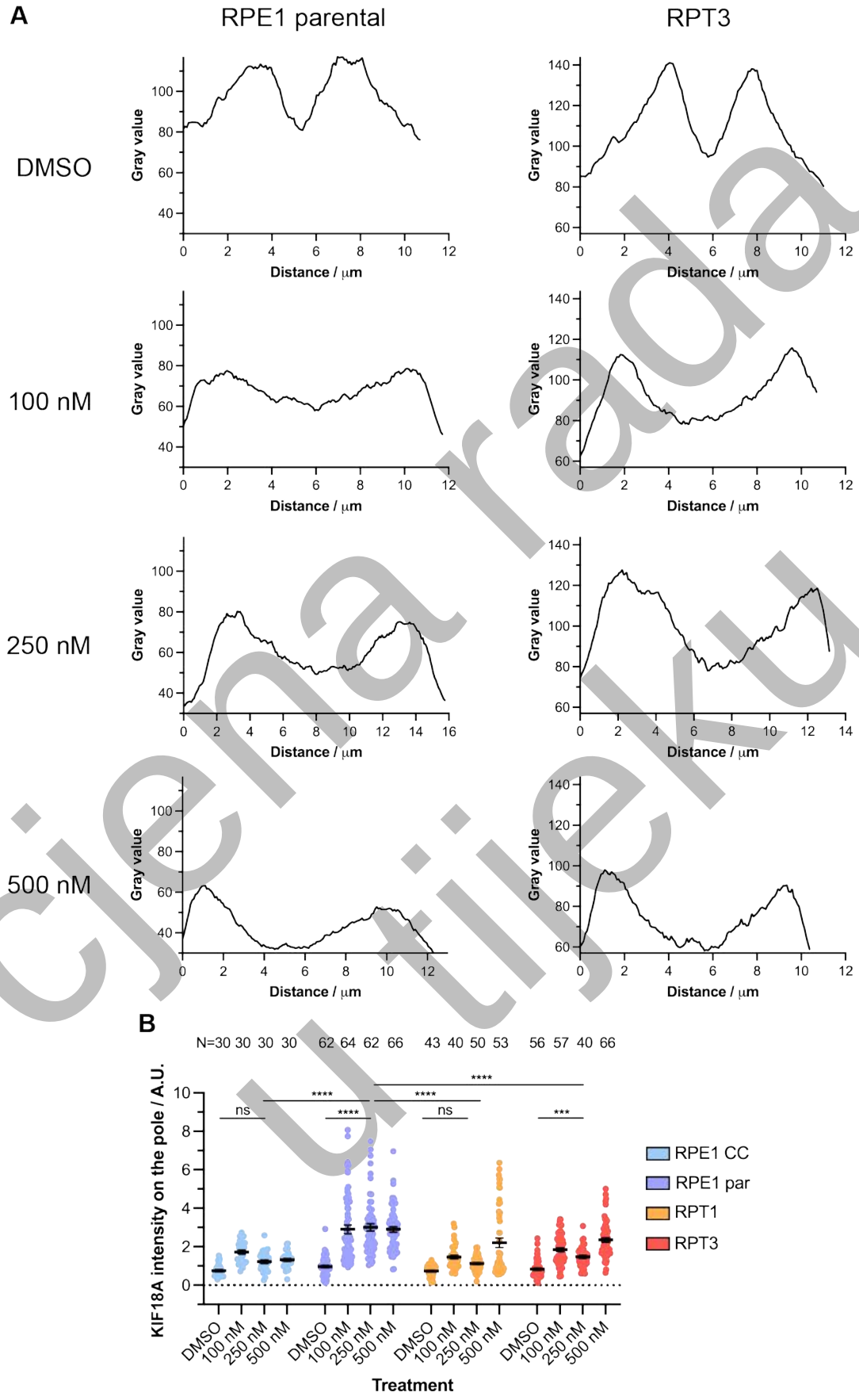

Figure 23. Caption on the following page.

Figure 23. KIF18A is localized on the spindle poles after sovilnesib treatment. A) Line profile intensity of KIF18A signal on the spindle, for RPE1 parental and RPT3 cells shown in Figure 22. **B)** KIF18A intensity on the spindle pole in RPE1 CC, RPE1 parental, RPT1 and RPT3 after sovilnesib treatment. Error bars represent mean value and SEM. Results were obtained from three independent experiments for all cell lines except for RPE1 CC, where one experiment was done. Statistical analysis: Kruskal-Wallis test with post-hoc Dunn's test was performed on a total number of cells for each cell line and sovilnesib concentration.

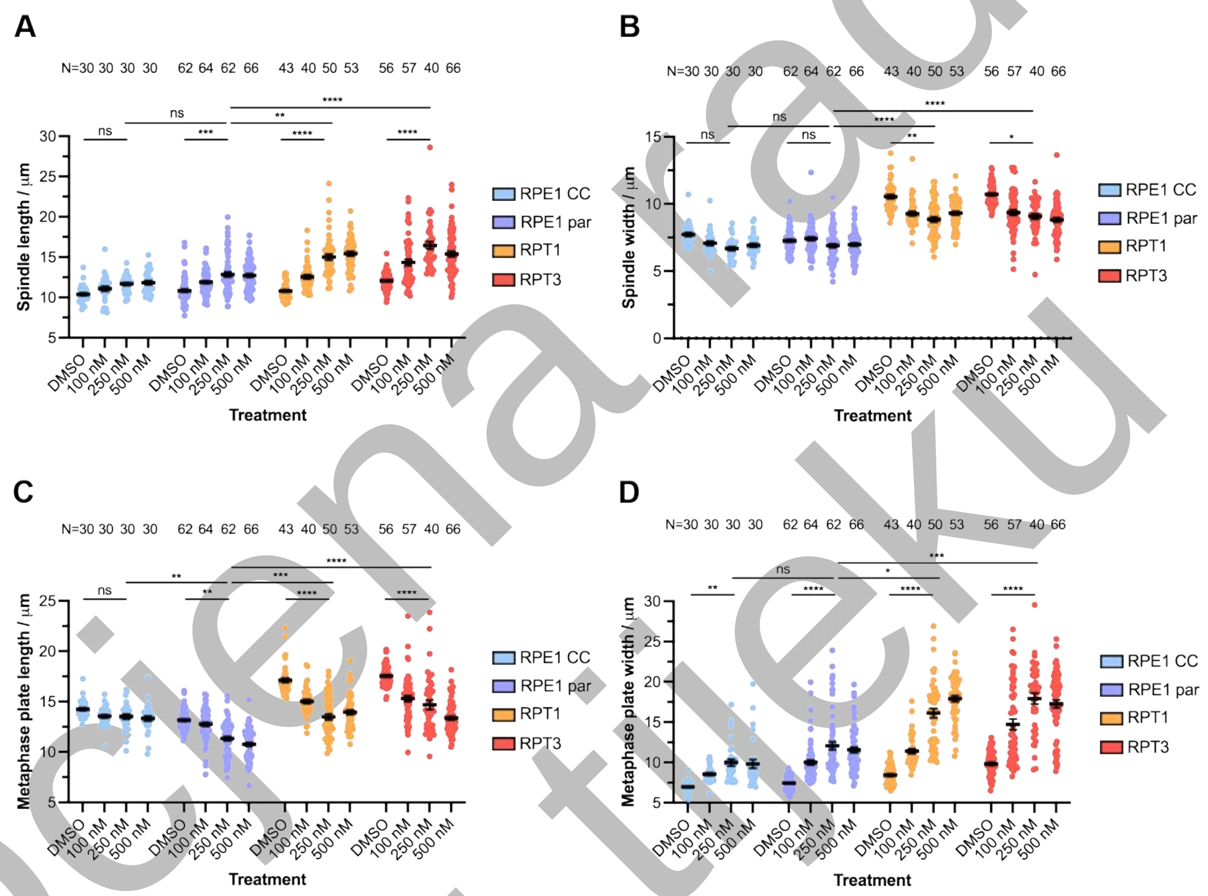

Figure 24. KIF18A inhibition affects spindle parameters. A) Spindle length after sovilnesib treatment in RPE1 CC, RPE1 parental, RPT1 and RPT3 cell lines. **B)** Spindle width after sovilnesib treatment. **C)** Metaphase plate length after sovilnesib treatment. **D)** Metaphase plate width after sovilnesib treatment.

Error bars represent mean value and SEM. Results were obtained from three independent experiment for all cell lines except for RPE1 CC, where one experiment was done. Statistical analysis: Kruskal-Wallis test with post-hoc Dunn's test was performed on a total number of cells for each cell line and sovilnesib concentration.

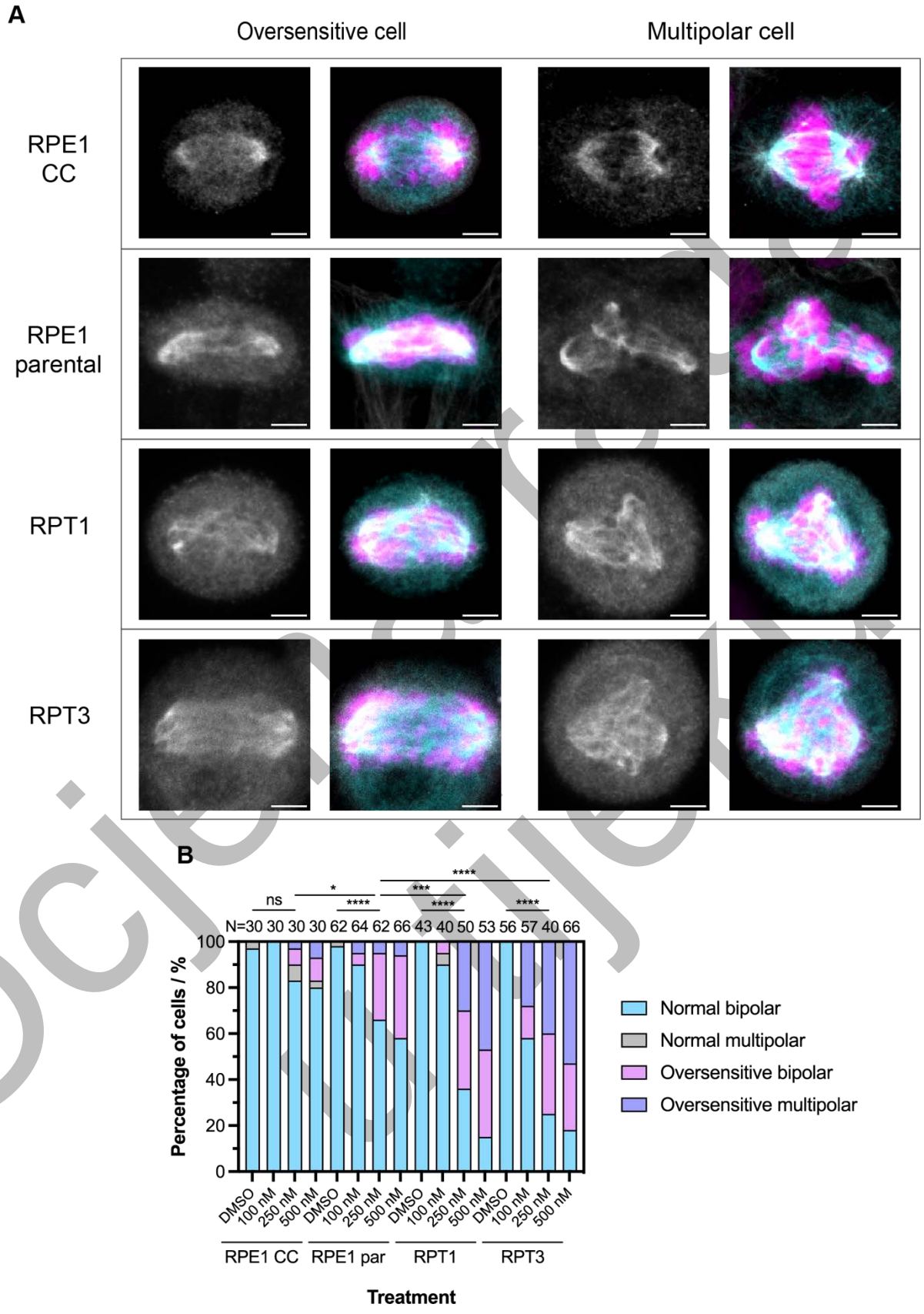

Figure 25. Caption on the following page.

Figure 25. A subpopulation of oversensitive cells occurs after KIF18A inhibition. A) Confocal images of immunostained RPE1 CC, RPE1 parental, RPT1 and RPT3 oversensitive and multipolar cells, treated with 250 nM sovilnesib. Cells were immunostained for KIF18A and tubulin, while DNA was labelled with DAPI. Left panels show KIF18A (grey), and right panels show merged images of KIF18A (cyan), tubulin (grey) and DNA (magenta) for RPE1 CC, RPE1 parental, RPT1 and RPT3. Images are shown as a SUM intensity projections. Scale bars, 5 μm. RPE1 CC is classified as a normal multipolar cell, while other multipolar cells shown are oversensitive multipolar. **B)** Distribution of phenotypes after sovilnesib treatment. Results were obtained from three independent experiments for all cell lines except for RPE1 CC, where one experiment was done. Statistical analysis: Chi-square test was performed. Ratio of outcomes was determined from a total number of cells for each incubation time for each cell line and sovilnesib concentration.

4.4. Low concentrations of sovilnesib have minor effects on diploid and PT cells

To determine whether previously used concentrations, 100 nM to 500 nM, were too high, and if lower doses could still inhibit KIF18A, RPE1 parental and RPT3 cells were treated with 10, 30, 50, and 70 nM sovilnesib and incubated for 24 hours before fixation and immunostaining. Control cells were treated with 0.014% DMSO, matching the amount used in the 70 nM sovilnesib treatment. Cells were immunostained for KIF18A and tubulin, while DNA was visualized with DAPI (Figure 26A). KIF18A localization on the spindle poles was not as clearly observed after treatment with low concentrations of sovilnesib compared to higher doses (Figure 26A). Line intensity profiles showed minimal differences between treated and control cells (Figure 26B). The greatest shift of KIF18A signal intensity toward spindle poles occurred at 50 nM and 70 nM concentrations. Quantification confirmed a slight increase in KIF18A intensity on spindle poles compared to controls (Figure 27B). Differences between RPE1 parental and RPT3 were observed only at 10 nM and 50 nM, but this could be due to microscopy limitations.

No significant changes in spindle length were observed (Figure 27B). Variations in spindle width and metaphase plate length reflected differences in ploidy levels (Gudlin et al., 2025) (Figures 27C-D). Increases in metaphase plate width were minor in both cell lines (Figure 27E). Low sovilnesib concentrations did not induce oversensitive cells, except a small fraction of oversensitive multipolar cells in RPT3 after 70 nM treatment (Figure 28). Normal multipolar cells were present in all RPT3 treatments, potentially due to the sovilnesib. In summary, low concentrations of sovilnesib caused only minor effects on KIF18A localization and spindle parameters, with minimal induction of oversensitive cells, suggesting limited effectiveness at low concentrations.

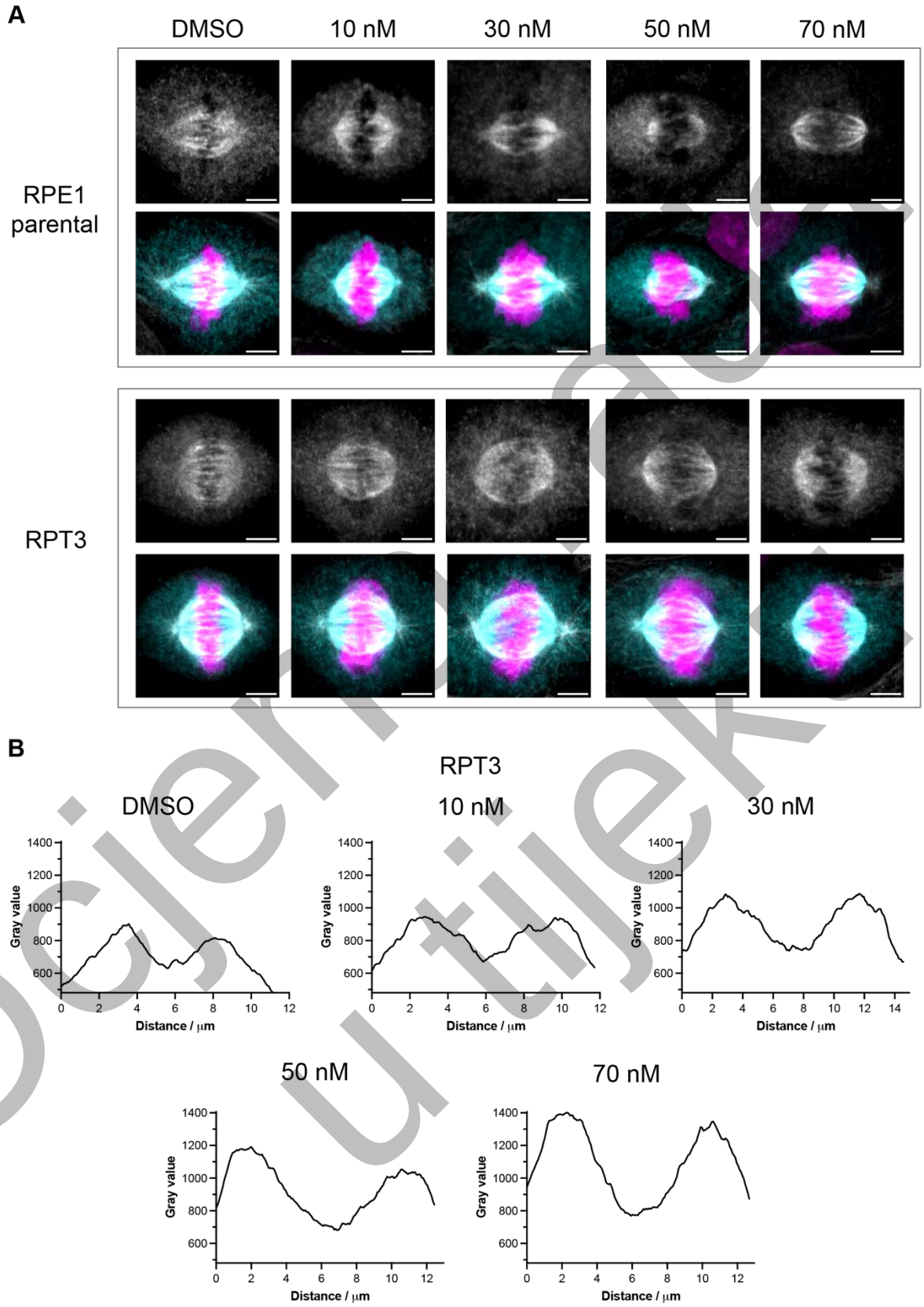

Figure 26. Caption on the following page.

Figure 26. Treatment with low doses of sovilnesib. A) Confocal images of immunostained RPE1 parental and RPT3 cells, treated with 10 nM, 30 nM, 50 nM and 70 nM sovilnesib. Control cells were treated with 0.014% DMSO. Cells were fixed 24 hours after the treatment and immunostained for KIF18A and tubulin, while DNA was labelled with DAPI. Upper panels show KIF18A (grey), and lower panels show merged images of KIF18A (cyan), tubulin (grey) and DNA (magenta) for RPE1 parental and RPT3. Images are shown as a SUM intensity projections. Scale bars, 5 μm. **B)** Line profile intensity of KIF18A signal on the spindle, for RPT3 cells shown in **A**.

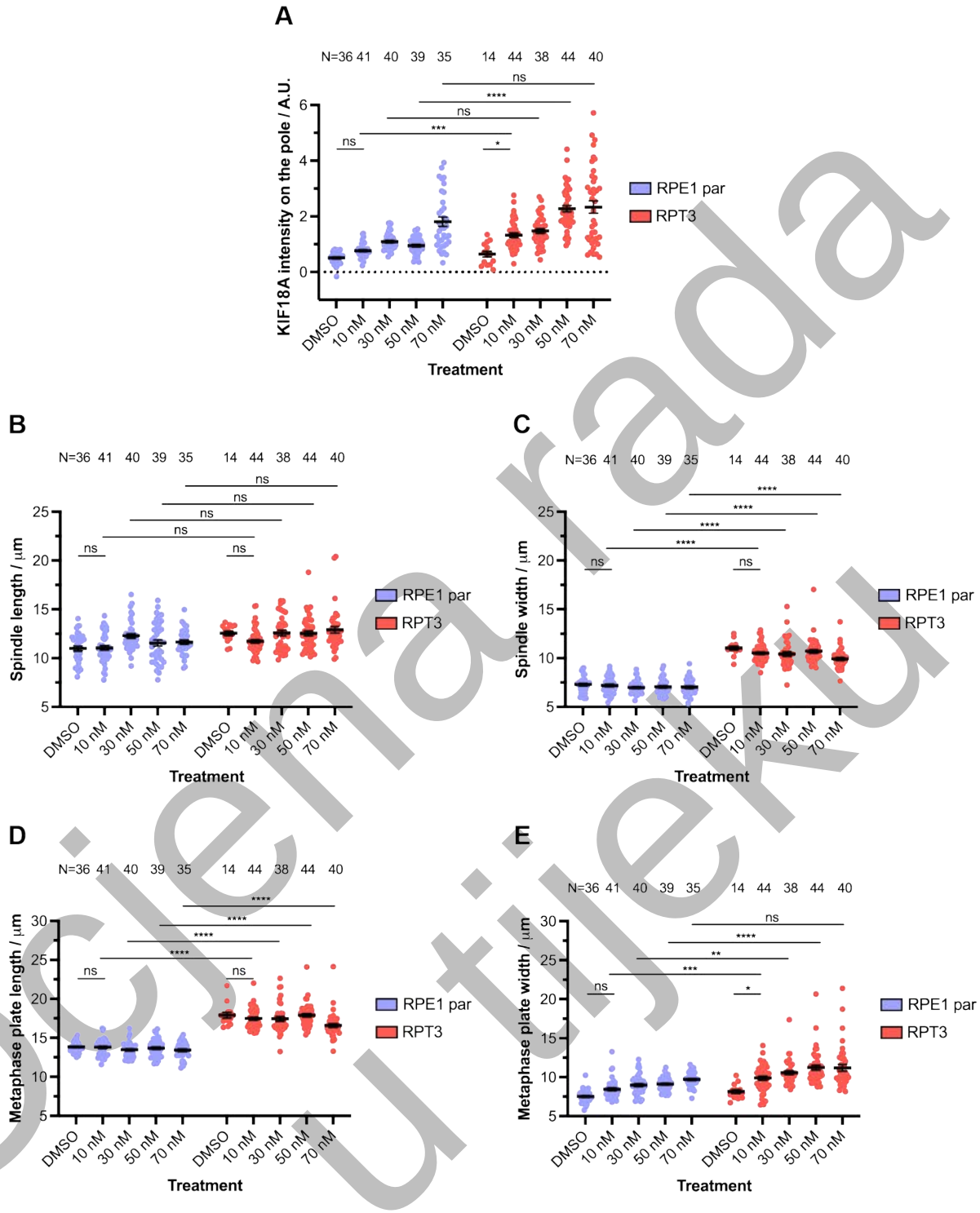

Figure 27. Caption on the following page.

Figure 27. Low doses of sovilnesib mildly affect spindle parameters. A) KIF18A intensity on the spindle pole in RPE1 parental and RPT3 cell lines after low doses sovilnesib treatment. **B)** Spindle length after low doses sovilnesib treatment. **C)** Spindle width after low doses sovilnesib treatment. **D)** Metaphase plate length after low doses sovilnesib treatment. **E)** Metaphase plate width after low doses sovilnesib treatment.

Error bars represent mean value and SEM. Results were obtained from three independent experiments for RPE1 parental, and from two independent experiments for RPT3. Statistical analysis: Kruskal-Wallis test with post-hoc Dunn's test was performed on a total number of cells for each sovilnesib concentration.

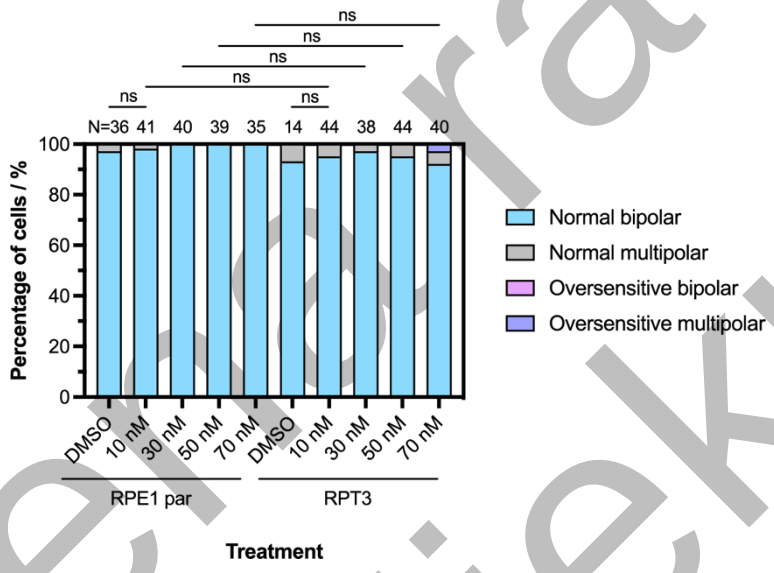

Figure 28. Most cells retain normal phenotype after low doses sovilnesib treatment. Distribution of phenotypes in RPE1 parental and RPT3 after low doses sovilnesib treatment. Results were obtained from three independent experiment for RPE1 parental, and from two independent experiments for RPT3. Statistical analysis: Fisher's exact test when compared groups had two outcomes, and Chi-square test if there were more than two outcomes (RPE1 par vs RPT3 – 70 nM). Ratio of outcomes was determined from a total number of cells for each sovilnesib concentration.

4.5. Sovilnesib effectively inhibits Kif18a for a minimum of seven days

Sovilnesib has proven to successfully inhibit KIF18A after 24 hours of treatment. To evaluate how its effectiveness changes over time, RPE1 parental and RPT3 cells were treated with 250 or 500 nM sovilnesib and incubated for up to seven days. Cells treated with 250 nM were fixed and immunostained after 24, 48, 72, 96 hours, and seven days, while those treated with 500 nM were fixed after 24, 48, 72 hours, and six days. Control cells received 0.05% and 0.1% DMSO, corresponding to the respective sovilnesib treatments.

After the treatment, KIF18A remained localized at the spindle poles for up to seven days in both cell lines (Figure 29, images shown for 250 nM treatment). Line intensity profiles across the spindle poles were generated for RPT3 cells treated with 250 nM sovilnesib (Figure 30A). The strongest KIF18A signal peak appeared at 24 hours. Smaller peaks persisted at later time points, though their intensity may vary due to differences in overall cell staining or microscopy conditions. Quantification of KIF18A intensity at spindle poles showed no significant differences between RPE1 parental and RPT3 cells for either treatment, except at 24 hours with 250 nM sovilnesib, when RPE1 parental cells exhibited higher intensity (Figures 30B-C).

Spindle length increased in both cell lines after both treatments, with RPT3 cells displaying generally longer spindles than RPE1 parental (Figures 31A-B). Spindle width and metaphase plate length slightly decreased following treatments but remained larger in RPT3 cells, consistent with their ploidy levels (Gudlin et al., 2025) (Figures 31C-F). Metaphase plate width increased significantly in RPT3 cells under both treatments, indicating persistent chromosome alignment defects for up to seven days (Figures 31G-H). An oversensitive subpopulation appeared after treatment with both 250 nM and 500 nM sovilnesib (Figure 32). The proportion of oversensitive cells was significantly higher in RPT3 compared to RPE1 parental. Notably, oversensitive RPE1 parental cells increased at the higher drug concentration but began to decline after 72 hours. To conclude, sovilnesib successfully inhibits KIF18A protein for up to seven days in both cell lines. Inhibition leads to altered spindle morphology and increased problems with chromosome alignment, which are more evident in PT cells.

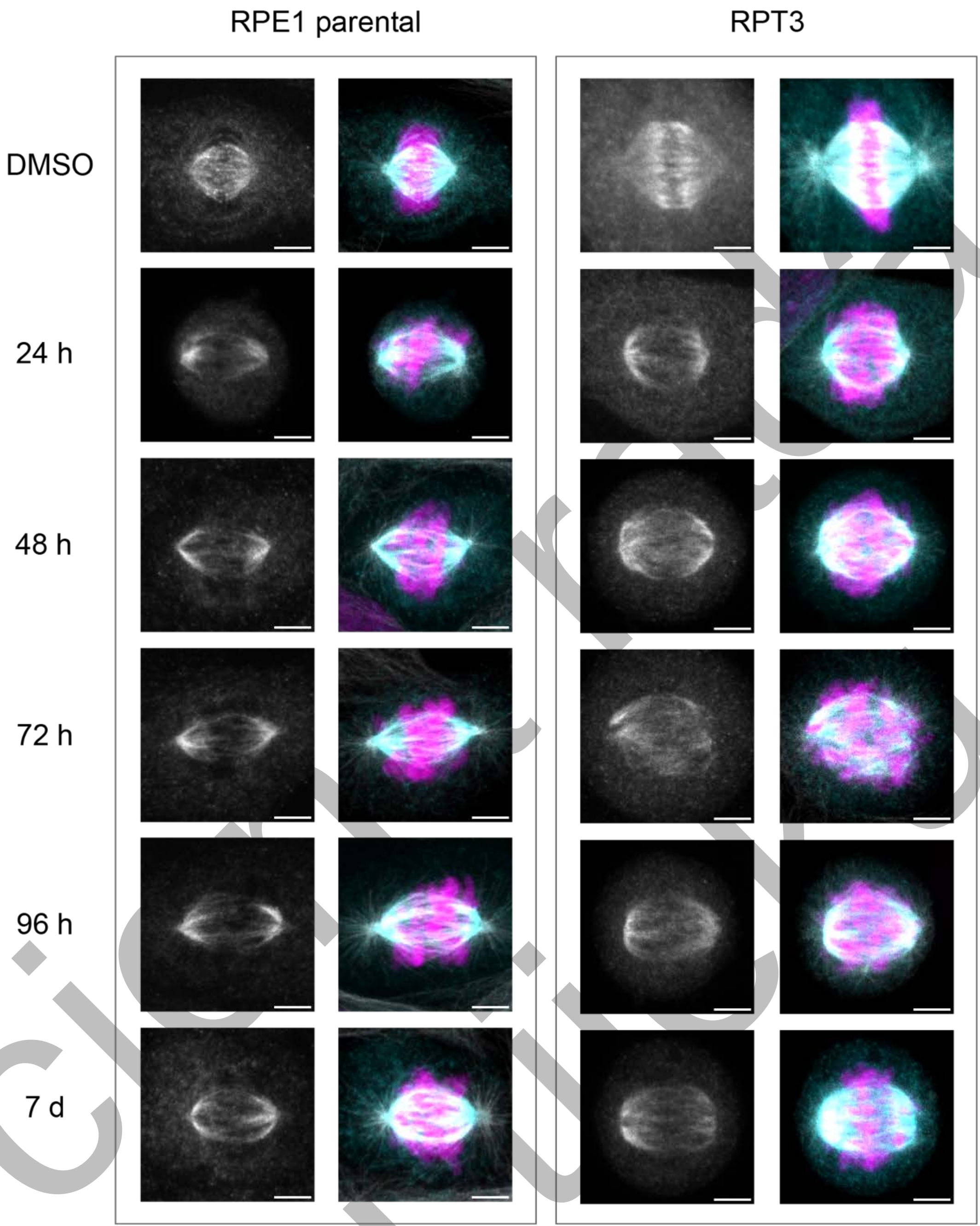

Figure 29. KIF18A inhibition effect lasts for seven days. Confocal images of immunostained RPE1 parental and RPT3 cells, treated with 250 nM sovilnesib for 24, 48, 72 96 hours and seven days. Control cells were treated with 0.05% DMSO and incubated for 24 hours. Cells were immunostained for KIF18A and tubulin, while DNA was labelled with DAPI. Left panels show KIF18A (grey), and right panels show merged images for KIF18A (cyan), tubulin (grey) and DNA (magenta) for RPE1 parental and RPT3 cells. Images are shown as a SUM intensity projections. Scale bars, 5 µm.

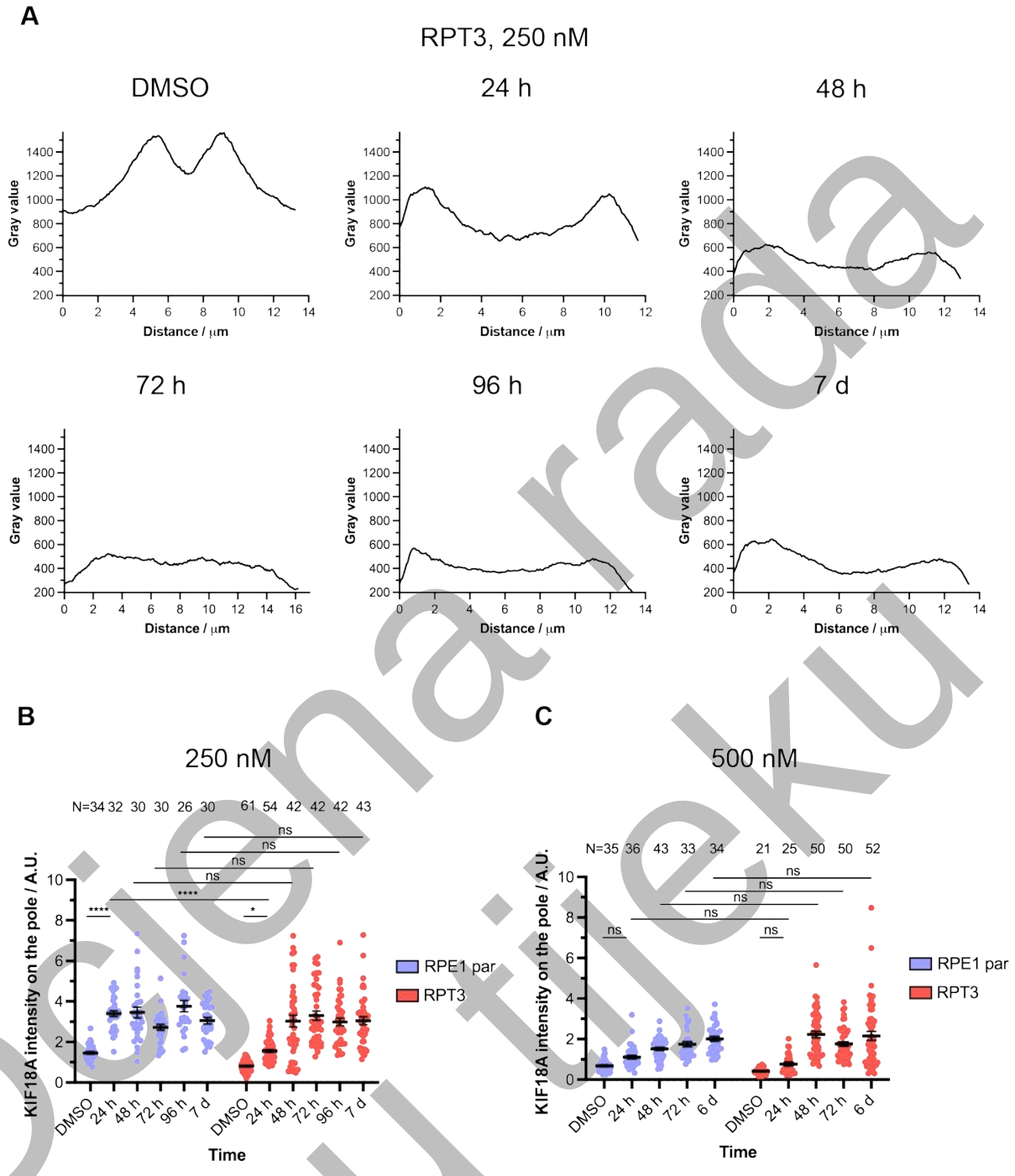

Figure 30. Caption on the following page.

Figure 30. KIF18A remains on the spindle poles for up to seven days following sovilnesib treatment. A) Line profile intensity of KIF18A signal on the spindle, for RPT3 cells shown in Figure 29. **B)** KIF18A intensity on the spindle pole in RPE1 parental and RPT3 after 250 nM sovilnesib treatment. Results were obtained from one experiment for RPE1 parental, and from two independent experiments for RPT3. **C)** KIF18A intensity on the spindle pole in RPE1 parental and RPT3 after 500 nM sovilnesib treatment. Cells were incubated for 24, 48, 72, hours and six days. Results were obtained from three independent experiments for each cell line. Error bars represent mean value and SEM. Statistical analysis: Kruskal-Wallis test with post-hoc Dunn's test was performed on a total number of cells for each incubation time.

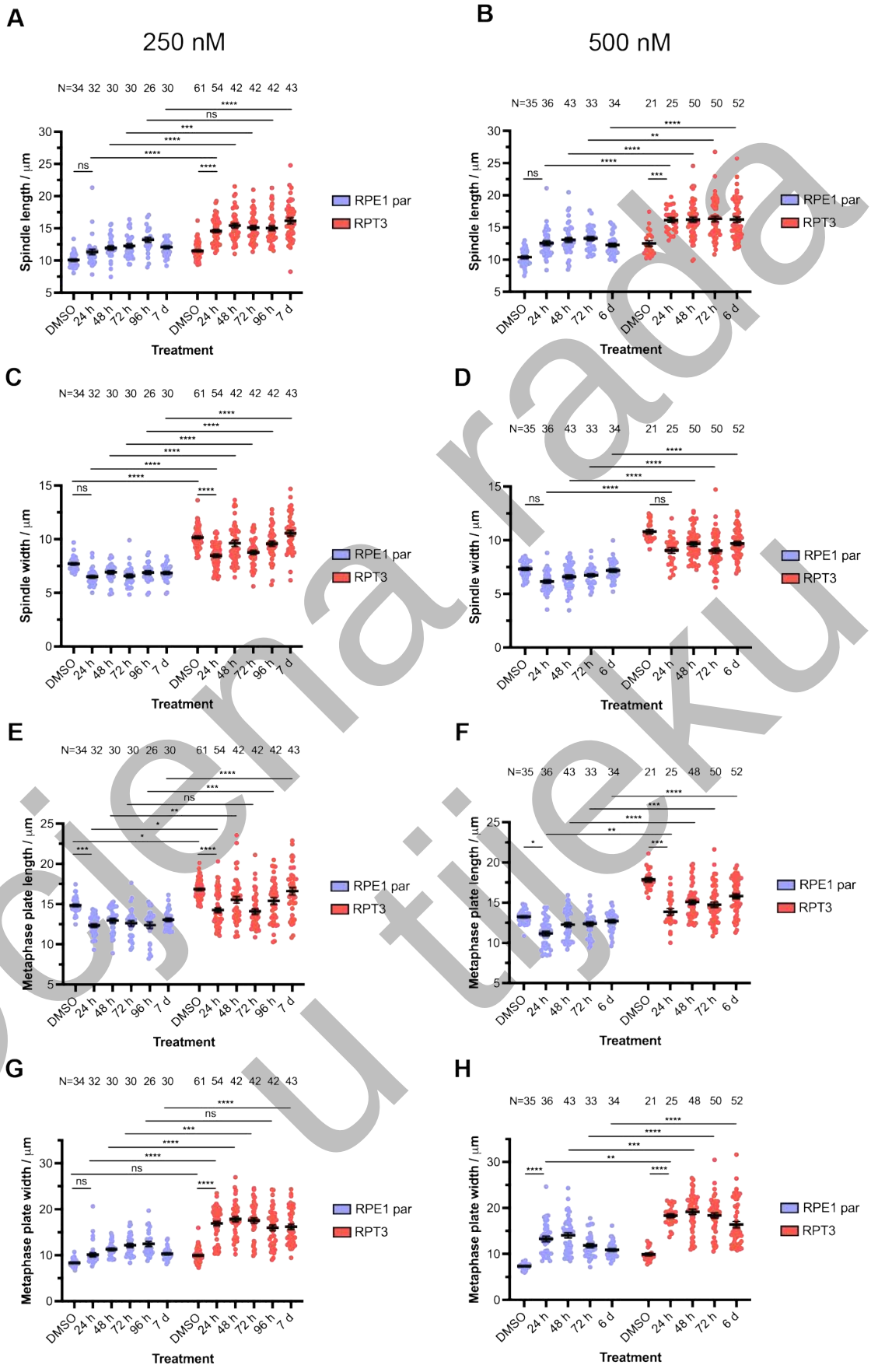

Figure 31. Caption on the following page.

Figure 31. Long-term treatment with sovilnesib affects spindle parameters. A) Spindle length after 250 nM sovilnesib treatment in RPE1 parental and RPT3 cells. **B)** Spindle length after 500 nM sovilnesib treatment. **C)** Spindle width after 250 nM sovilnesib treatment. **D)** Spindle width after 500 nM sovilnesib treatment. **E)** Metaphase plate length after 250 nM sovilnesib treatment. **F)** Metaphase plate length after 500 nM sovilnesib treatment. G) Metaphase plate width after 250 nM sovilnesib treatment. **H)** Metaphase plate width after 500 nM sovilnesib treatment.

Error bars represent mean value and SEM. Results for 250 nM sovilnesib treatment were obtained from one experiment for RPE1 parental, and from two independent experiments for RPT3. Results for 500 nM sovilnesib treatment were obtained from three independent experiments for both cell lines. Statistical analysis: Kruskal-Wallis test with post-hoc Dunn's test was performed on a total number of cells for each incubation time.

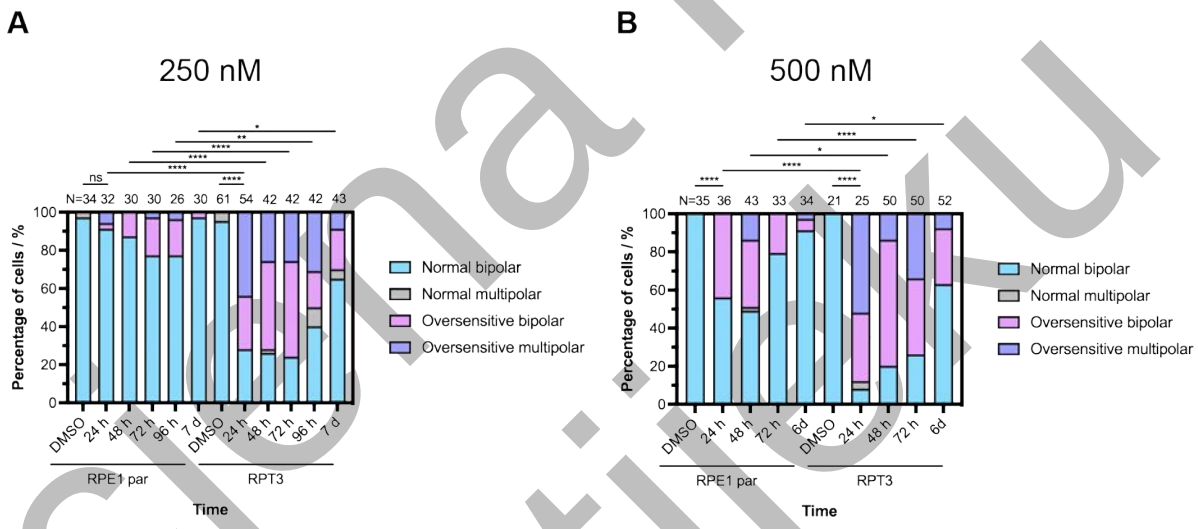

Figure 32. A subpopulation of oversensitive cells occurs after the long-term sovilnesib treatment. A) Distribution of phenotypes in RPE1 parental and RPT3 cells after long-term 250 nM sovilnesib treatment. Results were obtained from one experiment for RPE1 parental, and from two independent experiments for RPT3. **B)** Distribution of phenotypes in RPE1 parental and RPT3 cells after long-term 500 nM sovilnesib treatment. Results were obtained from three independent experiments for each cell line.

Statistical analysis: Fisher's exact test when compared groups had two outcomes (RPE1 par – DMSO vs 24 h, 500 nM), and Chi-square test if there were more than two outcomes. Ratio of outcomes was determined from a total number of cells for each incubation time.

4.6. Effects of dual KIF18A depletion and inhibition on diploid and PT cell lines

It was unexpected that sovilnesib had such a severe effect on both diploid and PT RPE1 cells, which are generally considered to be independent on KIF18A for proliferation (Gliech et al., 2024). This could indicate either a high inhibitor efficiency or potential non-specific effects of sovilnesib. To investigate this, a double treatment was performed in which RPE1 parental and RPT3 cells were exposed to both 100 nM KIF18A siRNA and 250 nM sovilnesib. Cells were incubated for 24, 48, and 72 hours before fixation and immunostaining. Control cells were treated with 100 nM non-targeting siRNA and 0.05% DMSO and incubated for 24 hours.

After KIF18A was both depleted and inhibited there was no KIF18A localization on the spindle in both RPE1 parental and RPT3 (Figure 33A). Line intensity profiles confirmed the absence of KIF18A signal peaks after double treatment, although total signal intensity varied in some cases, such as in RPT3 cells shown in the example image, which may be attributed to variability in immunostaining or microscopy (Figures 33A-B). Quantification revealed a significant decrease in KIF18A intensity both across the spindle and at the spindle poles, with no differences between the cell lines (Figures 33C-D).

Spindle length slightly increased after the treatment, but there was no difference between the cell lines (Figure 34A). Differences in spindle width and metaphase plate length were consistent with variations in ploidy, as observed in previous experiments (Gudlin et al., 2025) (Figures 34B-C). Metaphase plate width increased as expected but remained similar between the cell lines (Figure 34D). A subpopulation of oversensitive cells significantly increased in both cell lines following the double treatment, with RPT3 exhibiting a higher proportion of oversensitive multipolar cells (Figure 35).

Double treatment was also compared to KIF18A depletion alone. No differences were observed in KIF18A spindle intensity or spindle length between the two treatments at 24 hours in either cell line (Figures 36A-B). Metaphase plate width remained the same in both conditions in RPT3 but was larger in RPE1 parental following double treatment (Figure 36C).

The proportion of oversensitive cells was higher after the double treatment than after KIF18A depletion alone in both cell lines (Figure 21C, Figure 35B). However, RPT3 cells exhibited a much greater fraction of oversensitive cells following treatment with the inhibitor alone (Figure 32A). The combined KIF18A depletion and inhibition treatment results in spindle phenotypes comparable to the depletion alone (Figure 36). However, the proportion of oversensitive cells is higher than with the depletion alone, but for PT cells not as high than with the inhibition alone (Figure 36D). It is not clear whether this is the synergistic effect of siRNA and inhibitor combined, or the inhibitor itself has some off-target binding sites, but this is yet to be determined in further studies.

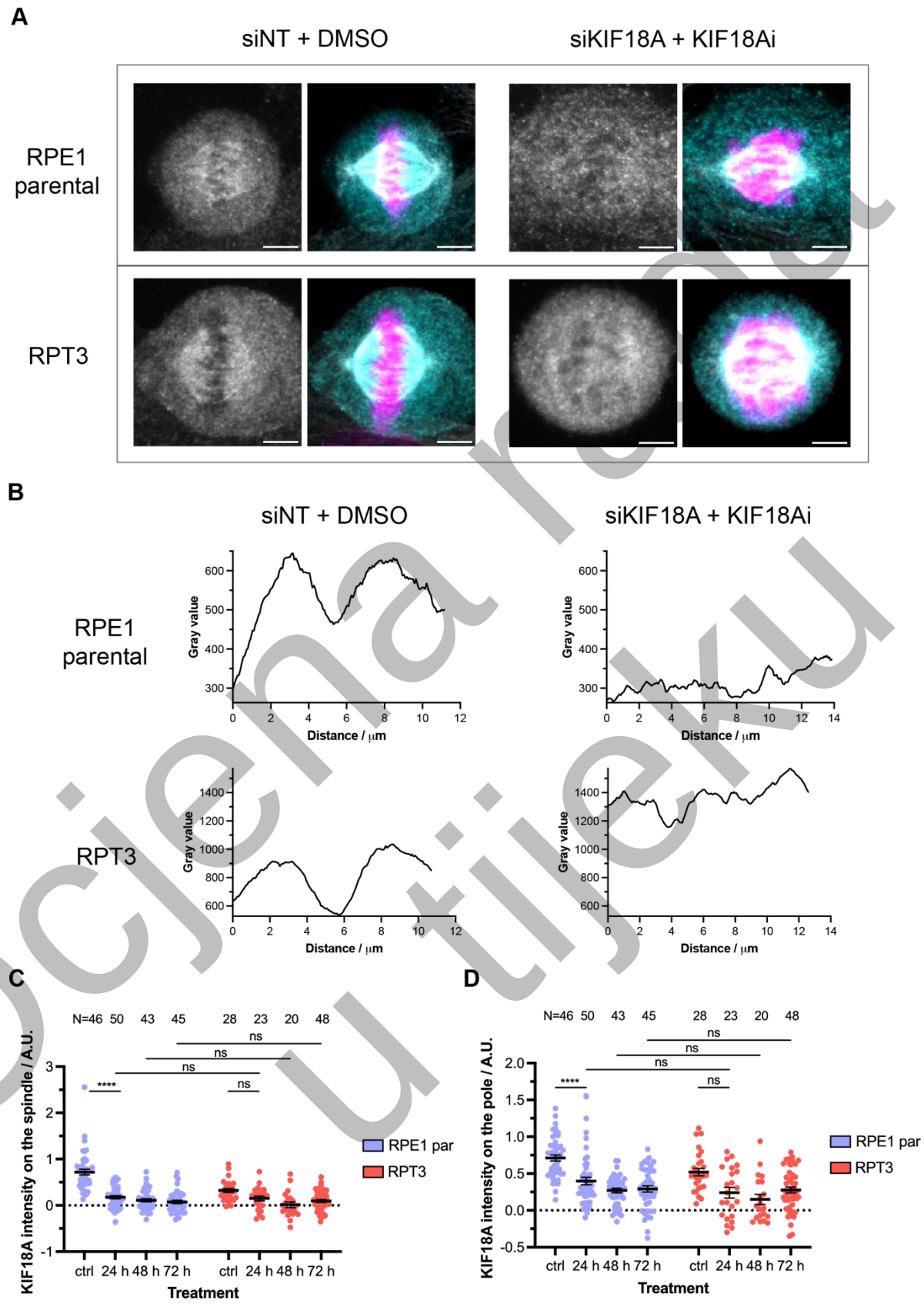

Figure 33. Caption on the following page.

Figure 33. KIF18A does not localize on the spindle after the double treatment. A) Confocal images of immunostained RPE1 parental and RPT3 cells, treated with 100 nM KIF18A siRNA and 250 nM sovilnesib for 24, 48 and 72 hours. Control cells were treated with 100 nM non-targeting siRNA and 0.05% DMSO and incubated for 24 hours. Cells were immunostained for KIF18A and tubulin, while DNA was labelled with DAPI. Left panels show KIF18A (grey), and right panels show merged images for KIF18A (cyan), tubulin (grey) and DNA (magenta) for RPE1 parental and RPT3 cells. Images are shown as a SUM intensity projections. Scale bars, 5 μm. **B)** Line profile intensity of KIF18A signal on the spindle, for RPE1 parental and RPT3 cells shown in **A**. **C)** KIF18A intensity on the spindle after the double treatment. The percentage of silencing efficiency in RPE1 parental is following: 24 h – 75.2%, 48 h – 84.5% and 72 h – 89.4%. Silencing efficiency in RPT3 is following: 24 h – 53.2%, 48 h – 95.7% and 72 h – 70.5%. **D)** KIF18A intensity on the spindle pole after the double treatment. Error bars represent mean value and SEM. Results were obtained from three independent experiments for RPE1 parental, and for RPT3 cells one experiment was done for control group, 24 and 48 hours, while two independent experiments were done for 72 hours. Statistical analysis: Kruskal-Wallis test with post-hoc Dunn's test was performed on a total number of cells for each incubation time.

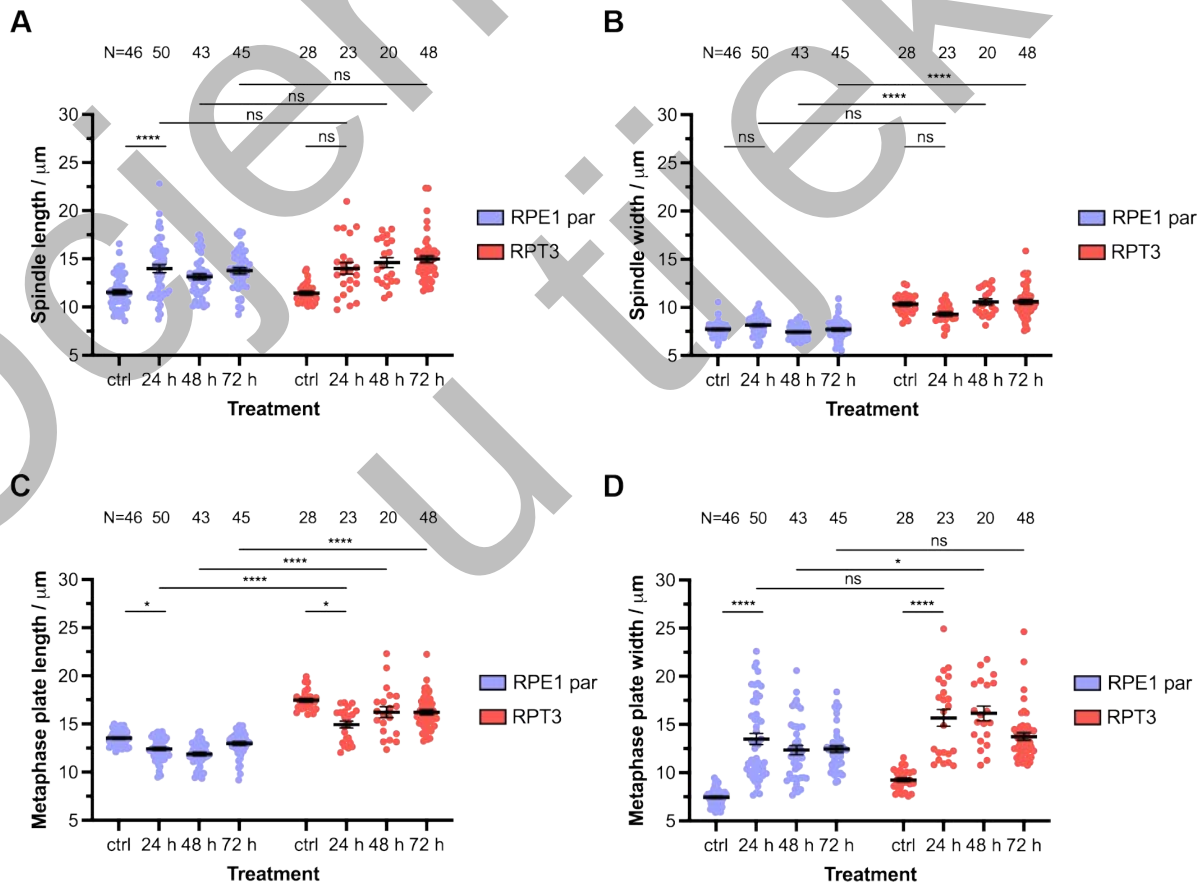

Figure 34. Caption on the following page.

Figure 34. Double treatment affects spindle parameters. A) Spindle length after the double treatment in RPE1 parental and RPT3. **B)** Spindle width after the double treatment. **C)** Metaphase plate length after the double treatment. **D)** Metaphase plate width after the double treatment.

Error bars represent mean value and SEM. Results were obtained from three independent experiments for RPE1 parental, and for RPT3 cells one experiment was done for control group, 24 and 48 hours, while two independent experiments were done for 72 hours. Statistical analysis: Kruskal-Wallis test with post-hoc Dunn's test was performed on a total number of cells for each incubation time.

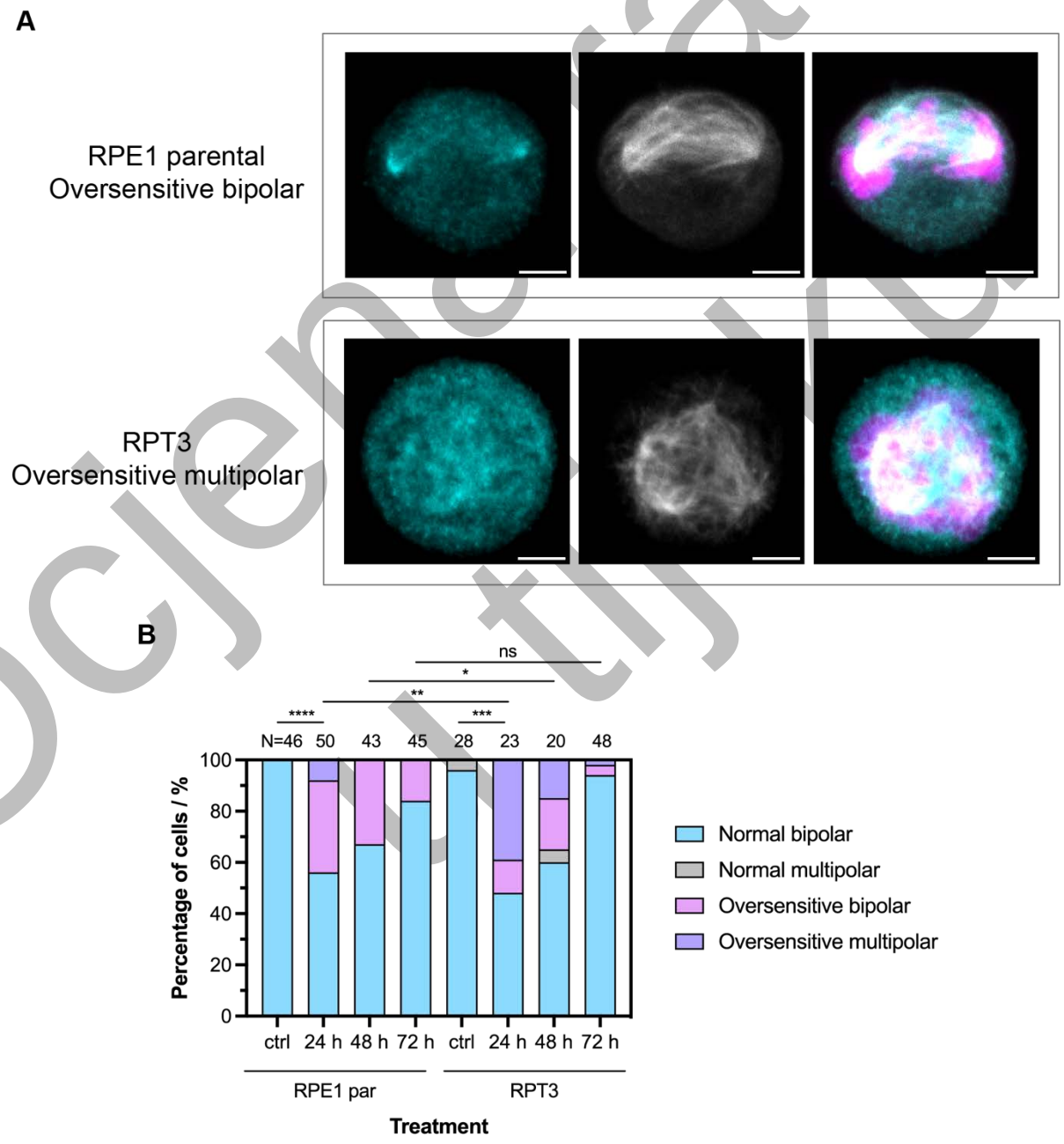

Figure 35. Caption on the following page.

Figure 35. A subpopulation of oversensitive cells occurs after double treatment. A) Confocal images of immunostained RPE1 parental and RPT3 cells, treated with 100 nM KIF18A siRNA and 250 nM sovilnesib. Control cells were treated with 100 nM non-targeting siRNA and 0.05% DMSO. Cells were fixed 24 hours after the treatment and immunostained for KIF18A and tubulin, while DNA was labelled with DAPI. Left panels show KIF18A (cyan), middle panel shows tubulin (grey), and right panels show merged images with DNA (magenta) for RPE1 parental and RPT3. **B)** Distribution of phenotypes after double treatment in RPE1 parental and RPT3 cells. Results were obtained from three independent experiments for RPE1 parental, and for RPT3 cell line one experiment was done for control group, 24 and 48 hours, while two independent experiments were done for 72 hours. Statistical analysis: Chi-square test was performed. Ratio of outcomes was determined from a total number of cells for each incubation time.

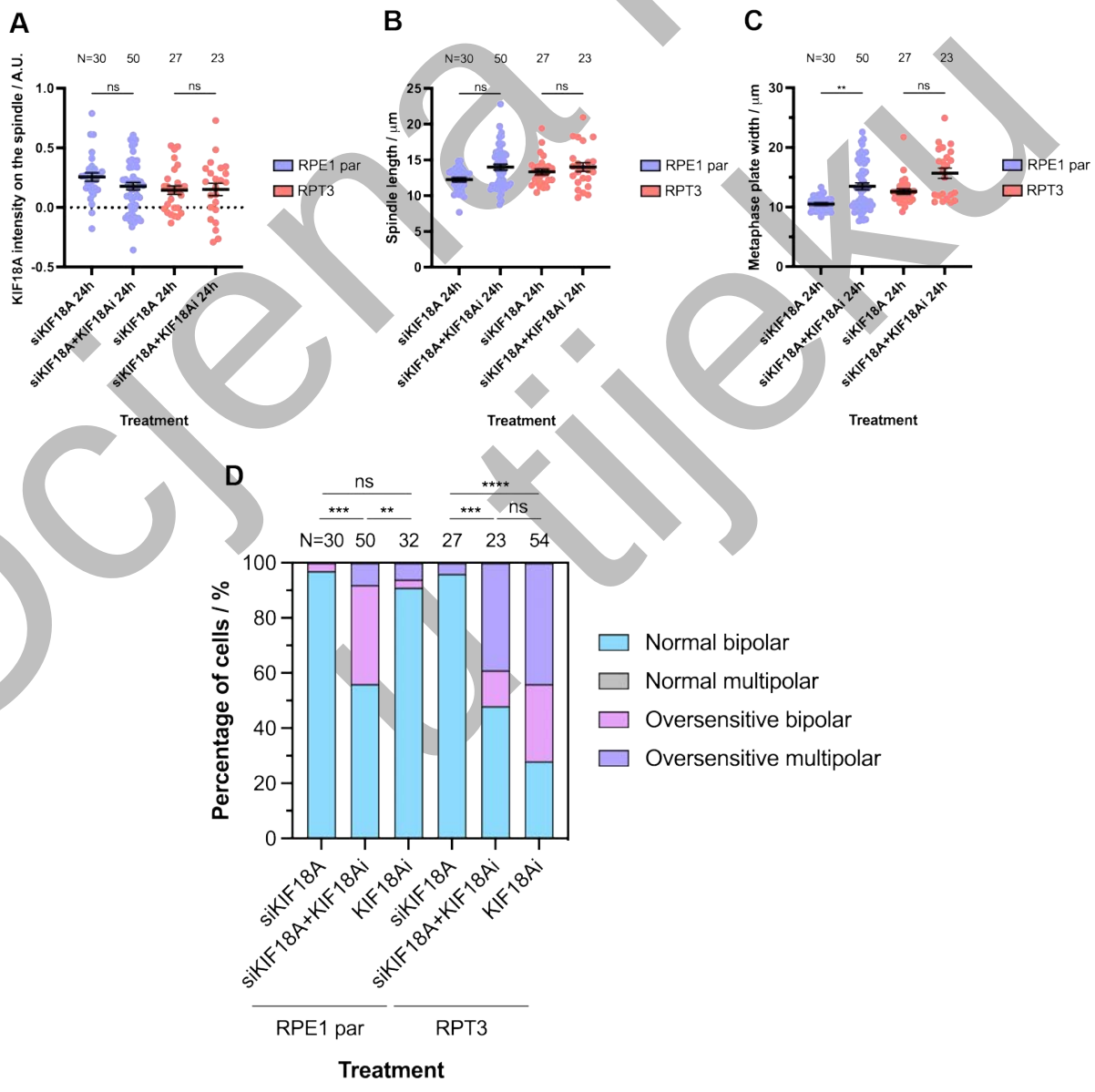

Figure 36. Comparison of double treatment with KIF18A depletion. Comparison of RPE1 parental and RPT3 cells treated with 100 nM KIF18A siRNA (Figure 19-20) and with the double treatment: 100 nM KIF18A siRNA and 250 nM sovilnesib (Figure 33-34) and incubated for 24 hours. **A)** Comparison of KIF18A intensity on the spindle after KIF18A depletion and double treatment. **B)** Comparison of spindle length after KIF18A depletion and double treatment. **C)** Comparison of metaphase plate width after KIF18A depletion and double treatment.
Error bars represent mean value and SEM. Results were obtained from one experiment for KIF18A depletion and from three independent experiments for RPE1 parental and one experiment for RPT3 cells for double treatment. Statistical analysis: Kruskal-Wallis test with post-hoc Dunn's test was performed on a total number of cells for each cell line and each treatment. **D)** Comparison of phenotypes ratios after KIF18A depletion, double treatment and KIF18A inhibition in RPE1 parental and RPT3 cells after 24 hours treatment. Numbers of independent experiments are stated in Figure 21C, Figure 35B and Figure 32A. Statistical analysis: Chi-square test. Ratio of outcomes was determined from a total number of cells for each cell line and each treatment.

4.7. Mitosis duration is severely affected with KIF18A depletion and inhibition

It was shown that KIF18A depletion and inhibition cause only minor mitosis prolongation in insensitive cells, that does not lead to mitotic arrest or mis-segregation errors (Cohen-Sharir et al., 2021; Gliech et al., 2024; Marquis et al., 2021; Quinton et al., 2021). Moreover, oversensitive cells have not been described in detail so far. A similar phenotype was reported by Marquis and colleagues, who showed that it results from PCM fragmentation in CIN+ cells, such as MDA-MB-231 and HT29 (Marquis et al., 2021). To investigate potential differences in mitotic duration between diploid and PT cell lines after depletion or inhibition, and to analyze mitotic behavior of oversensitive cells, live-cell imaging was performed. RPE1 CC, RPE1 parental, RPT1, and RPT3 cells were treated with 100 nM KIF18A siRNA or 250 nM sovilnesib. Control cells were treated with 100 nM non-targeting siRNA or 0.05% DMSO, respectively.

Mitotic cells were classified into three subpopulations: normal cells, cells with anaphase errors, and oversensitive cells (Figure 37A). Cells were considered normal only if they divided into two daughter cells without any anaphase errors or micronuclei formation before or after mitosis. To ensure accuracy, cells were defined as normal only if all M-phase subphases were imaged, from prophase to cytokinesis, and if the entire cell was within the field of view. Cells with anaphase errors included those displaying misaligned chromosomes in anaphase, lagging chromosomes, chromosome bridges, or micronuclei. Normal multipolar cells were also categorized in this subpopulation. Oversensitive cells included both bipolar

and multipolar cells characterized by extreme mitotic delay and specific phenotypes, even when full mitosis was not captured. These cells were characterized by severe chromosome misalignment and hyperoscillations. Chromosomes are behind spindle poles, and they move back and forth between spindle pole and spindle midzone, and they often had longer spindle.

Cells for which subpopulation classification was not possible were labeled as “not determined” or N.D. These included cells without a complete progression through mitosis, cells partially out of frame, or those that were out of focus. The proportion of N.D. cells was approximately 30% to 50% for depletion experiments and 10% to 30% for inhibition experiments. This percentage was consistent across the groups, and did not affect the statistical analysis, so these cells were excluded from subpopulation analysis. Mitosis duration was measured from NEBD to anaphase onset. As many cells with extremely prolonged mitosis were only partially imaged, and since this influenced the mean mitotic duration, analysis guidelines were applied: all fully imaged mitoses and partially imaged mitoses that lasted longer than 200 minutes were included. For all mitoses lasting over 200 minutes, whether full or partial, their duration was set to a maximum of 200 minutes. Oversensitive cells had extremely prolonged mitosis, that lasted up to 30 hours.

Mitosis duration was prolonged after both KIF18A depletion and inhibition in all cell lines, except for RPT3 cells following KIF18A depletion, which may be due to shorter imaging (Figure 37B-C). Interestingly, RPE1 parental cells exhibited a significant increase in mitotic duration after both depletion and inhibition. In a previous study, the mean mitotic duration following KIF18A inhibition with AM-1882 in diploid RPE1 cells was 55 minutes (Gliech et al., 2024), whereas in this experiment, treatment with Sovilnesib resulted in a mean duration of 93 minutes for RPE1 parental (Figure 37C). There should be no difference between the two diploid RPE1 cell lines, but the observed variation in mitotic duration may be due to differences in the potency of the two KIF18A inhibitors. The increase in mitotic duration following KIF18A depletion and inhibition was notably smaller in RPE1 CC cells compared to RPE1 parental cells, which was unexpected, considering that both cell lines are diploid.

After silencing, there was no difference in mitotic duration between RPE1 parental and PT cell lines, which differs from the results obtained in a previous study, where mitotic duration was longer in PT cell lines. Also, mitosis lasted shorter in all cell lines compared to the results obtained in this experiment (Cohen-Sharir et al., 2021) (Figure 37B). In the study by Cohen-Sharir and colleagues, the same cell lines and KIF18A siRNA from the same manufacturer were used, but at a lower concentration of 25 nM (Cohen-Sharir et al., 2021), compared to 100 nM siRNA used in this experiment, which could explain the stronger effects observed here.

Sovilnesib treatment caused an even greater increase in mitotic duration compared to depletion (Figure 37C). Notably, the difference between diploid and PT cell lines became more apparent after inhibition, suggesting that PT cells have increased sensitivity to KIF18A inhibition, despite being classified as insensitive (Gliech et al., 2024). Interestingly, after KIF18A depletion fraction of cells with anaphase errors was similar in all cell lines. After sovilnesib treatment fraction of cells with anaphase errors was higher in diploid cell lines, compared to PT cell lines, but this is probably because oversensitive subpopulation predominates after KIF18A inhibition.

After KIF18A depletion, there was no difference in the distribution of mitotic subpopulations among RPE1 parental, RPT1, and RPT3 cells. Similar to results for mitotic timing, RPE1 CC cells did not follow this pattern, they showed only an increase in the proportion of cells with anaphase errors, while the fraction of oversensitive cells remained below 5%. In contrast, KIF18A inhibition revealed a clear distinction between diploid and PT cell lines, with no significant difference between diploids themselves, as expected. Notably, the oversensitive subpopulation predominated after inhibition, indicating that these cells are highly sensitive to KIF18A inhibition with sovilnesib.

Overall, the results show that KIF18A depletion and inhibition both prolonged mitosis across all cell lines, with sovilnesib having a stronger effect than siRNA. While depletion did not reveal significant differences between diploid and PT cell lines, inhibition highlighted increased mitotic duration and a higher proportion of oversensitive cells specifically in PT lines. RPE1 CC cells showed a milder phenotype, compared to RPE1 parental.

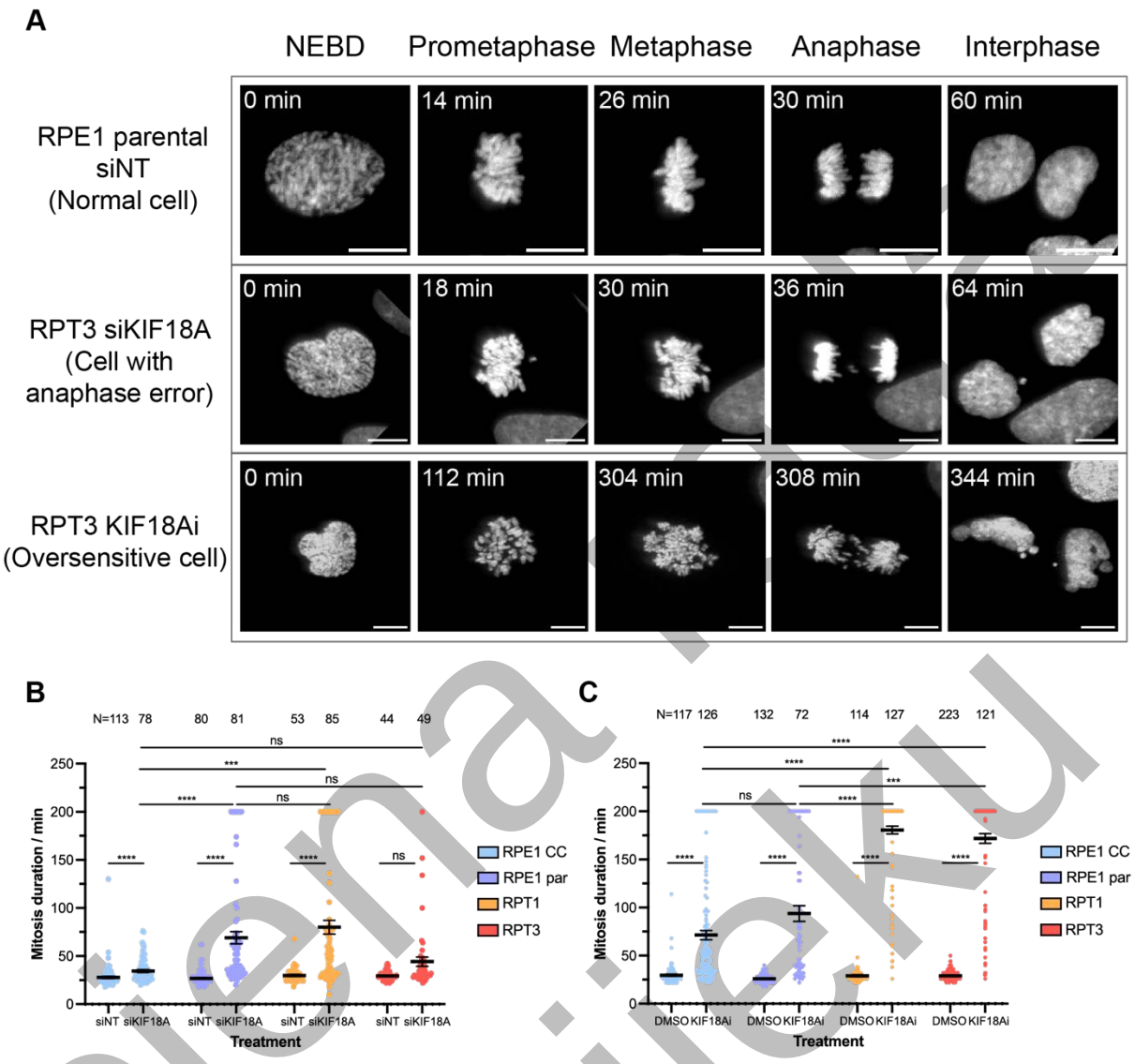

Figure 37. Caption on the following page.

Figure 37. KIF18A depletion and inhibition severely affect mitosis duration. A) Time-lapse images from lattice lightsheet of RPE1 parental and RPT3 cells stably expressing H2B-GFP (grey) throughout mitosis. Images show normal cell that divided without mis-segregation errors (upper panel, RPE1 parental, non-targeting siRNA), cell with anaphase error (middle panel, RPT3, KIF18A siRNA) and oversensitive cell (lower panel, RPT3, sovilnesib). Images show maximum intensity projections. Scale bars, 10 μm. **B)** Mitosis duration in RPE1 CC, RPE1 parental, RPT1 and RPT3, treated with 100 nM KIF18A siRNA. Control cells were treated with 100 nM non-targeting siRNA. Results were obtained from the following number of independent experiments: RPE1 CC; siNT – two, siKIF18A – four, RPE1 parental; siNT – four, siKIF18A – five, RPT1; siNT and siKIF18A – eight, RPT3; siNT – seven, siKIF18A – six. **C)** Mitosis duration in RPE1 CC, RPE1 parental, RPT1 and RPT3, treated with 250 nM sovilnesib. Control cells were treated with 0.05% DMSO. Results were obtained from the following number of independent experiments: RPE1 CC; DMSO and KIF18Ai – two, RPE1 parental; DMSO – two, KIF18Ai – three, RPT1; DMSO – two, KIF18Ai – three, RPT3 DMSO and KIF18Ai – three.

Error bars represent mean value and SEM. Statistical analysis: Kruskal-Wallis test with post-hoc Dunn's test was performed on a total number of cells for each cell line and each treatment.

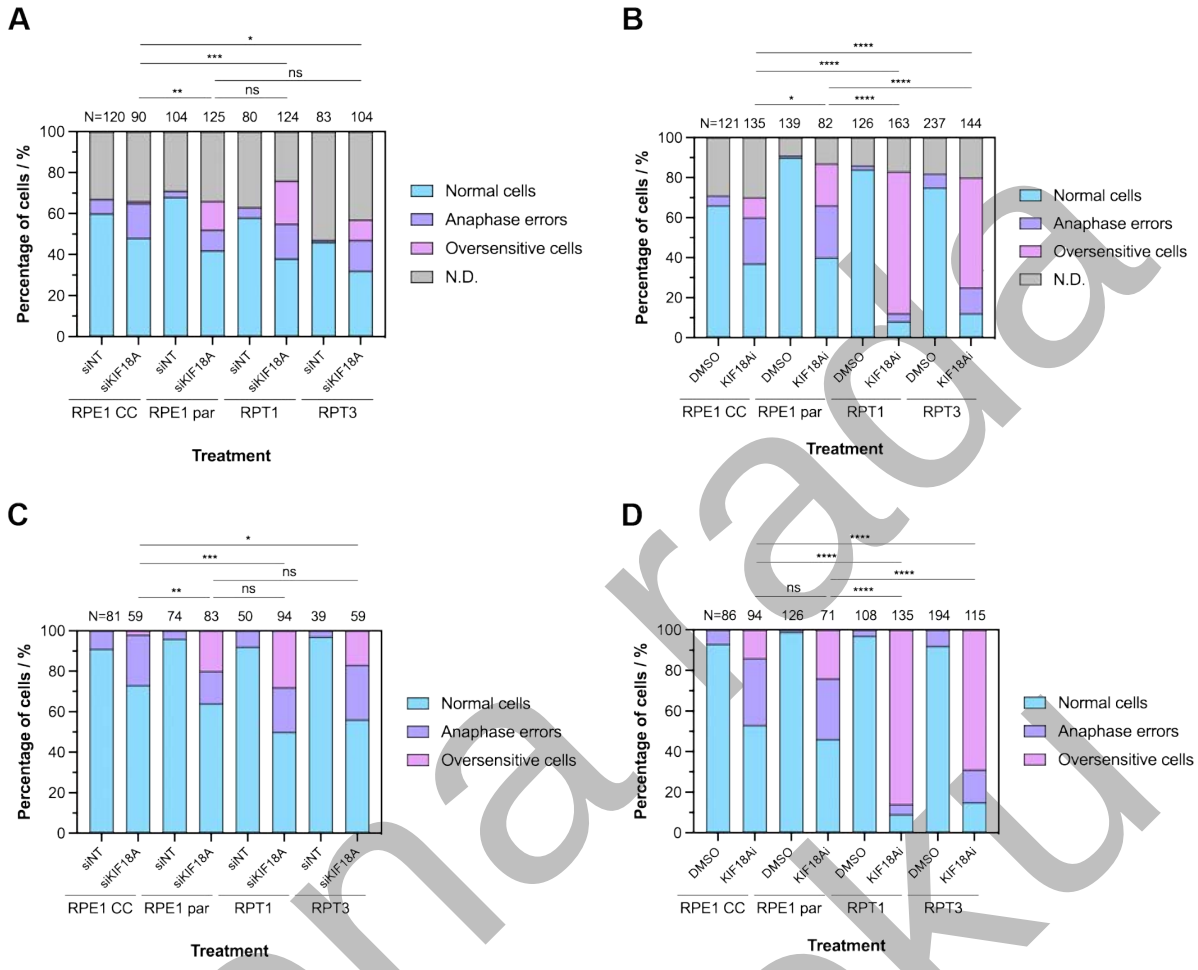

Figure 38. Live-cell imaging shows that a fraction of oversensitive cells differ after KIF18A depletion and inhibition. A) Distribution of phenotypes after KIF18A depletion in RPE1 CC, RPE1 parental, RPT1 and RPT3 cells. Results were obtained from the following number of independent experiments: RPE1 CC; siNT – two, siKIF18A – four, RPE1 parental; siNT – four, siKIF18A – five, RPT1; siNT and siKIF18A – eight, RPT3; siNT – seven, siKIF18A – six. **B)** Distribution of phenotypes after KIF18A inhibition in RPE1 CC, RPE1 parental, RPT1 and RPT3 cells. Results were obtained from the following number of independent experiments: RPE1 CC; DMSO and KIF18Ai – two, RPE1 parental; DMSO – two, KIF18Ai – three, RPT1; DMSO – two, KIF18Ai – three, RPT3 DMSO and KIF18Ai – three.

C) The same data shown in **A**, but N.D. is excluded. **D)** The same data shown in **B**, but N.D. is excluded.

Statistical analysis: Chi-square test was performed. Ratio of outcomes was determined from a total number of cells for each cell line and each treatment.

4.8. Sovilnesib treatment induces dynamic changes in spindle polarity

Experiments on fixed cells revealed that many oversensitive cells are also multipolar, and their frequency increased after sovilnesib treatment. Live-cell imaging showed that spindle polarity changes over time (Figure 39A). Spindles transitioned from bipolar to tripolar, tetrapolar, and even pentapolar spindles, back and forth (Figure 39B). In some transitions only minor poles formed (Figure 39A, Cell 2, middle panel), while others exhibited characteristic tripolar or tetrapolar shape. Although only chromosomes were visible in these images, spindle shape can be predicted, as in oversensitive cells chromosomes are localized behind spindle poles. It has been shown that KIF18A loss can cause multipolar spindles due to PCM fragmentation in sensitive CIN+ cells (Marquis et al., 2021). This may explain the formation of multipolar spindles during mitosis rather than at the beginning of mitosis.

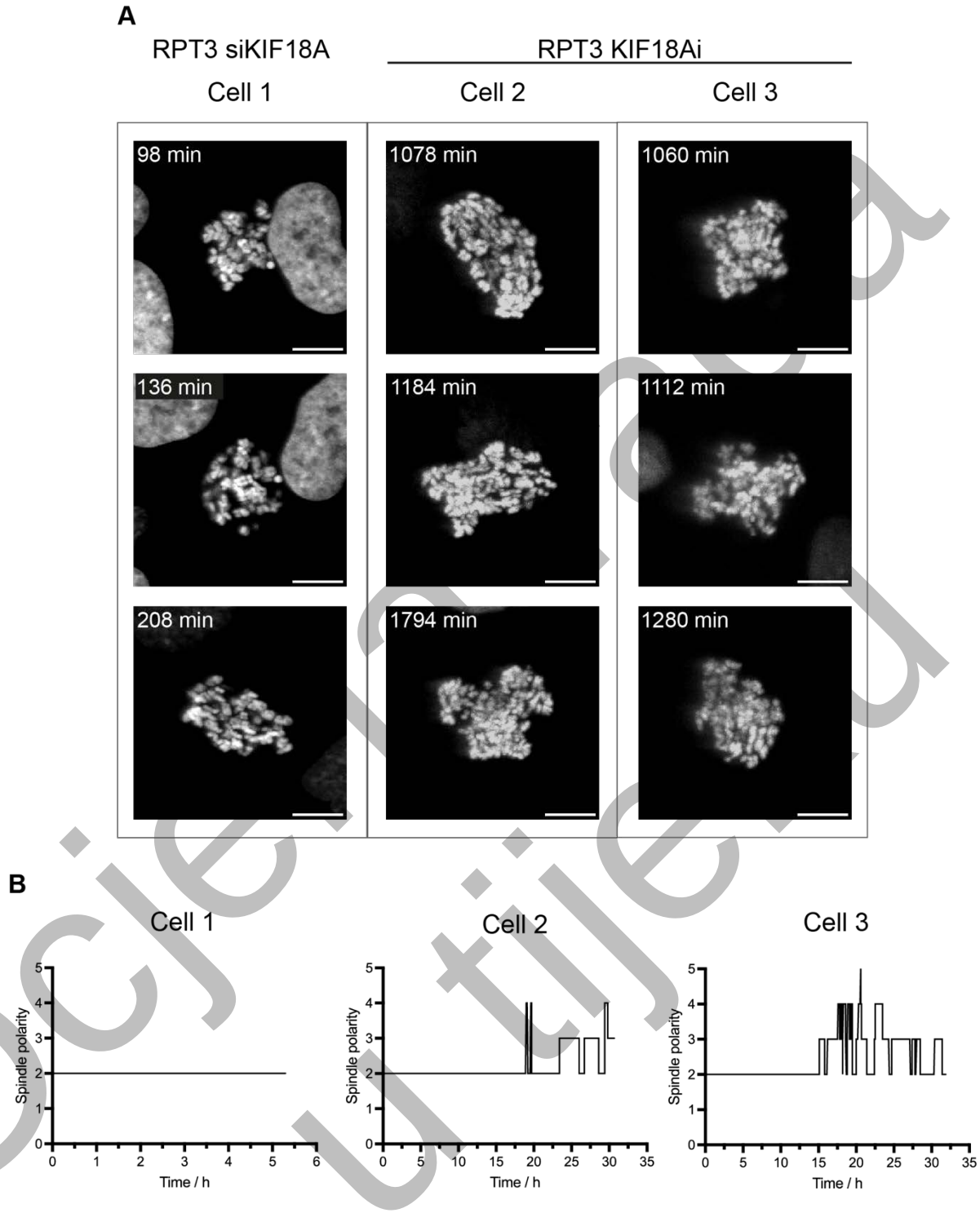

Figure 39. Caption on the following page.

Figure 39. Spindle polarity dynamically changes in oversensitive cells after sovilnesib treatment. A) Time-lapse images from lattice lightsheet of RPT3 cells stably expressing H2B-GFP (grey) throughout mitosis. Cell 1 was treated with 100 nM KIF18A siRNA and represents oversensitive bipolar cell. Cells 2 and 3 were treated with 250 nM sovilnesib and represent oversensitive multipolar cells with changes in spindle polarity. Images show maximum intensity projections. Scale bars, 10 μm. **B)** Changes of spindle polarity through time during mitosis in RPT3 cells.

4.9. Microtubule foci increased in oversensitive RPT3 cells after sovilnesib treatment

To investigate the relation between spindle polarity, centrosome number, and microtubule foci, RPE1 parental and RPT3 cells were treated with 250 nM sovilnesib and incubated for 72 hours prior to fixation and immunostaining. Cells were labeled with antibodies for centrin and tubulin to visualize both centrosomes and microtubule foci, while DNA was visualized with DAPI. This allowed for the identification of spindle poles with or without associated centrosomes. Since centrin is not a marker for PCM, additional experiments are required to determine whether poles lacking centrosomes still contain PCM components.

Based on spindle morphology and the number of microtubule foci, without considering centrosome number, oversensitive cells were classified according to their spindle architecture (Figure 40A). Some bipolar spindles contained the expected two microtubule foci, while others exhibited a third, indicating the presence of an additional minor pole, while maintaining overall bipolar geometry. In the same way, most tripolar spindles had three microtubule foci, though a subset displayed a fourth, consistent with the formation of another minor pole without a change in tripolar geometry (Figure 40A).

There was no significant difference in the proportion of bipolar versus multipolar cells between RPE1 parental and RPT3 lines (Figure 40B). However, the two cell lines differed in centrosome number. The RPT3 cell line had a significantly higher number of oversensitive cells with more than two centrosomes per cell (Figure 40C), possibly due to centrosome fragmentation (Marquis et al., 2021). A similar pattern was observed for microtubule foci, 80% of oversensitive RPT3 cells had more than two foci, further supporting the presence of additional minor spindle poles.

To further explore the relation between spindle polarity and the number of microtubule foci, bipolar and tripolar spindles were analyzed in both cell lines (Figure 40D). In RPE1 parental cells, 85% of bipolar spindles contained two foci, while 15% had three, indicating a third minor pole. All tripolar spindles in this cell line had three microtubule foci. In contrast, only 25% of bipolar spindles in RPT3 cells had two microtubule foci, the majority had either three or four. Similarly, only 25% of tripolar spindles in RPT3 had the expected three foci, while the rest of the cells exhibited an additional fourth pole. These findings indicate that 75% of RPT3 spindles formed at least one extra minor pole. One tetrapolar RPT3 cell with four microtubule foci was identified but excluded from quantification due to the low sample size. Further studies will be necessary to determine whether the additional microtubule foci in RPT3 cells arise from PCM fragmentation or altered microtubule dynamics.

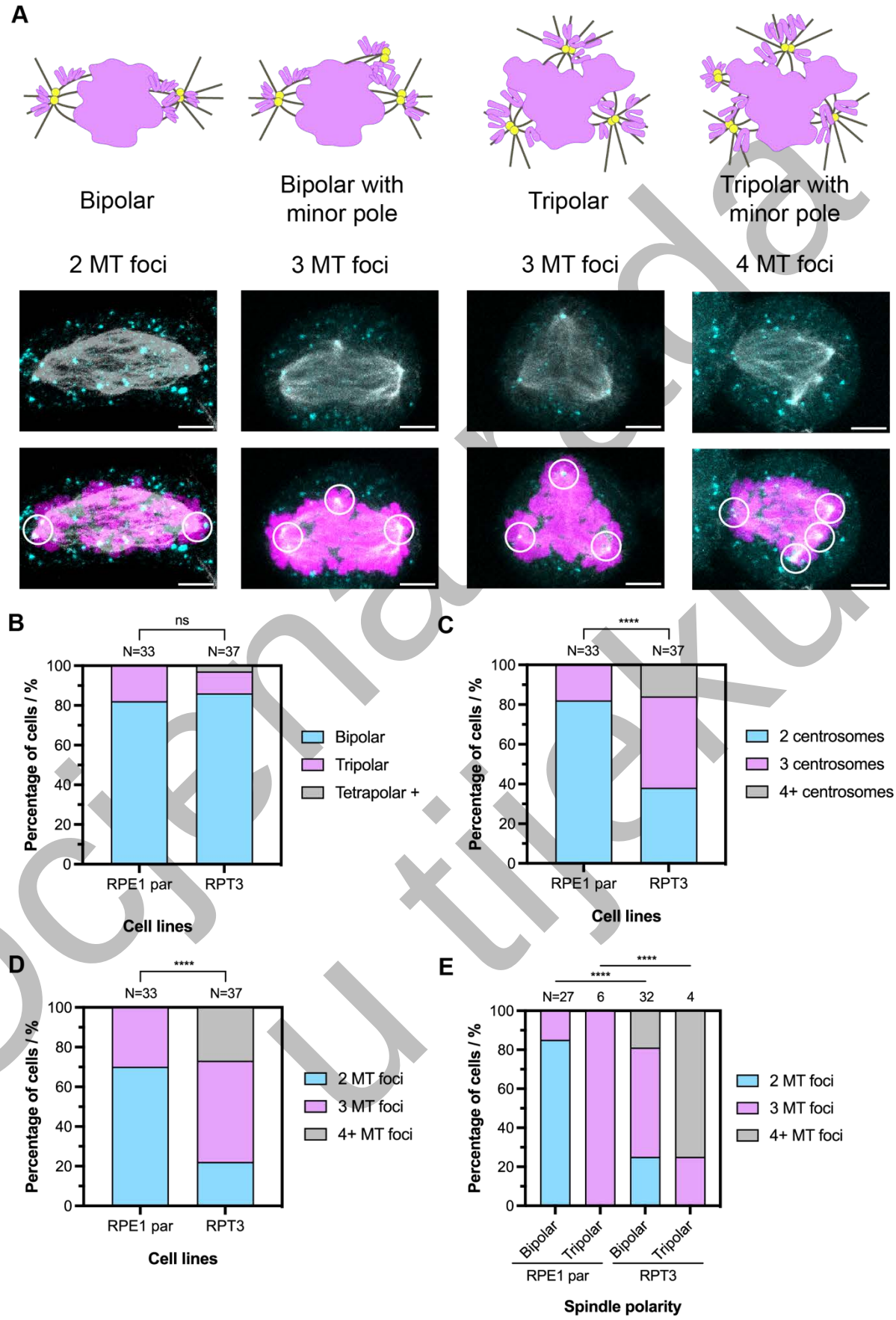

Figure 40. Caption on the following page.

Figure 40. Number of microtubule foci increases in oversensitive cells after sovilnesib treatment in RPT3. A) Schematic representation of spindle polarity and number of microtubule (MT) foci in oversensitive RPT3 cells with corresponding images. Confocal images of immunostained RPT3 cells, treated with 250 nM sovilnesib. Cells were fixed 72 hours after the treatment and immunostained for centrin and tubulin, while DNA was labelled with DAPI. Upper panels show centrin and tubulin (cyan and grey, respectively), and lower panels show merged images with DNA (magenta). Spindle poles are encircled on merged images. Images are shown as a SUM intensity projections. Scale bars, 5 μm. **B)** Spindle polarity in oversensitive RPE1 parental and RPT3 cells. **C)** Centrosome number in oversensitive cells. **D)** Number of microtubule foci in oversensitive cells. **E)** Number of microtubule foci based on spindle polarity in oversensitive cells.
Results were obtained from three independent experiments for RPE1 parental, and from four independent experiments for RPT3. Statistical analysis: Fisher's exact test when compared groups had two outcomes, and Chi-square test if there were more than two outcomes. Ratio of outcomes was determined from a total number of cells for each group.

4.10. STED imaging reveals altered spindle architecture after KIF18A depletion

To gain a more detailed understanding of spindle organization after KIF18A loss, RPE1 parental, RPT1, and RPT3 cells were imaged using superresolution STED microscopy. This approach overcomes the resolution limits of confocal microscopy and allows for the examination of the relationship between distinct classes of microtubules (Hell & Wichmann, 1994; Klar & Hell, 1999). KIF18A was depleted in RPE1 parental, RPT1 and RPT3 cells with 100 nM KIF18A siRNA, and control cells were treated with 100 nM non-targeting siRNA. Metaphase spindles were imaged in control cells, while after KIF18A depletion it is difficult to distinguish metaphase from later phases of prometaphase, due to chromosome alignment defects, so late prometaphase and metaphase spindles were imaged in these groups.

In control cells k-fibers and overlapping microtubules were clearly distinguishable. K-fibers in these cells typically terminated near the spindle midzone. In contrast, following KIF18A depletion, the distinction between k-fibers and overlapping microtubules became less apparent, especially in oversensitive cells. In these cells, individual microtubule fibers were harder to resolve, k-fibers were absent, and spindles were instead composed of long, disorganized fibers (Figure 41).

Line profile intensity measurements of the tubulin signal, taken along the spindle axis from pole to pole, supported these observations (Figure 42). In control cells, two prominent peaks corresponding to k-fiber localization were clearly visible, with a central dip marking the spindle midzone, where microtubule density is lower. After KIF18A depletion, this signal pattern became irregular, and in oversensitive cells, the typical spatial organization was completely lost. Oversensitive spindles also showed a noticeable reduction in astral microtubules. These observations indicate that KIF18A depletion leads to a severe structural disruption of the mitotic spindle in oversensitive cells, marked by the loss of k-fibers and disorganized microtubules, suggesting impaired spindle integrity and function.

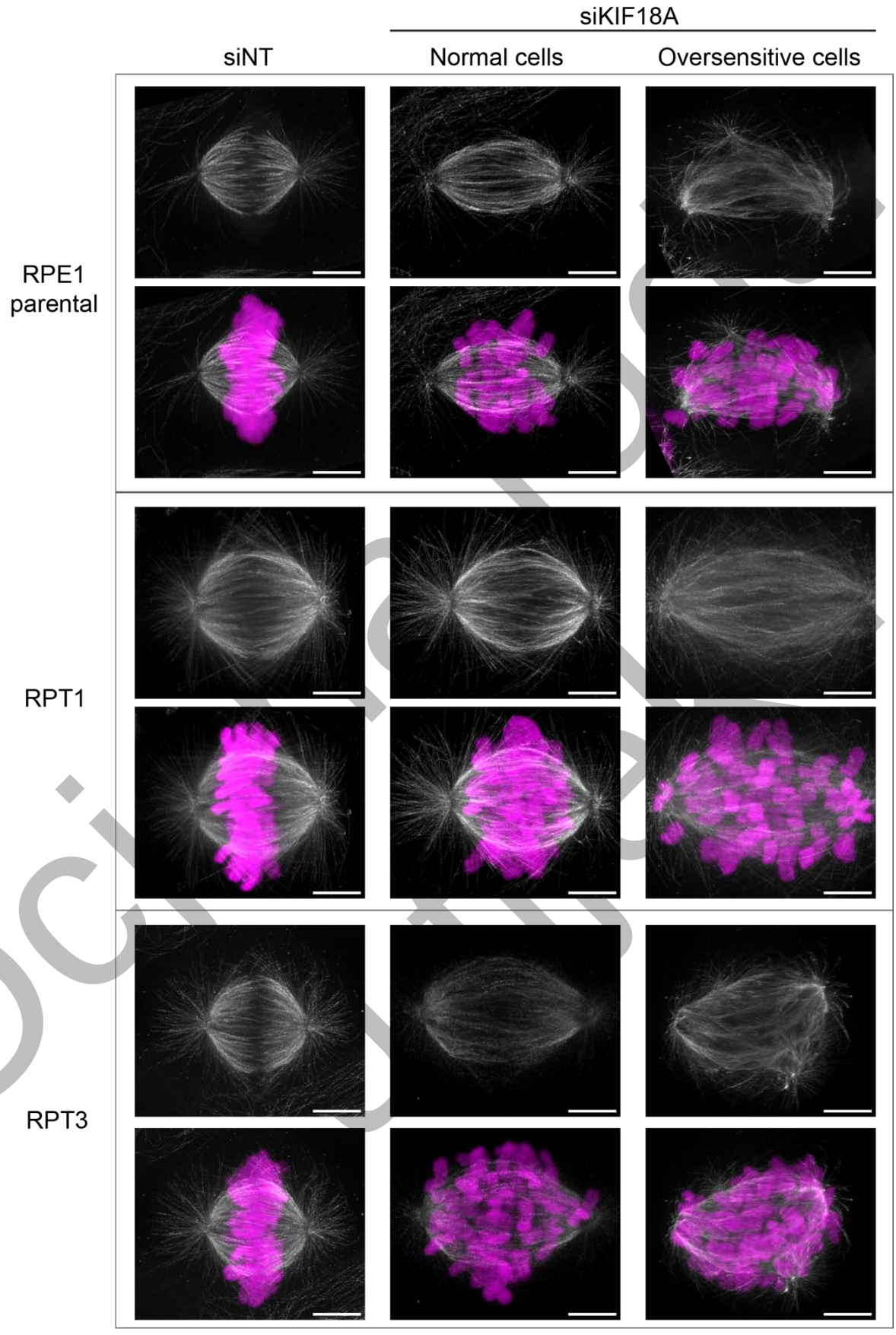

Figure 41. Caption on the following page.

Figure 41. Spindle architecture changes after KIF18A depletion. STED superresolution images of RPE1 parental, RPT1 and RPT3 cells after 100 nM KIF18A siRNA treatment. Control cells were treated with 100 nM non-targeting siRNA. Cells were fixed 24 hours after the treatment and immunostained for tubulin (grey, upper panels), imaged in superresolution. Confocal images of DNA, labelled with DAPI (magenta), are shown in merged imaged (lower panels). Images show maximum intensity projections. Scale bars, 5 µm. Results were obtained from one experiment.

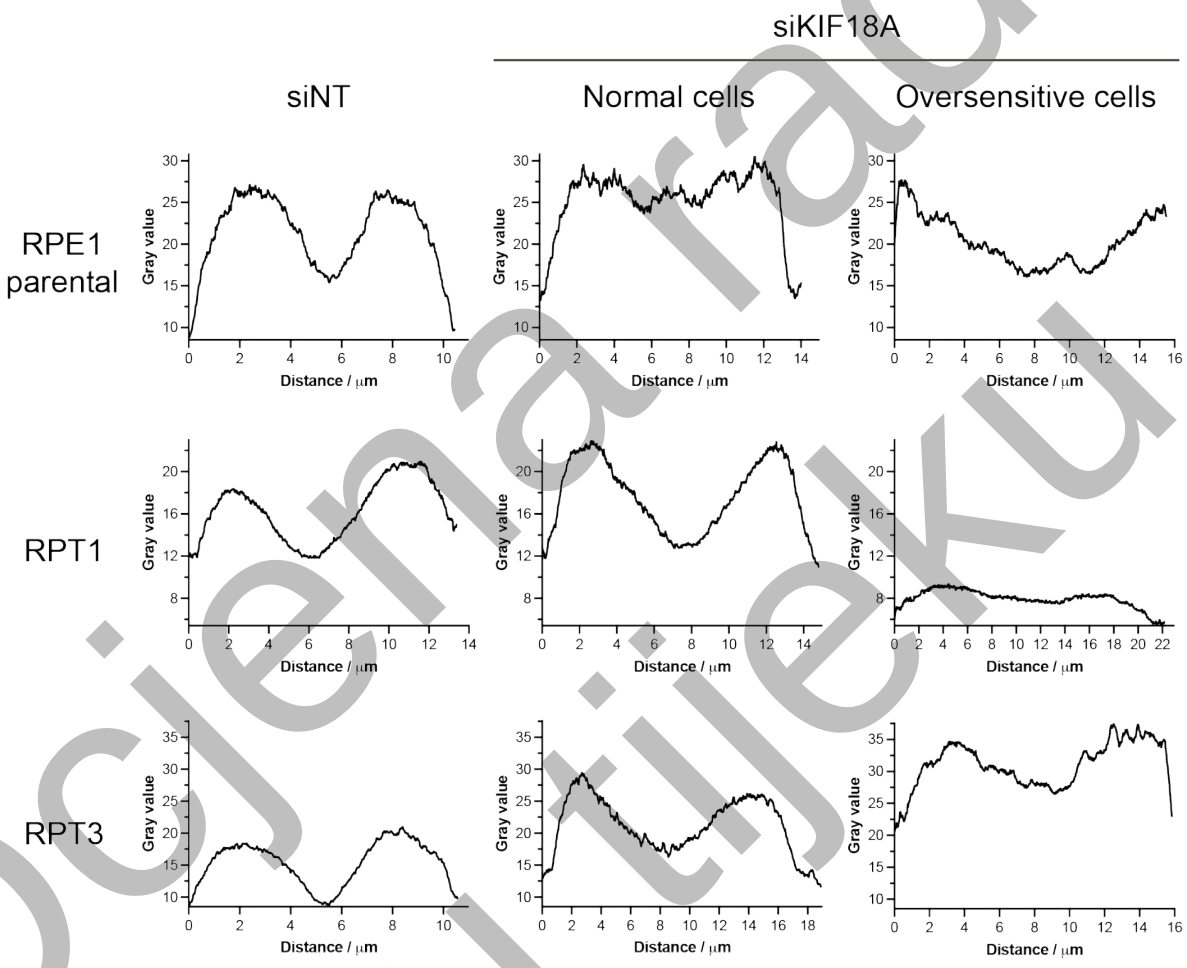

Figure 42. KIF18A depletion disrupts k-fibers in oversensitive cells. Line profile intensity of tubulin signal on the spindle, measured from one spindle pole to the other, for RPE1 parental, RPT1 and RPT3 cells shown in Figure 41.

In summary, KIF18A depletion and inhibition disrupted mitotic progression and spindle organization in both diploid and PT RPE1 cell lines. While cell confluency remained largely unaffected, clear mitotic defects were observed in all lines. This included spindle elongation, chromosome misalignment, and a higher frequency of oversensitive cells with abnormal spindle geometry and dynamic spindle pole transitions, and these defects were more pronounced in PT cell lines. Mitosis was significantly prolonged, particularly after sovilnesib treatment, and STED imaging revealed loss of k-fibers and disorganized spindle structure in oversensitive cells. These findings suggest that both diploid and PT RPE1 cell lines show some levels of sensitivity to KIF18A perturbations, although these cell lines are considered insensitive to KIF18A loss (Gliech et al., 2024).

4.11. Spheroids generation using magnetic cell levitation method

Spheroids were successfully generated using the magnetic cell levitation method in following cell lines: RPE1 p53KD, MDA-MB-231, U2OS and OVSAHO. Tumor cell spheroids were incubated for seven days prior to immunostaining, while RPE1 p53KD spheroids were incubated for five days. In all cell lines and replicates, cells formed a single compact spheroid. Cells began levitating within 20 minutes of exposure to the magnet. Between first and third day, the cell aggregates were loosely connected, whereas by day five, they had formed a compact spheroid. Spheroids exhibited irregular shapes, varying from round to elongated forms (Figure 43A), and they were flattened when viewed in the z dimension (Figure 43B). The spheroids did not form the perfect spheres, but rather irregular shapes, as shown for RPE p53KD (Figure 43C). Previous studies have also reported irregularly shaped spheroids, with morphology varying between different cell lines (Haisler et al., 2013; G. R. Souza et al., 2010).

Results for all further analyses were obtained from a following number of independent experiments for monolayers: RPE1 p53KD – three, MDA-MB-231 – five, U2OS – six and OVSAHO – three. Results were obtained from a following number of generated spheroids: RPE1 p53KD – 19, MDA-MB-231 – 15, U2OS – six and OVSAHO – six.

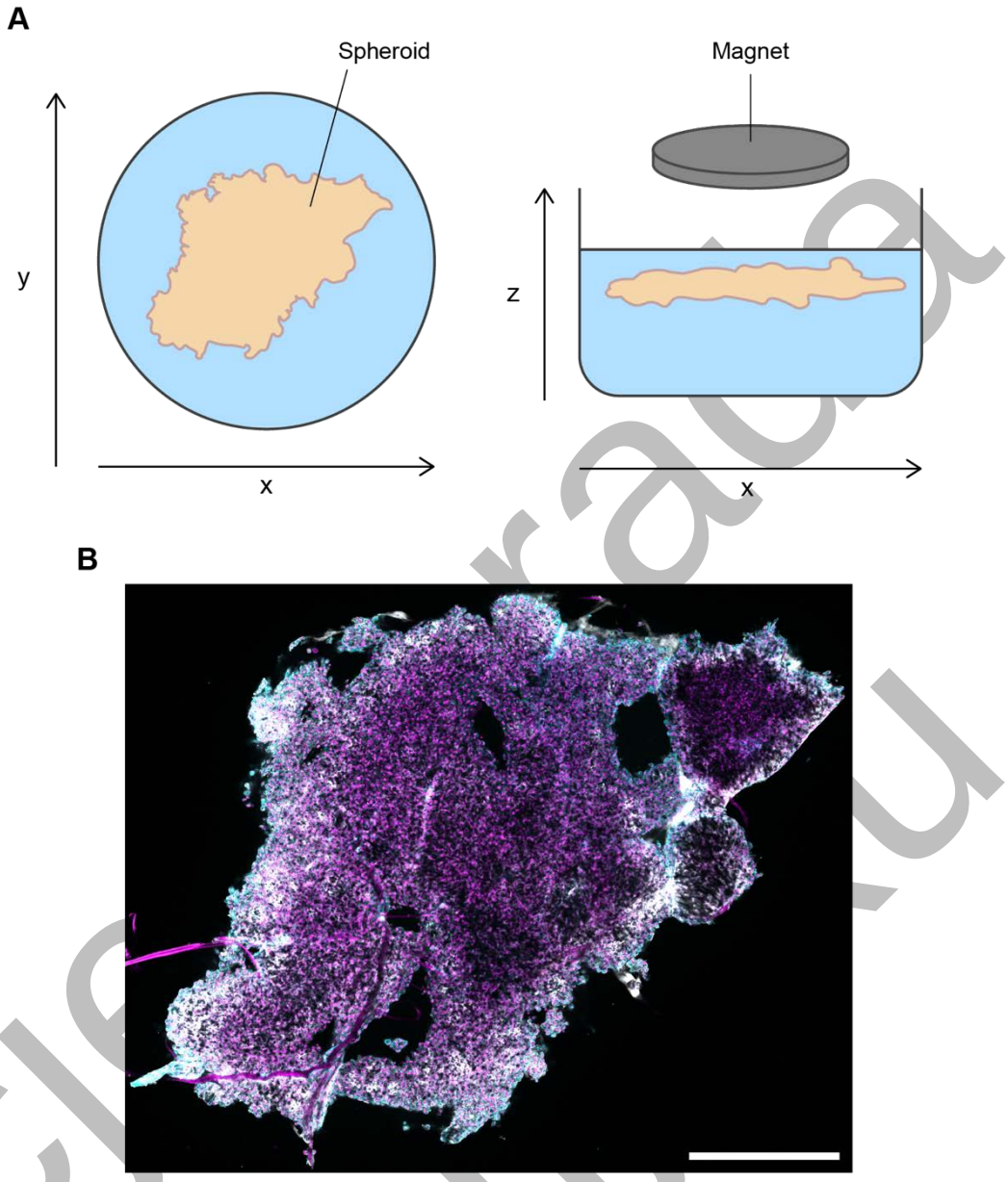

Figure 43. Magnetic cell levitation produces spheroids with variable shapes. A) Schematic representation of irregular spheroid shape viewed in x and y dimensions (left panel). Spheroids are flattened when viewed in x and z dimension (right panel). **B)** Confocal image of whole RPE1 p53KD spheroid. Merged image shows tubulin labelled with immunostaining (white), DNA labelled with DAPI (magenta) and cell membrane labelled with WGA membrane dye (cyan). One z-slice is shown. Scale bar, 500 μm.

4.12. Interphase cell morphology differs between monolayer and spheroid models

Numerous differences between cells cultured in 2D and 3D systems have been described. These cultures vary in cell shape, cell-cell interactions, proliferation, ECM production, etc. Although these factors influence mitosis, cell division is still predominantly studied in monolayer cultures (Ćosić & Petelinec, 2024; Cukierman et al., 2001; Desoize & Jardillier, 2000; Kapałczyńska et al., 2018; Langhans, 2018; Pampaloni et al., 2007; A. G. Souza et al., 2018). To characterize differences in mitosis between models, cells were cultured both as spheroids and monolayers.

Cells in monolayers grow attached to a flat surface and mostly display elongated and branched shapes, except for the OVSAHO cell line, where cells are round. In spheroids, cells are predominantly round in all lines except RPE1 p53KD, where some cells retain an elongated shape. Monolayer cells have enough space to spread and migrate without spatial organization, except OVSAHO cells, which grow in clumps. Additionally, cells in spheroids are smaller than those in monolayers (Figure 44).

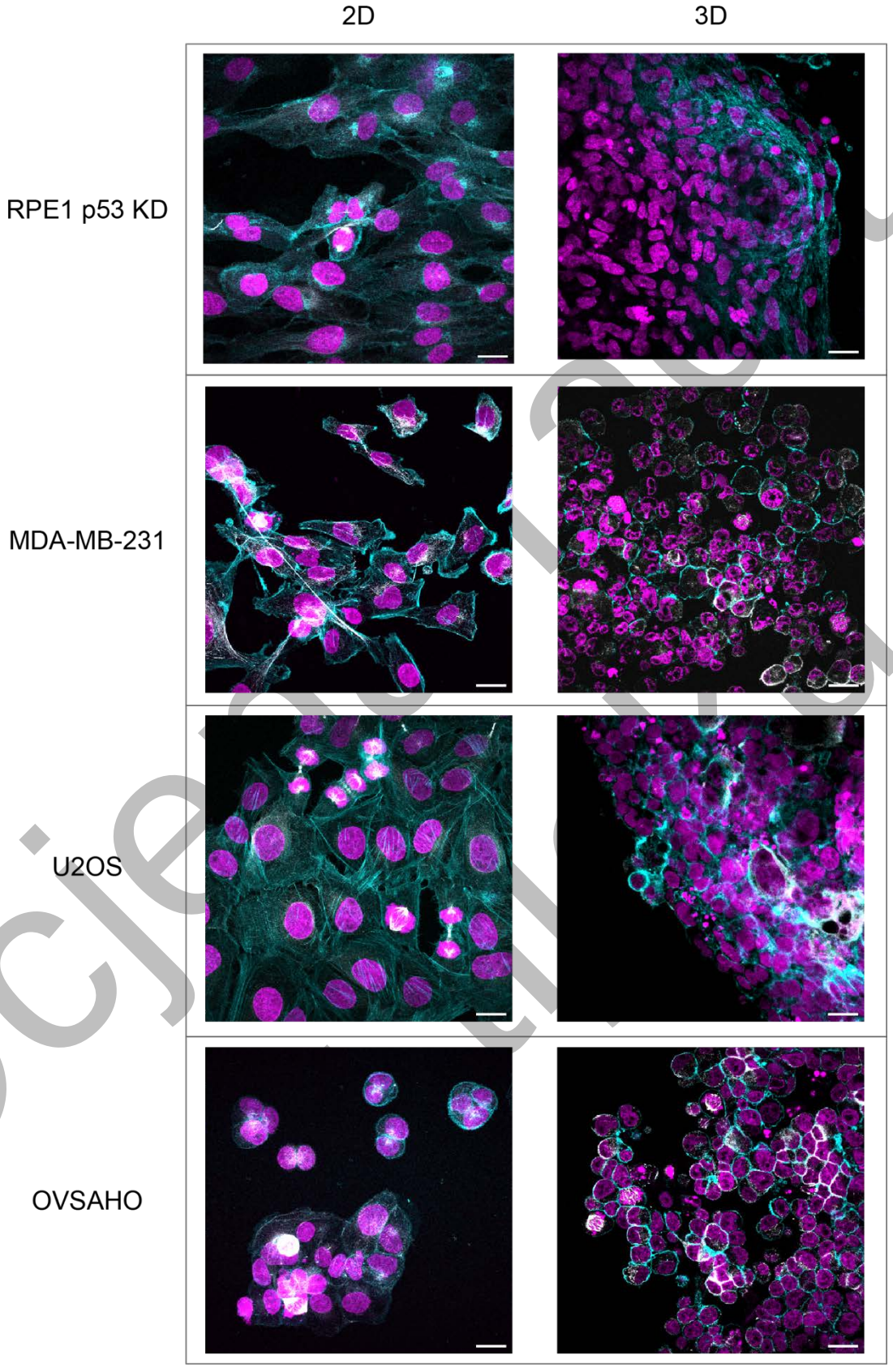

Figure 44. Caption on the following page.

Figure 44. Differences between 2D and 3D cell cultures. Confocal images of immunostained RPE1 p53KD, MDA-MB-231, U2OS and OVSAHO cell lines cultured as monolayers (left panels) and as spheroids (right panels). Cells were immunostained for tubulin (grey), DNA was labelled with DAPI (magenta) and cell membrane was stained with SiR-actin dye in all cell lines, excpet in RPE1 p53KD and OVSAHO monolayers, where it was stained with WGA membrane dye (cyan). Images show maximum intensity projections for all cell lines, except MDA-MB-231 and OVSAHO spheroid where one z-slice is shown. Scale bars, 20 μm.

4.13. Mitotic cells are distributed throughout the spheroid

To analyze the distribution of mitotic cells within spheroids, they were divided into three layers based on the distance of each mitotic cell from the culture edge (Figure 45A-B). This division is arbitrary and does not correspond to the typical classification of spheroids into proliferative, quiescent, and necrotic zones (Desoize & Jardillier, 2000; Hirschhaeuser et al., 2010; Laurent et al., 2013; Lin & Chang, 2008; Sutherland, 1988). Mitotic cells located directly at the spheroid edge were assigned to the outer layer. Those with one to three cell layers between them and the edge were classified as middle layer. Due to the irregular shape of the spheroids, the distance was determined in at least one direction. Mitotic cells with four or more cells between them and the spheroid edge were categorized as inner layer.

The proportion of mitotic cells In each layer varied among cell lines (Figure 45C). For example, 43% of mitoses in RPE1 p53KD spheroids occurred in the inner layers, whereas in OVSAHO spheroids, 44% were in the outer layer. Since the percentages were similar across layers within each cell line, the distribution of mitotic cells appears random. Furthermore, mitotic cells were observed throughout the whole spheroids, particularly in RPE1 and OVSAHO, suggesting that these spheroids cannot be classically divided into proliferative, quiescent, and necrotic zones, possibly due to their flattened shape.

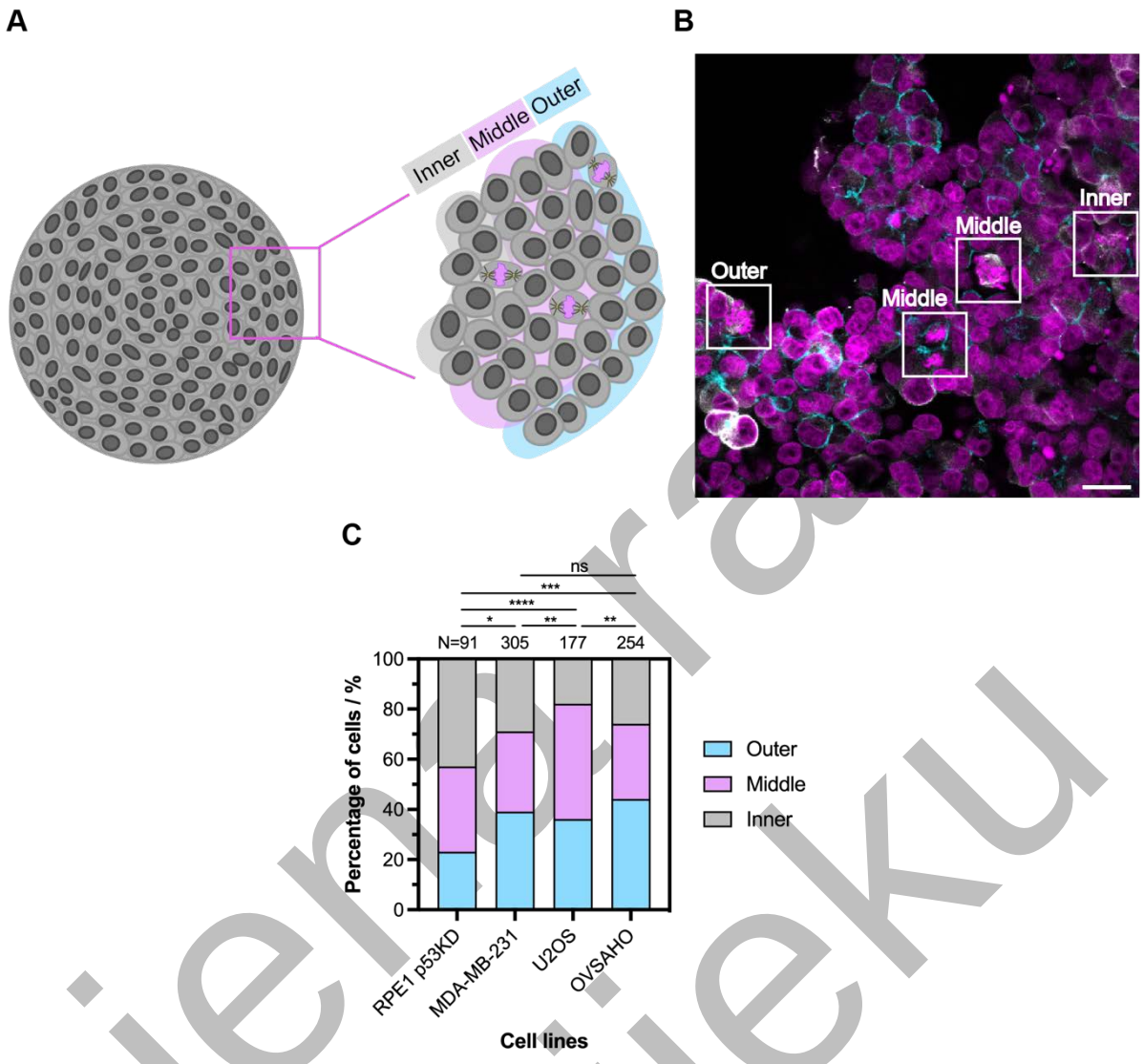

Figure 45. Mitotic cells can be found in the whole spheroid. A) Schematic representation of mitotic cells categorized into outer, middle, and inner layers of the spheroid based on their distance from the spheroid edge. Cells in outer layer are on the edge of the spheroid, cells in the middle layer have one to three layers of cells between them and the edge, and cells in inner layers have four or more layers of cells between them and the edge. **B)** Confocal image of OVSAHO spheroid, immunostained for tubulin (grey), while DNA was labelled with DAPI (magenta), and cell membrane with SiR-actin dye (cyan). Image is shown as a SUM intensity projection. Scale bar, 20 μm. **C)** Distribution of mitotic cells in different layers of spheroids. Statistical analysis: Chi-square test was performed. Ratio of outcomes was determined from a total number of cells for each cell line.

4.14. The fraction of prometaphase cells increases in tumor spheroids

A previous study showed that mitotic cells in spheroids can enter prometaphase arrest when exposed to mechanical stress, suggesting that confinement can interfere with mitotic progression (Desmaison et al., 2018). To determine whether a similar pattern is present in these spheroid model, the distribution of mitotic phases was quantified and compared to monolayer cultures. A higher proportion of cells in prometaphase may indicate mitotic arrest associated with the 3D growth environment.

Mitotic phases were grouped into those occurring before anaphase onset: prophase, prometaphase, and metaphase, and those occurring after anaphase onset: anaphase, telophase, and cytokinesis (Figure 46A). In the non-tumor RPE1 p53KD cell line, there was no significant difference in the proportion of cells before and after anaphase onset between spheroids and monolayers. In contrast, all tumor cell spheroids had significantly fewer cells that progressed to anaphase. The largest difference was observed in MDA-MB-231 spheroids, where only 8% of mitotic cells were in phases after anaphase onset, compared to 23% in monolayers, suggesting difficulty progressing into anaphase.

Further analysis of individual mitotic phases showed that RPE1 p53KD spheroids had a similar phase distribution to monolayers, with a modest 12% increase in prometaphase cells (Figure 46B). Tumor spheroids, especially MDA-MB-231 and U2OS, showed a substantial increase in prometaphase cells, with approximately 60% of mitotic cells in this phase. In OVSAHO spheroids, the distribution was more balanced, with a slight increase in metaphase and a decrease in the fraction of anaphase cells. A consistent reduction in prophase cells was observed in all spheroid lines, possibly due to difficulty detecting prophase cells during imaging, as they can resemble interphase cells and can be overlooked in crowded 3D environment. Overall, the elevated percentage of cells in prometaphase and metaphase in tumor spheroids suggests a prometaphase arrest likely due to the confinement in 3D environment.

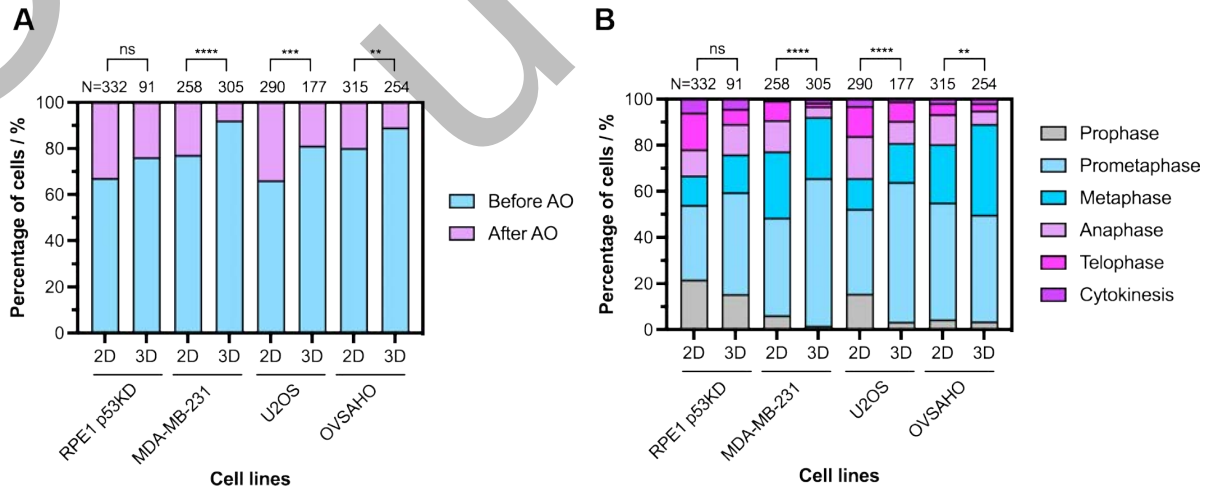

Figure 46. Prometaphase accumulation is elevated in tumor spheroids versus monolayers. A) Distribution of mitotic cells in phases before and after anaphase onset (AO) in monolayers and spheroids. Statistical analysis: Fisher's exact test. **B)** Distribution of mitotic cells in different phases of mitosis in monolayers and spheroids. Statistical analysis: Chi-square test. Ratio of outcomes was determined from a total number of cells for each cell line and a type of cell culture.

4.15. Prometaphase errors increased in RPE1 p53KD and MDA-MB-231 spheroids

Molla et al. reported that mitotic cells in spheroids had a higher occurrence of lagging chromosomes (Molla et al., 2017). Cells in spheroids could have difficulties with chromosome alignment which leads to prometaphase arrest. When chromosomes are not properly aligned, mis-segregation errors can happen during anaphase. To evaluate error rates in spheroids, mitotic errors were divided into prometaphase – unaligned and misaligned chromosomes, anaphase – lagging chromosomes and chromosome bridges, and cytokinesis errors – micronuclei and chromosomes bridges (Figure 47 and Figure 48A). For this analysis, cells in late prometaphase and metaphase that had already formed a metaphase plate were examined to determine the percentage of unaligned and misaligned chromosomes. Only anaphase cells with sufficiently separated chromosomes were analyzed to identify mis-segregation errors in anaphase. Cells in telophase and cytokinesis were analyzed to assess cytokinesis errors.

Only RPE1 p53KD and MDA-MB-231 spheroids showed an increase in prometaphase errors (Figure 48B). In RPE1 p53KD, error rates increased by 11%, while in MDA-MB-231 spheroids by 21%. The significant increase in unaligned and misaligned chromosomes in MDA-MB-231 spheroids was expected, given that approximately 60% of mitotic cells were in prometaphase (Figure 46B). Conversely, it was surprising that RPE1 cells showed an increase in prometaphase errors, while U2OS, which also has many cells in prometaphase, did not.

Moreover, none of the cell lines showed an increase in anaphase or cytokinesis errors (Figure 48C-D). This could be due to the smaller number of cells analyzed, or it is possible that cells experiencing prolonged prometaphase and failing to properly align chromosomes undergo mitotic slippage. Thus, only cells with correct chromosome alignment proceed to anaphase and divide without errors. Since the increase in prometaphase cells was not caused by more unaligned or misaligned chromosomes, cellular and spindle parameters were further investigated.

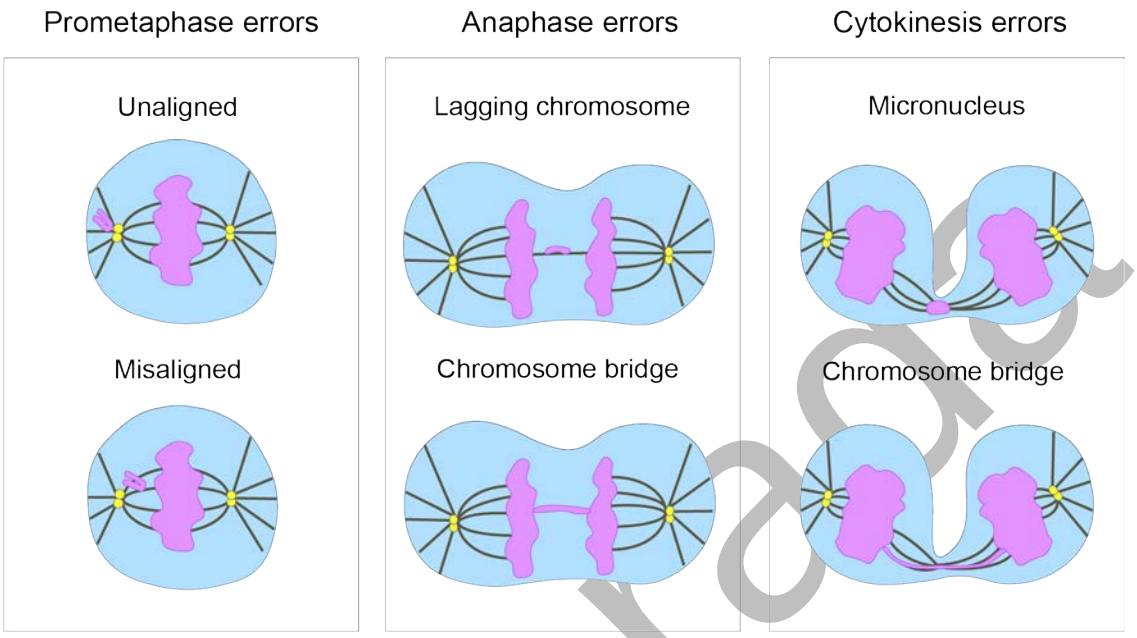

Figure 47. Cells can exhibit prometaphase, anaphase and cytokinesis errors. Schematic representation of different types of mitotic errors. Prometaphase errors can be unaligned and misaligned chromosomes (left panel), that can cause further mis-segregation errors in anaphase if they do not align properly to the metaphase plate before the anaphase onset. Anaphase errors can be lagging chromosomes (middle panel), which are left between two segregating masses, or chromosome bridges, which form when sister chromatids do not fully separate. Cytokinesis errors can be micronuclei, often formed from lagging chromosomes or chromosome bridges (right panel).

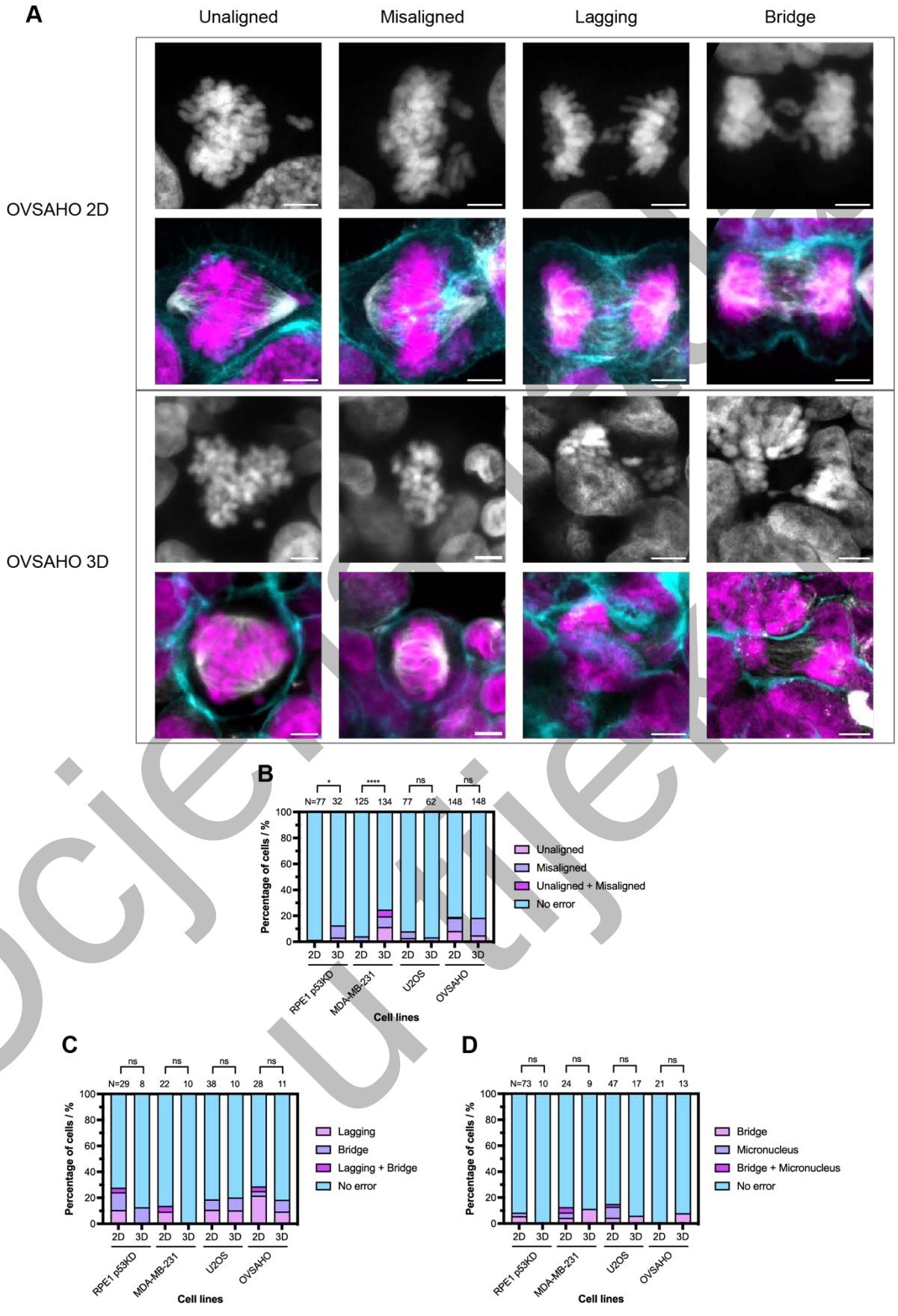

Figure 48. Caption on the following page.

Figure 48. Mitotic errors remain low in spheroids. A) Confocal images of immunostained OVSAHO cells in monolayers and spheroids. Upper panels show DNA labelled with DAPI (grey), and lower panels show merged images of immunostained tubulin (grey), DNA (magenta), and cell membrane stained with SiR-actin in spheroids and WGA membrane dye in monolayers (cyan). Images are shown as a SUM intensity projections. Scale bars, 5 µm. **B)** Frequency of prometaphase errors in monolayers and spheroids. Only cells in late prometaphase and metaphase were analyzed. **C)** Frequency of anaphase errors in monolayers and spheroids. Only anaphase cells with sufficiently separated chromosomes were analyzed. **D)** Frequency on cytokinesis errors in monolayers and spheroids. Cells in telophase and cytokinesis were analyzed.
Statistical analysis: Fisher's exact test when compared groups had two outcomes, and Chi-square test if there were more than two outcomes. Ratio of outcomes was determined from a total number of cells for each cell line and a type of cell culture.

4.16. Mitotic cell morphology differs in 3D environment

It was observed that interphase cells change shape when they are cultured as spheroids (Figure 44). To determine if mitotic cell shape also changes, mitotic cells in prometaphase, late prometaphase, metaphase, and anaphase onset, phases in which cells are rounded and their shape is stable, were classified into four categories: round, elongated, branched, and irregular (Figure 49A-B).

OVSAHO mitotic cells showed similar shape distributions in monolayers and spheroids, consistent with their interphase morphology (Figure 49C). RPE1 p53KD cells showed a minor shift, with a 20 percent increase in round cells and a decrease in branched shapes in spheroids. In MDA-MB-231 spheroids, 10% of mitotic cells were irregular. U2OS cells showed the most significant shift. While half of the cells in monolayers were elongated and the rest were divided between round and branched, over 70% of cells in spheroids were round.

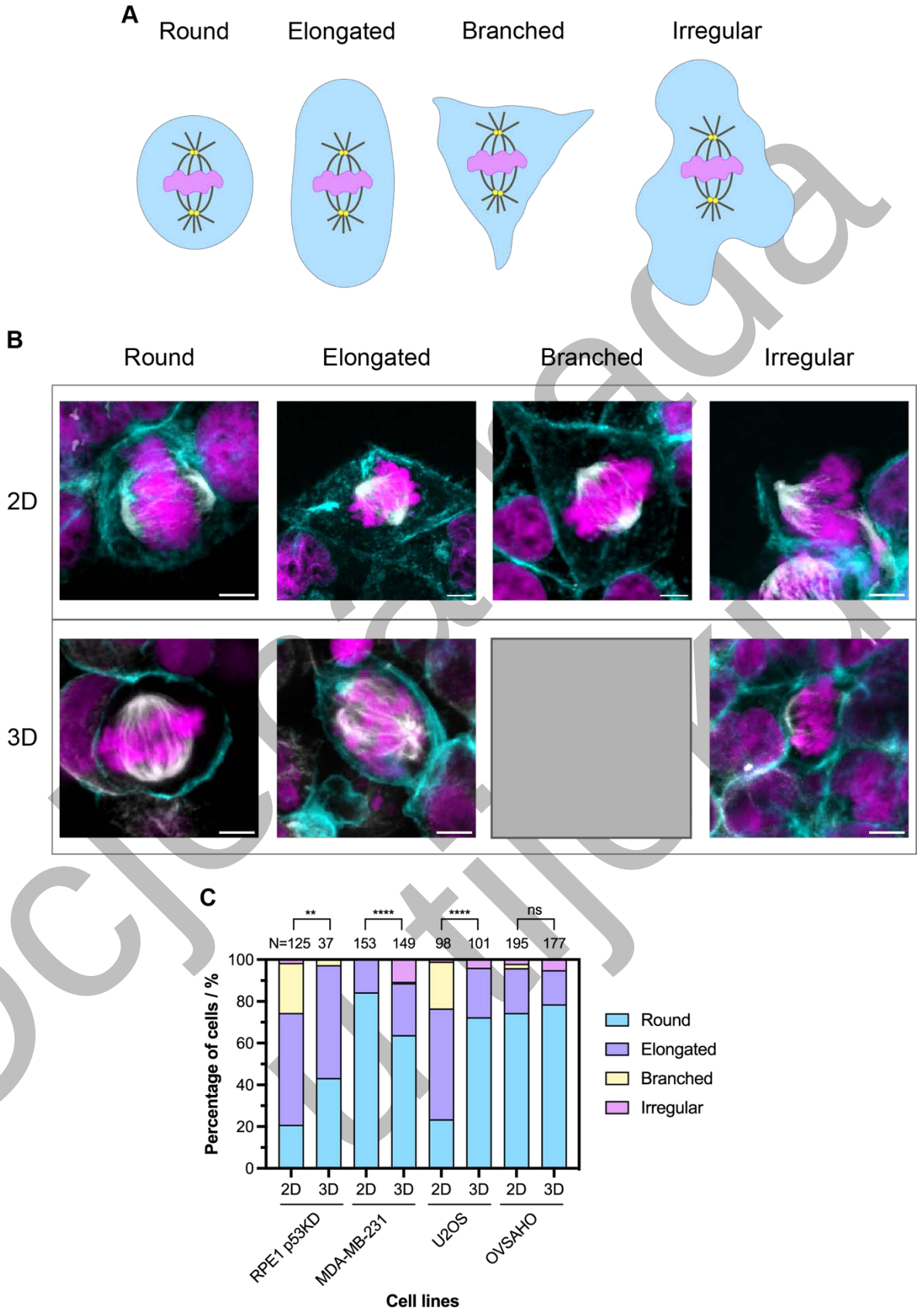

Figure 49. Caption on the following page.

Figure 49. Mitotic cell shape differs between monolayers and spheroids. A) Schematic representation of different cell shapes. Cells can exhibit round, elongated, branched and irregular shapes. **B)** Confocal images of immunostained OVSAHO cells in monolayers and spheroids. Merged images show tubulin labelled with immunostaining (white), DNA labelled with DAPI (magenta), and cell membrane stained with SiR-actin in spheroids and WGA membrane dye in monolayers (cyan). Images are shown as a SUM intensity projections. Scale bars, 5 μm. There were no branched cells in OVSAHO spheroids. **C)** Frequency of different cell shapes in monolayers and spheroids. Only mitotic cells entirely in the field of view were analyzed. Statistical analysis: Chi-square test was performed. Ratio of outcomes was determined from a total number of cells for each cell line and a type of cell culture.

4.17. Mitotic cells are smaller in spheroids

Cells in spheroids generally appear smaller compared to monolayers. To quantify this difference, cell dimensions were measured along the x and y axes using the same set of mitotic cells analyzed for cell shape. The longest and shortest dimensions of each cell were measured at the points where the cell appeared most extended and most narrow, regardless of spindle orientation. Number of z-planes imaged per cell was similar between spheroids and monolayers, which indicates that cell dimension in z axis remained relatively constant. Therefore, only the dimensions of cells in x and y axes were measured (Figure 50A).

A reduction in both the long and short axes was observed in spheroids across all cell lines (Figure 50B-C). This analysis confirmed that mitotic cells in spheroids are significantly smaller than those in monolayers (Figure 50D-E). Scatter plots of individual cells show smaller values on both axes for spheroids, indicating a more compact and rounded shape, than in monolayers. The most pronounced difference in size between 2D and 3D cultures was observed in U2OS cells. In RPE1 p53KD, the reduction was more prominent in length than in width.

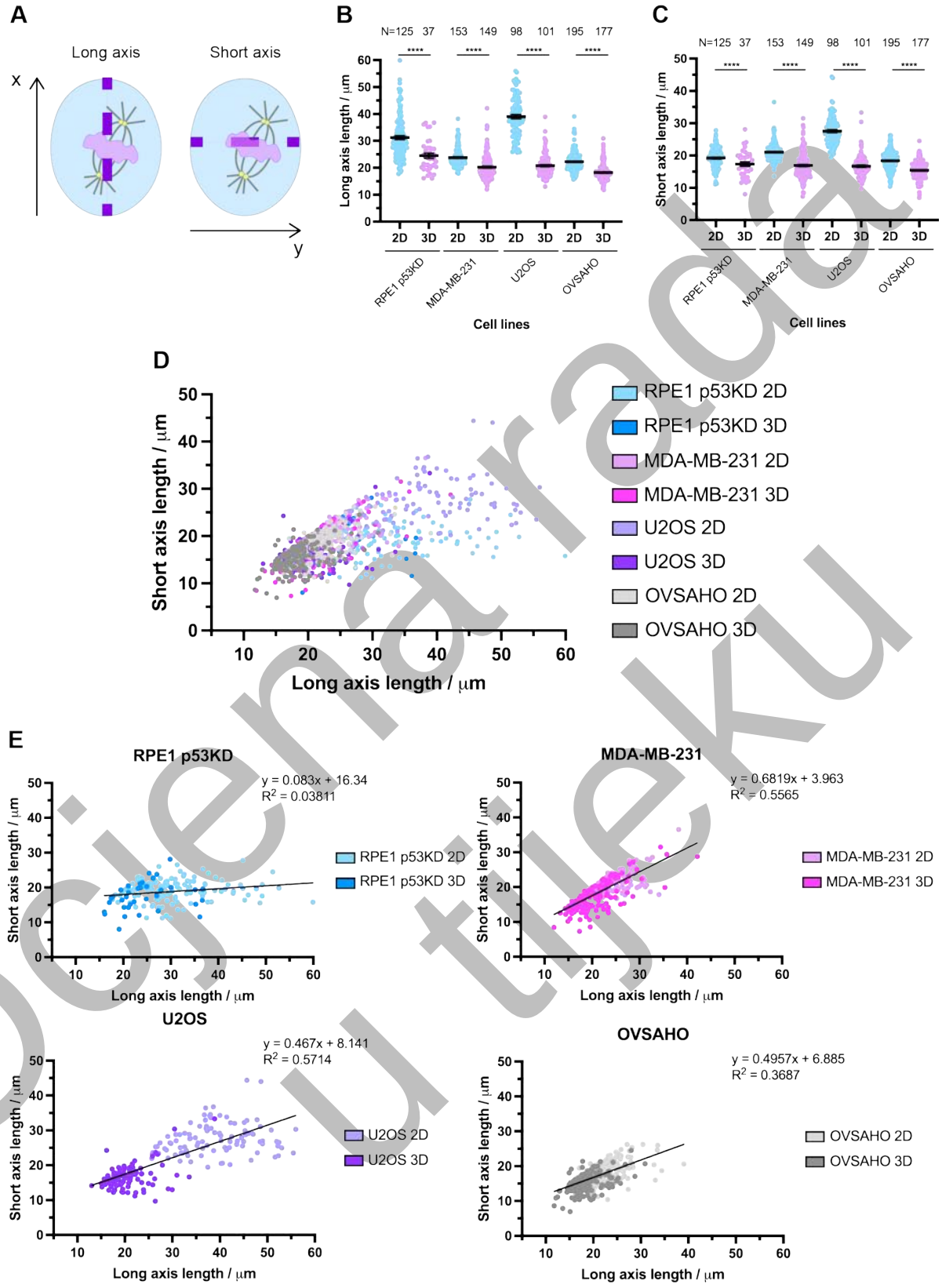

Figure 50. Caption on the following page.

Figure 50. Mitotic cells are smaller in spheroids compared to monolayers. A) Schematic representation of cell dimensions that were measured to determine the cell size. **B)** Long cell axis length of cells measured in monolayers and spheroids. **C)** Short cell axis length of cells measured in monolayers and spheroids. **B-C)** Only mitotic cells in prometaphase, metaphase and anaphase onset, and entirely in the field of view were analyzed. Error bars represent mean value and SEM. Statistical analysis: Kruskal-Wallis test with post-hoc Dunn's test was performed on a total number of cells for each cell line and a type of cell culture. **D)** Scatter plot of long versus short cell axis lengths in monolayers and spheroids in all cell lines. Each point represents a single cell. **E)** Scatter plots of long versus short cell axis lengths in monolayers and spheroids shown separately for each cell line.

4.18. Spindle orientation shifts in OVSAHO and U2OS spheroids

Spindles are typically oriented on the long axis of the cell, a principle known as Hertwig's rule (Hertwig & Hertwig, 1884). To test whether this rule also applies in spheroids, spindle orientation was analyzed and compared with monolayers. The same set of mitotic cells used for shape and size analysis was used here, but only bipolar spindles were included. Spindle orientation was classified as aligned with the long axis, short axis, or tilted (Figure 51A–B).

In RPE1 p53KD and MDA-MB-231, spindle orientation did not differ between monolayers and spheroids. However, while most RPE1 p53KD cells had spindles oriented on the long axis, only 40% of MDA-MB-231 cells showed this orientation (Figure 51C). OVSAHO cells showed a minor shift, with a slight increase in spindles oriented on the short axis in spheroids. The largest change was seen in U2OS cells. In monolayers, 65% of spindles were oriented on the long axis and 14% on the short axis, while in spheroids, 33% were oriented on the long axis and 52% on the short axis. Across all groups, tilted spindles ranged from 10% to 20%.

While spindles are generally positioned centrally, some cells in spheroids displayed an off-center spindle position, on one side of the cell (Figure 51D–E). This was quantified using the same set of cells. The greatest increase in off-center spindles between monolayers and spheroids was seen in RPE1 p53KD and MDA-MB-231, with an approximate 15% increase (Figure 51F). No difference was observed in U2OS, and OVSAHO cells showed only a minor shift.

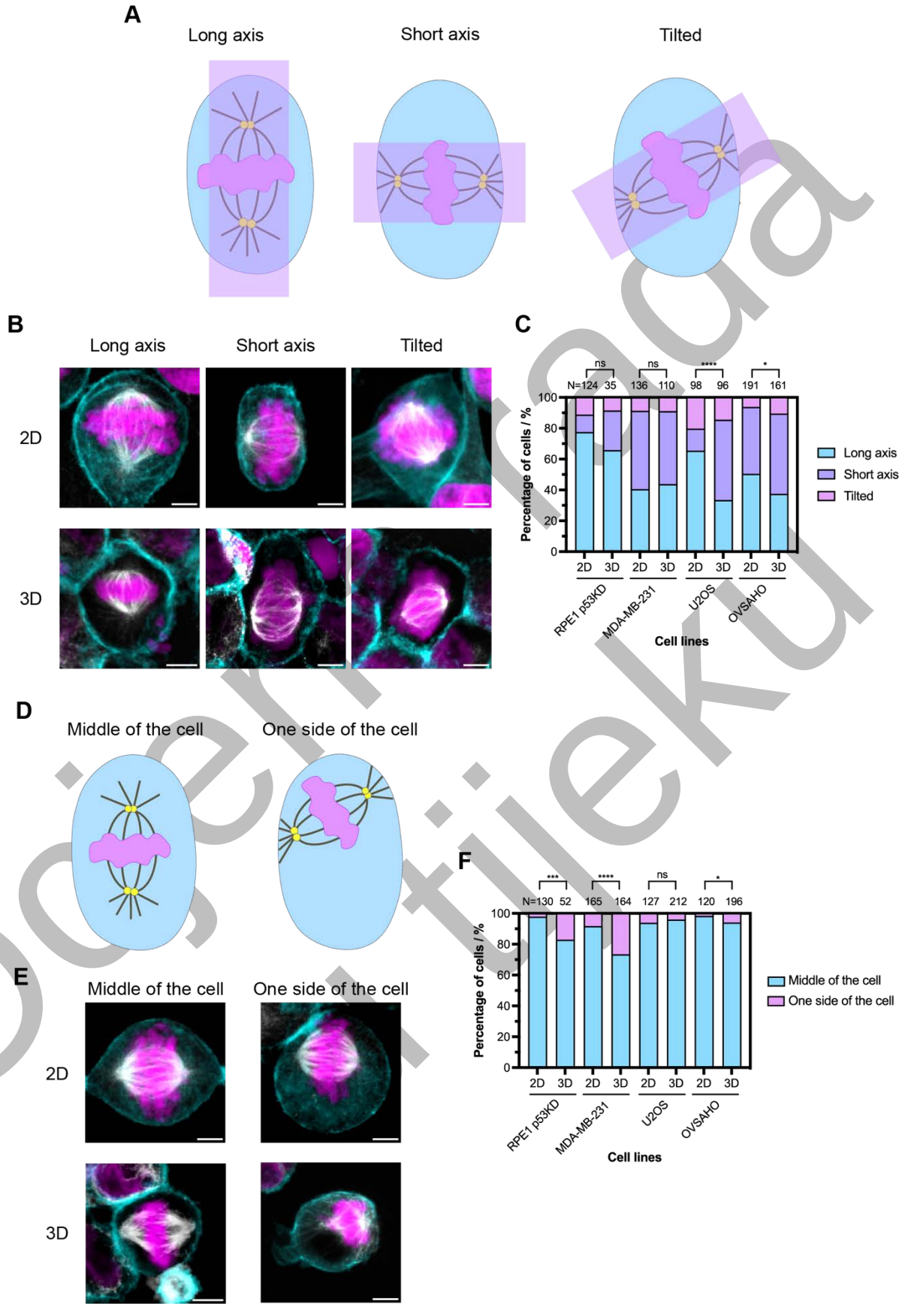

Figure 51. Caption on the following page.

Figure 51. Spindle orientation and positioning differ between monolayers and spheroids. A) Schematic representation of different spindle orientations. Spindles can be oriented on the long axis of the cell, short axis of the cell or tilted. **B, E)** Confocal images of immunostained MDA-MB-231 cells in monolayers and spheroids. Merged images show tubulin labelled with immunostaining (white), DNA labelled with DAPI (magenta), and cell membrane stained with SiR-actin (cyan). Images are shown as a SUM intensity projections. Scale bars, 5 μm. **C)** Distribution of mitotic cells with different spindle orientation in monolayers and spheroids. Only bipolar prometaphase, metaphase and cells at the anaphase onset were analyzed. Statistical analysis: Chi-square test. **D)** Schematic representation of spindle positioning in the cell. Spindles can be positioned in the middle of the cell, or at one side of the cell. **F)** Distribution of mitotic cells with different spindle positioning in monolayers and spheroids. Only prometaphase, metaphase and cells at the anaphase onset were analyzed. Multipolar cells were included in this analysis. Statistical analysis: Fisher's exact test was performed. Ratio of outcomes was determined from a total number of cells for each cell line and a type of cell culture.

4.19. Spindle shape variations in spheroids is cell line dependent

To test how 3D architecture affects the shape of mitotic spindle, spindles were categorized into following categories: round and elongated, which are normal spindle shapes, irregular and multipolar spindles (Figure 52 and Figure 53). Spindle shapes were determined in mitotic cells that were in prometaphase, late prometaphase, metaphase and anaphase onset. Cells in early prometaphase were excluded from the analysis because spindle formation is not completed.

Spindle shapes changed in all cell lines when comparing monolayers and spheroids (Figure 54A). The proportion of multipolar spindles increased in spheroids of tumor cell lines, particularly in MDA-MB-231. Irregular spindles were more frequent in MDA-MB-231 and U2OS spheroids. In contrast, RPE1 p53KD spheroids showed an increase in round spindles. The frequency of elongated spindles decreased in all cell lines.

To assess whether spindle shape is influenced by the mitotic cell's position within the spheroid, spindle shape distribution was analyzed across the outer, middle, and inner layers. No significant differences were observed in any of the cell lines (Figure 54B). Spindle shape varies between spheroids and monolayers in all tested cell lines, but these changes are not associated with the spatial position of mitotic cells within the spheroid.

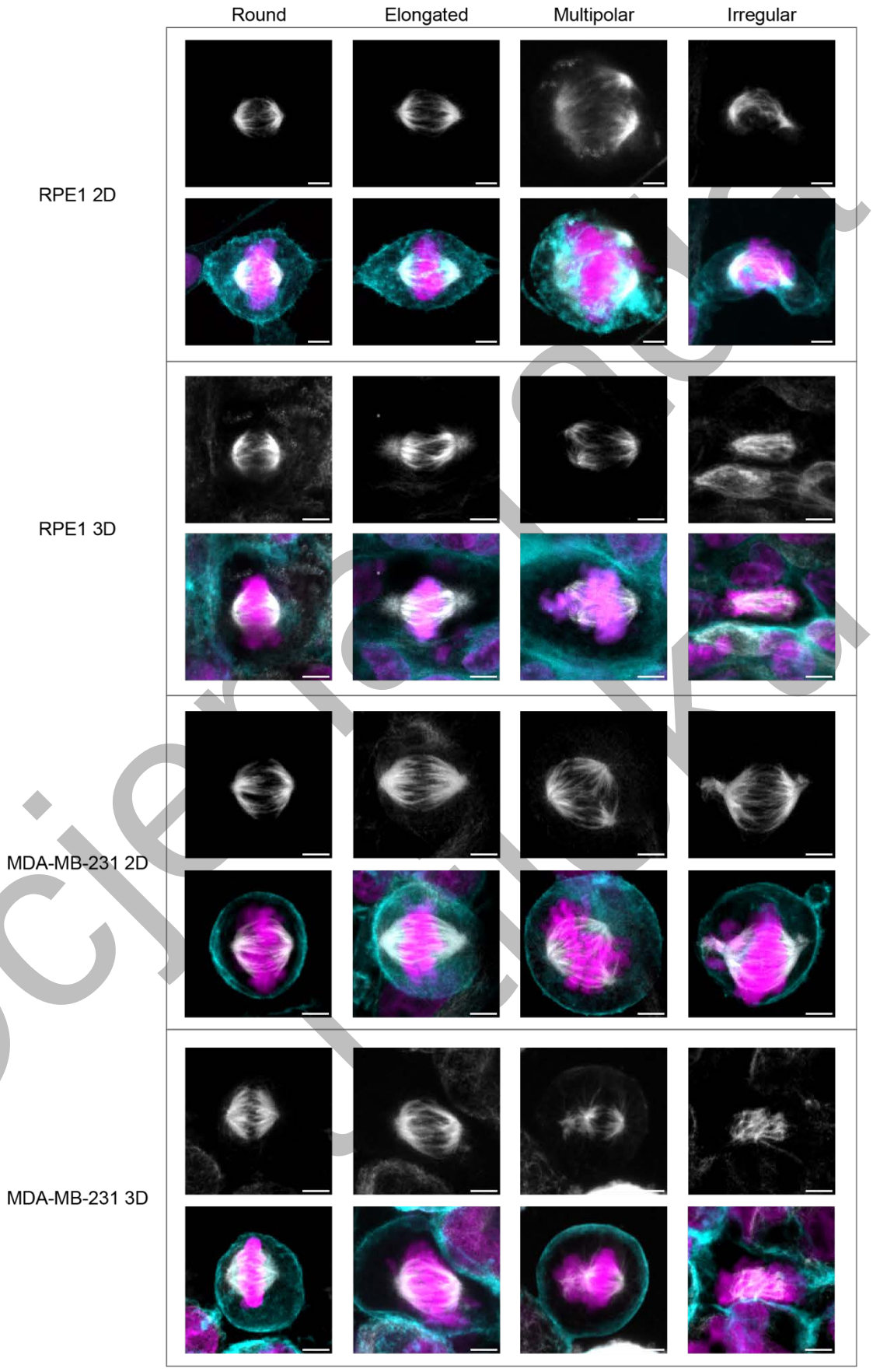

Figure 52. Caption on the following page.

Figure 52. Different spindle shapes observed in RPE1 p53KD and MDA-MB-231 monolayers and spheroids. Confocal images of immunostained RPE1 p53KD and MDA-MB-231 cells in monolayers and spheroids. Upper panels show images of immunostained tubulin (grey), and lower panels show merged images of immunostained tubulin (grey), DNA (magenta), and cell membrane stained with SiR-actin in MDA-MB-231 cells or WGA membrane dye in RPE p53KD cells (cyan). Images are shown as a SUM intensity projections. Scale bars, 5 μm.

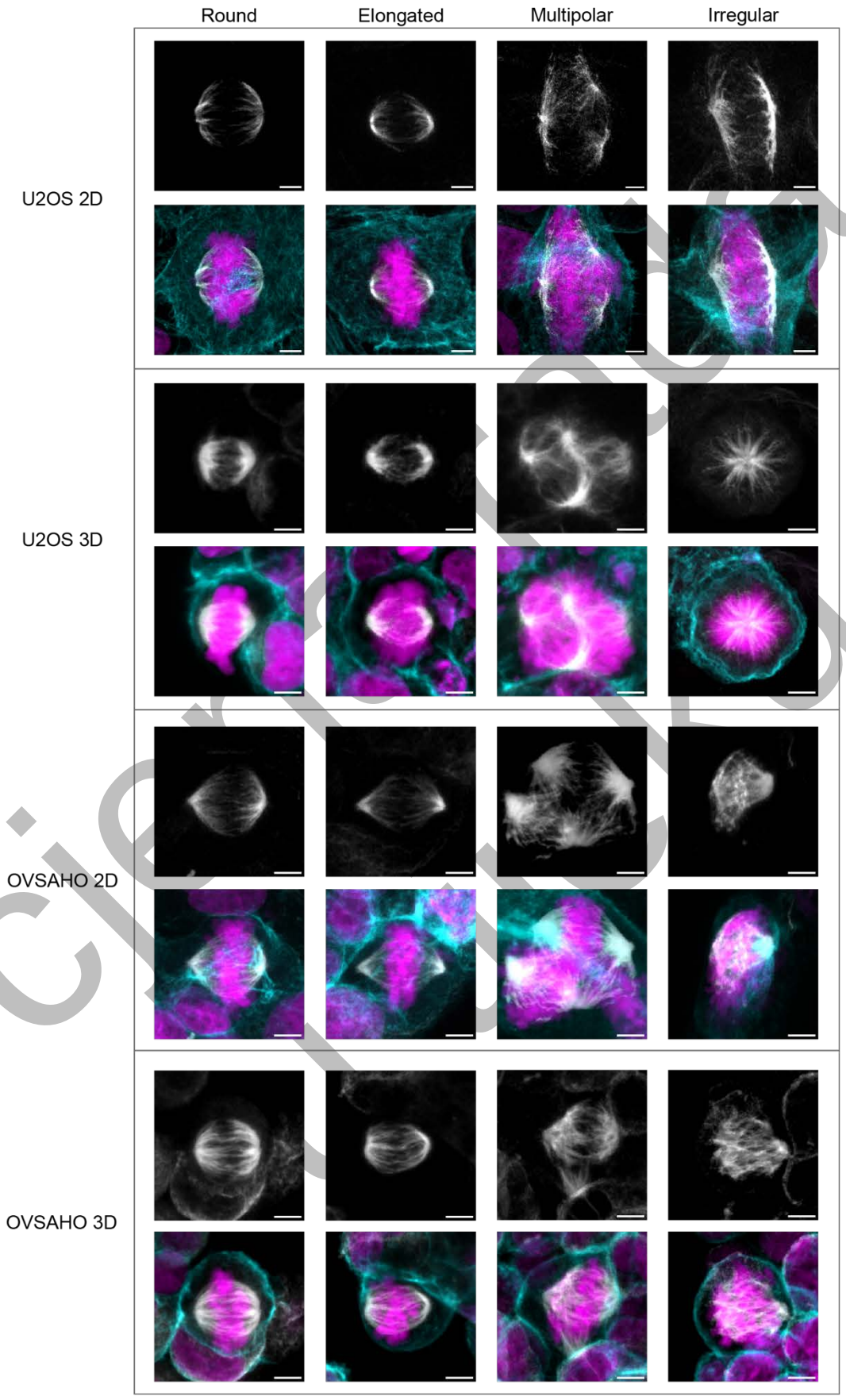

Figure 53. Caption on the following page.

Figure 53. Different spindle shapes observed in U2OS and OVSAHO monolayers and spheroids. Confocal images of immunostained U2OS and OVSAHO cells in monolayers and spheroids. Upper panels show images of immunostained tubulin (grey), and lower panels show merged images of immunostained tubulin (grey), DNA (magenta), and cell membrane stained with SiR-actin or WGA membrane dye in OVSAHO monolayers (cyan). Images are shown as a SUM intensity projections. Scale bars, 5 µm.

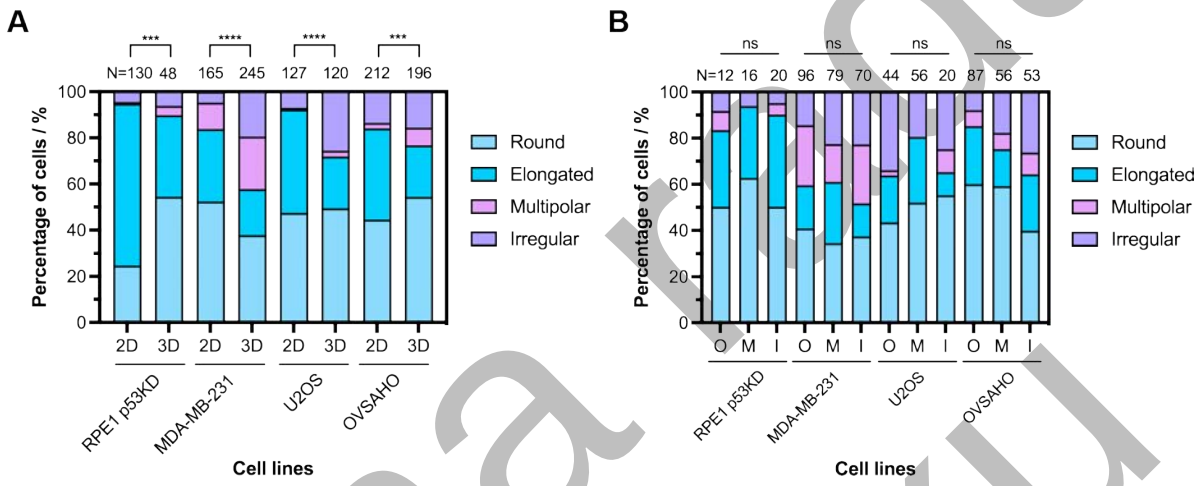

Figure 54. Cell line-specific variations in spindle shape between monolayers and spheroids. A) Frequency of different spindle shapes in monolayers and spheroids. **B)** Frequency of different spindle shapes in different layers of spheroids. Spindle shapes distribution was determined in outer (O), middle (M) and inner (I) layers (See Figure 45).

Cells in prometaphase and metaphase are analyzed, but early stages of prometaphase are excluded from this analysis. Statistical analysis: Chi-square test was performed. Ratio of outcomes was determined from a total number of cells for each cell line and a type of cell culture.

4.20. Spindle polarity is altered in tumor spheroids

The proportion of multipolar spindles increased in tumor cell spheroids, so spindle polarity was examined in more detail. Spindles were classified as monopolar, bipolar, tripolar, and tetrapolar-plus, including spindles that had four or more poles (Figure 55A). Tumor cell lines showed a higher percentage of multipolar spindles in spheroids, with the most pronounced increase in MDA-MB-231 cells (Figure 54A and Figure 55B). Notably, a small fraction of monopolar spindles was also detected in tumor spheroids. Although this fraction ranged only from 1% to 3%, it may indicate defects in centrosome separation and challenges in forming a proper bipolar spindle in spheroids (Tillement et al., 2009). This was also observed in a previous study, where freely growing HCT116 spheroids showed a small percentage of monopolar spindles, which increased to 22% under conditions of mechanical stress (Desmaison, Frongia, et al., 2013), further supporting the hypothesis that confinement affects bipolar spindle formation.

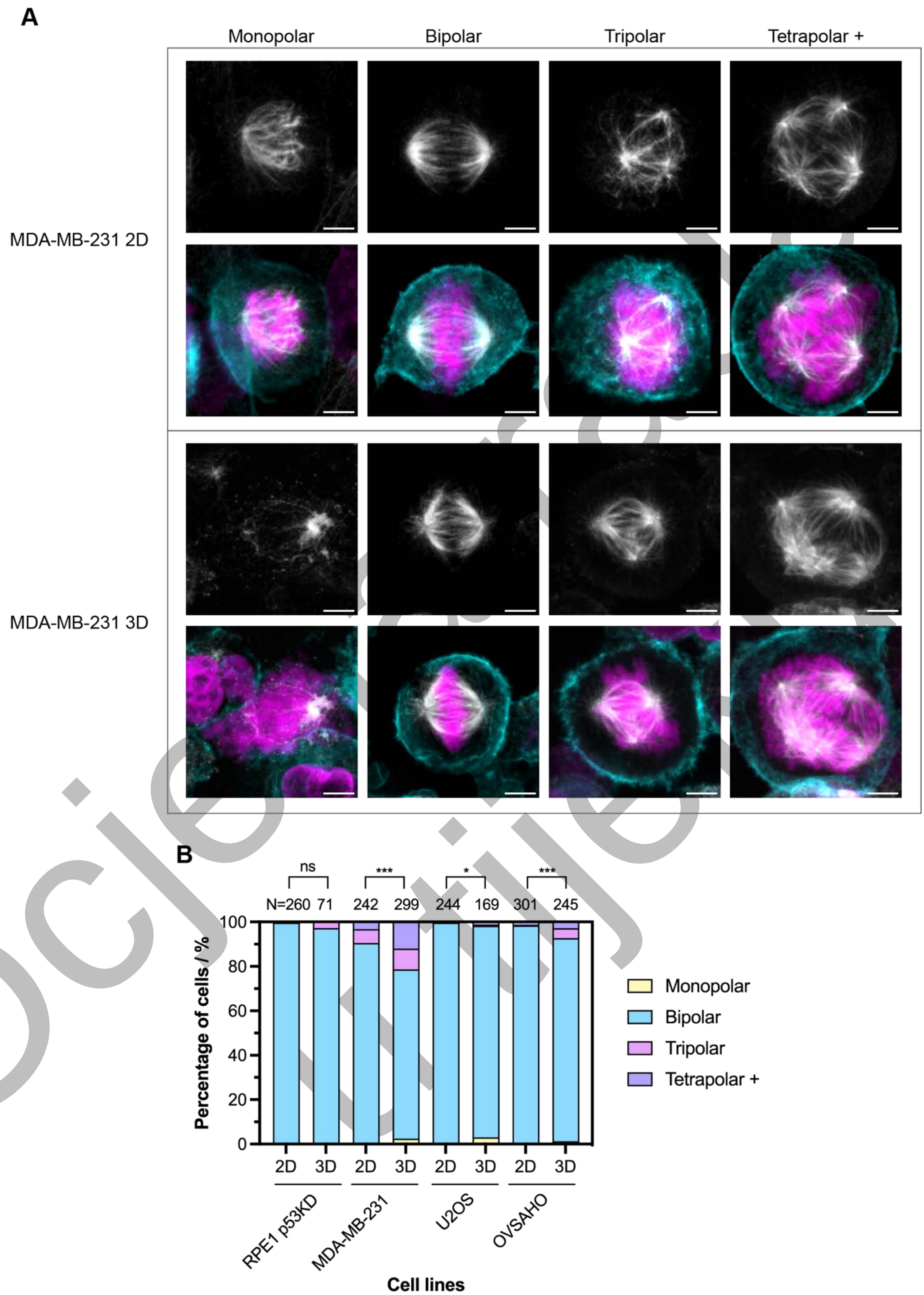

Figure 55. Caption on the following page.

Figure 55. Fraction of multipolar spindles increases in tumor spheroids. A) Confocal images of immunostained MDA-MB-231 cells in monolayers and spheroids. Upper panels show images of immunostained tubulin (grey), and lower panels show merged images of immunostained tubulin (grey), DNA (magenta), and cell membrane stained with SiR-actin (cyan). Images are shown as a SUM intensity projections. Scale bars, 5 µm. **B)** Frequency of of spindles with different polarity in monolayers and spheroids determined by the number of microtubule foci. Spindles that have four or more spindle poles are labelled as Tetrapolar +. Cells in prometaphase and metaphase are analyzed, but early stages of prometaphase are excluded from this analysis. Statistical analysis: Fisher's exact test when compared groups had two outcomes (RPE1 2D vs 3D), and Chi-square test if there were more than two outcomes. Ratio of outcomes was determined from a total number of cells for each cell line and a type of cell culture.

4.21. Spindle size scales with cell size in spheroids

Some studies have shown that spindle size scales with cell size, as observed in early zebrafish embryos and *Xenopus* egg extracts (Rieckhoff et al., 2020). In contrast, other research reported that spindle length does not scale with ploidy levels in yeast (Storchová et al., 2006). Similarly, the first part of this thesis demonstrated that spindle length does not scale with ploidy in diploid and PT RPE1 cell lines, consistent with previous findings (Bloomfield et al., 2021; Gudlin et al., 2025). To investigate whether spindle size scales with cell size under 3D culture conditions, spindle length and width were measured in metaphase cells (Figure 56A).

A significant reduction in both spindle length and width was observed in all cell lines cultured as spheroids compared to monolayers, except for spindle width in RPE1 p53KD, where no significant difference was detected (Figure 56B). The most pronounced difference was found in U2OS cells, which also showed the greatest reduction in cell size (Figure 50E). These results indicate that spindle dimensions scale with cell size in spheroids.

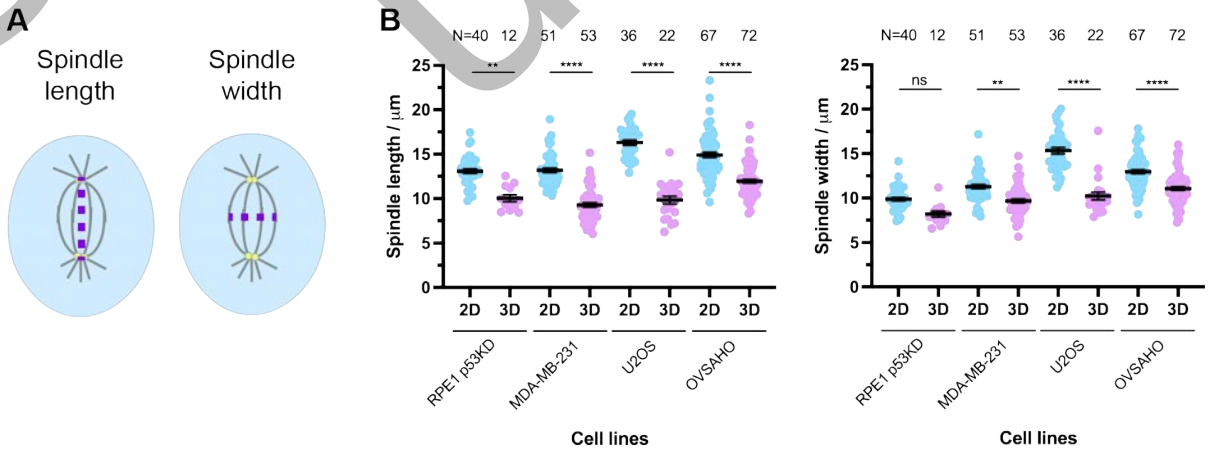

Figure 56. Spindles are significantly smaller in spheroids. A) Schematic representation of spindle dimensions that were measured to determine the spindle size. **B)** Spindle length of metaphase cells measured in monolayers and spheroids (left graph). Spindle width of metaphase cells measured in monolayers and spheroids (right graph). Only bipolar cells were analyzed. Error bars represent mean value and SEM. Statistical analysis: Kruskal-Wallis test with post-hoc Dunn's test was performed on a total number of cells for each cell line and a type of cell culture.

Multipolar spindles are more frequent in irregularly shaped cells in MDA-MB-231 spheroids. Finally, the relationship between cell shape, spindle shape, and prometaphase errors was examined in MDA-MB-231 cells. The only clear trend observed was that irregularly shaped cells had a higher proportion of multipolar spindles compared to round cells (Figure 57A). No significant differences were found between round and elongated cells, or between elongated and irregular cells. Overall, cell shape did not influence spindle polarity (Figure 57B). In addition, neither cell shape nor spindle shape was associated with an increased frequency of unaligned or misaligned chromosomes (Figure 57C-D).

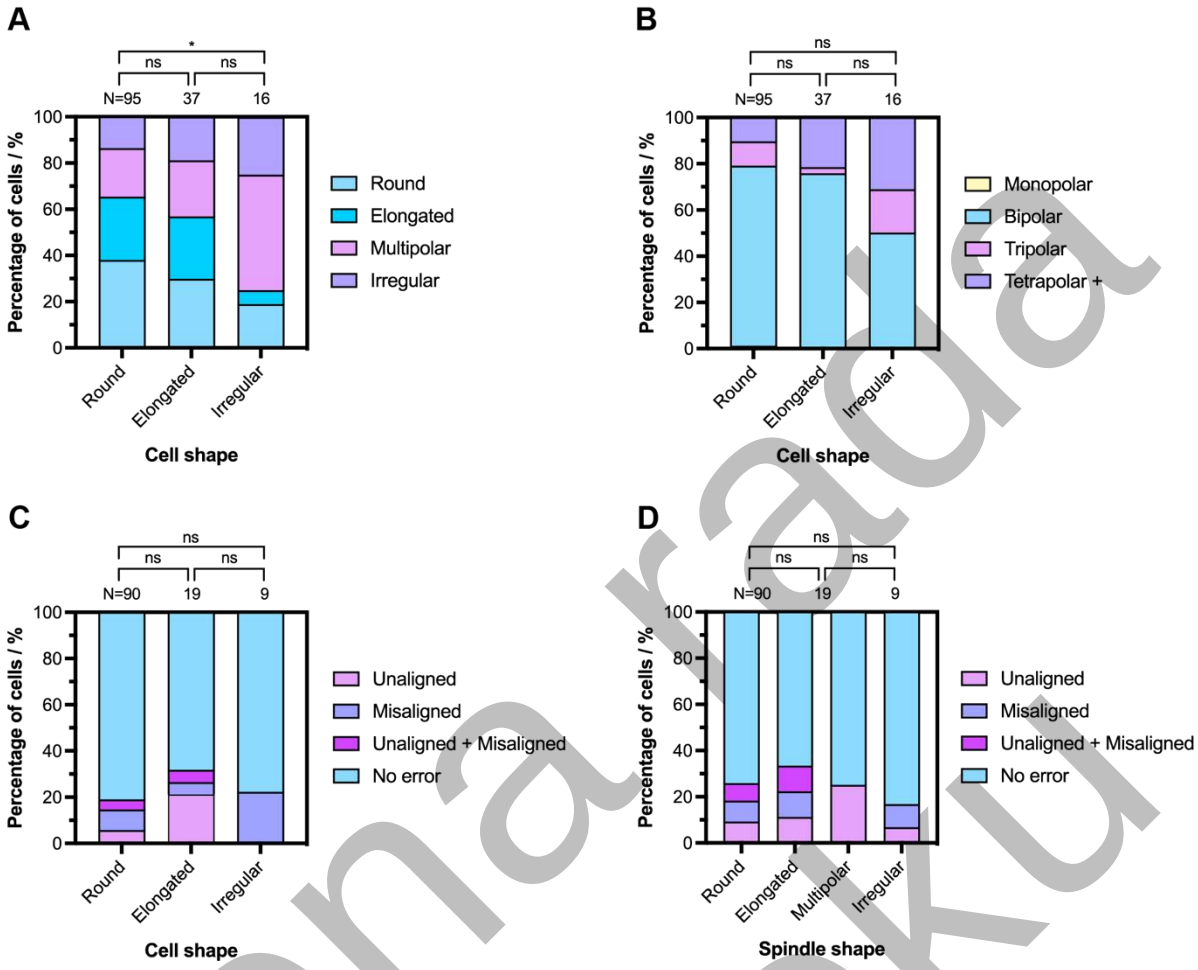

Figure 57. Irregular cell shape is linked to increased frequencies of multipolar spindles in MDA-MB-231 spheroids. A) Frequency of different spindle shapes across different cell shapes in MDA-MB-231 spheroids. **B)** Frequency of different spindle polarities across different cell shapes in MDA-MB-231 spheroids. **C)** Frequency of prometaphase errors across different cell shapes in MDA-MB-231 spheroids. **D)** Frequency of prometaphase errors across different spindle shapes in MDA-MB-231 spheroids.Statistical analysis: Chi-square test was performed. Ratio of outcomes was determined from a total number of cells for each cell line and a type of cell culture.

To conclude, this study demonstrates that culturing cells as spheroids induces significant changes in spindle organization and cell morphology compared to conventional 2D monolayers. Mitotic cells in spheroids were smaller and more rounded, with cell line-specific alterations in spindle shape, orientation, and polarity. Spindle size scales with cell size in all cell lines. While an increased proportion of prometaphase cells was observed in all tumor spheroids, a rise in prometaphase errors was observed only in MDA-MB-231, and non-tumor RPE1 p53KD, compared to monolayers. Anaphase error rates did not increase, suggesting that confinement in 3D affects early mitotic stages more than chromosome segregation. Overall, the data shows how 3D organization influences mitotic features in a cell line-dependent manner.

5. DISCUSSION

This thesis investigates two topics closely related to tumors. In the first part it was explored how diploid and PT RPE1 cells respond to KIF18A perturbations. Although RPE1 are non-tumor cells, they are of particular interest, because in some theories non-tumor tetraploid cells are considered potential precursors of tumorigenesis (Davoli & de Lange, 2011; Kirsch-Volders et al., 2024, 2025; Storchova & Kuffer, 2008; Storchova & Pellman, 2004). Novel KIF18A inhibitors are already being tested in clinical studies conducted by Volastra (*Volastra - Short Circuiting Cancer's Chaos*, 2025), showing promising results for tumor treatment. This study provides a detailed analysis of how KIF18A depletion and inhibition affect cells that may act as precursors to tumor development and thus represent a potential threat to the organism.

In the second part, the influence of 3D spatial organization on the mitosis of tumor and non-tumor cells was investigated. Characteristics of mitotic cells were compared between traditional 2D monolayer cultures and 3D spheroid cell cultures. This comparison is important because many studies on the mitotic spindle have been conducted in monolayers, which differ significantly from tissues. These structural differences may influence mitotic behavior and spindle architecture, and consequently the efficacy of novel antitumor compounds targeting mitotic cells.

5.1. Evaluation of sensitivity to KIF18A loss in diploid and PT cell lines

The sensitivity of different cell lines to KIF18A loss has been previously studied from different perspectives, including comparisons of aneuploid and polyploid, tumor and non-tumor, and CIN+ and CIN- cell types. It has been shown that tumor cells that have undergone WGD and exhibit elevated CIN are particularly sensitive to KIF18A loss due to activation of SAC (Cohen-Sharir et al., 2021; Marquis et al., 2021; Quinton et al., 2021). Recent work shows that sensitivity is not only linked to SAC activation but also to a weakened APC/C. Cells are considered sensitive to KIF18A loss if they exhibit persistent SAC signaling, which increases with ploidy, and weakened APC/C, altogether leading to mitotic arrest (Gliech et al., 2024). These studies have largely focused on tumor cell lines, but the effect of KIF18A loss on RPE1 cells, which were classified as insensitive, has also been examined (Gliech et al., 2024). In this thesis, KIF18A was perturbed by two approaches: siRNA-mediated knockdown and chemical inhibition using a small molecule inhibitor sovilnesib. Two diploid RPE1 cell lines were used, differing only in their expression of fluorescently labeled proteins. Also, two PT cell lines, derived from RPE1 parental, that share the same modal chromosome number were used.

5.2. KIF18A perturbations do not affect cell confluency

First, to test the impact of KIF18A depletion and inhibition on cell proliferation, changes in cell confluency over time were measured. In this study, no significant differences in cell confluency were observed following either depletion or inhibition in any cell line.

Similar results were reported by Gliech and colleagues, who showed a slightly slower increase in confluency in tetraploid RPE1 cells after KIF18A inhibition (Gliech et al., 2024). However, after seven days, the inhibited cells reached approximately 90% confluency compared to 100% in controls, which is insignificant difference. A more pronounced growth defect emerged only when APC/C activity was also inhibited (Gliech et al., 2024). Quinton and colleagues showed reduced viability in 4N RPE1 cells after KIF18A depletion (Quinton et al., 2021), but this cannot be directly compared with confluency since viable cells in the culture can still divide and increase the confluency. On the other hand, in tumor cells KIF18A depletion has been associated with reduced proliferation, such as in HPT cells (Cohen-Sharir et al., 2021) and MDA-MB-231 (Marquis et al., 2021).

5.3. KIF18A depletion exhibits the same effect on diploid and PT cell lines

KIF18A was successfully depleted in both diploid and PT cells for four days. siRNA-mediated knockdown efficiency varied, particularly in the double treatment experiments, but the protein's loss was confirmed through other parameters. Variability in the percentages of siRNA efficiency likely reflects microscope inconsistencies affecting signal intensity.

Following depletion, the protein was no longer localized on the spindle, spindle length increased, and metaphase plate was significantly wider, which indicates chromosome misalignment, as previously reported (Mayr et al., 2007; Stumpff et al., 2008). No consistent differences in these parameters were observed between diploid and PT cells over time, suggesting a similar response to KIF18A depletion. In the future, the immunofluorescence experiments should be repeated to collect bigger amounts of data which would be additional confirmation of the KIF18A depletion as well as the inhibition. In this study, experiments were performed to optimize ideal conditions, such as concentrations and incubation time. Also, other methods, such as Western blot, could be implemented to optimize the effectiveness of the study.

Live-cell imaging showed significantly prolonged mitosis following depletion, but unexpectedly, there was no difference between RPE1 parental and PT cell lines. An inconsistency was observed between the two diploid cell lines, where RPE1 parental had significantly longer mitosis than RPE1 CC, despite the same mitosis duration in control samples, and both cell lines have the low levels of CIN. This discrepancy may reflect uncharacterized mutations or adaptations accumulated over generations. Mitosis duration was longer than reported in a previous study (Cohen-Sharir et al., 2021), despite using the same protocol and cell lines. The

only difference was siRNA concentration, in this study 100 nM KIF18A siRNA was used, compared to 25 nM KIF18A siRNA in a previous study, suggesting that higher siRNA concentrations enhance the effect but diminish the difference between diploids and PTs.

5.4. Sovilnesib treatment has a stronger effect on PT cell lines

Novel small molecule KIF18A inhibitors: AM-0277, AM-1882, AM-5308 and AM-9022 have been described in the literature (Gliech et al., 2024; Payton et al., 2024). Although the exact differences between sovilnesib and these other compounds are unknown, they should all have the same mechanism of action. They inhibit the KIF18A motor domain, preventing its walking on microtubules and causing protein accumulation at spindle poles (Gliech et al., 2024; Payton et al., 2024), due to poleward flux (Varga et al., 2006).

The results demonstrate that sovilnesib successfully inhibits KIF18A in both diploid and PT RPE1 cell lines, with effects lasting up to seven days. Immunostaining experiments show that after sovilnesib treatment KIF18A is localized on the spindle poles. Concentrations between 100 nM and 500 nM were most effective, while low concentration showed only minor effects. 250 nM concentration was chosen as optimal. Protein inhibition had a similar effect on the mitotic spindle as depletion, with the key difference being that following inhibition, KIF18A remained localized at the spindle poles, whereas after depletion, the protein was no longer detectable on the spindle. Spindle length increased, as did metaphase plate width, indicating problems with chromosome alignment. Unlike depletion, in this case a distinction between diploid and PT cell lines was evident, with PTs showing broader metaphase plates, suggesting more pronounced chromosome alignment defects. Live-cell imaging confirmed these findings, with PT cells exhibiting prolonged mitosis.

Mitosis duration in diploids was greater than reported when AM-1882 inhibitor was used (Gliech et al., 2024), suggesting that sovilnesib may be more potent. Since different studies used different inhibitors (Gliech et al., 2024; Payton et al., 2024), it is not possible to directly compare their effect on mitotic cells, and sovilnesib's relative potency remains undetermined. In future studies sovilnesib should be compared to other inhibitors to precisely evaluate its efficiency, and possible differences in mechanism of action. It remains unclear whether KIF18A accumulation at spindle poles affects microtubules or if KIF18A interacts with proteins localized at the spindle pole. Sovilnesib inhibits the ATP-dependent motor domain, but the ATP-independent microtubule-binding domain likely remains intact and could still interact with other structures and have a role in centrosomes fragmentation. To investigate this, interactome analysis should be performed, and untreated cells should be compared with cells treated with sovilnesib.

5.5. A subpopulation of cells exhibits increased sensitivity to KIF18A loss

Both depletion and inhibition gave rise to a subpopulation of cells with a specific phenotype, referred to as oversensitive cells. These cells had severe chromosome alignment defects and hyper-oscillating chromosomes scattered across the spindle. Superresolution STED microscopy revealed disrupted spindle architecture and loss of k-fibers. These cells often entered prolonged mitotic arrest. After depletion, the fraction of oversensitive cells was comparable between diploid and PT lines. However, after inhibition, PT cells exhibited a significantly higher fraction of oversensitive cells, as shown by both live-cell imaging and immunostaining. These findings suggest that KIF18A inhibition uncovers differences in sensitivity between diploid and PT cells that are not detectable following depletion. Oversensitive cells were further classified as bipolar or multipolar. PT cell lines had a higher fraction of oversensitive multipolar cells after both depletion and inhibition, emphasizing another key difference, and indicating that PT cells are more prone to centrosome fragmentation. Live-cell imaging revealed that some oversensitive cells dynamically change spindle polarity from bipolar to multipolar spindles, back and forth. No prior reports of this phenomenon were found in the literature. Similar phenotypes with hyper-oscillating chromosomes, centrosome fragmentation and mitotic arrest lasting for up to 20 hours, have been noted in tumor cells, but they have not been extensively characterized (Marquis et al., 2021; Quinton et al., 2021).

KIF18A regulates microtubule dynamics (Gupta et al., 2006; Mayr et al., 2007; Stumpff et al., 2008; Varga et al., 2006), and its loss causes increased polymerization and centrosome fragmentation in CIN+ cells, leading to chromosome alignment defects. Marquis and colleagues proposed a model for selective dependance of CIN+ cells to KIF18A. In this model, increased microtubule polymerization and chromosome number lead to severe chromosome alignment defects. One fraction of cells will complete mitosis after a mitotic delay, followed with mis-segregation errors and micronuclei formation. Other fraction will have further deregulation of microtubule dynamics which leads to extended mitotic delay and disrupted integrity of mitotic spindle leading to centrosome fragmentation. The outcome of mitosis for this fraction is often cell death (Marquis et al., 2021).

Based on the results from this thesis, chromosomes hyper-oscillations and loss of k-fibers could have an important role in centrosome fragmentation. Microtubule stability and organization are highly disrupted and together with hyper-oscillating chromosomes accumulated behind the spindle pole this could cause centrosome fragmentation and dynamic changes of spindle polarity (Figure 58).

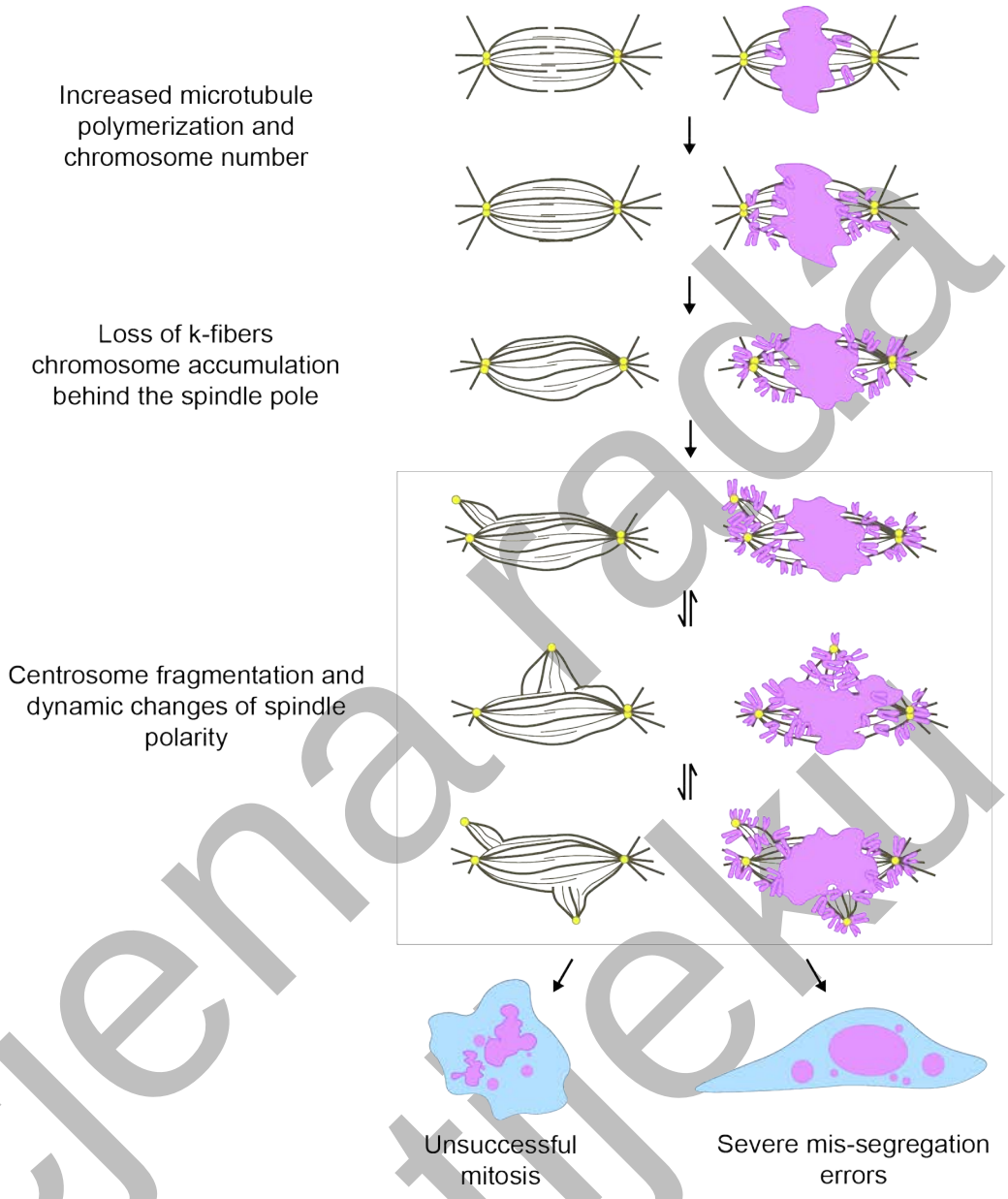

Figure 58. Unsuccessful mitosis in oversensitive cell after KIF18A loss. Oversensitive cells have increased microtubule polymerization and chromosome number, which leads to the loss of k-fibers and chromosome hyperoscillations. Chromosomes accumulate behind the spindle pole. Centrosomes fragment, and due to increased microtubule polymerization, they dynamically change spindle polarity. Mitosis ends unsuccessfully or with severe mis-segregation errors.

In the future, the reasons why oversensitive PT cells have more multipolar spindles than diploids should be determined. This could simply be because of higher chromosome number, which causes more hyper-oscillations which will have greater impact on microtubule stability. This could easily be tested by counting chromosome number in diploid and PT oversensitive cells. Also, because chromosome number differs in PT cells, chromosome number between oversensitive bipolar and oversensitive multipolar cells should be compared. In another approach, ploidy levels could be increased to get newly formed tetraploids and octoploids as described in previous study (Gudlin et al., 2025), and fraction of oversensitive cells after KIF18A loss could be compared among the RPE1 cell lines with different ploidy levels. Furthermore, microtubule poleward flux should be measured to see if microtubule dynamics is even more disturbed in oversensitive cells after KIF18A perturbations.

On the other hand, expression levels of proteins that regulate spindle polarity could be different in oversensitive PTs in comparison with diploids. For example, Aurora A kinase regulates bipolar spindle formation, and its overexpression can lead to centrosomes overgrowth and multipolar spindle formation (Willems et al., 2018). Also, NuMA is important for spindle assembly, and its overexpression induces spindle multipolarity (Quintyne et al., 2005). It could be possible that oversensitive PT cells have slightly higher expression levels of these proteins, compared to diploids, which in combination with disrupted microtubules dynamics leads to multipolarity.

Further studies using live-cell imaging with tubulin label and PCM markers, such as γ -tubulin, are needed to clarify the exact timing and mechanisms involved in dynamic changes of spindle polarity. Analysis of chromosome number and expression levels of proteins involved in maintaining spindle polarity would help to clarify why oversensitive PT cells have more multipolar spindles.

5.6. Combined treatment with KIF18A siRNA and sovilnesib

The strong effect of sovilnesib treatment, compared to siRNA-mediated depletion was unexpected. To test if the inhibitor has some non-specific effects, cells were treated with a combination of KIF18A siRNA and sovilnesib. While spindle parameters were largely like depletion alone, the proportion of oversensitive cells increased compared to depletion alone. Sovilnesib is a relatively new inhibitor and available data about its properties remains limited. Whether this differences between double treatment and depletion alone reflects a synergistic interaction of siRNA and inhibitor, or off-target effects of sovilnesib remains unclear. Further studies using precise approaches, such as thermal proteome profiling (George et al., 2023; Mateus et al., 2022) or in vitro binding assays (Takeda et al., 2006), are needed to clarify this.

In summary, sovilnesib is a novel KIF18A inhibitor which is already used in a phase Ib clinical trials in patients with high grade serous ovarian cancer (HGSOC) (*Volastra - Short Circuiting Cancer's Chaos*, 2025), so it is important to know its mechanism of action in both tumor and non-tumor cells. This study demonstrates that KIF18A perturbation, through both siRNA-mediated depletion and chemical inhibition with sovilnesib, disrupts mitotic spindle organization and chromosome alignment in both diploid and PT RPE1 cell lines. While both approaches were efficient, sovilnesib induced more pronounced phenotypes, particularly in PT cells. A key observation was the emergence of an oversensitive subpopulation, especially in PT cells, characterized by dynamic changes in spindle polarity during mitosis, a phenomenon not previously reported. These defects suggest that spindle instability may be a unique vulnerability of polyploid or highly aneuploid cells.

5.7. Cell shape adaptations in monolayer and spheroid cell cultures

In this study spheroids of three tumor cell lines: MDA-MB-231, U2OS and OVSAHO and a non-tumor cell line RPE1 p53KD were successfully generated using the magnetic cell levitation method and compared to cells cultured in monolayers. Cell shape changes were observed between monolayers and spheroids and were specific to each cell line. RPE1 p53KD cells retained a partially elongated shape, OVSAHO cells showed no notable difference, while MDA-MB-231 and U2OS cells changed from elongated, branched morphologies to more rounded shapes in spheroids.

5.8. Increased fraction of prometaphase cells indicates mitotic arrest in tumor spheroids

Mitotic cells were found in all parts of the spheroids, indicating that in this system there is no typical division into proliferative, quiescent, and necrotic zones. This is probably because the spheroids have a flattened and irregular shape, and they are not thick enough for cells in the inner layers to experience a lack of oxygen and nutrients. To obtain spheroids with a regular shape, other methods for spheroid generation should be used, such as the hanging drop method.

All tumor spheroids showed an accumulation of cells in prometaphase and metaphase, with a corresponding decrease in anaphase and telophase cells, suggesting prolonged prometaphase and possible mitotic arrest due to chromosome alignment defects. Future studies should investigate whether SAC remains active in these cells, because it prevents progression into anaphase until all kinetochores are properly attached (Lara-Gonzalez et al., 2021). This could be tested by determining the levels of the mitotic arrest deficiency 2 (Mad2) protein or with live-cell imaging of cells with labeled Mad2. This protein is a part of SAC

complex, it accumulates on unattached kinetochores and prevents anaphase onset until all kinetochores are properly attached to microtubules.

Live-cell imaging would provide information on mitosis duration and outcomes. So far, prometaphase arrest has only been reported in spheroids under mechanical stress (Desmaison et al., 2018). Future experiments should test whether mechanical stress further increases the fraction of prometaphase cells, which would support the hypothesis that confinement in spheroids contributes to mitotic arrest compared to monolayers. In spheroids the fraction of cells with anaphase errors did not increase, compared to monolayers, but low sample size could influence this result. In contrary, previous report noted increased frequency of lagging chromosomes in spheroids (Molla et al., 2017), but this could also be a cell lines-specific result. It is possible that due to the SAC activation cells in spheroids arrest in prometaphase until all the faulty attachments are corrected and chromosomes are properly aligned in metaphase, so when cells proceed to anaphase there will be no mis-segregation errors, which would explain high fraction of prometaphase cells, and low fraction of anaphase cells, that are mostly without mis-segregation errors. Long-term live-cell imaging of a whole spheroid would confirm this assumption.

5.9. Impact of confinement on cell and spindle morphology in spheroids

In all cell lines, both mitotic cells and spindles were generally smaller in spheroids, with observed decrease in both length and width. Also, cells and spindles had different shapes in spheroids compared to monolayers. Interphase cells also appeared smaller, although this was not quantified. Changes in spindle shape were cell line-specific and partially mirrored changes in cell shape. For example, RPE1 p53KD spheroids had more round cells and round spindles, MDA-MB-231 showed an increase in irregular cells and irregular and multipolar spindles and U2OS had fewer elongated cells and spindles. OVSAHO cells maintained the same cell shape in monolayers and spheroids but showed altered spindle shape, indicating that other factors also affect spindle morphology in spheroids.

A decrease in cell size in spheroids most likely occurred due to confined conditions and mechanical forces exerted by adjacent cells. Confinement also affected cell shape, resulting in more rounded and irregular shapes, because the cells did not have enough space to spread, and were squashed by neighboring cells, unlike in monolayers, where cells have enough space to expand. This was especially significant in MDA-MB-231 and U2OS spheroids. Spheroid confinement likely compresses cells in all directions, leading both spindle length and width to scale with reduced cell size. Spindle shape adapts to this confined environment.

Previous research on mechanical stress in spheroids mostly focused on proliferative cell distribution (Desmaison, Frongia, et al., 2013; Dolega et al., 2017), while spindle properties remain unexplored. Bipolar spindle formation impairment was reported in both confined (Desmaison, Frongia, et al., 2013) and freely growing spheroids (Molla et al., 2017), which is also found in this study, and implies that cells are under mechanical stress in spheroids. Also, it was shown that multipolar spindles, which were observed in high fraction in MDA-MB-231 spheroids can also be found in breast cancer tissue (Ibrahim et al., 2022).

In a study where MDA-MB-231 cells were injected into mice and formed tumors, histological samples showed that mitotic cells were rounded, but the spacing between neighboring nuclei appeared larger (Wiebe et al., 2013). This suggests that the cells were larger and subjected to less mechanical stress from adjacent cells than in the spheroids, indicating that spheroids are a good model for tumor regions under confined conditions. In some cells, the metaphase plate was positioned to one side of the cell (Wiebe et al., 2013), which was also observed in this study, where MDA-MB-231 cells in spheroids showed the highest percentage of spindles located asymmetrically. Changes of spindle orientation and symmetry in spheroids indicate that ECM and neighboring cells influence cell cortex and its interaction with spindle, which should be investigated in the future studies, by examining localization and expression levels of ECM components, and proteins involved in spindle orientation, such as LGN, NuMA and dynein (McNally, 2013; Zheng et al., 2010).

Previous studies demonstrated that spindle size does not always scale with cell size or ploidy. For example, spindle width increased by approximately 20% in tetraploid human cells, but spindle length remained unchanged (Bloomfield et al., 2021). Study on yeast also showed that spindle length does not scale with ploidy (Storchová et al., 2006). However, these studies focused on monolayer cultures where cell size changes due to increased ploidy, unlike this study where spheroid culture conditions cause size changes, independent of ploidy. In a recent study, spindles were squeezed by compressing them with the agarose gel. The forces were applied parallel to the surface and to the long axis of spindle, and caused changes in spindle height, but not in spindle length (Gudlin et al., 2025). In this study cells were confined from all directions which caused the change of both spindle length and width.

In the future, the level of mechanical stress on cells in spheroids should be explored using different approaches. Mechanical stress can directly be measured by using micro-beads (Cheng et al., 2009) or magnetic tweezers (Bonakdar et al., 2014). Also, additional forces can be applied on the spheroids to see if additional changes of size and shape will occur. In another approach, change of cell size, as an indicator of mechanical stress, could be measured in time. Cell size could be compared between cells in suspension, in early stages of spheroid formation and in fully formed spheroids. This approach would show whether mechanical stress gradually increases or if a certain number of cells is required for confined conditions to

develop. Other parameters that could influence spindle shape should be explored. It is not clear if ECM components could influence spindle shape. Also, various MAPs influence spindle shape, such as KIF18A (Gupta et al., 2006; Mayr et al., 2007; Stumpff et al., 2008; Varga et al., 2006), HSET (Cai et al., 2009) and Eg5 (Yang et al., 2016). Expression levels of proteins that regulate spindle length should be compared between monolayers and spheroids, by using proteomics and immunofluorescence methods, as it was shown that protein expression vary between monolayers and spheroids (Kumar et al., 2008).

5.10. Differences between tumor and non-tumor cell lines spheroids

Although many of the observed changes were cell line-specific, some consistent differences emerged between tumor and non-tumor cell lines (Figure 59). In non-tumor cells, there was no change in the distribution of mitotic phases between monolayers and spheroids. In contrast, tumor cells spheroids showed a higher fraction of cells in prometaphase and metaphase, suggesting prolonged prometaphase and potential mitotic arrest. Additionally, irregular cell shapes were observed only in tumor spheroids. Non-tumor spheroids exhibited fewer irregular spindle shapes, and an insignificant number of multipolar spindles. Furthermore, there were no monopolar spindles in non-tumor spheroids. These results emphasize the importance of using 3D models in tumor research, as the results obtained from spheroids and monolayers significantly differ.

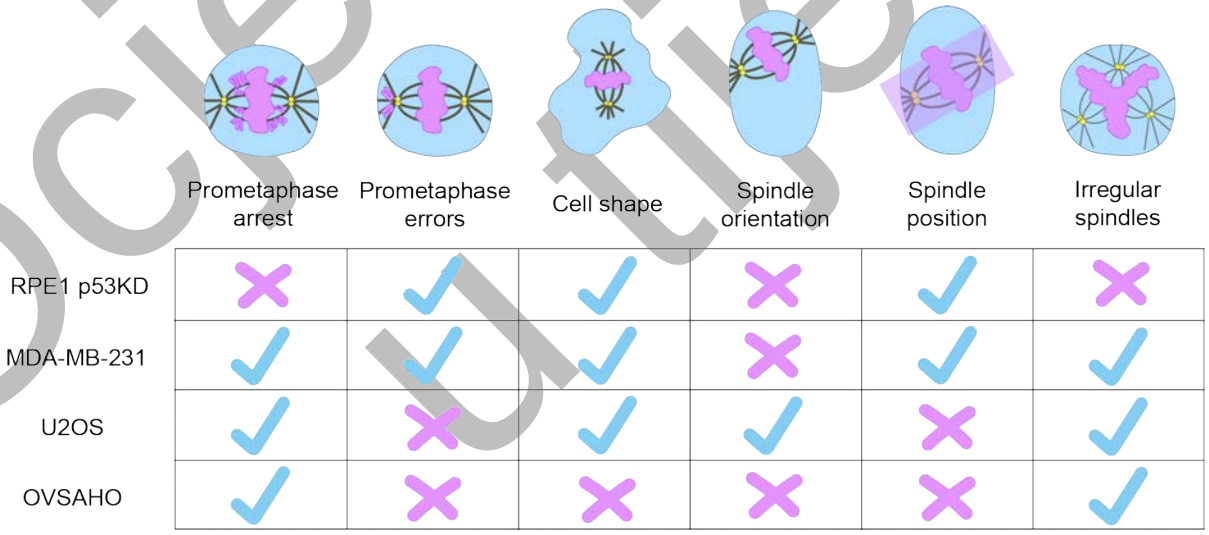

Figure 59. Caption on the following page.

Figure 59. Variability in mitotic patterns between monolayers and spheroids is cell line specific. The fraction of cells in prometaphase, occurrence of prometaphase errors, changes in cell shape, spindle orientation, spindle position within the cells, and spindle morphology were compared between monolayers and spheroids in different cell lines. A check mark denotes a change in mitotic pattern between monolayers and spheroids, whereas a cross mark denotes no observed change for a given cell line.

In summary, significant changes between monolayers and spheroids were observed in both tumor and non-tumor cell lines, and some of these changes are cell line specific. The biggest difference in mitotic patterns between spheroids and monolayers was observed in MDA-MB-231, which showed increased prometaphase fraction, altered cell shape, irregular and multipolar spindles, spindle positioning changes, and prometaphase errors. In contrast, OVSAHO showed fewer differences, limited to increase in metaphase fraction, spindle positioning, and spindle polarity changes.

This study highlights the importance of choosing appropriate models for research, as both cell line and culture type can influence the results. Multicellular tumor spheroids display smaller cell and spindle sizes with altered shapes, indicating confinement. These features make spheroids a relevant model to study non-vascularized, compressed tumor regions (Johnson et al., 2025; Sutherland, 1988). Confined conditions and disorganization of cells in space does not reflect the architecture of a healthy tissue. To study properties of non-tumor cells, other 3D models such as organoids, are more appropriate. Organoids reflect tissue architecture with cells strictly organized in space and well-defined cell polarity (Clevers, 2016).

Future research should focus on establishing protocols for long-term live-cell imaging of whole spheroids, to obtain information about mitosis duration and duration of each mitotic phase, which would indicate possible mitotic arrest and problems with chromosome alignment, the spatial distribution of mitotic cells, mitotic index and the rate of mis-segregation errors. Furthermore, the levels of confinement and their effect on mitotic cells should be described in detail. Lastly genomic or proteomic analyses should be conducted to explore the variability in mitotic patterns in spheroids among the cell lines.

6. CONCLUSION

In this thesis two topics that are relevant for gaining novel insights on tumor biology were explored. The first part examined differences in sensitivity to KIF18A depletion and inhibition in diploid and PT non-tumor cell lines, while the second part investigated the influence of 3D component in cell cultures on mitosis.

Both KIF18A depletion and inhibition led to prolonged mitosis, spindle elongation, and chromosome alignment defects. While depletion caused a similar effect in both diploid and PT cell lines, inhibition had a stronger overall impact, with more pronounced effects in PT cells. Mitosis prolongation was even longer in PT cells, and chromosome alignment defects were more severe.

A subpopulation of cells showing increased sensitivity to both depletion and inhibition was described for the first time in both diploid and PT cell lines. These cells were characterized by severe mitotic arrest, hyperoscillating chromosomes, and spindles that dynamically change their polarity throughout the mitosis. This subpopulation significantly increased following inhibition, and it was more prevalent in PT cells than in diploids. To conclude, KIF18A inhibition with sovilnesib, significantly affects RPE1 cells, even though they were classified as insensitive.

3D tumor and non-tumor cell cultures were successfully established using the magnetic levitation method, and mitotic cells in classical 2D monolayer cultures were compared with those in spheroids. An increased proportion of cells in prometaphase was observed in spheroids, indicating possible mitotic arrest.

In all tested cell lines, both the cells and the spindles were smaller in spheroids. To some extent, changes in cell shape are followed with changes in spindle shape. Considering that spindle size scales with cell size, and that an increased proportion of irregular shapes was observed, it can be concluded that cells within spheroids are under confinement, which may contribute to mitotic arrest. To conclude, this is the first study to characterize spindle differences between monolayer cultures and spheroids, offering a more realistic picture of cell division in confined conditions that resemble tumor architecture.

7. REFERENCES

Adcock, A. F., Trivedi, G., Edmondson, R., Spearman, C., & Yang, L. (2015). Three-Dimensional (3D) Cell Cultures in Cell-based Assays for in-vitro Evaluation of Anticancer Drugs. *Journal of Analytical & Bioanalytical Techniques*, *6*(3), Article 3. https://doi.org/10.4172/2155-9872.1000249

Aguilera, A., & Gómez-González, B. (2008). Genome instability: A mechanistic view of its causes and consequences. *Nature Reviews Genetics*, *9*(3), 204–217. https://doi.org/10.1038/nrg2268

Alberts, B., Johnson, A., Lewis, J., Raff, M., Roberts, K., & Walter, P. (2002). *Molecular Biology of the Cell* (4th ed.). Garland Science. https://doi.org/10.1093/aob/mcg023

Alfaro-Aco, R., & Petry, S. (2015). Building the Microtubule Cytoskeleton Piece by Piece*. *Journal of Biological Chemistry*, *290*(28), 17154–17162. https://doi.org/10.1074/jbc.R115.638452

Aumailley, M., & Gayraud, B. (1998). Structure and biological activity of the extracellular matrix. *Journal of Molecular Medicine*, *76*(3), 253–265. https://doi.org/10.1007/s001090050215

Bakhoum, S. F., Genovese, G., & Compton, D. A. (2009). Deviant kinetochore microtubule dynamics underlie chromosomal instability. *Current Biology: CB*, *19*(22), 1937–1942. https://doi.org/10.1016/j.cub.2009.09.055

Baudoin, N. C., Nicholson, J. M., Soto, K., Martin, O., Chen, J., & Cimini, D. (2020). Asymmetric clustering of centrosomes defines the early evolution of tetraploid cells. *eLife*, *9*, e54565. https://doi.org/10.7554/eLife.54565

Ben-David, U., & Amon, A. (2020). Context is everything: Aneuploidy in cancer. *Nature Reviews Genetics*, *21*(1), 44–62. https://doi.org/10.1038/s41576-019-0171-x

Bloomfield, M., Chen, J., & Cimini, D. (2021). Spindle Architectural Features Must Be Considered Along With Cell Size to Explain the Timing of Mitotic Checkpoint Silencing. *Frontiers in Physiology*, *11*. https://doi.org/10.3389/fphys.2020.596263

Boiron, M., Guillemain, B., Bernard, C., Peries, J., & Chuat, J. C. (1968). Presence in murine sarcoma virus stocks of a 3d component which alone initiates cellular conversion. *Nature*, *219*(5155), 748–749. https://doi.org/10.1038/219748a0

Bonakdar, N., Schilling, A., Lennert, P., Spörrer, M., Gerum, R. C., Alonso, J. L., & Goldmann, W. H. (2014). Measuring mechanical properties in cells: Three easy methods for biologists. *Cell Biology International*, *38*(10), 1227–1232. https://doi.org/10.1002/cbin.10303

Breslin, S., & O'Driscoll, L. (2013). Three-dimensional cell culture: The missing link in drug discovery. *Drug Discovery Today*, *18*(5), 240–249. https://doi.org/10.1016/j.drudis.2012.10.003

Bulysheva, A. A., Bowlin, G. L., Petrova, S. P., & Yeudall, W. A. (2013). Enhanced chemoresistance of squamous carcinoma cells grown in 3D cryogenic electrospun scaffolds. *Biomedical Materials (Bristol, England)*, *8*(5), 055009. https://doi.org/10.1088/1748-6041/8/5/055009

Burrell, R. A., McGranahan, N., Bartek, J., & Swanton, C. (2013). The causes and consequences of genetic heterogeneity in cancer evolution. *Nature*, *501*(7467), 338–345. https://doi.org/10.1038/nature12625

Cai, S., Weaver, L. N., Ems-McClung, S. C., & Walczak, C. E. (2009). Kinesin-14 Family Proteins HSET/XCTK2 Control Spindle Length by Cross-Linking and Sliding Microtubules. *Molecular Biology of the Cell*, *20*(5), 1348–1359. https://doi.org/10.1091/mbc.E08-09-0971

Carroll, T. D., Langlands, A. J., Osborne, J. M., Newton, I. P., Appleton, P. L., & Näthke, I. (2017). Interkinetic nuclear migration and basal tethering facilitates post-mitotic daughter separation in intestinal organoids. *Journal of Cell Science*, *130*(22), 3862–3877. https://doi.org/10.1242/jcs.211656

Cheeseman, I. M., Chappie, J. S., Wilson-Kubalek, E. M., & Desai, A. (2006). The Conserved KMN Network Constitutes the Core Microtubule-Binding Site of the Kinetochore. *Cell*, *127*(5), 983–997. https://doi.org/10.1016/j.cell.2006.09.039

Chen, Q., & Wang, Y. (2020). The application of three-dimensional cell culture in clinical medicine. *Biotechnology Letters*, *42*(11), 2071–2082. https://doi.org/10.1007/s10529-020-03003-y

Cheng, G., Tse, J., Jain, R. K., & Munn, L. L. (2009). Micro-Environmental Mechanical Stress Controls Tumor Spheroid Size and Morphology by Suppressing Proliferation and Inducing Apoptosis in Cancer Cells. *PLOS ONE*, *4*(2), e4632. https://doi.org/10.1371/journal.pone.0004632

Cherry, A. B. C., & Daley, G. Q. (2012). Reprogramming cellular identity for regenerative medicine. *Cell*, *148*(6), 1110–1122. https://doi.org/10.1016/j.cell.2012.02.031

Chignola, R., Schenetti, A., Andrighetto, G., Chiesa, E., Foroni, R., Sartoris, S., Tridente, G., & Liberati, D. (2000). Forecasting the growth of multicell tumour spheroids: Implications for the dynamic growth of solid tumours. *Cell Proliferation*, *33*(4), 219–229. https://doi.org/10.1046/j.1365-2184.2000.00174.x

Chin, H. M. S., Nandra, K., Clark, J., & Draviam, V. M. (2014). Need for multi-scale systems to identify spindle orientation regulators relevant to tissue disorganization in solid cancers. *Frontiers in Physiology*, *5*. https://doi.org/10.3389/fphys.2014.00278

Cimini, D., Howell, B., Maddox, P., Khodjakov, A., Degrassi, F., & Salmon, E. D. (2001). Merotelic Kinetochore Orientation Is a Major Mechanism of Aneuploidy in Mitotic Mammalian Tissue Cells. *The Journal of Cell Biology*, *153*(3), 517–528.

Clevers, H. (2013). The intestinal crypt, a prototype stem cell compartment. *Cell*, *154*(2), 274–284. https://doi.org/10.1016/j.cell.2013.07.004

Clevers, H. (2016). Modeling Development and Disease with Organoids. *Cell*, *165*(7), 1586–1597. https://doi.org/10.1016/j.cell.2016.05.082

Cohen-Sharir, Y., McFarland, J. M., Abdusamad, M., Marquis, C., Bernhard, S. V., Kazachkova, M., Tang, H., Ippolito, M. R., Laue, K., Zerbib, J., Malaby, H. L. H., Jones, A., Stautmeister, L.-M., Bockaj, I., Wardenaar, R., Lyons, N., Nagaraja, A., Bass, A. J., Spierings, D. C. J., … Ben-David, U. (2021). Aneuploidy renders cancer cells vulnerable to mitotic checkpoint inhibition. *Nature*, *590*(7846), 486–491. https://doi.org/10.1038/s41586-020-03114-6

Conduit, P. T., Wainman, A., & Raff, J. W. (2015). Centrosome function and assembly in animal cells. *Nature Reviews Molecular Cell Biology*, *16*(10), 611–624. https://doi.org/10.1038/nrm4062

Ćosić, M., & Petelinec, A. (2024). The role of 3D cell cultures in understanding mitosis and tissue architecture. *Periodicum Biologorum*, *126*(1–2), Article 1–2. https://doi.org/10.18054/pb.v126i1-2.32856

Cukierman, E., Pankov, R., Stevens, D. R., & Yamada, K. M. (2001). Taking Cell-Matrix Adhesions to the Third Dimension. *Science*, *294*(5547), 1708–1712. https://doi.org/10.1126/science.1064829

Dagenbach, E. M., & Endow, S. A. (2004). A new kinesin tree. *Journal of Cell Science*, *117*(Pt 1), 3–7. https://doi.org/10.1242/jcs.00875

Davoli, T., & de Lange, T. (2011). The causes and consequences of polyploidy in normal development and cancer. *Annual Review of Cell and Developmental Biology*, *27*, 585–610. https://doi.org/10.1146/annurev-cellbio-092910-154234

Desmaison, A., Frongia, C., Grenier, K., Ducommun, B., & Lobjois, V. (2013). Mechanical Stress Impairs Mitosis Progression in Multi-Cellular Tumor Spheroids. *PLOS ONE*, *8*(12), e80447. https://doi.org/10.1371/journal.pone.0080447

Desmaison, A., Guillaume, L., Triclin, S., Weiss, P., Ducommun, B., & Lobjois, V. (2018). Impact of physical confinement on nuclei geometry and cell division dynamics in 3D spheroids. *Scientific Reports*, *8*(1), 8785. https://doi.org/10.1038/s41598-018-27060-6

Desmaison, A., Lorenzo, C., Rouquette, J., Ducommun, B., & Lobjois, V. (2013). A versatile sample holder for single plane illumination microscopy. *Journal of Microscopy*, *251*(2), 128–132. https://doi.org/10.1111/jmi.12051

Desoize, B., & Jardillier, J.-C. (2000). Multicellular resistance: A paradigm for clinical resistance? *Critical Reviews in Oncology/Hematology*, *36*, 193–207. https://doi.org/10.1016/S1040-8428(00)00086-X

Dhiman, H. K., Ray, A. R., & Panda, A. K. (2005). Three-dimensional chitosan scaffold-based MCF-7 cell culture for the determination of the cytotoxicity of tamoxifen. *Biomaterials*, *26*(9), 979–986. https://doi.org/10.1016/j.biomaterials.2004.04.012

Dolega, M. E., Delarue, M., Ingremeau, F., Prost, J., Delon, A., & Cappello, G. (2017). Cell-like pressure sensors reveal increase of mechanical stress towards the core of multicellular spheroids under compression. *Nature Communications*, *8*(1), 14056. https://doi.org/10.1038/ncomms14056

Dumont, S., & Mitchison, T. J. (2009). Force and Length in the Mitotic Spindle. *Current Biology*, *19*(17), R749–R761. https://doi.org/10.1016/j.cub.2009.07.028

Eiraku, M., & Sasai, Y. (2012). Self-formation of layered neural structures in three-dimensional culture of ES cells. *Current Opinion in Neurobiology*, *22*(5), 768–777. https://doi.org/10.1016/j.conb.2012.02.005

Fallica, B., Maffei, J. S., Villa, S., Makin, G., & Zaman, M. (2012). Alteration of Cellular Behavior and Response to PI3K Pathway Inhibition by Culture in 3D Collagen Gels. *PLOS ONE*, *7*(10), e48024. https://doi.org/10.1371/journal.pone.0048024

Fayad, W., Rickardson, L., Haglund, C., Olofsson, M. H., D'Arcy, P., Larsson, R., Linder, S., & Fryknäs, M. (2011). Identification of Agents that Induce Apoptosis of Multicellular Tumour Spheroids: Enrichment for Mitotic Inhibitors with Hydrophobic Properties. *Chemical Biology & Drug Design*, *78*(4), 547–557. https://doi.org/10.1111/j.1747-0285.2011.01170.x

Fink, J., Carpi, N., Betz, T., Bétard, A., Chebah, M., Azioune, A., Bornens, M., Sykes, C., Fetler, L., Cuvelier, D., & Piel, M. (2011). External forces control mitotic spindle positioning. *Nature Cell Biology*, *13*(7), 771–778. https://doi.org/10.1038/ncb2269

Ford, J. H., & Correll, A. T. (2011). Chromosome errors at mitotic anaphase. *Genome*. https://doi.org/10.1139/g92-107

Frantz, C., Stewart, K. M., & Weaver, V. M. (2010). The extracellular matrix at a glance. *Journal of Cell Science*, *123*(24), 4195–4200. https://doi.org/10.1242/jcs.023820

Fujiwara, T., Bandi, M., Nitta, M., Ivanova, E. V., Bronson, R. T., & Pellman, D. (2005). Cytokinesis failure generating tetraploids promotes tumorigenesis in p53-null cells. *Nature*, *437*(7061), 1043–1047. https://doi.org/10.1038/nature04217

Ganem, N. J., Godinho, S. A., & Pellman, D. (2009). A mechanism linking extra centrosomes to chromosomal instability. *Nature*, *460*(7252), 278–282. https://doi.org/10.1038/nature08136

George, A. L., Sidgwick, F. R., Watt, J. E., Martin, M. P., Trost, M., Marín-Rubio, J. L., & Dueñas, M. E. (2023). Comparison of Quantitative Mass Spectrometric Methods for Drug Target Identification by Thermal Proteome Profiling. *Journal of Proteome Research*, *22*(8), 2629–2640. https://doi.org/10.1021/acs.jproteome.3c00111

Gliech, C. R., Yeow, Z. Y., Tapias-Gomez, D., Yang, Y., Huang, Z., Tijhuis, A. E., Spierings, D. C., Foijer, F., Chung, G., Tamayo, N., Bahrami-Nejad, Z., Collins, P., Nguyen, T. T., Plata Stapper, A., Hughes, P. E., Payton, M., & Holland, A. J. (2024). Weakened APC/C activity at mitotic exit drives cancer vulnerability to KIF18A inhibition. *The EMBO Journal*, *43*(5), 666–694. https://doi.org/10.1038/s44318-024-00031-6

Glimelius, B., Norling, B., Nederman, T., & Carlsson, J. (1988). Extracellular matrices in multicellular spheroids of human glioma origin: Increased incorporation of proteoglycans and flbronectin as compared to monolayer cultures. *APMIS*, *96*(1–6), 433–444. https://doi.org/10.1111/j.1699-0463.1988.tb05327.x

Godek, K. M., Kabeche, L., & Compton, D. A. (2015). Regulation of kinetochore–microtubule attachments through homeostatic control during mitosis. *Nature Reviews Molecular Cell Biology*, *16*(1), 57–64. https://doi.org/10.1038/nrm3916

Gudlin, L., Vukušić, K., Novak, M., Trupinić, M., Ljulj, M., Dundović, I., Petelinec, A., Petrušić, L., Hertel, A., Ravesteyn, T. van, Trakala, M., Kops, G. J. P. L., Storchová, Z., Tambača, J., Pavin, N., & Tolić, I. M. (2025). *A Universal Scaling Law for Mitotic Spindles Driven by Chromosome Crowding* (p. 2025.03.05.641650). bioRxiv. https://doi.org/10.1101/2025.03.05.641650

Gupta, M. L., Carvalho, P., Roof, D. M., & Pellman, D. (2006). Plus end-specific depolymerase activity of Kip3, a kinesin-8 protein, explains its role in positioning the yeast mitotic spindle. *Nature Cell Biology*, *8*(9), 913–923. https://doi.org/10.1038/ncb1457

Haisler, W. L., Timm, D. M., Gage, J. A., Tseng, H., Killian, T. C., & Souza, G. R. (2013). Three-dimensional cell culturing by magnetic levitation. *Nature Protocols*, *8*(10), 1940–1949. https://doi.org/10.1038/nprot.2013.125

Hanahan, D. (2022). Hallmarks of Cancer: New Dimensions. *Cancer Discovery*, *12*(1), 31–46. https://doi.org/10.1158/2159-8290.CD-21-1059

Hell, S. W., & Wichmann, J. (1994). Breaking the diffraction resolution limit by stimulated emission: Stimulated-emission-depletion fluorescence microscopy. *Optics Letters*, *19*(11), 780–782. https://doi.org/10.1364/ol.19.000780

Hertwig, O., & Hertwig, R. (1884). *Untersuchungen zur Morphologie und Physiologie der Zelle*. Fischer.

Hirschhaeuser, F., Menne, H., Dittfeld, C., West, J., Mueller-Klieser, W., & Kunz-Schughart, L. A. (2010). Multicellular tumor spheroids: An underestimated tool is catching up again. *Journal of Biotechnology*, *148*(1), 3–15. https://doi.org/10.1016/j.jbiotec.2010.01.012

Hohenester, E., & Engel, J. (2002). Domain structure and organisation in extracellular matrix proteins. *Matrix Biology*, *21*(2), 115–128. https://doi.org/10.1016/S0945-053X(01)00191-3

Hong, Y., Zhang, H., & Gartner, A. (2021). The Last Chance Saloon. *Frontiers in Cell and Developmental Biology*, *9*. https://doi.org/10.3389/fcell.2021.671297

Howe, G. A., & Addison, C. L. (2012). β1 integrin: An emerging player in the modulation of tumorigenesis and response to therapy. *Cell Adhesion & Migration*, *6*(2), 71–77. https://doi.org/10.4161/cam.20077

Hynes, R. O., & Naba, A. (2012). Overview of the Matrisome—An Inventory of Extracellular Matrix Constituents and Functions. *Cold Spring Harbor Perspectives in Biology*, *4*(1), a004903. https://doi.org/10.1101/cshperspect.a004903

Ibrahim, A., Lashen, A., Toss, M., Mihai, R., & Rakha, E. (2022). Assessment of mitotic activity in breast cancer: Revisited in the digital pathology era. *Journal of Clinical Pathology*, *75*(6), 365–372. https://doi.org/10.1136/jclinpath-2021-207742

Jagrić, M., Risteski, P., Martinčić, J., Milas, A., & Tolić, I. M. (2021). Optogenetic control of PRC1 reveals its role in chromosome alignment on the spindle by overlap length-dependent forces. *eLife*, *10*, e61170. https://doi.org/10.7554/eLife.61170

Janssen, L. M. E., Averink, T. V., Blomen, V. A., Brummelkamp, T. R., Medema, R. H., & Raaijmakers, J. A. (2018). Loss of Kif18A Results in Spindle Assembly Checkpoint Activation at Microtubule-Attached Kinetochores. *Current Biology*, *28*(17), 2685-2696.e4. https://doi.org/10.1016/j.cub.2018.06.026

Johnson, A. M., Froman-Glover, C., Mistry, A., Yaddanapudi, K., & Chen, J. (2025). The impact of compression and confinement in tumor growth and progression: Emerging concepts in cancer mechanobiology. *Frontiers in Materials*, *12*. https://doi.org/10.3389/fmats.2025.1492438

Kajtez, J., Solomatina, A., Novak, M., Polak, B., Vukušić, K., Rüdiger, J., Cojoc, G., Milas, A., Šumanovac Šestak, I., Risteski, P., Tavano, F., Klemm, A. H., Roscioli, E., Welburn, J., Cimini, D., Glunčić, M., Pavin, N., & Tolić, I. M. (2016). Overlap microtubules link sister

k-fibres and balance the forces on bi-oriented kinetochores. *Nature Communications*, *7*(1), 10298. https://doi.org/10.1038/ncomms10298

Kapałczyńska, M., Kolenda, T., Przybyła, W., Zajączkowska, M., Teresiak, A., Filas, V., Ibbs, M., Bliźniak, R., Łuczewski, Ł., & Lamperska, K. (2018). 2D and 3D cell cultures – a comparison of different types of cancer cell cultures. *Archives of Medical Science : AMS*, *14*(4), 910–919. https://doi.org/10.5114/aoms.2016.63743

Kapitein, L. C., & Peterman, E. J. G. (2009). Chapter 2 - Single Molecule Experiments and the Kinesin Motor Protein Superfamily: Walking Hand in Hand. In A. E. Knight (Ed.), *Single Molecule Biology* (pp. 35–60). Academic Press. https://doi.org/10.1016/B978-0-12-374227-8.00002-X

Kirsch-Volders, M., Mišík, M., & de Gerlache, J. (2024). Tetraploidy as a metastable state towards malignant cell transformation within a systemic approach of cancer development. *Mutation Research - Genetic Toxicology and Environmental Mutagenesis*, *896*, 503764. https://doi.org/10.1016/j.mrgentox.2024.503764

Kirsch-Volders, M., Mišík, M., & Fenech, M. (2025). Tetraploidy in normal tissues and diseases: Mechanisms and consequences. *Chromosoma*, *134*(1), 3. https://doi.org/10.1007/s00412-025-00829-1

Klar, T. A., & Hell, S. W. (1999). Subdiffraction resolution in far-field fluorescence microscopy. *Optics Letters*, *24*(14), 954–956. https://doi.org/10.1364/ol.24.000954

Kleinman, H. K., Philp, D., & Hoffman, M. P. (2003). Role of the extracellular matrix in morphogenesis. *Current Opinion in Biotechnology*, *14*(5), 526–532. https://doi.org/10.1016/j.copbio.2003.08.002

Klimek, K., & Ginalska, G. (2020). Proteins and Peptides as Important Modifiers of the Polymer Scaffolds for Tissue Engineering Applications—A Review. *Polymers*, *12*(4), Article 4. https://doi.org/10.3390/polym12040844

Kumar, H. R., Zhong, X., Hoelz, D. J., Rescorla, F. J., Hickey, R. J., Malkas, L. H., & Sandoval, J. A. (2008). Three-dimensional neuroblastoma cell culture: Proteomic analysis between monolayer and multicellular tumor spheroids. *Pediatric Surgery International*, *24*(11), 1229–1234. https://doi.org/10.1007/s00383-008-2245-2

Kuznetsova, A. Y., Seget, K., Moeller, G. K., de Pagter, M. S., de Roos, J. A. D. M., Dürrbaum, M., Kuffer, C., Müller, S., Zaman, G. J. R., Kloosterman, W. P., & Storchová, Z. (2015). Chromosomal instability, tolerance of mitotic errors and multidrug resistance are promoted by tetraploidization in human cells. *Cell Cycle (Georgetown, Tex.)*, *14*(17), 2810–2820. https://doi.org/10.1080/15384101.2015.1068482

Kyriakopoulou, K., Koutsakis, C., Piperigkou, Z., & Karamanos, N. K. (2023). Recreating the extracellular matrix: Novel 3D cell culture platforms in cancer research. *The FEBS Journal*, *290*(22), 5238–5247. https://doi.org/10.1111/febs.16778

Lancaster, M. A., & Knoblich, J. A. (2014). Organogenesis in a dish: Modeling development and disease using organoid technologies. *Science (New York, N.Y.)*, *345*(6194), 1247125. https://doi.org/10.1126/science.1247125

Lancaster, O. M., Le Berre, M., Dimitracopoulos, A., Bonazzi, D., Zlotek-Zlotkiewicz, E., Picone, R., Duke, T., Piel, M., & Baum, B. (2013). Mitotic Rounding Alters Cell Geometry to Ensure Efficient Bipolar Spindle Formation. *Developmental Cell*, *25*(3), 270–283. https://doi.org/10.1016/j.devcel.2013.03.014

Langhans, S. A. (2018). Three-Dimensional in Vitro Cell Culture Models in Drug Discovery and Drug Repositioning. *Frontiers in Pharmacology*, *9*. https://doi.org/10.3389/fphar.2018.00006

Lara-Gonzalez, P., Pines, J., & Desai, A. (2021). Spindle assembly checkpoint activation and silencing at kinetochores. *Seminars in Cell & Developmental Biology*, *117*, 86–98. https://doi.org/10.1016/j.semcdb.2021.06.009

Laurent, J., Frongia, C., Cazales, M., Mondesert, O., Ducommun, B., & Lobjois, V. (2013). Multicellular tumor spheroid models to explore cell cycle checkpoints in 3D. *BMC Cancer*, *13*(1), 73. https://doi.org/10.1186/1471-2407-13-73

Lefort, C. T., Wojciechowski, K., & Hocking, D. C. (2011). N-cadherin Cell-Cell Adhesion Complexes Are Regulated by Fibronectin Matrix Assembly*. *Journal of Biological Chemistry*, *286*(4), 3149–3160. https://doi.org/10.1074/jbc.M110.115733

Lin, R.-Z., & Chang, H.-Y. (2008). Recent advances in three-dimensional multicellular spheroid culture for biomedical research. *Biotechnology Journal*, *3*(9–10), 1172–1184. https://doi.org/10.1002/biot.200700228

Lingle, W. L., Lutz, W. H., Ingle, J. N., Maihle, N. J., & Salisbury, J. L. (1998). Centrosome hypertrophy in human breast tumors: Implications for genomic stability and cell polarity. *Proceedings of the National Academy of Sciences of the United States of America*, *95*(6), 2950–2955. https://doi.org/10.1073/pnas.95.6.2950

Lodish, H. F. (2008). *Molecular Cell Biology*. W. H. Freeman.

Lu, M. S., & Johnston, C. A. (2013). Molecular pathways regulating mitotic spindle orientation in animal cells. *Development (Cambridge, England)*, *140*(9), 1843–1856. https://doi.org/10.1242/dev.087627

Luca, A. C., Mersch, S., Deenen, R., Schmidt, S., Messner, I., Schäfer, K.-L., Baldus, S. E., Huckenbeck, W., Piekorz, R. P., Knoefel, W. T., Krieg, A., & Stoecklein, N. H. (2013). Impact of the 3D Microenvironment on Phenotype, Gene Expression, and EGFR Inhibition of Colorectal Cancer Cell Lines. *PLoS ONE*, *8*(3), e59689. https://doi.org/10.1371/journal.pone.0059689

Magidson, V., O'Connell, C. B., Lončarek, J., Paul, R., Mogilner, A., & Khodjakov, A. (2011). The spatial arrangement of chromosomes during prometaphase facilitates spindle assembly. *Cell*, *146*(4), 555–567. https://doi.org/10.1016/j.cell.2011.07.012

Maiato, H., Gomes, A. M., Sousa, F., & Barisic, M. (2017). Mechanisms of Chromosome Congression during Mitosis. *Biology*, *6*(1), Article 1. https://doi.org/10.3390/biology6010013

Manchester, K. L. (1995). Theodor Boveri and the origin of malignant tumours. *Trends in Cell Biology*, *5*(10), 384–387. https://doi.org/10.1016/s0962-8924(00)89080-7

Marquis, C., Fonseca, C. L., Queen, K. A., Wood, L., Vandal, S. E., Malaby, H. L. H., Clayton, J. E., & Stumpff, J. (2021). Chromosomally unstable tumor cells specifically require KIF18A for proliferation. *Nature Communications*, *12*(1), 1213. https://doi.org/10.1038/s41467-021-21447-2

Mateus, A., Kurzawa, N., Perrin, J., Bergamini, G., & Savitski, M. M. (2022). Drug Target Identification in Tissues by Thermal Proteome Profiling. *Annual Review of Pharmacology and Toxicology*, *62*, 465–482. https://doi.org/10.1146/annurev-pharmtox-052120-013205

Mayr, M. I., Hümmer, S., Bormann, J., Grüner, T., Adio, S., Woehlke, G., & Mayer, T. U. (2007). The Human Kinesin Kif18A Is a Motile Microtubule Depolymerase Essential for

Chromosome Congression. *Current Biology*, *17*(6), 488–498. https://doi.org/10.1016/j.cub.2007.02.036

McIntosh, J. R., Molodtsov, M. I., & Ataullakhanov, F. I. (2012). Biophysics of mitosis. *Quarterly Reviews of Biophysics*, *45*(2), 147–207. https://doi.org/10.1017/S0033583512000017

McKinley, K. L., Sekulic, N., Guo, L. Y., Tsinman, T., Black, B. E., & Cheeseman, I. M. (2015). The CENP-L-N Complex Forms a Critical Node in an Integrated Meshwork of Interactions at the Centromere-Kinetochore Interface. *Molecular Cell*, *60*(6), 886–898. https://doi.org/10.1016/j.molcel.2015.10.027

McKinley, K. L., Stuurman, N., Royer, L. A., Schartner, C., Castillo-Azofeifa, D., Delling, M., Klein, O. D., & Vale, R. D. (2018). Cellular aspect ratio and cell division mechanics underlie the patterning of cell progeny in diverse mammalian epithelia. *eLife*, *7*, e36739. https://doi.org/10.7554/eLife.36739

McNally, F. J. (2013). Mechanisms of spindle positioning. *The Journal of Cell Biology*, *200*(2), 131–140. https://doi.org/10.1083/jcb.201210007

Meerson, A., Milyavsky, M., & Rotter, V. (2004). P53 mediates density-dependent growth arrest. *FEBS Letters*, *559*(1), 152–158. https://doi.org/10.1016/S0014-5793(04)00027-4

Milane, L. S. (2022). Chapter One—The hallmarks of cancer and immunology. In M. M. Amiji & L. S. Milane (Eds.), *Cancer Immunology and Immunotherapy* (pp. 1–17). Academic Press. https://doi.org/10.1016/B978-0-12-823397-9.00001-6

Mitchison, T. J. (1989). Polewards microtubule flux in the mitotic spindle: Evidence from photoactivation of fluorescence. *The Journal of Cell Biology*, *109*(2), 637–652. https://doi.org/10.1083/jcb.109.2.637

Mittal, K., Kaur, J., Jaczko, M., Wei, G., Toss, Michael. S., Rakha, E. A., Janssen, E. A. M., Søiland, H., Kucuk, O., Reid, M. D., Gupta, M. V., & Aneja, R. (2021). Centrosome amplification: A quantifiable cancer cell trait with prognostic value in solid malignancies. *Cancer Metastasis Reviews*, *40*(1), 319–339. https://doi.org/10.1007/s10555-020-09937-z

Molla, A., Couvet, M., & Coll, J.-L. (2017). Unsuccessful mitosis in multicellular tumour spheroids. *Oncotarget*, *8*(17), 28769–28784. https://doi.org/10.18632/oncotarget.15673

Muranen, T., Selfors, L. M., Worster, D. T., Iwanicki, M. P., Song, L., Morales, F. C., Gao, S., Mills, G. B., & Brugge, J. S. (2012). Inhibition of PI3K/mTOR Leads to Adaptive Resistance in Matrix-Attached Cancer Cells. *Cancer Cell*, *21*(2), 227–239. https://doi.org/10.1016/j.ccr.2011.12.024

Musacchio, A., & Desai, A. (2017). A Molecular View of Kinetochore Assembly and Function. *Biology*, *6*(1), 5. https://doi.org/10.3390/biology6010005

Nestor-Bergmann, A., Goddard, G., & Woolner, S. (2014). Force and the spindle: Mechanical cues in mitotic spindle orientation. *Seminars in Cell & Developmental Biology*, *34*, 133–139. https://doi.org/10.1016/j.semcdb.2014.07.008

Nunes, A. S., Barros, A. S., Costa, E. C., Moreira, A. F., & Correia, I. J. (2019). 3D tumor spheroids as in vitro models to mimic in vivo human solid tumors resistance to therapeutic drugs. *Biotechnology and Bioengineering*, *116*(1), 206–226. https://doi.org/10.1002/bit.26845

Orr, B., Godek, K. M., & Compton, D. (2015). Aneuploidy. *Current Biology: CB*, *25*(13), R538-542. https://doi.org/10.1016/j.cub.2015.05.010

Otto, S. P. (2007). The evolutionary consequences of polyploidy. *Cell*, *131*(3), 452–462. https://doi.org/10.1016/j.cell.2007.10.022

Ovsianikov, A., Mironov, V., Stampfl, J., & Liska, R. (2012). Engineering 3D cell-culture matrices: Multiphoton processing technologies for biological and tissue engineering applications. *Expert Review of Medical Devices*, *9*(6), 613–633. https://doi.org/10.1586/erd.12.48

Pampaloni, F., Reynaud, E. G., & Stelzer, E. H. K. (2007). The third dimension bridges the gap between cell culture and live tissue. *Nature Reviews Molecular Cell Biology*, *8*(10), 839–845. https://doi.org/10.1038/nrm2236

Payton, M., Belmontes, B., Hanestad, K., Moriguchi, J., Chen, K., McCarter, J. D., Chung, G., Ninniri, M. S., Sun, J., Manoukian, R., Chambers, S., Ho, S.-M., Kurzeja, R. J. M., Edson, K. Z., Dahal, U. P., Wu, T., Wannberg, S., Beltran, P. J., Canon, J., … Hughes, P. E. (2024). Small-molecule inhibition of kinesin KIF18A reveals a mitotic vulnerability enriched in chromosomally unstable cancers. *Nature Cancer*, *5*(1), 66–84. https://doi.org/10.1038/s43018-023-00699-5

Pihan, G. A., Purohit, A., Wallace, J., Knecht, H., Woda, B., Quesenberry, P., & Doxsey, S. J. (1998). Centrosome defects and genetic instability in malignant tumors. *Cancer Research*, *58*(17), 3974–3985.

Pihan, G. A., Purohit, A., Wallace, J., Malhotra, R., Liotta, L., & Doxsey, S. J. (2001). Centrosome defects can account for cellular and genetic changes that characterize prostate cancer progression. *Cancer Research*, *61*(5), 2212–2219.

Polak, B., Risteski, P., Lesjak, S., & Tolić, I. M. (2017). PRC1-labeled microtubule bundles and kinetochore pairs show one-to-one association in metaphase. *EMBO Reports*, *18*(2), 217–230. https://doi.org/10.15252/embr.201642650

Potapova, T., & Gorbsky, G. J. (2017). The Consequences of Chromosome Segregation Errors in Mitosis and Meiosis. *Biology*, *6*(1), 12. https://doi.org/10.3390/biology6010012

Prasad, K., & Ben-David, U. (2023). A balancing act: How whole-genome doubling and aneuploidy interact in human cancer. *Oncotarget*, *14*, 382–383. https://doi.org/10.18632/oncotarget.28374

Prosser, S. L., & Pelletier, L. (2017). Mitotic spindle assembly in animal cells: A fine balancing act. *Nature Reviews Molecular Cell Biology*, *18*(3), 187–201. https://doi.org/10.1038/nrm.2016.162

Quinton, R. J., DiDomizio, A., Vittoria, M. A., Kotýnková, K., Ticas, C. J., Patel, S., Koga, Y., Vakhshoorzadeh, J., Hermance, N., Kuroda, T. S., Parulekar, N., Taylor, A. M., Manning, A. L., Campbell, J. D., & Ganem, N. J. (2021). Whole-genome doubling confers unique genetic vulnerabilities on tumour cells. *Nature*, *590*(7846), 492–497. https://doi.org/10.1038/s41586-020-03133-3

Quintyne, N. J., Reing, J. E., Hoffelder, D. R., Gollin, S. M., & Saunders, W. S. (2005). Spindle Multipolarity Is Prevented by Centrosomal Clustering. *Science*, *307*(5706), 127–129. https://doi.org/10.1126/science.1104905

Ravid, K., Lu, J., Zimmet, J. M., & Jones, M. R. (2002). Roads to polyploidy: The megakaryocyte example. *Journal of Cellular Physiology*, *190*(1), 7–20. https://doi.org/10.1002/jcp.10035

Rieckhoff, E. M., Berndt, F., Elsner, M., Golfier, S., Decker, F., Ishihara, K., & Brugués, J. (2020). Spindle Scaling Is Governed by Cell Boundary Regulation of Microtubule Nucleation. *Current Biology*, *30*(24), 4973-4983.e10. https://doi.org/10.1016/j.cub.2020.10.093

Rieder, C. L., & Salmon, E. D. (1994). Motile kinetochores and polar ejection forces dictate chromosome position on the vertebrate mitotic spindle. *The Journal of Cell Biology*, *124*(3), 223–233. https://doi.org/10.1083/jcb.124.3.223

Risteski, P., Božan, D., Jagrić, M., Bosilj, A., Pavin, N., & Tolić, I. M. (2022). Length-dependent poleward flux of sister kinetochore fibers promotes chromosome alignment. *Cell Reports*, *40*(5), 111169. https://doi.org/10.1016/j.celrep.2022.111169

Risteski, P., Martinčić, J., Jagrić, M., Tintor, E., Petelinec, A., & Tolić, I. M. (2024). Microtubule poleward flux as a target for modifying chromosome segregation errors. *Proceedings of the National Academy of Sciences*, *121*(47), e2405015121. https://doi.org/10.1073/pnas.2405015121

Saleh, J., Fardin, M.-A., Barai, A., Soleilhac, M., Frenoy, O., Gaston, C., Cui, H., Dang, T., Gaudin, N., Vincent, A., Minc, N., & Delacour, D. (2023). Length limitation of astral microtubules orients cell divisions in murine intestinal crypts. *Developmental Cell*, *58*(17), 1519-1533.e6. https://doi.org/10.1016/j.devcel.2023.06.004

Sato, N., Mizumoto, K., Nakamura, M., Nakamura, K., Kusumoto, M., Niiyama, H., Ogawa, T., & Tanaka, M. (1999). Centrosome abnormalities in pancreatic ductal carcinoma. *Clinical Cancer Research: An Official Journal of the American Association for Cancer Research*, *5*(5), 963–970.

Sato, T., Stange, D. E., Ferrante, M., Vries, R. G. J., Es, J. H. van, Brink, S. van den, Houdt, W. J. van, Pronk, A., Gorp, J. van, Siersema, P. D., & Clevers, H. (2011). Long-term Expansion of Epithelial Organoids From Human Colon, Adenoma, Adenocarcinoma, and Barrett's Epithelium. *Gastroenterology*, *141*(5), 1762–1772. https://doi.org/10.1053/j.gastro.2011.07.050

Sato, T., Vries, R. G., Snippert, H. J., van de Wetering, M., Barker, N., Stange, D. E., van Es, J. H., Abo, A., Kujala, P., Peters, P. J., & Clevers, H. (2009). Single Lgr5 stem cells build crypt-villus structures in vitro without a mesenchymal niche. *Nature*, *459*(7244), 262–265. https://doi.org/10.1038/nature07935

Schooley, A. M., Andrews, N. M., Zhao, H., & Addison, C. L. (2012). B1 integrin is required for anchorage-independent growth and invasion of tumor cells in a context dependent manner. *Cancer Letters*, *316*(2), 157–167. https://doi.org/10.1016/j.canlet.2011.10.032

Seldin, L., Poulson, N. D., Foote, H. P., & Lechler, T. (2013). NuMA localization, stability, and function in spindle orientation involve 4.1 and Cdk1 interactions. *Molecular Biology of the Cell*, *24*(23), 3651–3662. https://doi.org/10.1091/mbc.E13-05-0277

Senbanjo, L. T., & Chellaiah, M. A. (2017). CD44: A Multifunctional Cell Surface Adhesion Receptor Is a Regulator of Progression and Metastasis of Cancer Cells. *Frontiers in Cell and Developmental Biology*, *5*. https://doi.org/10.3389/fcell.2017.00018

Shackney, S. E., Smith, C. A., Miller, B. W., Burholt, D. R., Murtha, K., Giles, H. R., Ketterer, D. M., & Pollice, A. A. (1989). Model for the genetic evolution of human solid tumors. *Cancer Research*, *49*(12), 3344–3354.

Shao, G., Zhou, H., Zhang, Q., Jin, Y., & Fu, C. (2019). Advancements of Annexin A1 in inflammation and tumorigenesis. *OncoTargets and Therapy*, *12*, 3245–3254. https://doi.org/10.2147/OTT.S202271

Sjöblom, T., Jones, S., Wood, L. D., Parsons, D. W., Lin, J., Barber, T. D., Mandelker, D., Leary, R. J., Ptak, J., Silliman, N., Szabo, S., Buckhaults, P., Farrell, C., Meeh, P., Markowitz, S. D., Willis, J., Dawson, D., Willson, J. K. V., Gazdar, A. F., … Velculescu, V. E. (2006). The consensus coding sequences of human breast and colorectal cancers. *Science (New York, N.Y.)*, *314*(5797), 268–274. https://doi.org/10.1126/science.1133427

Skibbens, R., Skeen, V., & Salmon, E. (1993). Directional instability of kinetochore motility during chromosome congression and segregation in mitotic newt lung cells: A push-

pull mechanism. *Journal of Cell Biology*, *122*(4), 859–875. https://doi.org/10.1083/jcb.122.4.859

Soto, M., García-Santisteban, I., Krenning, L., Medema, R. H., & Raaijmakers, J. A. (2018). Chromosomes trapped in micronuclei are liable to segregation errors. *Journal of Cell Science*, *131*(13), jcs214742. https://doi.org/10.1242/jcs.214742

Souza, A. G., Silva, I. B. B., Campos-Fernandez, E., Barcelos, L. S., Souza, J. B., Marangoni, K., Goulart, L. R., & Alonso-Goulart, V. (2018). Comparative Assay of 2D and 3D Cell Culture Models: Proliferation, Gene Expression and Anticancer Drug Response. *Current Pharmaceutical Design*, *24*(15), 1689–1694. https://doi.org/10.2174/1381612824666180404152304

Souza, G. R., Molina, J. R., Raphael, R. M., Ozawa, M. G., Stark, D. J., Levin, C. S., Bronk, L. F., Ananta, J. S., Mandelin, J., Georgescu, M.-M., Bankson, J. A., Gelovani, J. G., Killian, T. C., Arap, W., & Pasqualini, R. (2010). Three-dimensional tissue culture based on magnetic cell levitation. *Nature Nanotechnology*, *5*(4), 291–296. https://doi.org/10.1038/nnano.2010.23

Storchová, Z., Breneman, A., Cande, J., Dunn, J., Burbank, K., O'Toole, E., & Pellman, D. (2006). Genome-wide genetic analysis of polyploidy in yeast. *Nature*, *443*(7111), 541–547. https://doi.org/10.1038/nature05178

Storchova, Z., & Kuffer, C. (2008). The consequences of tetraploidy and aneuploidy. *Journal of Cell Science*, *121*(23), 3859–3866. https://doi.org/10.1242/jcs.039537

Storchova, Z., & Pellman, D. (2004). From polyploidy to aneuploidy, genome instability and cancer. *Nature Reviews Molecular Cell Biology*, *5*(1), 45–54. https://doi.org/10.1038/nrm1276

Streuli, C. (1999). Extracellular matrix remodelling and cellular differentiation. *Current Opinion in Cell Biology*, *11*(5), 634–640. https://doi.org/10.1016/S0955-0674(99)00026-5

Stumpff, J., von Dassow, G., Wagenbach, M., Asbury, C., & Wordeman, L. (2008). The kinesin-8 motor Kif18A suppresses kinetochore movements to control mitotic chromosome alignment. *Developmental Cell*, *14*(2), 252–262. https://doi.org/10.1016/j.devcel.2007.11.014

Sutherland, R. M. (1988). Cell and environment interactions in tumor microregions: The multicell spheroid model. *Science (New York, N.Y.)*, *240*(4849), 177–184. https://doi.org/10.1126/science.2451290

Takeda, H., Fukumoto, A., Miura, A., Goshima, N., & Nomura, N. (2006). High-throughput kinase assay based on surface plasmon resonance suitable for native protein substrates. *Analytical Biochemistry*, *357*(2), 262–271. https://doi.org/10.1016/j.ab.2006.07.002

Taubenberger, A. V., Girardo, S., Träber, N., Fischer-Friedrich, E., Kräter, M., Wagner, K., Kurth, T., Richter, I., Haller, B., Binner, M., Hahn, D., Freudenberg, U., Werner, C., & Guck, J. (2019). 3D Microenvironment Stiffness Regulates Tumor Spheroid Growth and Mechanics via p21 and ROCK. *Advanced Biosystems*, *3*(9), 1900128. https://doi.org/10.1002/adbi.201900128

Taylor, M. V. (2002). Muscle differentiation: How two cells become one. *Current Biology: CB*, *12*(6), R224-228. https://doi.org/10.1016/s0960-9822(02)00757-1

Théry, M., Racine, V., Pépin, A., Piel, M., Chen, Y., Sibarita, J.-B., & Bornens, M. (2005). The extracellular matrix guides the orientation of the cell division axis. *Nature Cell Biology*, *7*(10), 947–953. https://doi.org/10.1038/ncb1307

Thompson, S. L., Bakhoum, S. F., & Compton, D. A. (2010). Mechanisms of chromosomal instability. *Current Biology: CB*, *20*(6), R285-295. https://doi.org/10.1016/j.cub.2010.01.034

Tillement, V., Remy, M.-H., Raynaud-Messina, B., Mazzolini, L., Haren, L., & Merdes, A. (2009). Spindle assembly defects leading to the formation of a monopolar mitotic apparatus. *Biology of the Cell*, *101*(1), 1–11. https://doi.org/10.1042/BC20070162

Tolić, I. M. (2018). Mitotic spindle: Kinetochore fibers hold on tight to interpolar bundles. *European Biophysics Journal*, *47*(3), 191–203. https://doi.org/10.1007/s00249-017-1244-4

Tolić, I. M., & and Pavin, N. (2016). Bridging the gap between sister kinetochores. *Cell Cycle*, *15*(9), 1169–1170. https://doi.org/10.1080/15384101.2016.1157976

Trédan, O., Galmarini, C. M., Patel, K., & Tannock, I. F. (2007). Drug Resistance and the Solid Tumor Microenvironment. *JNCI: Journal of the National Cancer Institute*, *99*(19), 1441–1454. https://doi.org/10.1093/jnci/djm135

Trivedi, P., & Stukenberg, P. T. (2016). A centromere-signaling network underlies the coordination among mitotic events. *Trends in Biochemical Sciences*, *41*(2), 160–174. https://doi.org/10.1016/j.tibs.2015.11.002

Tse, H. T. K., Weaver, W. M., & Carlo, D. D. (2012). Increased Asymmetric and Multi-Daughter Cell Division in Mechanically Confined Microenvironments. *PLOS ONE*, *7*(6), e38986. https://doi.org/10.1371/journal.pone.0038986

Tucker, J. B., Bonema, S. C., García-Varela, R., Denu, R. A., Hu, Y., McGregor, S. M., Burkard, M. E., & Weaver, B. A. (2023). Misaligned Chromosomes are a Major Source of Chromosomal Instability in Breast Cancer. *Cancer Research Communications*, *3*(1), 54–65. https://doi.org/10.1158/2767-9764.CRC-22-0302

Ullah, Z., Kohn, M. J., Yagi, R., Vassilev, L. T., & DePamphilis, M. L. (2008). Differentiation of trophoblast stem cells into giant cells is triggered by p57/Kip2 inhibition of CDK1 activity. *Genes & Development*, *22*(21), 3024–3036. https://doi.org/10.1101/gad.1718108

Varga, V., Helenius, J., Tanaka, K., Hyman, A. A., Tanaka, T. U., & Howard, J. (2006). Yeast kinesin-8 depolymerizes microtubules in a length-dependent manner. *Nature Cell Biology*, *8*(9), 957–962. https://doi.org/10.1038/ncb1462

Volastra—Short Circuiting Cancer's Chaos. (2025, May 27). Volastra. https://www.volastratx.com/

Vukušić, K., Buđa, R., Bosilj, A., Milas, A., Pavin, N., & Tolić, I. M. (2017). Microtubule Sliding within the Bridging Fiber Pushes Kinetochore Fibers Apart to Segregate Chromosomes. *Developmental Cell*, *43*(1), 11-23.e6. https://doi.org/10.1016/j.devcel.2017.09.010

Vukušić, K., Buđa, R., & Tolić, I. M. (2019). Force-generating mechanisms of anaphase in human cells. *Journal of Cell Science*, *132*(18), jcs231985. https://doi.org/10.1242/jcs.231985

Vukušić, K., & Tolić, I. M. (2022). Polar Chromosomes-Challenges of a Risky Path. *Cells*, *11*(9), 1531. https://doi.org/10.3390/cells11091531

Walczak, C. E., Cai, S., & Khodjakov, A. (2010). Mechanisms of chromosome behaviour during mitosis. *Nature Reviews. Molecular Cell Biology*, *11*(2), 91–102. https://doi.org/10.1038/nrm2832

Watanabe, T., Shimada, H., & Tanaka, Y. (1978). Human hepatocytes and aging: A cytophotometrical analysis in 35 sudden-death cases. *Virchows Archiv. B, Cell Pathology*, *27*(4), 307–316. https://doi.org/10.1007/BF02889003

Weaver, L. N., Ems-McClung, S. C., Stout, J. R., LeBlanc, C., Shaw, S. L., Gardner, M. K., & Walczak, C. E. (2011). Kif18A Uses a Microtubule Binding Site in the Tail for Plus-End Localization and Spindle Length Regulation. *Current Biology*, *21*(17), 1500–1506. https://doi.org/10.1016/j.cub.2011.08.005

Weaver, V. M., Petersen, O. W., Wang, F., Larabell, C. A., Briand, P., Damsky, C., & Bissell, M. J. (1997). Reversion of the Malignant Phenotype of Human Breast Cells in Three-Dimensional Culture and In Vivo by Integrin Blocking Antibodies. *Journal of Cell Biology*, *137*(1), 231–245. https://doi.org/10.1083/jcb.137.1.231

Wiebe, J. P., Zhang, G., Welch, I., & Cadieux-Pitre, H.-A. T. (2013). Progesterone metabolites regulate induction, growth, and suppression of estrogen- and progesterone receptor-negative human breast cell tumors. *Breast Cancer Research*, *15*(3), R38. https://doi.org/10.1186/bcr3422

Willems, E., Dedobbeleer, M., Digregorio, M., Lombard, A., Lumapat, P. N., & Rogister, B. (2018). The functional diversity of Aurora kinases: A comprehensive review. *Cell Division*, *13*, 7. https://doi.org/10.1186/s13008-018-0040-6

Yahya, G., Menges, P., Amponsah, P. S., Ngandiri, D. A., Schulz, D., Wallek, A., Kulak, N., Mann, M., Cramer, P., Savage, V., Räschle, M., & Storchova, Z. (2022). Sublinear scaling of the cellular proteome with ploidy. *Nature Communications*, *13*(1), 6182. https://doi.org/10.1038/s41467-022-33904-7

Yamada, K. M., Pankov, R., & Cukierman, E. (2003). Dimensions and dynamics in integrin function. *Brazilian Journal of Medical and Biological Research*, *36*, 959–966. https://doi.org/10.1590/S0100-879X2003000800001

Yang, C.-F., Tsai, W.-Y., Chen, W.-A., Liang, K.-W., Pan, C.-J., Lai, P.-L., Yang, P.-C., & Huang, H.-C. (2016). Kinesin-5 Contributes to Spindle-length Scaling in the Evolution of Cancer toward Metastasis. *Scientific Reports*, *6*(1), 35767. https://doi.org/10.1038/srep35767

Zack, T. I., Schumacher, S. E., Carter, S. L., Cherniack, A. D., Saksena, G., Tabak, B., Lawrence, M. S., Zhsng, C.-Z., Wala, J., Mermel, C. H., Sougnez, C., Gabriel, S. B., Hernandez, B., Shen, H., Laird, P. W., Getz, G., Meyerson, M., & Beroukhim, R. (2013). Pan-cancer patterns of somatic copy number alteration. *Nature Genetics*, *45*(10), 1134–1140. https://doi.org/10.1038/ng.2760

Zheng, Z., Zhu, H., Wan, Q., Liu, J., Xiao, Z., Siderovski, D. P., & Du, Q. (2010). LGN regulates mitotic spindle orientation during epithelial morphogenesis. *Journal of Cell Biology*, *189*(2), 275–288. https://doi.org/10.1083/jcb.200910021

Zhu, C., Zhao, J., Bibikova, M., Leverson, J. D., Bossy-Wetzel, E., Fan, J.-B., Abraham, R. T., & Jiang, W. (2005). Functional Analysis of Human Microtubule-based Motor Proteins, the Kinesins and Dyneins, in Mitosis/Cytokinesis Using RNA Interference. *Molecular Biology of the Cell*, *16*(7), 3187–3199. https://doi.org/10.1091/mbc.e05-02-0167

8. SUMMARY

Mitosis is a dynamic part of the cell cycle that ensures the proper distribution of genetic material into two daughter cells. Chromosomes are accurately segregated by mitotic spindle, a complex micromachinery composed of microtubules and various proteins. Errors during cell division can lead to aneuploidy, and failure to divide properly can result in polyploid cells. Frequent mitotic errors cause chromosomal instability (CIN). Recent studies have shown that tetraploid cells with CIN exhibit increased sensitivity to the loss of the motor protein kinesin-8/KIF18A, although the exact mechanism remains unclear.

The KIF18A protein regulates spindle length and reduces oscillations of properly aligned kinetochores at the metaphase plate. Loss of KIF18A in tumor cell lines dependent on this protein causes chromosome alignment defects, prolongs mitosis, and reduces proliferation. Tetraploid cells can form by cytokinesis failure, and in subsequent divisions they lose some chromosomes and form stable post-tetraploid (PT) clones. Some theories consider them to be precursors of tumor cells, due to CIN.

Most cell division studies use two-dimensional (2D) cultures, where cells grow as a monolayer, differing significantly from cells in tissues. In three-dimensional (3D) systems cells produce an extracellular matrix, have complex cell-cell interactions, limited space, and are heterogeneous. To more accurately study cellular processes, various 3D cell culture models have been developed.

KIF18A protein was perturbed by small interfering RNA (siRNA) or the inhibitor sovilnesib, which has shown promising results in clinical trials for cancer treatment. Confocal, super-resolution, and live-cell microscopy revealed that both silencing and inhibition prolonged mitosis, caused chromosome misalignment, and led to spindle elongation. Silencing had a similar effect in diploid and PT cells, while inhibition had a stronger effect, especially in PTs.
A subpopulation highly sensitive to KIF18A loss was described, showing prolonged mitosis, chromosome hyperoscillations, and dynamic changes of spindle polarity during mitosis. This subpopulation was larger after inhibition than depletion, and PT cells showed a larger fraction of this subpopulation after inhibition.

Furthermore, spheroids were successfully generated using magnetic cell levitation method from tumor cell lines MDA-MB-231, U2OS, OVSAHO, and the non-tumor RPE1 p53KD line. For the first time, mitotic cells in monolayers were compared to those in spheroids. Tumor spheroids had more prometaphase cells, indicating mitotic arrest. Cells and mitotic spindles were smaller in spheroids in all cell lines, and proportion of irregularly shaped cells increased, which implies that neighboring cells limit space and compress mitotic cells, which may contribute to mitotic arrest.

In conclusion, this work provides a detailed description of the effect of sovilnesib on mitosis duration and mitotic cell phenotypes in diploid and PT cells, showing their increased sensitivity compared to depletion, which is of great importance for further research on sovilnesib in cancer treatment. Furthermore, this thesis characterizes differences between mitotic spindles in monolayers and spheroids, providing a more realistic view of mitosis in a system that mimics tumor regions confined by limited space and pressure from surrounding tissues. This work highlights the importance of choosing appropriate cell lines and experimental models, as both influence different mitotic patterns, and ultimately the response to various treatments.

9. SAŽETAK

Mitoza je dinamičan dio staničnog ciklusa koji osigurava pravilnu podjelu genetičkog materijala na dvije stanice kćeri. Tijekom mitoze genetički materijal je u obliku kromosoma, kondenziranih molekula DNA, koji se pravilno podijele uz pomoć diobenog vretena, kompleksnog sustava sastavljenog od mikrotubula i raznih proteina.

Pogreške u diobi stanica mogu dovesti do aneuploidije, a ako se stanica ne može podijeliti na dvije stanice kćeri, često nastaju poliploidne stanice. Učestale mitotske greške tijekom dioba uzrokuju kromosomsku nestabilnost, koja pripada širem pojmu genomske nestabilnosti, a jedna je od obilježja tumora. Nedavna istraživanja pokazala su da tetraploidne stanice s kromosomskom nestabilnosti imaju veću osjetljivost na gubitak motornog proteina kinezina-8/KIF18A, iako još uvijek nije u potpunosti razjašnjeno koje su predispozicije potrebne za izazivanje osjetljivosti.

Protein KIF18A ima važnu ulogu u regulaciji duljine diobenog vretena te smanjuje oscilacije kinetohora koje su pravilno poravnate u metafaznoj ploči. Gubitak proteina KIF18A u tumorskim staničnim linijama, koje su ovisne o proteinu, uzrokuje teškoće u poravnanju kromosoma, značajno produljuje mitozu i smanjuje proliferaciju. Tetraploidne stanice mogu nastati inhibicijom citokineze, čime se sprječava da se stanica podijeli na dvije stanice kćeri. U narednim diobama stanice gube dio kromosoma i nastaju stabilni post-tetraploidni klonovi. Prema nekim teorijama, smatra se da su te stanice zbog kromosomske nestabilnosti prekursori tumorskih stanica. Iz tog razloga bitno je istražiti kako gubitak proteina KIF18A utječe na njihovu diobu.

Brojne značajke tumorskih i ne-tumorskih stanica otkrivene su kroz istraživanja provedena na staničnim kulturama. Stanice se tradicionalno uzgajaju u 2D staničnim kulturama gdje rastu u jednom sloju i prianjaju na podlogu. Njihova obilježja značajno se razlikuju od stanica koje se nalaze u tkivima. Za razliku od 2D sustava, u 3D sustavima stanice stvaraju izvanstanični matriks, imaju kompleksne međustanične interakcije, ograničen prostor za rast i diobu i heterogene su. Kako bi se preciznije istražili procesi koji se događaju u tkivima, razvijeni su različiti modeli 3D staničnih kultura.

U ovom radu istražene su dvije teme bitne za razumijevanje razvoja tumora. U prvom dijelu istražen je utjecaj gubitka proteina KIF18A na diploidne i post-tetraploidne ne-tumorske RPE1 stanice. Drugi dio istražuje utjecaj 3D arhitekture na diobu stanica, kako bi se dobio bolji uvid u mitozu u tumorskim tkivima.

Protein KIF18A utišan je pomoću male interferirajuće RNA ili kemijski inhibiran koristeći inhibitor sovilnesib, koji je pokazao obećavajuće rezultate u kliničkim istraživanjima za liječenje tumora. Učinak gubitka proteina KIF18A istražen je pomoću konfokalne, superrezolucijske i mikroskopije živih stanica. Inhibicija i utišanje proteina KIF18A uzrokovali

su produljeno trajanje mitoze, probleme s poravnanjem kromosoma i elongaciju diobenog vretena. Utišanje proteina imalo je sličan učinak u diploidnim i post-tetraploidnim stanicama, dok je inhibicija imala snažniji učinak, osobito u post-tetraploidnim stanicama. Opisana je i subpopulacija stanica koja pokazuje iznimnu osjetljivost na gubitak proteina. Takve stanice imaju značajno produljeno trajanje mitoze, hiperoscilacije kromosoma i diobeno vreteno koje dinamično mijenja polarnost tijekom mitoze. Ova subpopulacija je bila veća nakon inhibicije nego utišanja proteina, a post-tetraploidne stanice su nakon inhibicije pokazale veću frakciju izrazito osjetljive populacije. Inhibicija proteina KIF18A imala je snažan efekt na stanice i pokazala da su i RPE1 stanice, osjetljive na gubitak proteina.

U ovom istraživanju uspješno su generirani sferoidi pomoću metode magnetske levitacije stanica. Uspoređene su tumorske stanične linije MDA-MB-231, U2OS i OVSAHO te ne-tumorska stanična linija RPE1 p53KD. Po prvi puta uspoređene su mitotske stanice u klasičnim 2D staničnim kulturama sa stanicama u sferoidima. Sferoidi tumorskih stanica imali su veći udio prometafaznih stanica, što upućuje na zastoj u mitozi. Stanice i diobena vretena bili su manjih dimenzija u sferoidima svih staničnih linija. Budući da su stanice u sferoidima manjih dimenzija i povećan je udio stanica nepravilnog oblika, može se zaključiti da susjedne stanice ograničavaju prostor i pritišću mitotske stanice, što može pridonijeti zastoju mitoze.

Zaključno, u ovom radu detaljno je opisan utjecaj sovilnesiba na trajanje mitoze i fenotip mitotskih stanica u diploidnim i post-tetraploidnim RPE1 stanicama i pokazana je njihova povećana osjetljivost, u usporedbi s utišanjem proteina, što je bitno za daljnja istraživanja sovilnesiba u liječenju tumora. Nadalje, u ovom radu karakterizirane su razlike između diobenog vretena u 2D staničnim kulturama i sferoidima, čime je prikazana realističnija slika mitoze u sustavu koji nalikuje na dijelove tumora koji su u ograničenom prostoru i okolna tkiva vrše pritisak na njih. Ovaj rad ukazuje na važnost odabira prikladne stanične linije i eksperimentalnog modela, zato što i stanične linije i uvjeti u kojima se stanice uzgajaju mogu utjecati na tijek mitoze, fenotip mitotskih stanica i na kraju odgovor na različite tretmane.

10. AUTHOR BIOGRAPHY

Ana Petelinec was born on July 5th, 1997, in Pula, Croatia. She finished her elementary and high school education in Pula. In 2016 she became a student at the Faculty of Science, University of Zagreb, where she finished integrated undergraduate and graduate programme Biology and Chemistry Education in 2021. Her master thesis, titled “The role of 2D and 3D cell environment in the cellular stress response” was done in the Laboratory of Cell Biophysics, Department of Molecular Biology, at the Ruđer Bošković Institute, Zagreb.

During her studies, she was a teaching assistant in General Zoology Practicum at the Faculty of Science, University of Zagreb in 2019-2020. Also, she has done a Laboratory practice on the project “Changes in the pathogen composition and immune response during range expansion of successful crayfish invaders”, funded by Croatian Science Foundation, under the mentorship of Prof. Sandra Hudina, in Division of Zoology, at the Faculty of Science, University of Zagreb. In 2021 she finished the Laboratory Animal Science Course (LabAnim A, FELASA equivalent).

She continued her education at the Josip Juraj Strossmayer University in Osijek, where she enrolled in Postgraduate University Interdisciplinary Doctoral Study of Molecular Biosciences in 2021. Since then, she has been working as a research assistant in the Laboratory of Cell Biophysics, Department of Molecular Biology, at the Ruđer Bošković Institute, Zagreb, under the mentorship of Dr. Iva M. Tolić. She is the author on two papers, and she participated in three conferences. In 2022 she visited Koch Institute for Integrative Cancer Research At MIT, for a short-term stay. Also, she got a scholarship from Ruđer Bošković Insitute for funding young researchers’ international short-term stay, for an internship in the Laboratory of Quantitative Proteomics, in Eberhard Karls University of Tuebingen, Germany.

During her studies she participated in several events related to popularization of science, such as “Day and Night” at the Faculty of Science 2019 and 2021, Youth Science Camp in Višnjan 2020, Summer Science Factory 2021 and 2022, Bioteka workshop 2022 and Open days of Ruđer Bošković Institute 2022.

Publications:

Gudlin, L., Vukušić, K., Novak, M., Trupinić, M., Ljulj, M., Dundović, I., **Petelinec, A.,** Petrušić, L., Hertel, A., Ravesteyn, T. van, Trakala, M., Kops, G. J. P. L., Storchová, Z., Tambača, J., Pavin, N., & Tolić, I. M. (2025). A Universal Scaling Law for Mitotic Spindles Driven by Chromosome Crowding (p. 2025.03.05.641650). bioRxiv. https://doi.org/10.1101/2025.03.05.641650

Risteski, P., Martinčić, J., Jagrić, M., Tintor, E., **Petelinec, A.,** & Tolić, I. M. (2024). Microtubule poleward flux as a target for modifying chromosome segregation errors. Proceedings of the National Academy of Sciences, 121(47), e2405015121. https://doi.org/10.1073/pnas.2405015121

Ćosić, M., & **Petelinec, A.** (2024). The role of 3D cell cultures in understanding mitosis and tissue architecture. Periodicum Biologorum, 126(1–2), Article 1–2. https://doi.org/10.18054/pb.v126i1-2.32856

Dobrović, A., Geček, S., Klanjšček, T., Haberle, I., Dragičević, P., Pavić, D., **Petelinec, A.,** Boštjančić, L. L., Bonassin, L., Theissinger, K., & Hudina, S. (2022). Recurring infection by crayfish plague pathogen only marginally affects survival and growth of marbled crayfish. NeoBiota, 77, 155–177. https://doi.org/10.3897/neobiota.77.87474

Petelinec, A., Nikša, E., Grudiček, D., & Sertić Perić, M. (2020). Poučavanje teme Prehrana čovjeka putem istraživačkog učenja i osnovnih načela teorije izbora i kvalitetne škole. Educatio biologiae, 6., 65–79. https://doi.org/10.32633/eb.6.5

Conferences:

1. **Petelinec, A.,** Tolić I. M. “Tumor cells reveal different mitotic patterns in a three-dimensional environment”, 8th Faculty of Science PhD Student Symposium (26-27.4.2024.), oral presentation

2. **Petelinec, A.,** Tolić I. M. “A subpopulation of diploid and post-tetraploid RPE1 cells show increased sensitivity to KIF18A inhibition”, Cell Cycle Conference (15.10.2024), oral presentation

3. Dundović I., **Petelinec A.,** Tolić I. M. “Mitotic fidelity is preserved in organized tissue despite late centrosome separation”, Mitotic spindle: From living and synthetic systems to theory (16-19.4.2023.), poster presentation